NASA
Reference
Publication
1108

December 1983

Propagation Effects on Satellite Systems at Frequencies Below 10 GHz

A Handbook for Satellite Systems Design

Warren L. Flock

National Aeronautics and
Space Administration
Twenty-fifth Anniversary
1958-1983

NASA

NASA Reference Publication 1108

1983

Propagation Effects on Satellite Systems at Frequencies Below 10 GHz

A Handbook for Satellite Systems Design

Warren L. Flock
University of Colorado

Prepared for
Jet Propulsion Laboratory
California Institute of Technology

NASA
National Aeronautics
and Space Administration

Scientific and Technical Information Branch

1983

FOREWORD

The NASA Handbook *for Propagation Effects on Satellite* Systems at Frequencies Below 10 GHz was prepared by Dr. Warren G. Flock, University of Colorado, for NASA Jet Propulsion Laboratory (JPL). The Handbook was initiated two years ago when Prof. Flock was working at JPL while on leave from the University of Colorado, and it has evolved through an extensive review process at JPL.

The Handbook was developed under NASA's Propagation Studies and Measurements Program, which has been involved for over a decade in the study of radiowave propagation on earth-space paths. The objectives of the NASA Propagation Program are to provide an understanding of the basic propagation mechanisms which hinder reliable earth-space communications, and to develop predictive models for the quantitative evaluation of propagation effects in the bands allocated for space applications.

The frequency bands below 10 GHz are allocated for several space services, including broadcasting, land-, maritime-, and aeronautical-mobile, meteorological, and space operations. The propagation problems are primarily ionospheric effects, although tropospheric factors cannot be neglected, particularly at low elevation angles. This Handbook provides the first comprehensive development of propagation effects in the bands below 10 GHz which impact satellite system design and performance.

Dr. Ernest K. Smith, Jet Propulsion Laboratory Propagation Program Manager, was instrumental in the initial definition and structure of the Handbook, and coordinated the preparation and review process throughout its development.

A second NASA Handbook, published earlier, presents a summary of propagation effects above 10 GHz ("Propagation Effects Handbook for Satellite Systems Design - A Summary of Propagation Impairments on 10 to 100 GHz Satellite Links With Techniques for System Design", NASA Reference Publication 1082, December 1981). Together these two documents provide a comprehensive description of propagation factors affecting telecommunications systems involving earth-space links.

This Handbook was conceived as an evolving document, which will be updated periodically to provide the most recent developments in propagation research. Your comments or suggestions on the document are always welcome.

Dr. Louis J. Ippolito
Manager,
Propagation Studies &
Measurements Program
NASA Headquarters

PREFACE

The use of satellite communications is expanding at an impressive rate, with much of the expansion taking place at frequencies above 10 GHz where attenuation due to precipitation and atmospheric gases tends to be the highest. Frequencies below 10 GHz, however, will continue to provide a large fraction of satellite service, and new applications, including mobile satellite services, are planned at frequencies below 10 GHz. As frequencies decrease below 10 GHz, attenuation due to precipitation and gases decreases and ionospheric scintillation and Faraday rotation increase. Tropospheric refraction and fading affect frequencies above and below 10 GHz but appear to be relatively more important at lower frequencies where attenuation due to rain and gases is small.

A handbook on propagation effects in the 10-100 GHz range has been prepared under NASA sponsorship* and this handbook is intended to serve a similar purpose for the 100 MHz to 10 GHz range. Emphasis is on effects on satellite communications, but material that is pertinent to radionavigation satellite service and deep-space telecommunications is included as well.

Descriptive background material concerning the various propagation impairments is given in Chaps. 1 through 7, and Chap. 9 is devoted to the estimation or calculation of the magnitudes of these effects for use in system design. Link power budget equations and the role of propagation effects in these equations are the subjects of Chap. 10. The final two chapters include some repetition of material presented earlier so that they can be used independently of the earlier chapters to a considerable extent. To avoid excessive duplication, however, references are made in some cases to figures and tables of the earlier chapters. Chapter 8, dealing with the complex subject of propagation effects on interference, departs from the earlier chapters in that it includes both background material and a summary of procedures for ap-

*NASA Communications Division, NASA Headquarters, A Propagation Effects Handbook for Satellite Systems Design, A Summary of Propagation Impairments on 10-100 GHz Satellite Links, with Techniques for System Design, Second Edition, Dec. 1981, NASA Reference Publication 1082 (L. J. Ippolito, Program Manager; R. D. Kaul and R. G. Wallace, Authors).

plication of the material in the same chapter. Although it draws upon the previous chapters and is pertinent to Chap. 10, the material of Chap. 8 constitutes a distinct and interesting subject of its own.

The handbook is based upon the work of the many investigators cited in the lists of references. Research supported by the Communications Division of the Office of Space and Terrestrial Applications of NASA has contributed greatly to knowledge of satellite communications, including the propagation aspects considered here, and is well represented in the reference lists.

I would like to express my appreciation for assistance and cooperation in the preparation of this handbook to Dr. Louis J. Ippolito of NASA and Dr. Ernest K. Smith, Dr. Young Park, Mr. Alfred M. Goldman, Jr., Dr. Arydas J. Kliore, Dr. William J. Weber, Dr. Stephen D. Slobin, and Mr. Tomas A. Komarek of the Jet Propulsion Laboratory. In addition, I wish to thank the many other persons at the Jet Propulsion Laboratory for their help in providing information and assistance in the production of the handbook. Mr. Goldman provided especially valuable assistance by reviewing the manuscript, providing information for inclusion in Chaps. 9 and 10, and engaging in discussions of the nature and purpose of the handbook.

PROPAGATION EFFECTS ON SATELLITE SYSTEMS
AT FREQUENCIES BELOW 10 GHZ

A Handbook for Satellite Systems Design

TABLE OF CONTENTS

TABLE OF CONTENTS

TABLE OF CONTENTS

CHAPTER 1
INTRODUCTION

1.1 PROPAGATION EFFECTS ON SYSTEM PERFORMANCE

1.1.1 Performance of Earth-Space Links

A fundamental requirement for satisfactory satellite communications service is the maintenance of a sufficient signal-to-noise ratio. Propagation effects are important because they tend to cause transmission losses which adversely affect this ratio. The received carrier power C on a path of length d is given by

$$C = \frac{P_T G_T A_R}{4\pi d^2 L} \tag{1.1}$$

where P_T is the power supplied to the transmitting antenna, G_T is the gain of the transmitting antenna, A_R is the effective area of the receiving antenna, and L is a loss factor which includes all losses and margins not otherwise taken into account. In particular, L includes propagation losses. If the losses included in L reduce C to 0.5 of what its value would be if the losses were neglected, for example, L would have the value of 2. Transmission losses are frequently specified in terms of the losses exceeded for a certain percentage, such as 0.01 percent, of a year or worst month.

Equation (1.1) can be converted to

$$C = \frac{P_T G_T G_R}{L_{FS} L} \tag{1.2}$$

where, for the receiving antenna, use has been of the relation between gain and effective area A_{eff}, namely

$$G = \frac{4\pi A_{eff}}{\lambda^2} \tag{1.3}$$

The quantity L_{FS} is the so-called free-space loss and is given by

$$L_{FS} = \left(\frac{4\pi d}{\lambda}\right)^2 \tag{1.4}$$

In Eqs. (1.3) and (1.4), λ is wavelength. The noise power X in watts at the receiving antenna terminals is given by

$$X = k\, T_{sys}\, B \tag{1.5}$$

where k is Boltzmann's constant (1.38×10^{-23} J/K), T_{sys} is the system noise temperature (K), and B is bandwidth (Hz). The ratio C/X is given by

$$C/X = \frac{P_T G_T G_R}{L_{FS} L k T_{sys} B} = \frac{(EIRP) G_R}{L_{FS} L k T_{sys} B} \tag{1.6}$$

where EIRP (effective isotropically radiated power) has been substituted for the product $P_T G_T$. In some cases, however, P_T is taken to be the transmitter or power amplifier output rather than the transmitting antenna input. In that case

$$EIRP = \frac{P_T G_T}{L_T} \tag{1.7}$$

where L_T accounts for losses in switches, filters, cables, or waveguides between the power amplifier and the antenna terminals. The quantity C/X is commonly expressed in dB (decibel) values and then takes the form of

$$(C/X)_{dB} = (EIRP)_{dBW} - (L_{FS})_{dB} - L_{dB} + (G_R/T_{sys})_{dB} - k_{dBW} - B_{dB} \tag{1.8}$$

Here k is taken to be the product of 1.38×10^{-23} J/K times a 1 K temperature interval times a 1 Hz bandwidth so that it has units of dBW (power measured in dB with relation to one watt). Then T_{sys} and B are treated as nondimensional quantities which can be expressed in dB above unity. The L_{FS} value in dB is given by

$$(L_{FS})_{dB} = 10 \log(4\pi d/\lambda)^2 = 20 \log(4\pi d/\lambda) \tag{1.9}$$

The carrier power-to-noise density ratio, C/X_0, where X_0 is noise power per Hz and is equal to kT_{sys}, is frequently used as a measure of system performance. It differs from C/X only by the factor B, representing bandwidth, and is thus given by

$$C/X_o = \frac{(EIRP)G_R}{L_{FS}LT_{sys}k} \tag{1.10}$$

Some satellites serve a wide geographical area in which a number of earth stations are located. In such a case the satellite transmitter gain G_T and the corresponding value of EIRP that are utilized in the expressions for C/X or C/X_o must be the appropriate value for the location in question. It can not necessarily be assumed that the maximum antenna gain corresponding to the center of the antenna beam is the value to use. For satellites that are already operational or for which detailed antenna analyses and designs have been made, plots showing contours of constant EIRP superimposed on geographical maps may be available (Fig. 10.6). Such plots, commonly referred to as footprints, allow selecting the proper value of EIRP for use in Eqs. (1.6) or (1.10).

As the system designer may be required to provide a certain C/X_o ratio over a certain coverage area A_{cov}, it is instructive to show the relation of A_{cov} to C/X_o and the other system parameters. A relation accomplishing this purpose has been supplied by Pritchard (1977) who gives the following expression

$$A_{cov}\ C/X_o \propto \frac{P_T A_R}{T_{sys} L} \tag{1.11}$$

A similar expression involving C/X, which is related to C/X_o by $C/X_o = (C/X)B$ with B the bandwidth, is

$$A_{cov}B \propto \frac{P_T A_R}{T_{sys} L(C/X)} \tag{1.12}$$

Note that these relations show proportionality rather than equality. Numerical constants (k in particular) have been eliminated from Eqs. (1.11) and (1.12). Pritchard has stressed that Eqs. (1.11) and (1.12) are fundamental to appreciating the essential problems of space communication. Equations (1.11) and (1.12) display clearly the roles of T_{sys} and L in determining system performance. T_{sys} is not strictly a propagation effect but is a closely related quantity, is a subject of this report along with L, and plays a comparable role in determining system performance. L includes, and may

consist only of, propagation losses. A derivation and further discussion of Eq. (1.11) is given in Section 10.4.

1.1.2 Determination of Distance and Elevation Angle of Satellite

Geostationary satellites operate at an altitude of about 35,785 km above sea level. Unless an earth station is directly under a satellite, however, the distance d of Eq. (1.4) will be larger than 35,785 km. The value of d can be established by use of the law of cosines of plane trigonometry. Consider first that the earth station is on the same longitude as the subsatellite point, taken to be at 0° latitude. The subsatellite point is located where a straight line from the satellite to the center of the Earth intersects the Earth's surface. Referring to Fig. 1.1

$$d^2 = r_o^2 + (h + r_o)^2 - 2\, r_o (h + r_o) \cos \theta' \tag{1.13}$$

where θ' is latitude. The equatorial radius of the Earth is 6378.16 km, the polar radius is 6356.78 km, and the mean radius is 6371.03 km (Allen, 1976). To obtain the most accurate value of d, it would be necessary to take into account the departure of the Earth from sphericity, but an approximate value of d can be obtained by taking r_o, the earth radius, to be 6378 km and h, the height of the satellite above the Earth's surface, to be 35,785 km in Eq. (1.13). It is convenient to divide all terms by $(h + r_o)^2$ or $(42,163)^2$ giving

$$\left(\frac{d}{h + r_o}\right)^2 = f^2 + 1 - 2f \cos \theta' \tag{1.14}$$

where $f = \frac{r_o}{h + r_o} = 0.1513$. Once d is known then all three sides are known and the angle ψ can be determined by applying the law of cosines again. The applicable equation is

$$(h + r_o)^2 = d^2 + r_o^2 - 2 r_o\, d \cos \psi \tag{1.15}$$

The elevation angle θ measured from the horizontal at the earth station, is equal to $\psi - 90°$.

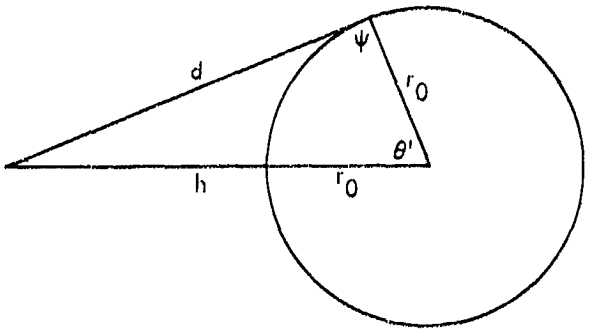

Figure 1.1. Geometry for calculation of distance d of satellite from earth station.

For an earth station not on the same meridian as the subsatellite point one can use

$$\cos Z = \cos\theta' \cos\phi' \tag{1.16}$$

in Eq. (1.13) in place of $\cos\theta'$, where ϕ' is the difference in longitude between subsatellite point and earth station. Cos Z is the angular distance of a great-circle path for the special case that one of the end points is at 0° latitude (Fig. 1.2). Also the expression follows from the "law of cosines for sides" of spherical trigonometry (ITT, 1968). The azimuth angle α of an earth-space path can be determined by using

$$\cos\alpha = \tan\theta' \cot Z \tag{1.17}$$

another relation applying to a right spherical triangle (ITT, 1968). The angle α is shown in Fig. 1.2a for an earth station located to the east of the subsatellite point. The azimuth angle measured from north in this case would be 180° + α. For an earth station location to the west of the subsatellite point as in Fig. 1.2b the angle from north is 180° - α. As an example, calculations for Boulder, Colorado, latitude 40°N, longitude 105°W and for Satcom-2, located at 119°W, with cos Z = cos 40° cos 14° = 0.743, give d = 37,501 km, elevation angle = 43.73°, and azimuthal angle = 201.2°.

In the above expression, r_0 is taken as a fixed sea-level value, but a larger value can be used for elevations above sea level. Local topography affects the angle of the path above the local horizon and can be taken into

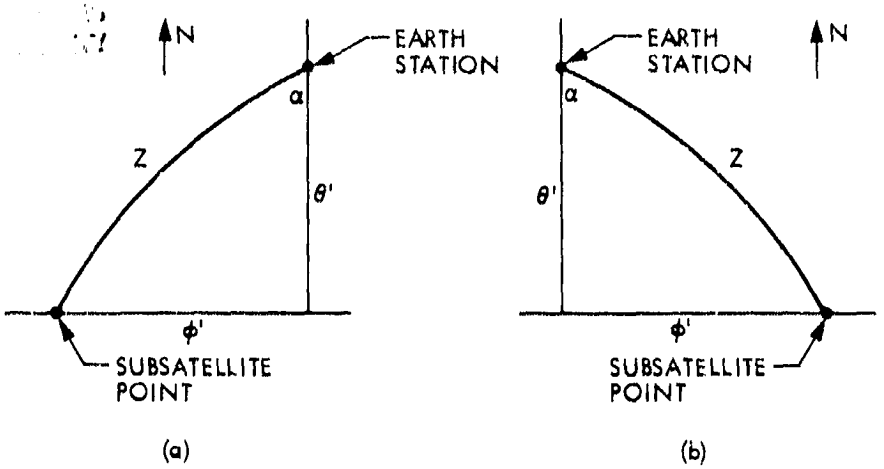

Figure 1.2. Projection of right spherical triangles on Earth's surface.

account to determine this angle for a particular location. Breuker and Walsh (1980) have developed a computer program to carry out such calculations for interference analysis as well as for determining the angle of a satellite above the local horizon. Propagation effects are a function of elevation angle and tend to become more serious with decreasing elevation angle. An elevation angle of 5° is often taken to be the minimum elevation angle that should normally be utilized. The procedure described here, essentially the same as that described by Dougherty (1980), is presented as suitable for link analysis and consideration of propagation effects rather than for precise aiming of antennas.

1.1.3 Propagation and Related Effects

Relatively small margins are utilized for satellite communications, and it is important to use no larger a margin than necessary. Thus, it is important to have as accurate information as practical about the propagation factors contributing to L even for the case of effects which might appear to be minor.

Frequencies in roughly the 1 to 4 GHz range tend to be affected only slightly by the Earth's atmosphere, but it is important nevertheless to know as closely as practical what the magnitudes of the effects are in this frequency range. Moving to higher frequencies, attenuation and noise due to rain, clouds and atmospheric gases increase. These effects may become limiting factors at frequencies above 10 GHz. The ionospheric effects of Faraday rotation, amplitude scintillation, and absorption, on the other hand, become increasingly significant with decreasing frequency. Tropospheric refraction and fading can affect transmissions over a wide range of frequencies extending above and below 10 GHz.

Depolarization or cross polarization may occur in propagation through the atmosphere or in reflection from terrestrial features. These terms refer to a degradation or change in polarization as from purely vertical linear polarization to linear polarization at an angle slightly different from vertical. This latter polarization is equivalent to a combination of vertical and horizontal polarization. In the process the originally vertically polarized wave is attenuated. Also the power converted to the orthogonal polarization may interfere with a channel having that polarization and thus make less effective the practice of frequency "reuse" (using the same frequency for two orthogonal polarizations in this case).

Electromagnetic radiation emitted by the atmosphere, commonly known as sky noise, is not strictly a propagation effect but is closely related and increases when attentuation increases. As is evident from the discussion of Sec. 1.1.1 [Eqs. (1.11) and 1.12) for example], T_{sys} affects system performance directly. Sky noise contributes to T_{sys}. When using a receiving system having a low noise temperature only a slight increase in sky noise may increase the system noise temperature, T_{sys}, significantly. It is important to know T_{sys}, as well as L, as accurately as practical.

A few references of a general nature, concerning either satellite systems or propagation effects, are appropriate for mention here. A comprehensive treatment of satellite communication engineering has been provided by Miya (1981), and Freeman (1981) includes satellite systems, as well as HF radio, line-of-sight terrestrial systems, and troposcatter systems, in his Telecommu-

nication Transmission Handbook. Martin (1978) discusses satellite communications from a largely non-technical viewpoint, as part of his popular series of books on communications and computers. An introductory treatment of radiowave propagation, earth-space links, and remote sensing has been prepared by Flock (1979). Hall (1979) has presented a summary of tropospheric effects on radio communications. NASA Reference Publication 1082 (Ippolito, Kaul, and Wallace, 1981) treats propagation effects at frequencies above 10 GHz, but many of the concepts and much of the material presented is pertinent to a broader range of frequencies.

1.2 FREQUENCY ASSIGNMENTS AND APPLICATIONS BELOW 10 GHZ

Frequencies below 10 GHz are used for a variety of purposes involving earth-space or space-space paths as shown in Table 1.1. The general categories of service are actually little different for frequencies above 10 GHz. A listing of frequency allocations for earth-space service at frequencies between 100 MHz and 10 GHz is given in Table 1.2. The entries in this table were taken from the Final Acts of the World Administrative Radio Conference, Geneva, 1979, Book I (ITU, 1979) for Region 2, which comprises North and South America and portions of the Atlantic and Pacific Oceans. This same reference also includes allocations for Region 1 (Europe, Africa, and Northern Asia) and Region 3 (Southern Asia and the South Pacific, including Australia and New Zealand). Allocations for the three regions tend to be similar but differ in details. The reference includes numerous footnotes giving information about exceptions for particular countries and periods, but information from the footnotes is omitted from Table 1.2, unless otherwise indicated. Allocations are also given in the Manual of Regulations and Procedures for Federal Radio Frequency Management (NTIA, 1979) and in the FCC Rules and Regulations.

The INTELSAT satellite system uses frequencies near 6 GHz for the uplink (earth-to-space path) and frequencies near 4 GHz for the downlink (space-to-earth path), and allocations used by INTELSAT are included in Table 1.2 as entries for fixed satellites, which refers to point-to-point service using geostationary satellites. Note that a number of space services utilize lower frequencies than the INTELSAT satellites. Included among these services are

Table 1.1 Satellite Services (ITU, 1976).

Aeronautical Mobile Satellite
Aeronautical Radionavigation Satellite
Amateur Satellite
Broadcasting Satellite
Earth Exploration Satellite
Fixed Satellite
Inter Satellite
Land Mobile Satellite
Maritime Mobile Satellite
Maritime Radionavigation Satellite
Meteorological Satellite
Mobile Satellite
Radiodetermination Satellite
Radionavigation Satellite
Space Operations
Space Research
Standard Frequency Satellite
Time Signal Satellite

Table 1.2 Frequency Allocations for Space Services (ITU, 1979).

Frequency (MHz)	Services
137 - 138	Space Operations and Research (Downlink) Meteorological Satellite (Downlink)
138 - 143.6	Space Research (Downlink)
143.6 - 143.65	Space Research (Downlink)
143.65 - 144	Space Research (Downlink)
144 - 146	Amateur Satellite
149.9 - 150.05	Radionavigation Satellite
267 - 272	Space Operation (Downlink)
272 - 273	Space Operation (Downlink)
322 - 328.6	Radio Astronomy
399.9 - 400.05	Radionavigation Satellite
400.05 - 400.15	Standard Frequency and Time Signal Satellite
400.15 - 401	Meteorological Satellite (Downlink) Space Research and Operation (Downlink)
401 - 402	Space Operation (Downlink) Earth Exploration Satellite (Uplink) Meteorological Satellite (Uplink)
402 - 403	Earth Exploration Satellite (Uplink) Meteorological Satellite (Uplink)
406 - 406.1	Mobile Satellite (Uplink)
406.1 - 410	Radio Astronomy
460 - 470	Meteorological Satellite (Downlink)
608 - 614	Radio Astronomy, Mobile Satellite (Uplink)
620 - 790	Broadcasting Satellite (Footnote 332A)
806 - 890	Mobile Satellite (Footnote 3670B)

Table 1.2 Frequency Allocations for Space Services (ITU, 1979) (cont'd).

Frequency (MHz)	Services
1215 - 1240	Radionavigation Satellite (Downlink)
1240 - 1260	Radionavigation Satellite (Downlink)
1400 - 1427	Radio Astronomy (1420 MHz neutral H line) Earth Exploration Satellite (Passive) Space Research (Passive)
1427 - 1429	Space Operation (Downlink)
1525 - 1530	Space Operation (Downlink) Earth Exploration Satellite
1530 - 1535	Space Operation (Downlink) Maritime Mobile Satellite (Downlink) Earth Exploration Satellite (Downlink)
1535 - 1544	Maritime Mobile Satellite (Downlink)
1544 - 1545	Mobile Satellite (Downlink)
1545 - 1559	Aeronautical Mobile Satellite (Downlink)
1559 - 1610	Radionavigation Satellite (Downlink)
1625.5 - 1645.5	Maritime Mobile Satellite (Uplink)
1645.5 - 1646.5	Mobile Satellite (Uplink)
1646.5 - 1660	Aeronautical Mobile Satellite (Uplink)
1660 - 1660.5	Aeronautical Mobile Satellite (Uplink) Radio Astronomy
1660.5 - 1668.4	Radio Astronomy Space Research (Passive)
1668.4 - 1670	Radio Astronomy
1670 - 1690	Meteorological Satellite (Downlink)
1690 - 1700	Meteorological Satellite (Downlink)

Table 1.2 Frequency Allocations for Space Services (ITU, 1979) (cont'd).

Frequency (MHz)	Services
1700 - 1710	Meteorological Satellite (Downlink)
2110 - 2120	Space Research (Deep Space Uplink, Footnote 3707B)
2290 - 2300	Space Research (Deep Space Downlink)
2500 - 2655	Fixed Satellite (Downlink) Broadcasting Satellite
2655 - 2690	Fixed Satellite (Downlink and Uplink) Broadcasting Satellite Earth Exploration Satellite (Passive) Radio Astronomy Space Research (Passive)
2690 - 2700	Earth Exploration Satellite (Passive) Radio Astronomy Space Research (Passive)
3400 - 3500	Fixed Satellite (Downlink)
3500 - 3700	Fixed Satellite (Downlink)
3700 - 4200	Fixed Satellite (Downlink)
4202	Standard Frequency and Time (Downlink)
4500 - 4800	Fixed Satellite (Downlink)
4800 - 4990	Radio Astronomy
4990 - 5000	Radio Astronomy Space Research (Passive)
5250 - 5255	Space Research
5650 - 5725	Space Research (Deep Space)
5725 - 5850	Fixed Satellite (Uplink)
5850 - 5925	Fixed Satellite (Uplink)

Table 1.2 Frequency Allocations for Space Services (ITU, 1979) (cont'd).

Frequency (MHz)	Services
5925 - 7025	Fixed Satellite (Uplink)
6427	Standard Frequency and Time (Uplink)
7125 - 7155	Space Operation (Uplink, Footnote 3762A)
7145 - 7190	Space Research (Deep Space only, Footnote 3763)
7145 - 7235	Space Research (Uplink, Footnote 3763)
5925 - 7075	Fixed Satellite (Uplink)
7250 - 7300	Fixed Satellite (Downlink)
7300 - 7450	Fixed Satellite (Downlink)
7450 - 7550	Fixed Satellite (Downlink) Meteorological Satellite (Downlink)
7550 - 7750	Fixed Satellite (Downlink)
7900 - 7975	Fixed Satellite (Uplink)
7975 - 8025	Fixed Satellite (Uplink)
8025 - 8175	Fixed Satellite (Uplink) Earth Exploration Satellite (Downlink)
8175 - 8215	Earth Exploration Satellite (Downlink) Fixed Satellite (Uplink) Meteorological Satellite (Downlink)
8215 - 8400	Earth Exploration Satellite (Downlink) Fixed Satellite (Uplink)
8400 - 8500	Space Research (Deep Space Downlink)

space research, involving the use of telemetry for transmitting data to the Earth, and space operations, including the functions of tracking and command. The frequency ranges of 2110 to 2120 MHz, 2290 and 2300 MHz, 5650 to 5725 MHz, and 8400 and 8500 MHz are listed as being for deep-space research. The proposed satellite power system (SPS) for collecting solar energy and transmitting it to the Earth would utilize 2450 MHz, according to present plans, for space-to-earth transmission.

The 806 - 890 MHz band which is used for land mobile service is being considered for Mobile Satellite services. These would be compatible with terrestrial land mobile service and would allow vehicles in remote areas to communicate by satellite.

Still lower frequencies, including prominently some in the 136-150 MHz range, are also assigned for space research and operation and for meteorological, radio navigation, earth exploration, mobile, standard time and frequency, and amateur satellite service. Amateur satellite service has assigned frequencies as low as 7 MHz.

Some of the services listed in Table 1.2, including radio astronomy, operate passively, which means that they record signals of natural origin which have followed earth-space paths and do not utilize manmade transmissions.

A listing or log of operational and planned geostationary satellites, by longitude, has been provided by Morgan (1980).

1.3 STRUCTURE OF THE EARTH'S ATMOSPHERE

Earth-space paths traverse both the Earth's troposphere and ionosphere, and the characteristics of these atmospheric regions are thus pertinent to satellite communications.

Troposphere

Temperature decreases with increasing altitude in the troposphere on the average, but temperature inversion layers provide exceptions to this general

characteristic. The height of the troposphere varies but extends to about 10 km over the poles and 16 km over the equator. The upper limit of the troposphere is known as the tropopause. A plot of atmospheric temperature versus altitude is shown in Fig. 1.3.

Atmospheric pressure tends to decrease exponentially in accordance with

$$p = p_o \, e^{-h/H} \tag{1.18}$$

where h is the height above a reference level where the pressure is p_o. The scale height H, however, is not a constant as it is a function of temperature T, the average mass m of the molecules present, and the acceleration of gravity g as indicated by

$$H = \frac{kT}{mg} \tag{1.19}$$

where k is Boltzmann's constant.

The rate of change of temperature with altitude in a dry atmosphere in an adiabatic state involving no input or loss of heat energy is given by $dT/dh = -9.8°C/km$. The dry adiabatic rate of change of temperature with height is of interest because the stability or instability of the atmosphere is determined in large part by the relative values of the actual rate of change of temperature with altitude and the dry adiabatic rate of change.

If the actual lapse rate of the atmosphere (rate of decrease of temperature with altitude) is 9.8°C/km, a parcel of air that is originally in equilibrium with its surroundings and which is then moved upwards or downwards will tend to remain in equilibrium, at the same temperature as its surroundings. The parcel of air will then not be subject to any restraining or accelerating force. Such a lapse rate of temperature is referred to as neutral. If the actual lapse rate of the atmosphere is greater than 9.8°C/km, a rising parcel of air will tend to cool only at the adiabatic rate and be warmer than its surroundings. As a result it will be lighter than the air around it and will be accelerated still further upwards. The air in this condition is unstable. If the lapse rate is less than 9.8°C/km, a parcel

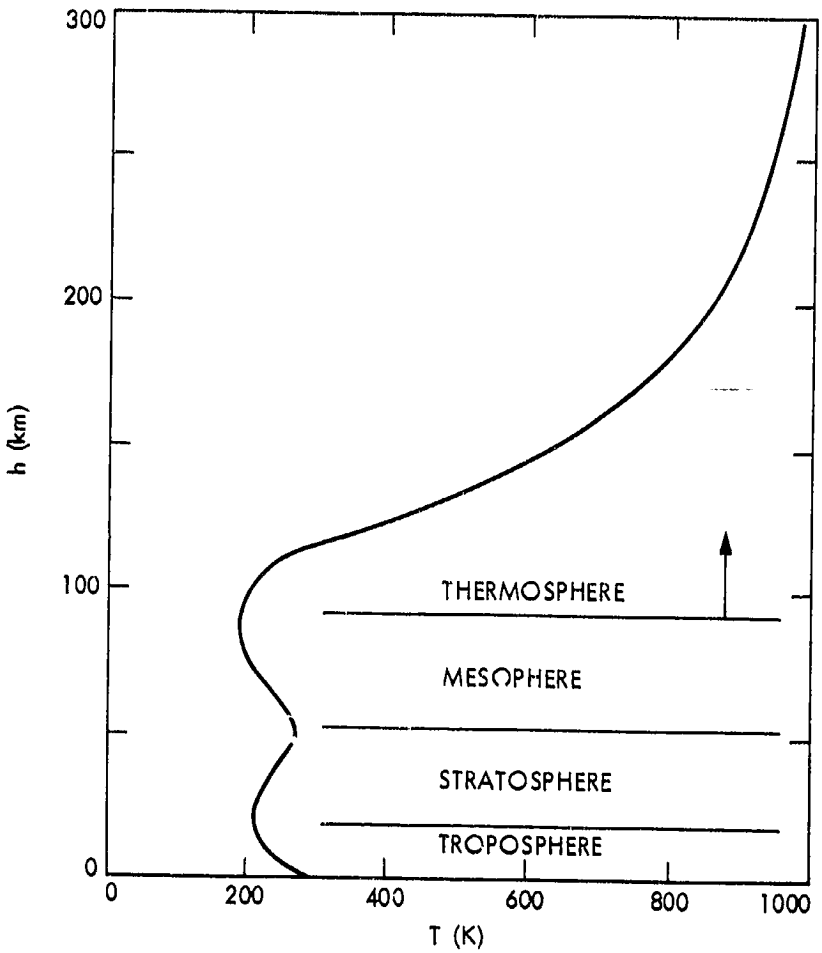

Figure 1.3. Atmospheric temperature versus altitude (values from U.S. Standard Atmosphere, 1976).

moved upwards would tend to cool at the adiabatic rate and be cooler than its surroundings. Thus, it would be subject to a force that inhibits vertical motion. Such a lapse rate, less than 9.8°C/km, is a stable lapse rate.

In an inversion layer temperature increases with altitude, and such a layer is highly stable. All vertical motions are strongly inhibited in an inversion layer, and pollution emitted below the layer tends to be confined below it. Also, if a source of water vapor exists below an inversion layer, it tends to be confined below the layer, with the result that large decreases in index of refraction may be encountered in upward passage through an inversion layer. Thus the occurrence of inversion layers may have an important effect on low-angle earth-space communication paths (Secs. 3.2 and 3.3).

Inversions tend to develop at night and in the winter, especially under conditions of clear sky as in the desert at night and in the arctic and subarctic in winter. Inversions may also form when warm air blows over a cool surface such as an ocean surface. Subsiding air is another cause of inversions, and this type of inversion is common because descending air is associated with developing or semipermanent anticyclones. The Pacific coast of the United States lies along the eastern edge of a semipermanent anticyclone that forms in the Pacific; this occurrence is a major factor in causing the pollution problems of the Los Angeles area.

Model atmospheres have been developed to present the best available estimates of the average values of pressure, density, temperature, and other parameters. One such model atmosphere is the U.S. Standard Atmosphere (1976). Temperature tends to decrease on the average at a rate of about 6.5°C/km, which is less than the dry adiabatic rate. When rainfall occurs at the Earth's surface a transition to ice and snow particles tends to occur at the height where the 0°C isotherm is reached. Water drops cause much higher attenuation than do ice particles and snow, so the 0°C isotherm marks the upper boundary of the region where most attentuation due to precipitation occurs.

A characteristic pattern of winds develops in the troposphere and is considered further in the following section (Sec. 1.4), where the natural regions of the Earth are listed.

Stratosphere, Mesosphere, Thermosphere

Above the troposphere temperature increases with height, to a maximum near 50 km, as a result of the absorption of solar ultraviolet radiation by ozone (Fig. 1.3). This region of increasing temperature with height is known as the stratosphere. The mesosphere, a region of decreasing temperature with height, occurs above the stratosphere and extends to about 85 km. Above 85 km is the thermosphere, in which temperature again increases with height as a result of the dissociation of atmosphere gases by solar ultraviolet radiation. Above 300 km temperatures change little with height for a considerable distance. Below about 100 km temperature varies little with time, but temperature above 120 km may vary by nearly a factor of 3 to 1, being highest in the daytime near the peak of the 11-year sunspot cycle.

The characteristic of the thermosphere of most importance to satellite communications is not the temperature structure itself but the ionization that occurs there. On the basis of the ionization, the region is known as the ionosphere. Actually the ionosphere commences at an altitude near 60 km, so it includes part of the mesosphere as well as the thermosphere.

Ionosphere

The ionosphere extends from about 60 km to a not very well defined upper limit of about 500 to 2000 km above the Earth's surface. As geostationary satellites operate at an altitude of about 35,785 km, transmission to and from these satellites pass through the entire ionosphere. The ionosphere, which is ionized by solar radiation in the ultraviolet and X-ray frequency ranges, is an ionized gas or plasma containing free electrons and positive ions such as to be electrically neutral. Only a fraction of the molecules are ionized, and large numbers of neutral molecules are also present. It is the free electrons that affect electromagnetic wave propagation in the frequency range considered in this report (100 MHz to 10 GHz).

Because different portions of the solar spectrum are absorbed at different altitudes, the ionosphere consists of several layers or regions. The layers are not sharply defined, distinct layers, and the transition from one to the other is generally gradual with no very pronounced minimum in electron

concentration in between. Representative plots of electron density versus height are shown in Fig. 1.4. Two good sources for further information about the characteristics of the ionosphere have been provided by Rishbeth and Garriott (1969) and Ratcliffe (1969).

D Region

The D region, the lowest of the ionospheric regions, extends from approximately 50 to 90 km with the maximum electron concentration of about $10^9/m^3$ occurring between 75 and 80 km in the daytime. At night electron concentrations throughout the D region drop to vanishingly small values.

As electron concentrations in the D region are very low it tends to have little effect on high-frequency waves. However, attenuation in the ionosphere occurs mainly through collisions of electrons with neutral particles, and as the D region is at a low altitude many neutral atoms and molecules are present and the collision frequency of electrons is high. Thus, transmissions in the AM broadcast band are highly attenuated in the daytime in the D region, but distant reception improves at night when the D region disappears.

E Region

The E region extends from about 90 to 140 km, and the peak electron concentration occurs between about 100 and 110 km. Electron densities in the E region vary with the 11-year sunspot cycle and may be about $10^{11}/m^3$ at noon at the minimum of the solar cycle and about 50 percent greater at the peak of the cycle. Electron concentrations drop by a factor of about 100 at night. Intense electrical currents flow in the equatorial and auroral ionospheres at E-region altitudes, these currents being known as equatorial and auroral electrojets. Radio waves are scattered from electron density structure associated with the electrojets at frequencies up to more than 1000 MHz. Backscatter echoes from the auroral electrojets are a manifestation of radio aurora. The phenomenon of sporadic E, thin, sporadic, often discontinuous layers of intense ionization, occurs in the E region, at times with electron densities well above $10^{12}/m^3$. The E layer can be useful for communications, as HF waves may be reflected from the E layer at frequencies which are a function of the time of day and period of the sunspot cycle. By causing interference between VHF stations, sporadic E tends to be a nuisance.

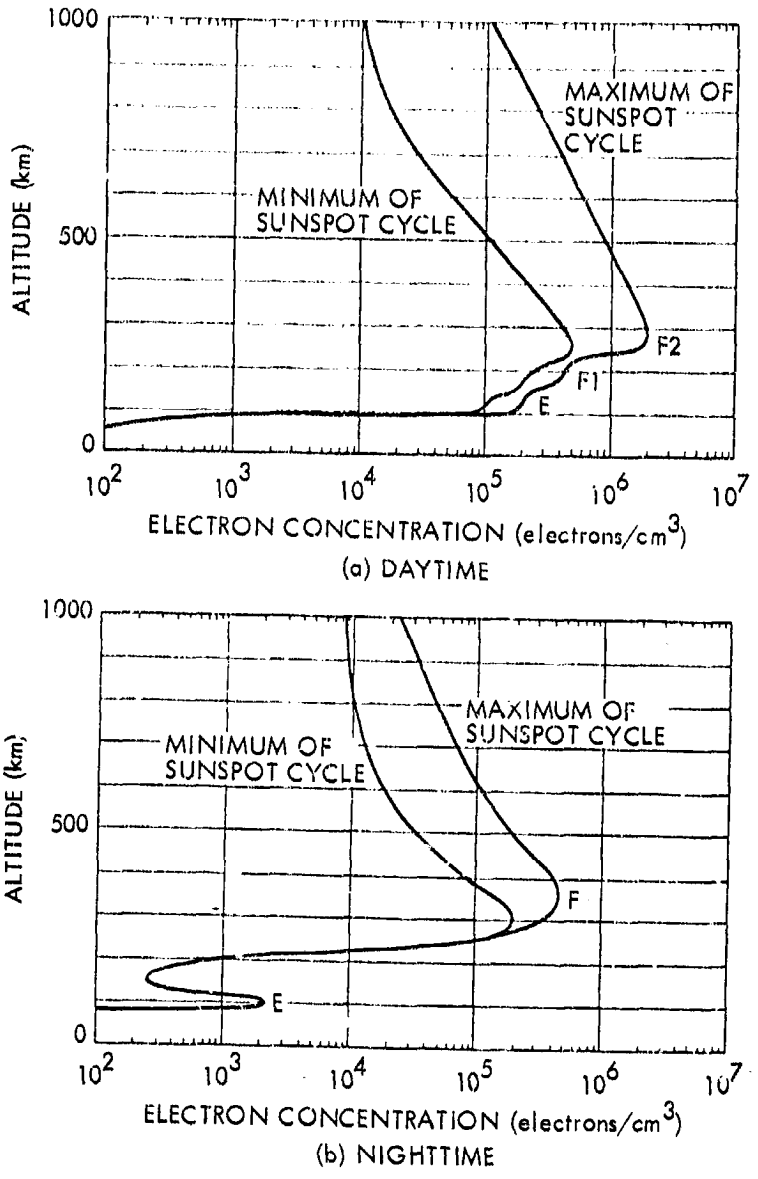

Figure 1.4. Electron density distributions at the extremes of the sunspot cycle (from Hanson, W.B., "Structure of the Ionosphere" in Johnson, F.S. (ed.), Satellite Environment Handbook, Stanford Univer. ity Press, 1965).

F Region

The F region has the highest electron densities of the ionosphere regions. It sometimes consists of two parts, the F_1 and F_2 layers. The F_1 layer largely disappears at night but has peak electron densities of about $2.5 \times 10^{11}/m^3$ at noon at the minimum of the solar cycle and $4 \times 10^{11}/m^3$ at noon at the maximum of solar cycle. The F_2 layer has the highest peak electron densities of any ionospheric region and the electron densities there remain higher at night than in other regions. The peak electron density is in the 200- to 400-km height range and may be between about $5 \times 10^{11}/m^3$ and $2 \times 10^{12}/m^3$ in the daytime and between $1 \times 10^{11}/m^3$ and $4 \times 10^{11}/m^3$ at night. Reflection from the F_2 layer is the major factor in HF communications which formerly handled a large fraction of long-distance, especially transoceanic, communications.

Plasmasphere and Magnetosphere

The upper limit of the ionosphere is not precisely defined but for the purposes of space communications may be taken to be 2000 km, this being the upper limit for significant Faraday rotation as discussed in Sec. 2.2. Above the ionosphere is the plasmasphere or protonosphere, which has an electron content of about 10 percent of the ionospheric content in the daytime and up to 50 percent of the ionospheric content at night, as defined along an earth-space path.

The Earth's magnetic field is confined inside an elongated cavity in the solar wind, that extends to about 10 earth radii in the direction towards the sun and has a long tail extending to about 60 earth radii or farther in the opposite direction. The boundary of this cavity is known as the magnetopause, and the region inside the boundary, above the ionosphere, is known as the magnetosphere. The magnetosphere can be defined as the region in which the Earth's field dominates the motion of charged particles, in contrast to the ionosphere where collisions play a major role. The Van Allen radiation belts, discovered in 1958 by use of Explorer 1, are in the magnetosphere. The plasmasphere, usually considerd to be above the ionosphere (or above 2000 km), is below the Van Allen belts and is the lowest region of the magnetosphere. The plasmasphere is bounded on the upper side at about 4 earth radii at the

equator by the plasmasphere where the plasma density drops by a factor of 10 to 100 or from about $10^8/m^3$ to $10^6/m^3$. The region above the plasmasphere is known as the plasmatrough.

Irregularities and Disturbed Conditions

A brief description has been provided of the ionospheric layers. Consideration of the ionosphere can be conveniently separated into the quiet ionospheric layers and their formation and ionospheric disturbances and irregularities, as occur at times of magnetic storms and essentially every night or day to some degree in the auroral and equatorial ionospheres. Both propagation in the quiet ionosphere and the effects of disturbances and irregularities are considered in the following Chap. 2.

1.4 NATURAL REGIONS OF THE EARTH, A GLOBAL VIEW OF PROPAGATION EFFECTS

The uneven heating of the Earth's surface by the Sun, the rotation of the Earth and the consequent Coriolis force, and surface features of the Earth determine a characteristic pattern of wind over the Earth. See, for example, a text on meteorology such as that by Donn (1975), p. 238. In good measure because of this pattern, corresponding characteristic patterns of climate, ecosystems, vegetation, tropospheric refractivity (Sec. 3.1), and rainfall (Chap. 4) also occur over the surface of the Earth. The living portions of ecosystems are referred to as biotic communities, and the major terrestrial biotic communities are known as biomes. A generalized pattern indicating the distribution of biomes over a theoretical flat continent corresponding roughly to a combination of North and South America or Eurasia and Africa is shown in Fig. 1.5, adapted from Trewarth (1968), and the numbered biomes of the figure are named and their locations are listed in Table 1.3. It can be seen that the names of the biomes represent the dominant type of vegetation (e.g., coniferous forest, grassland, desert) and are quite familiar. For most practical purposes the biomes can be referred to simply as natural regions. Many variations of such classifications exist, and local or regional conditions may cause departures from generalized distributions but the natural regions do occur in a regular way over the Earth. Regions of chaparral and Mediterranean climate (No. 9 in Fig. 1.5), for example, occur in similar locations in North and South America (California and Chile), Europe and

northern Africa, southern Africa, and Australia, in general agreement with the scheme of Fig. 1.5. The biomes of Fig. 1.5 correspond to the well-known Koppen system for classifying climate (Trewartha, 1963), but his letter designations and terminology have not been used in the figure. Maps of the natural regions of all the continents are included in the Aldine University Atlas (Fullard and Darley, 1969). The classification in Table 1.3, having been devised for biotic communities, does not include the surface areas consisting essentially of only ice and snow that occur in the Arctic and Antarctic.

The climatological, ecological, and geographical characteristics of a region are closely related and are pertinent to satellite communications within the region. Areas of tropical rainforest, for example, (the forests themselves are disappearing rapidly) can be expected to have heavy rainfall and a high atmospheric vapor content. The Arctic, on the other hand, has low precipitation and low values of water vapor. Some of the characteristics of the natural regions that may affect telecommunications are listed in Table 1.3 along with the names and locations of the regions.

A global model for estimating rainfall statistics has been developed and is discussed in Sec. 4.3.3, where rain rate regions are shown in Figs. 4.8, 4.9 and 4.10. Having this statistical model of rainfall allows formulating also a model of attentuation due to rainfall. To aid in comparing the natural regions listed in Table 1.3 and the rain rate regions of Figs. 4.8 - 4.10, the letter designations of the rain rate regions are included in Table 1.3, whenever a close correspondence occurs, in parentheses after the numbers assigned to the natural regions. Worldwide maps or tables are also available showing atmospheric water vapor content and features of the index of refraction, n, of the Earth's atmosphere, including surface values, Δn (the decrease in n in the first 1 km), and C_n^2 $[(n_1 - n_2)^2$ where n_1 and n_2 are indices of refraction at points located 1 m apart]. These parameters are discussed in Secs. 3.1 and 3.2.

The rain-rate classifications of Sec. 4.3 and the available data on index of refraction, etc., are not very detailed, however, and advantage should be taken of any more detailed information that may be available about the climate and related characteristics of a potential site for an earth station. Large

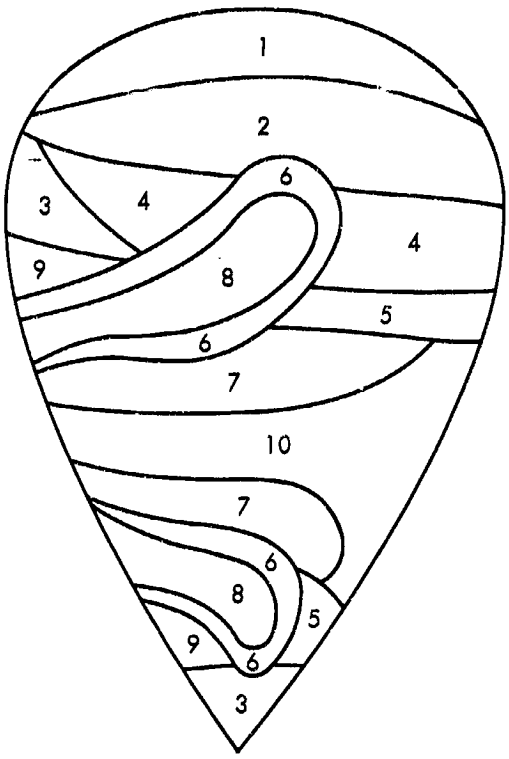

Figure 1.5. Generalized distribution of major natural regions (adapted from Trewartha, G.T., An Introduction to Climate, McGraw-Hill, 1968). The numbers correspond to the entries of Table 1.3.

Table 1.3 The Major Natural Regions, their Locations, and Characteristics Pertinent to Telecommunications.

	Natural Region	Characteristics
1. (A)	Tundra Circumpolar (Arctic)	Low atmospheric water vapor content, low precipitation, but fog common in summer. Polar-cap absorption.
2. (B)	Northern coniferous forest (taiga, boreal forest) Circumpolar, south of the tundra	Rather low atmospheric water vapor content and precipitation, winter temperature inversions and ice fog, the latter especially in settled areas (Fairbanks, Alaska). Auroral absorption, scatter, and scintillation.
3. (C)	Temperate rain forest (marine west coast climate) N. Pacific coast of N. America (Alaska to California), w. coast New Zealand, Tasmania and s.e. Australia, s. Chile.	Moderately high atmospheric water vapor content, considerable rain and overcast, but rain rates generally not extremely high, drier in summer, amount of rainfall influenced by location with respect to mountains (Pacific Northwest).
4. (D)	Temperate deciduous forest Eastern N. America, Europe, China, Japan, e. coast of Australia	Moderately high atmospheric water vapor content, moderately high precipitation more or less uniformly distributed throughout year
5. (E)	Broad-leafed evergreen subtropical forest (humid subtropical climate) S.e. U.S., central and s. Japan	High water vapor content, high rain rates and high total precipitation, more or less uniformly distributed throughout the year in United States except higher in summer in Florida.
6. (F)	Temperate grasslands and steppes Interior regions of N. America, e. Europe, central and w. Asia, Argentina, Australia	Rather low water vapor content and total precipitation but with some severe thunderstorms and blizzards. Precipitation greatest in early summer in Great Plains of United States.

Table 1.3 The Major Natural Regions, their Locations, and Characteristics Pertinent to Telecommunications (cont'd).

Natural Region	Characteristics
7. (G) Tropical savanna Central Africa, C. and S. America (n. and s. of Amazon basin), n. Australia, s.e. Asia	Alternating wet and dry seasons with corresponding variations in water vapor content (summer monsoon in India).
8. Desert — S.w. and intermountain N. America; n., s.w., and e. Africa; Mid East; central Asia; Peru and n. Chile; c. Australia	Low total rainfall and low water vapor content away from coast but some intense rainstorms in summer. (Maximum rain in the summer with a secondary maximum in the winter -in Arizona.) Deserts and mountains having higher precipitation are found in close proximity in western North America. Some coastal areas have very high -water vapor content (Persian Gulf). Drier desert areas subject to temperature inversions at night.
9. Mediterranean (chaparral, etc.) Mediterranean area, California, central Chile, Cape of Good Hope, s.w. and s. Australia	Moderate water vapor near coast, lower inland, winter rainy season, dry summers. Strong and persistent temperature inversions in summer and fall (southern California).
10. (H) Tropical forest (a) Rainforest Amazon basin, Brazilian coast of S. America, C. America, Congo, Niger, and Zambezi basins of Africa; Indonesia, Malaysia, Borneo, New Guinea, and Pacific islands. (b) Scrub and deciduous forest C. and S. America, Africa, Australia, s. Asia	Very high water vapor content and very high precipitation throughout most of year in rainforest areas, lower in scrub forests. Equatorial ionospheric scatter and scintillation.

variations in climate can occur on a local scale as well as on a global scale. Rainfall on the west slope of the Olympic Mountains of the state of Washington, for example, may be about 144 inches (12 feet) per year, whereas in the rain shadow on the northeast side of the mountains rainfall may total only about 16 inches.

The auroral and equatorial ionospheres exhibit irregularities and disturbed conditions more extensively than other regions. Magnetic latitude is the major determining factor in the case of the ionosphere, but it corresponds sufficiently closely to geographic latitude that Table 1.3 includes references to ionospheric characteristics for regions 1, 2, and 10.

REFERENCES

Allen, C.W., Astrophysical Quantities. London: University of London, The Athlone Press, 1978.

Breuker, D.J. and K.V. Walsh, "A Technical and Cost-Performance Model for Receive-Only Earth Satellite-Terminals (RESTS)," M.S. thesis. Boulder, CO; Department of Electrical Engineering, University of Colorado, 1980.

Donn, W.L., Meteorology, 4th ed. New York: McGraw-Hill, 1975.

Dougherty, H.T., "A consolidated model for UHF/SHF telecommunications links between earth and synchronous satellites," NTIA Report 80-45, U.S. Dept. of Commerce, Aug. 1980.

Flock, W.L., Electromagnetics and the Environment: Remote Sensing and Telecommunications. Englewood Cliffs, NJ: Prentice-Hall, 1979.

Freeman, R.L., Telecommunications Transmission Handbook, 2nd Ed., New York: Wiley, 1981.

Fullard, H. and H.C. Darby, Aldine University Atlas. Chicago: Aldine, 1969.

Hall, M.P.M., Effects of the Troposphere on Radio Communications. Stevenage, UK and New York: Peter Peragrinus Ltd. on behalf of the Institution of Electrical Engineers, 1979.

Ippolito, L.J., R.D. Kaul, and R.G. Wallace, Propagation Effects Handbook for Satellite Systems Design, A Summary of Propagation Impairments on 10 to 100 GHz Satellite Links with Techniques for System Design, NASA Reference Pub. 1082. Washington, D.C.: NASA Headquarters, 1981.

ITT, Reference Data for Radio Engineers, Fifth Edition. Indianapolis: Howard W. Sams & Co., 1968.

ITU (International Telecommunications Union), Radio Regulations, Edition of 1976. Geneva: ITU, 1976.

ITU (International Telecommunications Union), Final Acts of the World Administrative Radio Conference, Geneva, 1979, Book I of IV, Terminology, Technical Provisions, and Frequency Allocations. Geneva: ITU, 1979.

Martin, J., Communications Satellite Systems. Englewood Cliffs, NJ: Prentice-Hall, Inc., 1978.

Miya, K., Satellite Communications Technology. KDD Bldg. 3-2, Nishi-Shinjuku 2-chome, Shinjuku-ku, Tokyo 60, Japan, 1981.

Morgan, W.L., "Geosynchronous satellite log for 1980," COMSAT Tech. Rev., vol. 10, pp. 233-262, Spring, 1980.

NTIA (National Telecommunications and Information Administration), Manual of Regulations and Procedures for Federal Radio Frequency Management. Washington, D.C. 20230. NTIA, IRAC (Interdepartment Radio Advisory Committee), 1979.

Pritchard, W.L., "Satellite communication -- an overview of the problems and programs," Proc. IEEE, vol. 65, pp. 294-307, March, 1977.

Ratcliffe, J.A., An Introduction to the Ionosphere and Magnetosphere. Cambridge: Cambridge University Press, 1972.

Rishbeth, H. and O.K. Garriott, Introduction to Ionospheric Physics. New York: Academic Press, 1969.

Trewartha, G.T., An Introduction to Climate. New York: McGraw-Hill, 1968.

U.S. Standard Atmosphere, 1976, sponsored by NOAA, NASA, USAF. Washington, D.C.: Supt. of Documents, U.S. Government Printing Office, 1976.

CHAPTER 2
IONOSPHERIC EFFECTS

2.1 PROPAGATION IN HOMOGENEOUS PLASMAS

This chapter includes a brief treatment of ionospheric propagation. The reader interested in a more thorough analysis of this large and interesting subject is referred to references by Budden (1961), Davies (1965, 1969), Kelso (1964), and Ratcliffe (1972). An elementary treatment starting with Maxwell's equations is included in the text by Flock (1979).

2.1.1 Characteristic Waves

The Earth's ionosphere is a partially ionized gas or plasma which is rendered anisotropic by the presence of the Earth's magnetic field. The concept of characteristic waves is important in considering the propagation of electromagnetic waves in such a medium. These are the waves which propagate without changing their polarization, by which reference is made to whether a wave is linearly, circularly, or elliptically polarized and, in the case of linear polarization, to the direction of the electric field intensity vector of the wave (e.g. vertical, horizontal, or at an angle between vertical and horizontal). Changing from linear to elliptical polarization, for example, constitutes a change in polarization, and changing the direction of linear polarization also constitutes a change in polarization.

The nature of the characteristic waves that propagate in an anisotropic plasma such as the Earth's ionosphere can be determined by the application of Maxwell's equations. It develops that there are two characteristic waves and that the parameters of the characteristic waves depend upon the direction of propagation with respect to the Earth's magnetic field (the angle θ_B of Fig. 2.1).

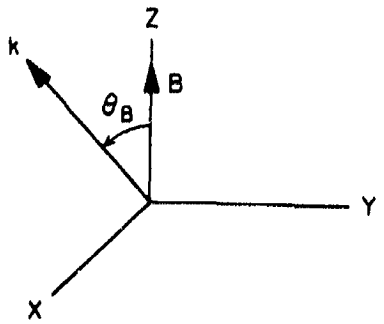

Figure 2.1. Coordinate system for considering propagation at an angle Θ_B from the direction of the Earth's magnetic field $\underset{\sim}{B}$. The quantity $\underset{\sim}{k}$ is a vector indicating the direction of propagation of the wave.

Parallel Propagation

For propagation parallel to the Earth's field B ($\Theta_B = 0^0$) in the lossless case the two characteristic waves are left and right circularly polarized and have indices of refraction n_ℓ and n_r given by

$$n_\ell^2 = K_\ell = 1 - \frac{\omega_p^2}{\omega(\omega + \omega_B)} \qquad (2.1)$$

and

$$n_r^2 = K_r = 1 - \frac{\omega_p^2}{\omega(\omega - \omega_B)} \qquad (2.2)$$

K_ℓ and K_r are the relative dielectric constants for the left and right circularly polarized waves. ω is the angular frequency of the wave and equals $2\pi f$ where f is frequency in Hz. ω_B is the angular gyro frequency of the electrons in the plasma and is given by

$$\omega_B = \frac{-qB}{m} \qquad (2.3)$$

where B is the Earth's magnetic field in Wb/m^2, $q = -e = -1.6022 \times 10^{-19}$ C is the charge of the electron, and m is the mass of the electron (9.1096×10^{-31}

kg). The Earth's field is roughly that of a magnetic dipole, inclined by about 12^{o} with respect to the rotational axis, for which the field decreases as the cube of the radius or distance from the center of the Earth. Figure 2.2 shows field values given by a dipole model. Other more accurate models take into account the observed departure of the Earth's field from that of a dipole. It must be recognized that the Earth's field changes with time and that a model developed for a certain period of time will not give the most accurate results for a later period. Emphasis was originally given to modeling the Earth's surface field, but for earth-space paths field values may be needed for a range of altitudes. The Environmental Data Service (1976) of NOAA, Boulder, Colorado can supply values of the Earth's magnetic field by making use of several mathematical models and has prepared a leaflet describing their services of this type. The World Data Center A for Rockets and Satellites, Code 601, NASA/Goddard Space Flight Center, Greenbelt, MD 20771 can supply information about computer programs for synthesizing field values. Coefficients for expansion of the International Geomagnetic Reference Field in spherical harmonics are given in the May 1982 issue of Geophysics (Peddie, 1982). This model of the Earth's geomagnetic field was developed by a working group of IAGA (The International Association of Geomagnetism and Aeronomy). A special issue of the Journal of Geomagnetism and Geoelectricity is scheduled to be devoted to the Earth's field but is not yet available at the time of writing. A computer algorithm for synthesizing the geomagnetic field has been prepared by Malin and Barraclough (1981).

The quantity ω_p^2 is the angular plasma frequency squared and can be calculated from

$$\omega_p^2 = \frac{Nq^2}{m\varepsilon_o} \tag{2.4}$$

N is electron density (el/m^3) and ε_o is the electric permittivity of empty space (8.854×10^{-12} F/m). For practical calculations using Eqs. (2.1) and (2.2) it may be convenient to convert from angular frequency to frequency in MHz for propagation at HF and higher frequencies. For this purpose

$$(f_B)_{MHz} = 2.7992 \times 10^4 \; B \tilde{=} 2.8 \times 10^4 \; B \tag{2.5}$$

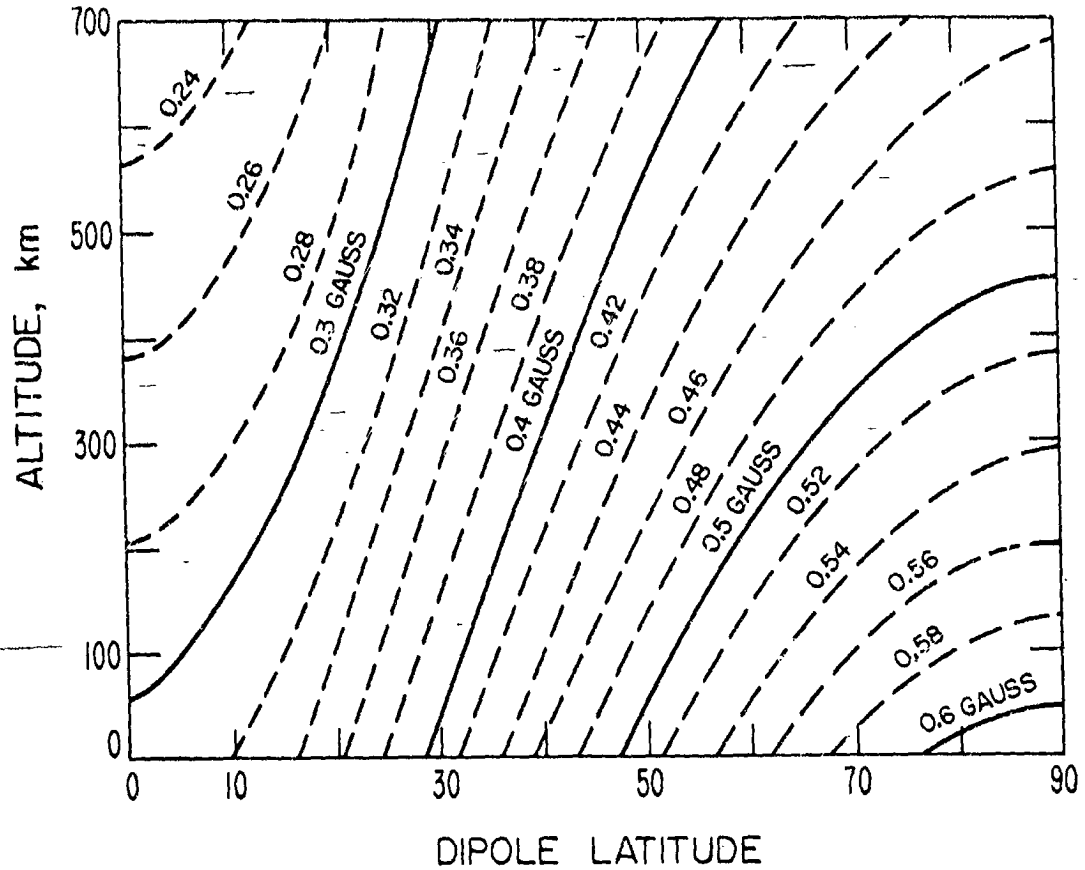

Figure 2.2. Total intensity of the Earth's magnetic field as a function of altitude and dipole latitude, assuming an earth-centered dipole of magnetic moment M = 7.95 x 10^{25} gauss cm^3 (after Smith, 1974).

with B in Wb/m^2, or $(f_B)_{MHz} \cong 2.8\ B$ with B in gauss. Also

$$(f_p)_{MHz} = 8.9788 \times 10^{-6} \sqrt{N} \tag{2.6}$$

with N the number of electrons per m^3. Then

$$n_\ell = \left[1 - \frac{f_p^2}{f\,(f + f_B)} \right]^{1/2} \tag{2.7}$$

and

$$n_r = \left[1 - \frac{f_p^2}{f\,(f - f_B)} \right]^{1/2} \tag{2.8}$$

A right circularly polarized wave has an electric field intensity vector of constant length that rotates with angular velocity ω in the right circular direction, which can be defined by the direction of the fingers of the right hand, if they are imagined to circle the thumb when the thumb points in the direction of propagation. A left circularly polarized wave rotates in the opposite direction.

Perpendicular Propagation

For propagation perpendicular to the magnetic field ($\Theta_B = 90^0$) one characteristic wave has its electric field intensity vector directed along the z axis of Fig. 2.1. The electric field in this case imparts a velocity to the free electrons in the z direction, with the result that the electrons are unaffected by the magnetic field, as no magnetic force is exerted on charged particles having velocities parallel to the magnetic field. The index of refraction n_o for this case is given by

$$n_o^2 = 1 - \frac{\omega_p^2}{\omega^2} = 1 - \frac{f_p^2}{f^2} \tag{2.9}$$

which is also the value for the case of no magnetic field. The subscript o stands for ordinary; traditionally this wave has been called the ordinary wave as it is unaffected by the magnetic field. If the electric field intensity is in the y direction in Fig. 2.1 (or in general perpendicular to B), the situation is somewhat more complicated. In this case, the index of refraction n_x is given by

$$n_x^2 = \frac{K_\ell K_r}{K_\perp} \qquad (2.10)$$

where

$$K_\perp = 1 - \frac{\omega_p^2}{\omega^2 - \omega_B^2}$$

This wave is referred to as the extraordinary wave. The two characteristic waves for propagation perpendicular to the magnetic field are linearly polarized in the plane perpendicular to the direction of propagation, but it develops that for the extraordinary wave there is a component of electric field intensity in the direction of propagation (the x direction if the transverse component is in the y direction) as well.

2.1.2 Role of Index of Refraction

The index of refraction of an electromagnetic wave is by definition the ratio of $c \approx 3 \times 10^8$ m/s, the velocity of an electromagnetic wave in empty space, to v_p, the phase velocity of the wave in question in the medium under consideration. (A more precise value of c is 2.9979×10^8 m/s.) Thus

$$n = \frac{c}{v_p} \qquad (2.11)$$

The phase constant β of an electromagnetic wave gives the phase lag of the wave with distance when used in

$$E = E_0 e^{-j\beta z} \qquad (2.12)$$

for the case of a wave propagating in the z direction and having an electric field intensity E_0 at a reference position where $z = 0$. β can be expressed in several ways as shown in Eq. 2.13, namely

$$\beta = \frac{2\pi}{\lambda} = \frac{\omega}{v_p} = \beta_o n \qquad (2.13)$$

where λ is wavelength and β_o is the phase constant for empty space. It can be seen that the two characteristic waves, for propagation either parallel or perpendicular to the magnetic field, have different values of index of refraction. Thus they have different phase velocities, phase constants, and wavelengths.

2.1.3 Reflection and Refraction

Reflection

Examination of Eqs. (2.1), (2.2), (2.9) and (2.10) reveals that it is possible for the index of refraction squared, or the relative dielectric constant, to be negative and thus for the index of refraction itself to become imaginary. The simplest case to consider is that of the ordinary wave (Eq. 2.9). For $\omega > \omega_p$, n_o is real but for $\omega < \omega_p$, n_o is imaginary. An imaginary value of index of refraction determines that β of Eq. (2.12) will be imaginary and that, instead of a propagating wave as indicated by Eq. (2.12) with β real, an evanescent condition will occur with $E = E_o e^{-\alpha z}$, when the $-j\beta$ of Eq. (2.12) has become $-j\beta_o\,(-j|n|) = -\alpha$. The different possibilities are summarized in Table 2.1.

Table 2.1 Characteristics of n and E(z) Corresponding to Different Relative Values of ω and ω_p.

ω	n	E(z)
$\omega > \omega_p$	real	$E = E_o e^{-j\beta z}$
$\omega = \omega_p$	0	$E = E_o$
$\omega < \omega_p$	imaginary	$E = E_o e^{-\alpha z}$

The condition $E = E_0 e^{-\alpha z}$ of Table 2.1 represents a field that attenuates with z, but the attenuation in the evanescent case is not dissipative. Instead it involves reflection and reversal of direction as suggested in Fig. 2.3b. In Fig. 2.3 an increase of electron density with height in the ionosphere is assumed. The frequency ω is much greater than ω_p in Fig. 2.3a, and the ray path is essentially unaffected by the ionosphere, whether the path is vertical or oblique. In Fig. 2.3b the condition $\omega < \omega_p$ is reached in the vertical path shown and the ray is reflected. The illustration of Fig. 2.3b

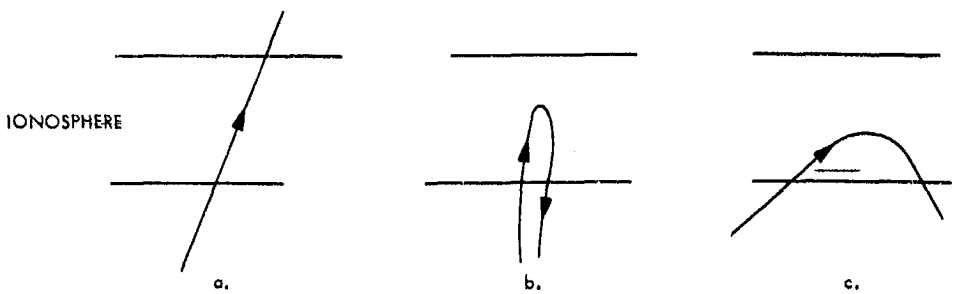

Figure 2.3. Ionospheric ray paths.

a. $\omega >> \omega_p$ throughout the ionosphere.
b. The condition $\omega \leq \omega_p$ is reached along the ray path.
c. Oblique-incidence path.

suggests the overall result, but the reflection process actually takes place over a range of heights, consistent with $E = E_0 e^{-\alpha z}$, rather than abruptly at a particular level. Furthermore, if the evanescent region is of limited extent and E still has a significant value at the far side of the region from the source, then a wave of diminished but measurable amplitude will be launched and will propagate beyond the evanescent region.

For the ordinary wave ω_p plays the role of a critical frequency with propagation occurring for $\omega > \omega_p$ and not for $\omega < \omega_p$. The situation is similar to propagation in a metallic waveguide having a certain cutoff frequency f_c. In a waveguide propagation occurs for $f > f_c$ and an evanescent condition

occurs for $f < f_c$. An evanescent section of waveguide, however, can serve as a waveguide-below-cutoff attenuator. For the left and right circularly polarized waves, Eqs. (2.1) and (2.2) show that the conditions,

$$\omega_p^2 = \omega^2 + \omega\omega_B \text{ and } \omega_p^2 = \omega^2 - \omega\omega_B,$$

respectively, separate propagating and nonpropagating regions for the left and right circularly polarized waves.

The above discussion is idealized in that dissipative attenuation does occur to some degree in the ionosphere so that for $\omega \to \omega_p$, $E(z) = e^{-j\beta z}e^{-\alpha z}$ where α now represents dissipative attenuation involving the conversion of electromagnetic energy into heat. The attenuation varies as $1/f^2$ for frequencies above 30 MHz and tends to be small for frequencies used on earth-space paths. The topic of absorptive or dissipative attenuation is treated in Section 2.7.

Refraction

In Figure 2.3c a ray is obliquely incident upon the ionosphere and is shown to experience reflection. In this case ω is always greater than ω_p, however, and while the overall result is usually viewed as reflection the process is basically one of refraction. Applying Snell's law with the angle χ measured from the zenith and neglecting the earth's curvature

$$n \sin \chi = n_0 \sin \chi_0$$

where χ_0 is the initial launch angle below the ionosphere and n_0, the index of refraction of the troposphere, is essentially unity. At the highest point in the path of Figure 2.3c the angle χ is 90^0. Therefore, at this point $n = \sin \chi_0$. For the ordinary wave for which

$$n^2 = 1 - (f_p/f)^2$$

with f_p the plasma frequency and f the operating frequency

$$n^2 = \sin^2 \chi_o = 1 - \left(\frac{f_p}{f}\right)^2 \tag{2.14}$$

from which $\cos \chi_o = f_p/f$ and

$$f = f_p \sec \chi_o \tag{2.15}$$

This expression gives the maximum frequency, f, which will be reflected, or refracted, from or below a height where the plasma frequency is f_p for a wave having a launch angle of χ_o. If f_p is the peak value of the ionosphere then f is the maximum usable frequency, in particular the maximum frequency that will be reflected for a launch angle of χ_o.

The above case can be considered to be an extreme example of refraction. At the frequencies of major interest in this handbook ionospheric refraction will be of rather minor importance but will cause a slight bending of a ray such that the apparent elevation angle or angle of arrival will be higher than the geometric elevation angle. For satellites well above most of the ionization the error in elevation angle $\Delta\Theta$ is given by

$$\Delta\Theta = \frac{(R+r_o \sin \Theta_o) r_o \cos \Theta_o}{[h_i(2r_o+h_i) + (r_o \sin \Theta_o)^2]} \frac{\Delta R}{R} \text{ rad} \tag{2.16}$$

where Θ_o is the apparent elevation angle, h_i is the height of the centroid of the electron content along the path (normally between 300 and 450 km), and ΔR is the range error [Eq. (2.34)]. For sufficiently low elevation angles or for long ranges corresponding to geostationary satellites for which $R > r_o \sin \Theta_o$

$$\Delta\Theta \cong \frac{\cos \Theta_o}{2h_i} \Delta R \quad \text{rad} \tag{2.17}$$

As ΔR, the range error, varies with time, the elevation angle error $\Delta\Theta$ also varies with time. Furthermore as $\Delta\Theta$ is the difference between the true and apparent elevation angles, the apparent elevation angle or direction of arrival varies with time.

These relations were developed by Millman and Reinsmith (1974). Klobuchar (1978) reports that for a frequency of 1.6 GHz, a worst case elevation angle of 5^0, and a TEC (total electron content) of 10^{19} electrons/m^2, $\Delta\Theta$ will be 0.3 mr. Equation (2.34) shows the range error and therefore the refraction or elevation angle to vary inversely with f^2.

2.1.4 QL Approximation

Propagation can occur at any angle Θ_B with respect to the magnetic field, and analysis for the general case is more complex than for strictly parallel or perpendicular propagation. The situation is considerably simplified, however, when the QL approximation is applicable. To state this approximation, we use the common practice of defining ω_p^2/ω^2 as X and ω_B/ω as Y. Using these quantities, Eqs. (2.1) and (2.2) take the forms

$$n_\ell^2 = K_\ell = 1 - \frac{X}{1 + Y} \tag{2.18}$$

and

$$n_r^2 = K_r = 1 - \frac{X}{1 - Y} \tag{2.19}$$

Also defining Y cos Θ_B as Y_L and Y sin Θ_B as Y_T, the condition for the QL approximation to apply is

$$4(1 - X)^2 Y_L^2 >> Y_T^4 \tag{2.20}$$

When this approximation applies the characteristic waves for propagation at an angle Θ_B with respect to the magnetic field are circularly polarized, as they are for $\Theta_B = 0^0$, and their indices of refraction have the forms

$$n_\ell^2 = K_\ell = 1 - \frac{X}{1 + Y_L} \tag{2.21}$$

and

$$n_r^2 = K_r = 1 - \frac{X}{1 - Y_L} \tag{2.22}$$

2.1.5 Application to Space Communications

The value of X in Eq. (2.20) is a major factor in determining if the QL approximation applies, and X is defined as ω_p^2/ω^2. For space communications ω tends to be high, X tends to be small, and the QL approximation tends to apply, even for large values of θ_B. Thus the characteristic waves on earth-space paths are normally left and right circularly polarized waves. Also examination of Eqs. (2.1) and (2.2) or (2.21) and (2.22) shows that n_ℓ and n_r have values only slightly less than unity for large values of ω and that these values approach closer to unity and to each other as ω increases. Thus for ω sufficiently large, n_ℓ and n_r are essentially unity, reflection does not occur, and the effect of the ionosphere can be neglected. Such is the case for frequencies above 10 GHz. Moving downward in frequency below 10 GHz, however, one reaches frequencies for which ionosphere effects are important, even though n_ℓ and n_r may still not be far from unity.

In this section consideration is given to uniform or homogeneous media, but the ionosphere is characterized by various disturbances and irregularities which also affect propagation and which are also most important for lower frequencies. These irregularities and their effects are treated in Secs. 2.5, 2.6, and 2.7.

2.2 FARADAY ROTATION

Analysis of the propagation of a linearly polarized high-frequency wave in the ionosphere shows that it experiences rotation of the plane of polarization such that a wave that is launched with vertical polarization, for example, does not remain vertical. Depending on the frequency, length of path in the ionosphere, and orientation with respect to the Earth's magnetic field the amount of rotation may vary from a negligible amount to amounts in excess of 360^0 to many complete rotations. The basis for such rotation, known as Faraday rotation, is that a linearly polarized wave consists of left and right circularly polarized components which have different indices of refraction.

That a linearly polarized wave can be separated into left and right circularly polarized components, or formed by combining the circular components, can be visualized with the aid of Fig. 2.4.

Consider that E_ℓ and E_r are the electric field intensity vectors of left and right circularly polarized waves. Small auxiliary arrows are used to indicate the direction of rotation for E_ℓ and E_r for a right-handed coordinate system with z, the direction of propagation, extending out of the plane of the paper. E_ℓ and E_r are the circularly polarized components of a linearly polarized wave having its electric field intensity in the x direction. Figure 2.4a shows an instant when E_ℓ and E_r both also lie along the x axis, and Fig. 2.4b shows conditions an instant later. It can be recognized that as the two vectors rotate their projections on the y axis cancel and the sum of their projections on the x axis provide cosinusoidal variation of the amplitude of $\underset{\sim}{E}$, with $\underset{\sim}{E}$ always lying along the x axis. Note that as E varies cosinusoidally, E_ℓ and E_r maintain constant lengths.

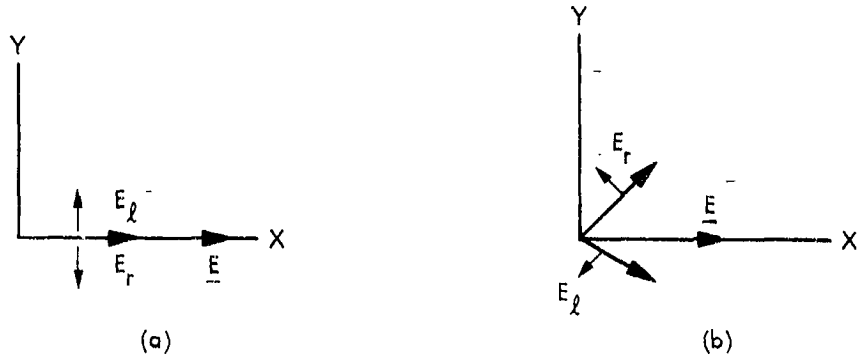

Figure 2.4. Illustration suggesting how circularly polarized waves combine to form a linearly polarized wave.

As the vectors E_ℓ and E_r propagate in the z direction, they continue to rotate with angular velocity ω in their respective directions but the phases of the rotations lag in accordance with the factors $e^{-j\beta_\ell z}$ and $e^{-j\beta_r z}$. The indices n_ℓ and n_r have different values and therefore β_ℓ and β_r have different values, in accordance with Eq. (2.13). Thus after propagating a distance z, the rotations are no longer symmetrical about the x axis, and the direction of the linearly polarized wave no longer lies along the x axis but at an angle ϕ from the original x axis where

$$\phi = \frac{\beta_\ell z - \beta_r z}{2} \tag{2.23}$$

for the case of a uniform ionosphere. The parameter β_ℓ is larger than β_r but its lag in phase of rotation is in the right circular direction. Thus, Fig. 2.5 shows a possible condition after propagation through some distance z, namely rotation of $\underset{\sim}{E}$ through an angle ϕ in the right circular direction.

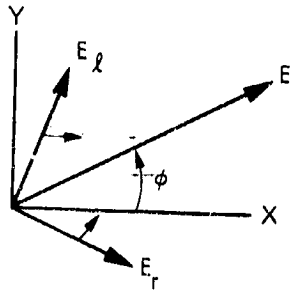

Figure 2.5. Faraday rotation through an angle ϕ from the conditions of Fig. 2.4.

Consider now propagation at an angle Θ_B with respect to the magnetic field when the QL approximation applies. For sufficiently high frequencies, the calculation of rotation can be simplified by noting that

$$\frac{\beta_\ell - \beta_r}{2} = \frac{\beta_o(n_\ell - n_r)}{2} = \frac{\beta_o}{2}\left[\left(1 - \frac{X}{1 + Y_L}\right)^{1/2} - \left(1 - \frac{X}{1 - Y_L}\right)^{1/2}\right]$$

$$\simeq \frac{\beta_o}{2}\left[1 - \frac{X}{2(1 + Y_L)} - 1 + \frac{X}{2(1 - Y_L)}\right] = \frac{\beta_o}{2} XY_L \qquad (2.24)$$

The electron density and magnetic field along the path will in general not be uniform but total rotation can be determined by first defining the differential rotation $d\phi$ in an increment of path length $d\ell$ and then integrating along the length of the path. Thus

$$d\phi = \frac{\beta_o}{2} XY_L \, d\ell \quad \text{rad} \qquad (2.25)$$

and, using the definitions of X and Y_L, the total rotation ϕ in radians along a path is given by

$$\phi = \frac{e^3}{2c\varepsilon_o m^2 \omega^2} \int N B \cos \theta_B \, d\ell \qquad \text{rad} \tag{2.26}$$

where $e = 1.6022 \times 10^{-19}$, $m = 9.1096 \times 10^{-31}$, $c = 3 \times 10^8$, $\varepsilon_o = 8.854 \times 10^{-12}$, and $\omega = 2\pi f$. Also

$$\phi = \frac{2.36 \times 10^4}{f^2} \int N B \cos \theta_B \, d\ell \qquad \text{rad} \tag{2.27}$$

with f in Hz and all quantities in SI units (N/m^3 and B, the earth's field, in Wb/m^2).

The total rotation can be seen to vary inversely with f^2 and to be proportional to the integral of electron density, weighted by the value of B cos θ_B along the path. If it is desired to carry out integration in the vertical direction, letting $d\ell = dh$, but the path is a slant path, a factor sec χ can be introduced inside the integral in Eq. (2.27), where χ is the zenith angle or angle of the path measured from the vertical. B decreases as the cube of radius and has very low values above about 2000 km, and Faraday rotation is insensitive to ionization above that level. Thus, Faraday rotation measurements of signals from geostationary satellites provide a measure of ionospheric total electron content but not of total electron content along the entire path to a satellite. The region above the ionosphere, above about 2000 km, may have an electron content that is about 10 percent of the electron content of the ionosphere in the daytime and 50 percent at night (Davies, Hartmann, and Leitinger, 1977).

For some situations, it is sufficiently accurate to replace B cos θ_B in Eq. (2.27) by an average value, namely $\overline{B_L}$ and take it outside the integral. The expression for the Faraday rotation angle ϕ then becomes

$$\phi = \frac{2.36 \times 10^4}{f^2} \bar{B}_L \overline{\int N \, d\ell} = \frac{2.36 \times 10^6 \bar{B}_L TEC}{f^2} \qquad (2.28)$$

where

$$\bar{B}_L = \frac{\int NB \cos \Theta_B \, d\ell}{\int N \, d\ell}$$

and TEC stands for the total ionospheric electron content along the path. Equation (2.28) can be inverted to find TEC by use of

$$TEC = \frac{\phi f^2}{2.36 \times 10^6 \bar{B}_L} \qquad (2.29)$$

On a fixed path, when the above procedure is applicable, the amount of Faraday rotation depends on the TEC, which exhibits a pronounced diurnal variation as well as a variation with the season, solar flare activity, and period of the solar cycle. When the form of the variation of electron density with altitude changes, however, the value of $\bar{B}_L$ may change also.

A practical consequence of Faraday rotation is that, in the frequency range where Faraday rotation is significant, one cannot transmit using one linear polarization and receive using an antenna with the same linear polarization without a high probability of a polarization loss which may be serious. Among the techniques for avoiding or dealing with the problem are to use a sufficiently high frequency for which Faraday rotation is negligible, to use a receiving antenna that can accept both orthogonal linear polarizations so that no polarization loss occurs, and to use circular rather than linear polarization. As a right or left circularly polarized wave is a characteristic wave, it does not change polarization as it propagates and thus presents no problem, as long as both transmitting and receiving antennas are designed for circular polarization. Another possibility, if Faraday rotation is not too great or highly variable, is to vary the orientation of a linear transmitting or receiving antenna to compensate for the Faraday rotation expected along the path, as a function of time of day, season, and period of the sunspot cycle.

As Faraday rotation and group delay and other topics of the following Sec. 2.3 are all functions of electron content along the path, numerical illustrations of Faraday rotation are deferred until Sec. 2.4 which deals with electron content.

2.3 GROUP DELAY, PHASE ADVANCE, DOPPLER FREQUENCY, AND BANDWIDTH COHERENCE

2.3.1 Group Delay

To consider ionospheric group delay at high frequencies, note that the integral $\int n \, d\ell$, evaluated along a path with n representing index of refraction, gives the true distance along the path if $n = 1$ but gives a value P, sometimes called the phase path length, which is different from the true distance if $n \neq 1$. Thus

$$P = \int n \, d\ell \tag{2.30}$$

and ΔP the difference between P and the true length is given by

$$\Delta P = \int (n - 1) \, d\ell \tag{2.31}$$

Neglecting refraction and considering that $f > 100$ MHz for which $n^2 \cong 1 - X$,

$$n^2 = 1 - \frac{f_p^2}{f^2} = 1 - \frac{80.6 \, N}{f^2} \tag{2.32}$$

where N is electron density (el/m^3) and f is frequency in Hz. Taking X as being small compared to unity as is the case for sufficiently high frequencies, including $f > 100$ MHz.

$$n \cong 1 - \frac{X}{2} = 1 - \frac{40.3 \, N}{f^2} \tag{2.33}$$

For group delay, however, one is concerned with the group velocity rather than phase velocity. As $v_g v_p = c^2$ for ionospheric propagation when $v_p > c$, where v_p is phase velocity and v_g is group velocity, one should use the group refractive index, $n_g = 1 + X/2$. The result is that

$$\Delta R = \int \frac{40.3\ N}{f^2}\, d\ell = \frac{40.3}{f^2} \int N\, d\ell \qquad \text{m} \qquad (2.34)$$

where ΔR is a positive range error and is the difference between the true range and that which would be inferred by assuming a velocity of c. (The true range is less than the inferred range.) Also, if the velocity c is assumed, ΔR corresponds to an error in time or a time delay of

$$\Delta t = \frac{40.3}{cf^2} \int N\, d\ell = \frac{1.34 \times 10^{-7}}{f^2} \int N\, d\ell \qquad \text{s} \qquad (2.35)$$

where $\int N\, d\ell$ is the total electron content (TEC) along the path (el/m^2). If the TEC is known or can be estimated closely, Δt can be determined from Eq. (2.35).

Use of a second lower frequency allows determining Δt and also TEC without any advance information. Let

$$\Delta t_1 = \frac{40.3\ TEC}{cf_1^2}$$

where f_1 is the frequency of primary interest and

$$\Delta t_2 = \frac{40.3\ TEC}{cf_2^2}$$

Then

$$\delta t = \Delta t_2 - \Delta t_1 = \frac{40.3\ TEC}{c} \left(\frac{1}{f_2^2} - \frac{1}{f_1^2} \right) \qquad (2.36)$$

It is now possible to solve for Δt_1 which is given by

$$\Delta t_1 = \frac{f_2^2}{f_1^2 - f_2^2} \delta t \tag{2.37}$$

Note that δt can be readily measured by suitably modulating both carrier frequencies but Δt as used in Eq. (2.35) cannot be readily measured directly for lack of a suitable reference signal.

For determining the TEC, one can use

$$\text{TEC} = \frac{\delta t\, c}{40.3} \frac{f_1^2 f_2^2}{f_1^2 - f_2^2} \tag{2.38}$$

Equation (2.37) allows calculating and correcting for Δt_1, at the expense of utilizing a second frequency. Such a correction is important in the case of satellite navigation systems such as the NAVSTAR Global Positioning System, where it is desired to determine positions precisely. In particular, it is desired to locate positions to an accuracy of a few meters, but if no allowance is made an electron content of 10^{18} electrons/m^2 can cause an error of 134 nanoseconds or 40 m in range at a frequency of 1 GHz (Klobuchar, 1978).

Another case where high accuracy is desired is that of the DSN (Deep Space Network) of the Jet Propulsion Laboratory, where it is desired to determine ranges to satellites with a precision of 3 m. Coded signals are transmitted to satellites at S band and retransmitted back to the station as X band. Also for determining the declination angle of a spacecraft near zero declination a range differencing procedure has been developed. This procedure involves determining the difference in distance to the satellite from Goldstone, California and Canberra, Australia. Correction for time delays is essential to this procedure.

Equation (2.38), when applied to an earth-space path, gives the total electron content along the entire path, in contrast to Faraday rotation measurements which gives the electron content of the ionosphere only. Numerical values of time delay are given in Sec. 2.4.

2.3.2 Phase Advance

The presence of the ionosphere advances the phase of a received signal with respect to the value which would be recorded for propagation through unionized air. Equation (2.34) can be used to determine $\Delta\phi$, the phase advance, by multiplying by the phase constant $\beta = 2\pi/\lambda = 2\pi f/c$. Thus

$$\Delta\phi = \frac{40.3\ (2\pi f)}{f^2 c}\ \text{TEC}$$

$$= \frac{8.44 \times 10^{-7}}{f}\ \text{TEC} \qquad \text{rad} \qquad (2.39)$$

Dividing by 2π gives the value of $\Delta\Theta$ in cycles so that

$$\Delta\phi = \frac{1.34 \times 10^{-7}}{f}\ \text{TEC} \qquad \text{cycles}$$

2.3.3 Doppler Frequency

Frequency and phase are related by

$$f = \frac{1}{2\pi}\frac{d\phi}{dt} \qquad (2.40)$$

with f in Hz and ϕ in radians. The Doppler shift in frequency, f_D, corresponding to the phase change described in Eq. (2.39) is given by

$$f_D = \frac{1}{2\pi}\,\frac{8.44 \times 10^{-7}}{f}\,\frac{d(\text{TEC})}{dt} = \frac{1.34 \times 10^{-7}}{f}\,\frac{d(\text{TEC})}{dt}$$

In terms of finite quantities, it becomes

$$f_D = \frac{1.34 \times 10^{-7}}{f}\,\frac{\Delta(\text{TEC})}{T_c} \qquad (2.41)$$

where the TEC changes by Δ(TEC) in the time interval or count time T_c and f_D is the average value during T_c.

2.3.4 Differenced Range versus Integrated Doppler (DRVID)

A technique known as differenced range versus integrated Doppler (DRVID) has been developed at the Jet Propulsion Laboratory for obtaining information about changes in columnar electron content (TEC) (Callahan, 1975). The basis for the technique is the difference in group and phase velocities, the group velocity being less than c and the phase velocity being greater than c. In terms of index of refraction,

$$n_g = 1 + \frac{40.3\ N}{f^2} \text{ and } n = 1 - \frac{40.3\ N}{f^2}$$

where n_g is the group index and n is the phase index, which is normally what one refers to when they speak of index of refraction. Total columnar electron content, TEC, and electron density, N, are related by $TEC = \int N dl$, where the integral is taken along the path length.

The Deep Space Network of the Jet Propulsion Laboratory has a system for measuring range delay by the use of two-way transmissions of coded pulse trains. For the time interval between t_o and t, this system provides a value ΔR_g which in general is a combination of a true change in range, $R(t) - R(t_o)$ and an apparent change in range represented by $40.3\ \Delta(TEC)/f^2$. Thus

$$\Delta R_g(t,t_o) = R(t) - R(t_o) + \frac{40.3\ \Delta(TEC)}{f^2} \tag{2.42}$$

A similar expression applies for $\Delta R_\phi\ (t, t_o)$, which is determined by a phase or Doppler frequency measurement such that

$$\Delta R_\phi\ (t,t_o) = R(t) - R(t_o) - \frac{40.3\ \Delta(TEC)}{f^2} \tag{2.43}$$

The difference $\Delta R_g - \Delta R_\phi$ is designated as DRVID, which is given by

$$DRVID(t) = \Delta R_g(t) - \Delta R_\phi(t) = \frac{80.6\ \Delta(TEC)}{f^2} \tag{2.44}$$

where DRVID, ΔR_g, and ΔR_ϕ all refer to values applying at a time t after t_o. From Eq. (2.44), the change in total electron content $\Delta(TEC)$ can be determined and if a series of consecutive measurements of this kind are made, a record of the variation of TEC can be constructed. Note that the absolute value of TEC

can not be determined by this method but that the effects of motion of the spacecraft and of the troposphere are cancelled out as n_g and n are the same for the troposphere.

The quantity ΔR_ϕ can be determined from

$$f_D = \frac{1}{\lambda_o} \frac{\Delta R_\phi}{T_c} \tag{2.45}$$

where T_c is the count time and equals $t - t_o$ or alternatively from

$$f_D = \frac{1}{2\pi} \frac{\Delta \phi}{T_c} \tag{2.46}$$

and

$$\Delta \phi = \frac{2\pi}{\lambda_o} \Delta R_\phi \tag{2.47}$$

where $\Delta \phi$ is the change in phase in the time T_c. Equation (2.46) has the form of Eq. (2.40) except that finite quantities $\Delta \phi$ and T_c are used in place of $d\phi$ and dt. The f_D of Eqs. (2.45) and (2.46) is the average Doppler frequency in the interval T_c. A limitation of the DRVID technique is that it tends to be noisy and not readily adaptable to recording rapid scintillation (Sec. 2.6).

2.3.5 Bandwidth Coherence

Time delay and phase advance on ionospheric paths are functions of frequency. The rate of change of time delay with frequency, or the time-delay dispersion, is found by taking the derivative of Eq. (2.35) yielding

$$\frac{dt}{df} = \frac{-80.6}{cf^3} \int N \, d\ell = \frac{-2.68 \times 10^{-7}}{f^3} \text{TEC} \tag{2.48}$$

The rate of change of phase angle with frequency or the phase-advance dispersion, is found by taking the derivative of Eq. (2.39) giving

$$\frac{d\phi}{df} = \frac{-8.44 \times 10^{-7}}{f^2} \text{TEC} \tag{2.49}$$

The effect of dispersion is to tend to introduce distortion into wideband signals. Note that all of the quantities of this Sec. 2.3 are closely related and that the other quantities can all be determined from the group delay.

2.4 ELECTRON CONTENTS OF IONOSPHERE AND PLASMASPHERE AND THEIR EFFECTS

Faraday rotation measurements on satellite to earth paths provide values of the electron content of the ionosphere, and group delay measurements give the total electron content (TEC) along the entire path. By taking the difference of the total and ionospheric values, the electron content of the plasmasphere or protonosphere is obtained. Most electron content data refer to ionospheric values, but data for the plasmasphere as well have been reported by Davies, Hartman, and Leitinger (1977), Klobuchar and Working Group (1978), and Davies (1980).

The ionospheric TEC shows pronounced diurnal variations consistent with the production of ionization by solar radiation in the daytime and the decay of ionization at night. Extreme values of the ionospheric TEC are given by Klobuchar (1978) as 10^{16} el/m^2 (min) and 10^{19} el/m^2 (max); CCIR Report 263-4 (CCIR, 1978) refers to 10^{18} el/m^2 as a maximum zenith value. These values apply to the electron content of a vertical column having a cross section of 1 m^2 and extending to a height of about 2000 km. Representative curves showing the diurnal variation of TEC for an invariant latitude of 54^o are given in Fig. 2.6. Invariant latitude equals $\cos^{-1}(1/L)^{1/2}$ and refers to the magnetic field line that is at a distance L, measured in earth radii; from the center of the earth, at the magnetic equator.

One effect of the TEC is to produce group time delay. Plots showing ionospheric time delay as a function of TEC and frequency are shown in Fig. 2.7.

The results of utilizing a worldwide model of ionospheric TEC to determine time delay at a frequency of 1.6 GHz are shown in Fig. 2.8.

Typical values of Faraday rotation as a function of ionospheric TEC and frequency for a northern mid-latitude station viewing a geostationary satellite near the station meridian are shown in Fig. 2.9.

Figures 2.6 and 2.9 provide information about the diurnal variation of TEC and how TEC affects group time delay and Faraday rotation. The data shown in these figures may be sufficient for some purposes, but solar-cycle variations and ionospheric disturbances and irregularities cause variations in TEC that may be important in certain cases.

Table 2-2, adapted from CCIR Report 263-4 and a draft revision of Report 565-1, gives a summary of ionospheric effects of frequencies from 100 MHz to 10 GHz. Included are effects proportional to TEC (Faraday rotation, propagation delay, and dispersion) and refraction and absorption.

Table 2.2 Estimated maximum ionospheric effects in the United States for elevation angles of about 30 degrees and one-way paths (derived from Table VI, Report 263-4).

Effect	Frequency Dependence	100 MHz	300 MHz	1 GHz	3 GHz	10 GHz
Faraday Rotation	$1/f^2$	30 rot.	3.3 rot.	108^0	12^0	1.1^0
Propagation delay	$1/f^2$	25 μs	2.8μs	0.25 μs	0.028 μs	0.0025 μs
Refraction	$1/f^2$	$\leq 1^0$	<7'	$\leq$0.6'	<4.2"	$\leq$0.36"
Variation in the direction of arrival	$1/f^2$	20 min of arc	2.2 min of arc	12 sec of arc	1.32 sec of arc	0.12 sec of arc
Absorption (auroral and polar cap)	$1/f^x$ $1<x\leq 2$	5 dB	1.1 dB	0.2 dB	0.04 dB	0.008 dB
Absorption (mid latitude)	$1/f^2$	<1 dB	0.1 dB	<0.01 dB	0.001 dB	$<10^{-4}$ dB
Dispersion	$1/f^3$	0.4 ps/Hz	0.015 ps/Hz	0.0004 ps/Hz	1.5×10^{-5} ps/Hz	4×10^{-7} ps/Hz

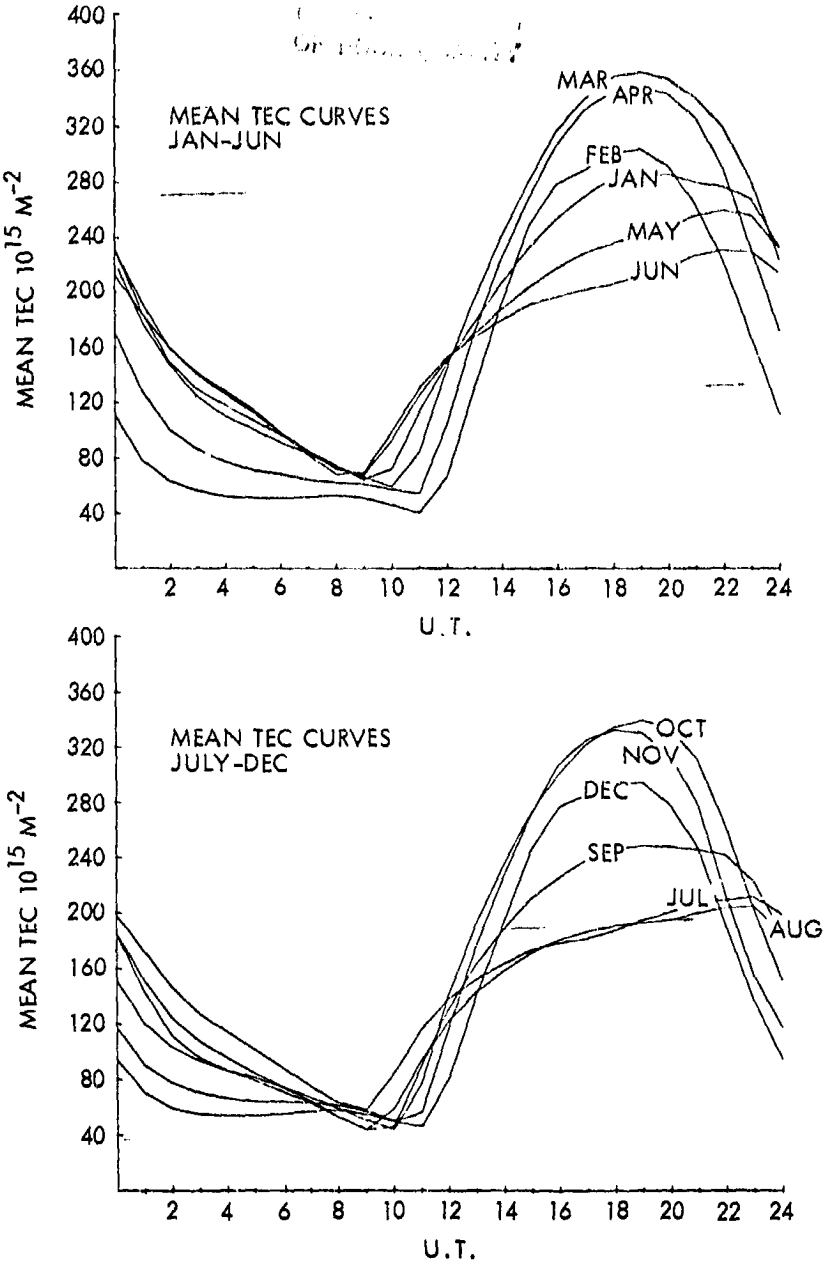

Figure 2.6. Diurnal variations in TEC, mean monthly curves for 1967 to 1973 as obtained at Sagamore Hill, MA using 136 MHz signals from ATS-3 (after Hawkins and Klobuchar, 1974).

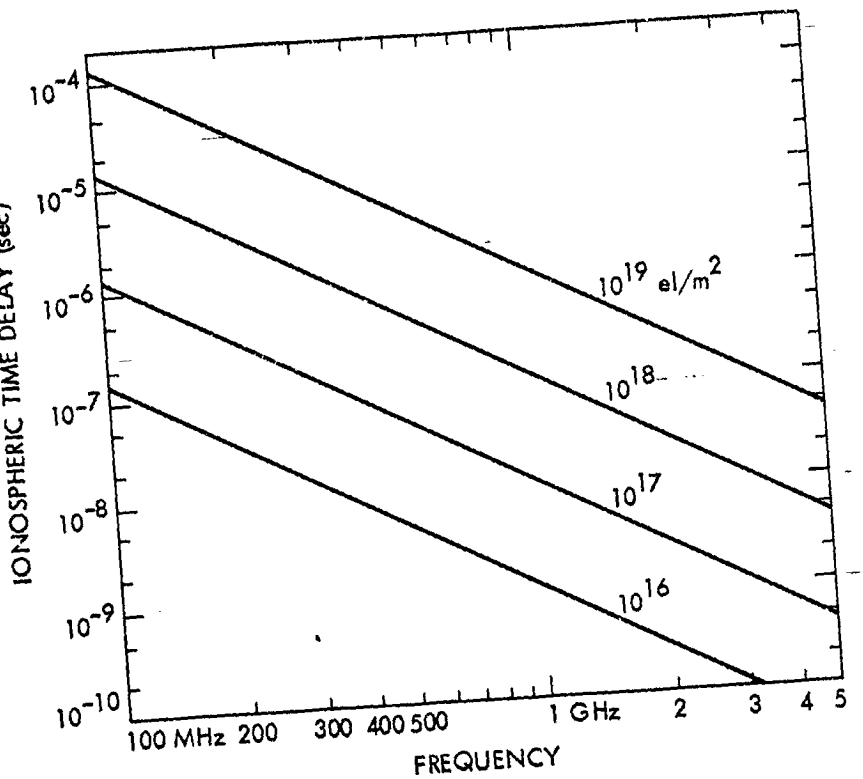

Figure 2.7. Ionospheric time delay as a function of ionospheric TEC and frequency (after Klobuchar, 1978).

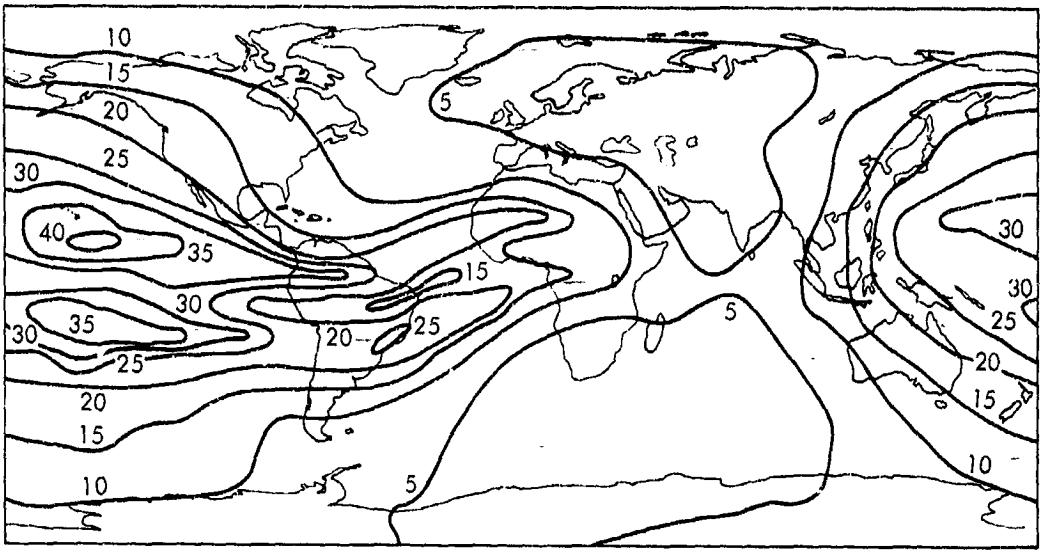

Figure 2.8. Ionospheric time delay in nanoseconds at a frequency of 1.6 GHz, based on the Bent model of ionospheric TEC (after Klobuchar, 1978).

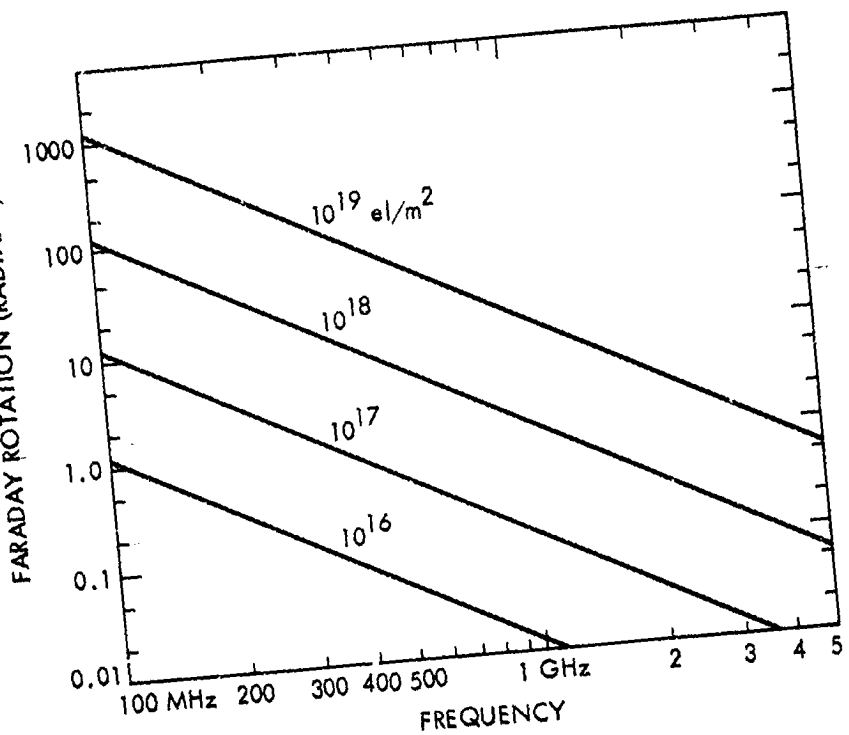

Figure 2.9. Faraday rotation as a function of ionospheric TEC and frequency (after Klobuchar, 1978).

2.5 IONOSPHERIC DISTURBANCES AND IRREGULARITIES

2.5.1 Equatorial Ionosphere

Because of atmospheric solar and lunar tidal forces and heating by the Sun, horizontal movements or winds occur in the ionosphere. As a result, electric fields are developed by the dynamo affect, described by $\underset{\sim}{E} = \underset{\sim}{v} \times \underset{\sim}{B}$, where $\underset{\sim}{E}$ is electric field intensity, $\underset{\sim}{v}$ is the velocity of the charged particles of the ionosphere, and $\underset{\sim}{B}$ is the Earth's magnetic field. (This is a vector equation and $\underset{\sim}{E}$ is perpendicular to both $\underset{\sim}{v}$ and $\underset{\sim}{B}$.) The electric fields in turn drive a current system in the ionosphere which involves two systems of current loops in the daytime hemisphere, one in the northern hemisphere and one in the southern hemisphere. The currents flow counterclockwise in the northern hemisphere and clockwise in the southern hemisphere so that the currents of both systems flow from west to east near the geomagnetic equator. Furthermore, the conductivity of the ionosphere becomes high over a restricted range of altitude in the E region. Also, the equatorial ionosphere is situated favorably to intercept solar radiation, which is the main agent causing ionization in the ionosphere. As a result of the factors mentioned, a strong, concentrated current, known as the equatorial electrojet, flows at heights near 110 km in the E region of the equatorial ionosphere. Electron density irregularities and variations associated with the electrojet cause scattering of electromagnetic waves which are incident upon and propagate through this region. Strong radar backscatter echoes are received from the equatorial electrojet. The Jicamarca Radar Observatory near Lima, Peru, operating at a frequency near 50 MHz, has provided a large amount of information concerning the equatorial ionosphere. It can record both discrete echoes from E and D region irregularities and weak incoherent-scatter echoes from the entire ionosphere (Evans, 1969; Farley, 1963; Balsley, 1969).

The occurrence of plasma bubbles (McClure et al., 1977) has been an object of investigation since Woodman and La Hoz (1976) reported the appearance of rising plume-like structures, using the Jicamarca radar. The bubbles typically have a width of 100 km and electron densities 1 to 2 orders of magnitude less than the surrounding (Heron, 1980). Such bubbles are considered further in Sec. 2.6.

2.5.2 Auroral Ionosphere

Energetic-particle precipitation into the auroral ionosphere causes the visible aurora, excess ionization which attenuates and scatters radio waves, and concentrated electrical currents known as auroral electrojets. The currents in turn cause characteristic variations in the geomagnetic field. These phenomena occur in the form of an oval (Fig. 2.10) which surrounds but is eccentric with respect to the Earth's magnetic dip pole, with the oval center displaced by about 3^0 toward the dark hemisphere (Akasofu, 1968). The oval is fixed approximately with respect to the Sun, and the Earth rotates beneath the oval. The term auroral zone is applied to the area that falls beneath the midnight portion of the auroral oval, where auroral activity occurs essentially every night to some degree.

The excess ionization occurs prominently in the E region and can be regarded as a variety of sporadic E. Intense radar backscatter or radar auroral echoes can be received at HF, VHF, and UHF frequencies. The irregularities in ionization are field aligned, having a considerable extent along the Earth's magnetic field lines and a small extent perpendicular to the lines. The line of sight to the echoing region must be close to perpendicular to the magnetic field to receive VHF-UHF echoes, which must therefore occur at ranges of 500-900 km in Alaska. An auroral radar facility at Anchorage, Alaska transmits data to the NOAA-USAF Space Environment Services Center in Boulder, Colorado. HF waves experience sufficient refraction in the auroral ionosphere to achieve near-perpendicularity without being launched originally in the perpendicular direction.

An ionospheric trough, namely a region of reduced ionization, separates the auroral and mid-latitude ionospheres. This trough appears to be linked by magnetic field lines to the plasmapause of the magnetosphere (Sec. 1.3).

The riometer (relative ionospheric opacity meter) has been a valuable tool for studying the auroral and polar ionospheres. It operates typically at a frequency of 30 MHz and, by recording the amplitude of cosmic noise, monitors auroral and polar-cap activity and the associated attenuation experienced by radio waves propagating through the auroral ionosphere. An incoherent scatter radar facility at Chatanika, Alaska, near Fairbanks, has been

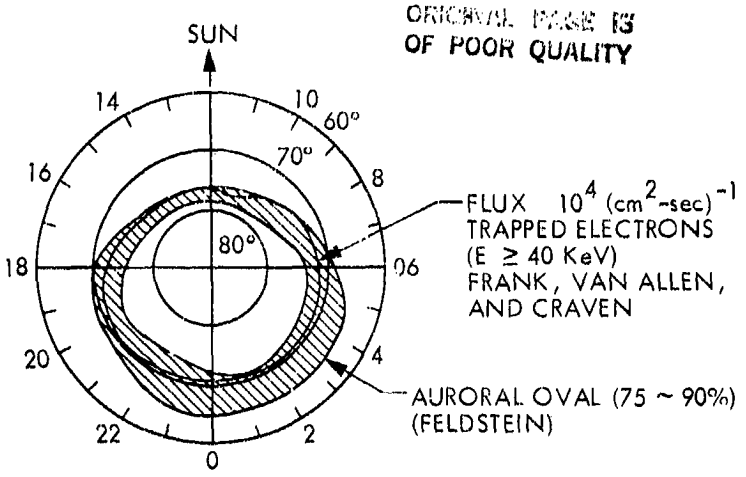

Figure 2.10. The auroral oval (Akasofu, 1968).

in operation since about 1972 and has provided extremely valuable information about the auroral ionosphere (Leadabrand et al., 1972; Baron, 1974; Hunsucker, 1974). Auroral absorption is considered further in Sec. 2.7.

2.5.3 SID's and Ionospheric Storms

The equatorial and auroral ionosphere are characterized by irregularities and disturbed conditions, to some degree and subject to diurnal variations, on a more or less continuous basis. The mid-latitude ionosphere exhibits less activity and disturbance generally but is subject to the effects of solar flares and sporadic E. Auroral activity is also enhanced by flare activity.

The effects of solar flares can be divided into the categories of simultaneous and delayed. The simultaneous effects result from the radiation of X-rays from the flares. X-rays propagate with the velocity c, the velocity of light. The simultaneous effects are known as sudden ionospheric disturbances (SID's), a term which covers a variety of phenomena including SWF (shortwave fadeout), SCNA (sudden cosmic noise absorption), SPA (sudden phase anomaly) and SFD (sudden frequency deviation). These effects tend to be important at HF frequencies. SWF refers to a decrease in amplitude of radio-wave transmissions, whereas SPA and SFD refer to variations in phase and frequency of radio-wave transmissions. Phase ϕ and frequency f are related by

$$f = \frac{1}{2\pi}\frac{d\phi}{dt} \qquad (2.50)$$

and if a change in phase occurs, a corresponding change in the frequency of the recorded signal also occurs. The change in frequency is similar to that encountered in reflection from a moving object and the term Doppler frequency is applied in both cases. Solar X-rays affect primarily the D region of the ionosphere.

Delayed effects from solar flares are caused by particles which are emitted from the Sun and may take 20 to 40 or more hours to reach the Earth. The particles cause magnetic and ionospheric storms (Rishbeth and Garriott, 1969), which can result in blackout of HF frequencies and also cause large variations in phase and Doppler frequency. Ionospheric storms strongly affect the F region of the ionosphere.

Magnetic storms are manifested by large irregular variations in the magnitude and direction of the Earth's magnetic field, as recorded by magnetometers, and are accompanied by ionospheric storms that strongly affect the F region of the ionosphere.

If it is not always possible to make a clear distinction between quiet ionospheric conditions and the disturbed conditions of magnetic storms. Some magnetic activity and associated ionospheric effects, especially the TID's and spread F discussed in the following subsection, tend to occur to some degree nearly every night even in temperate latitudes.

2.5.4 Traveling Ionospheric Disturbances and Spread F

Traveling ionospheric disturbances (TID's) propagate as acoustic-gravity waves in the Earth's ionosphere (Hines, 1974). These waves involve variations in pressure and corresponding variations in electron density. Measurements of the Faraday rotation of signals from satellites indicate a cyclical variation in total electron content as TID's propagate through an earth-space path. TID's frequently appear to originate in the auroral zone and to propagate toward the equator. The condition of spread F is commonly associated with TID's (Booker, 1979). Spread F manifests itself and was originally identified

on ionosonde records, which are made by vertically pointing radar systems whose frequency is varied periodically from about 0.5 to 25 MHz. Under quiet ionospheric conditions, the traces on an ionosonde record have the form shown in Fig. 2.11. In the ionogram, the virtual height of reflection is plotted as a function of frequency. The symbols f_0 and f_x in Fig. 2.11 stand for penetration frequencies of the ionospheric layers (E, F_1, and F_2) for the "ordinary" (unaffected by magnetic field) and "extraordinary" waves. The highest penetration frequency shown, f_xF_2 is about 7 MHz. Waves at higher frequencies pass through the ionosphere without reflection. A main point for present purposes is that the traces are relatively clean and distinct, although those of Fig. 2.11 have been redrawn to provide additional clarity.

When spread F occurs, the trace for the F region is broken up into a multiplicity of separate traces. Spread F has been divided into two main types, which are range spreading and frequency spreading. Range spreading involves two or more traces (often a multiplicity) having different virtual heights well below the penetration frequency as in Fig. 2.12a. The high-frequency portions of the traces are branched or blurred in frequency spreading as in Fig. 2.12b.

Spread F occurs for the largest percentage of the time in equatorial and auroral latitudes, but as mentioned previously tends to occur nearly every night in temperature latitudes to some degree as well. It is positively correlated with magnetic activity at high latitudes and negatively correlated at low latitudes (Rishbeth and Garriott, 1969).

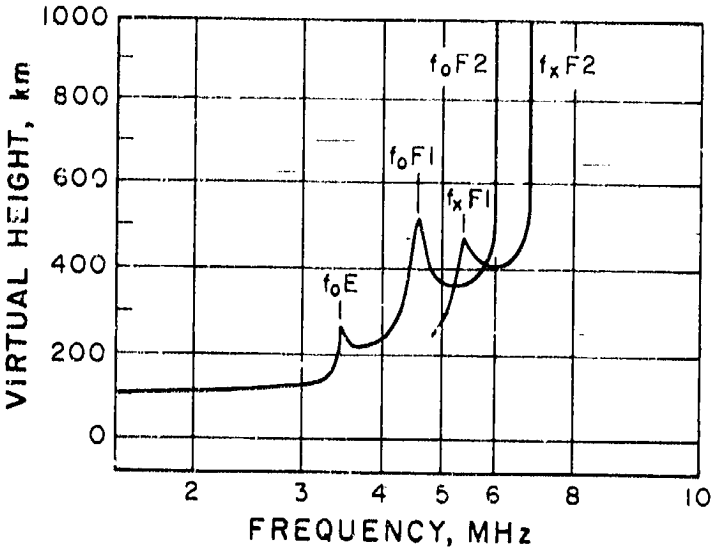

Figure 2.11. Ionospheric traces under quiet ionospheric conditions, Washington, D.C., June 3, 1962 (after Davies, 1969).

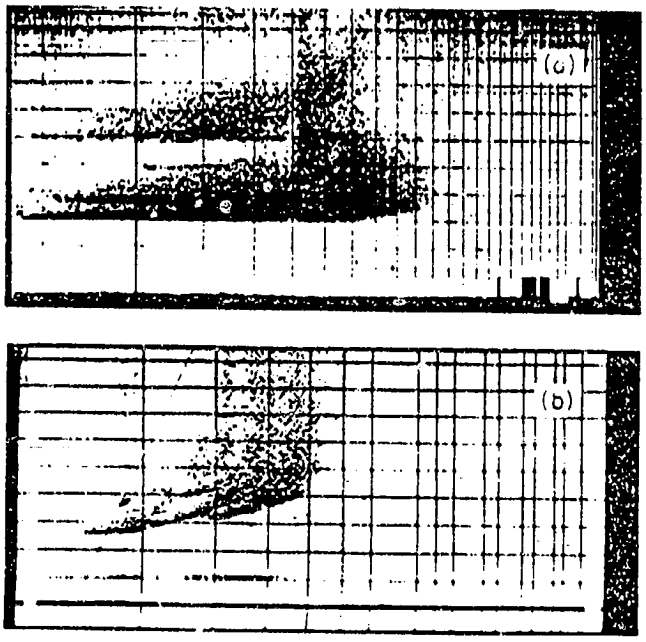

Figure 2.12. Ionograms showing spread-F. a) Range spreading, Huancayo, Peru, May 20, 1960. b) Frequency spreading, South Pole, August 1, 1960 (Davies, 1965). The vertical axis represents virtual height and the horizontal axis represents frequency.

2.5.5 Polar-cap Absorption

Very energetic protons or solar cosmic rays which may reach the Earth in only 15 minutes to several hours after a flare are associated with some intense solar flares. These particles are guided by the Earth's magnetic field to the polar regions, above about 64° in geomagnetic latitude, where they cause polar-cap absorption. Such polar-cap absorption events occur most frequently near the peak of the sunspot cycle and tend to last for several days. When the polar regions have periods of both daylight and darkness, the absorption decreases significantly at night with respect to daytime values. The auroral oval partially overlaps the equatorward edge of the region where polar-cap absorption occurs, and both polarcap and auroral absorption can occur in the auroral zone. A hypothetical illustration of polar-cap absorption is given in Sec. 2.7.

2.6 IONOSPHERIC SCINTILLATION

2.6.1 Introduction

Irregular variations or scintillations of the amplitude of radiowaves received from radio stars were first recorded by Hay, Parsons, and Phillips (1946) who reported variations in the amplitude of signals from Cygnus and Cassiopeia at 36 MHz. At first, it was thought that the emissions from the stars might be varying with time, but records obtained simultaneously from stations separated by 200 km showed no similarity whereas when the receiver separation was only about 1 km the records were closely similar (Smith, 1950; Little and Lovell, 1950). These results showed that the scintillations were not caused by the stars but were of localized origin, and it was concluded that their source was in the ionosphere. The scintillations were attributed by Hewish (1952) to a diffraction pattern formed at the ground by a steadily drifting pattern of irregularities in the ionosphere at a height of about 400 km. According to Aarons, Whitney, and Allen (1971), the irregularities are mostly in the F layer at heights predominantly from 225 to 400 km.

With the advent of satellites, scintillations of signals from such spacecraft were also observed (Yeh and Swenson, 1964). The signals from radio stars are incoherent and broadband and allow the recording of amplitude and angle-of-arrival scintillations but not phase scintillations. Coherent, mono-

chromatic signals from spacecraft have the advantage of allowing the recording of phase scintillations and spectral broadening as well as amplitude scintillations (Crane, 1977; Woo, 1977; Smith and Edelson, 1980). The early observations of scintillations were at comparatively low frequencies and, on the basis of the assumed form of decrease of scintillation intensity with frequency, it was expected that frequencies as high as those of the 4 and 6 GHz bands planned for the INTELSAT system would be free from scintillation effects. It developed, however, that scintillation occurs at frequencies at least as high as 6 GHz, with significant scintillation at 4 and 6 GHz in equatorial latitudes (Craft and Westerlund, 1972; Taur, 1973).

Scintillation may involve weak scattering or strong scattering. The strongest scattering is observed in the equatorial and auroral regions, especially the equatorial areas. The resulting scintillation is correspondingly intense and extends to higher frequencies than elsewhere. Scintillation tends to be weak at temperate latitudes. Maximum scintillation occurs at night in all three regions (before midnight in equatorial regions). The nighttime pattern of occurrence is shown in Fig. 2.13. It is generally agreed that the weak mid-latitude scintillation is due to diffractive scattering, and it has sometimes been assumed that such is the case for all scintillation. Certain analyses of strong scattering, including that responsible for scintillation at microwave (SHF) frequencies, however, have led to conclusions that such scintillation must be caused by a higher portion of the atmosphere, in particular the plasmasphere (Booker, 1975) or by a different mechanism, namely refractive scattering rather than diffractive scattering (Crain, Booker, and Ferguson, 1979). The refractive scattering is said to be caused by ionization structure in the form of "holes" of "bubbles" that is perpendicular to the line of sight. Refractive scattering is considered to involve irregularities of scale larger than the Fresnel scale, and diffractive scattering is assumed to involve irregularities having sizes near the Fresnel scale.

Several measures or indices of scintillation have been used. Attention was given to the subject of indices by Briggs and Parkin (1963) who introduced indices designated by S, S_1, S_2, S_3, and S_4. The index S_4, representing the standard deviation of received power divided by the mean value is said to be

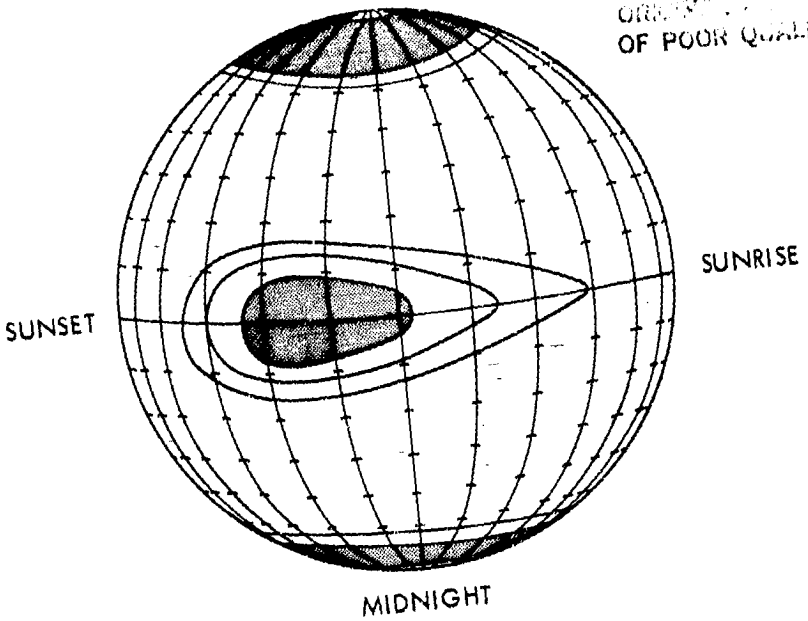

Figure 2.13. Pattern of occurrence of ionospheric scintillation (CCIR, 1978).

the most useful of the several indices (Klobuchar and Working Group, 1978). It is given by

$$S_4 = \frac{1}{\overline{E^2}} \left[\overline{(E^2 - \overline{E^2})^2} \right]^{1/2} \tag{2.51}$$

where E is field intensity. A similar index, m, has been defined as the ratio of rms fluctuation to mean value of power.

The index SI has been proposed as a convenient approximate measure of scintillation (Whitney, Aarons, and Malik, 1969). It is defined by

$$SI = \frac{P_{max} - P_{min}}{P_{max} + P_{min}}$$

where the P's represent power. In order to avoid overemphasizing extreme conditions, it was recommended that the third peak down from the maximum peak in an interval and the third minimum up from the absolute minimum be used to define P_{max} and P_{min}.

The parameters τ_c, the fade coherence time, is pertinent to digital communications. If τ_c is long compared to the time interval corresponding to one bit, the average bit error can be computed in terms of S_4. It has been asserted that knowledge of S_4, τ_c, and a rough measure of coherence bandwidth are what is needed for considering the effect of scintillation on transionospheric communication systems (Klobuchar and Working Group, 1978).

2.6.2 Theory

Discussions of ionospheric scintillation may refer to Fresnel scale sizes and distances. To introduce these concepts, consider a path of length d between transmitting and receiving locations. At distances d_T from the transmitter and d_R from the receiver, the first Fresnel zone radius F_1 is given by (Appendix 2.1)

$$F_1 = \sqrt{\frac{\lambda d_T d_R}{d}} \tag{2.52}$$

All the elements of radiation passing through the first Fresnel zone have components of electric field intensity that add constructively. If the distance to the transmitter d_T becomes very large compared to d_R, d_T approaches d and the first Fresnel zone radius is given by

$$F_1 = \sqrt{\lambda d_R} \tag{2.52a}$$

The first Fresnel zone is circular in cross section and has an area of πF_1^2. Converting to different symbols, corresponding to irregularities that occur with a radius or scale size L about equal to F_1 at a height h = z above a point of observation Eq. (2.52a) becomes

$$L = \sqrt{\lambda z} \tag{2.52b}$$

Upon rearrangement, one obtains

$$z = L^2/\lambda \tag{2.53}$$

In Eqs. (2.52b) and (2.53), L takes the place of F_1 and z takes the place of d_R. In some cases, one may wish to know the Fresnel distance z corresponding to a certain value of L. In other applications, one may wish to know the Fresnel scale size L corresponding to a certain distance z. If d_T is not sufficiently large to justify using Eq. (2.52a), one can revert to Eq. (2.52) which is sometimes written with $d_T d_R/d$ replaced by a single symbol which is referred to as reduced distance.

Some analyses of ionospheric scintillation are based on consideration of scattering in an ionospheric layer or screen containing identical roughly isotropic or ellipsoidal irregularities of scale size L, as Fig. 2.14. Let the irregularities of the layer be characterized by ΔN, the deviation in electron density from that of surroundings. The corresponding deviation Δn in index of refraction can be determined by use of Eq. (2.33) to be given by

$$\Delta n = -40.3\ \Delta N/f^2 \tag{2.54}$$

thus

$$\overline{(\Delta n)^2} = \frac{1.624 \times 10^3 \overline{(\Delta N)^2}}{f^4} \tag{2.55}$$

where the overbars indicate mean values. The phase change $\Delta\phi$ in traversing a single irregularity of size L is

$$\Delta\phi = (2\pi/\lambda)\ (L\Delta n) \tag{2.56}$$

where $2\pi/\lambda$ is the phase constant. Equation (2.55) can be written in an alternative form as

$$\frac{\overline{(\Delta n)^2}}{n} = \frac{1}{4\pi^2} r_e^2\ \lambda^4\ \overline{(\Delta N)^2} \tag{2.57}$$

Figure 2.14. Layer of irregularities of scale size L.

where r_e is the classical electron radius (2.82×10^{-15} m). Using this form and considering a layer of thickness D rather than a layer of negligible thickness, the total mean square phase fluctuation $\overline{(\Delta\phi)^2}$ in a layer of thickness D at a zenith angle χ is given by Booker (1975) as

$$\overline{(\Delta\phi)^2} = 4 r_e^2 \lambda^2 \overline{(\Delta N)^2} \, LD \sec \chi \tag{2.58}$$

Note that n of Eq. (2.57) is essentially unity and that Δn can be either a positive or negative quantity.

Only phase variations occur immediately below the layer of Fig. 2.14, but amplitude variations develop farther below the layer. The distance h that is required for amplitude fluctuations to develop is in the order of the Fresnel distance $z = L^2/\lambda$ of Eq. (2.53). In particular, if $h > \pi L^2/\lambda$ amplitude fluctuations are said to develop (Booker, 1975). The phasor diagram of Fig. 2.15 can help to visualize the association of phase fluctuations and amplitude fluctuations. A represents

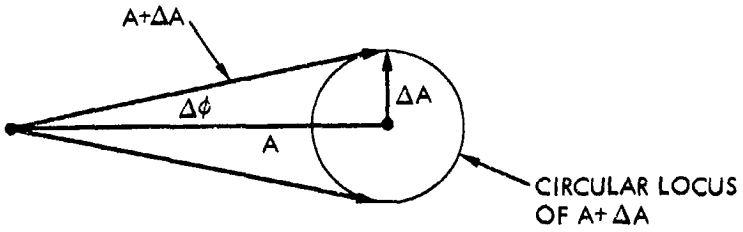

Figure 2.15. Phasor representation of amplitude and phase scintillation.

the undisturbed component of field intensity and $(\Delta A)^2 = (\Delta\Phi)^2 A^2$ so that

$$\left(\frac{\overline{\Delta A}}{A}\right)^2 = \overline{(\Delta\phi)^2} \tag{2.59}$$

in the fully developed case [see Eq. (2.62)]. In the diagram ΔA represents a quantity that adds with random phase to A to produce amplitude variations.

Using results obtained by Bowhill (1961) but expressing relations in his own notation, Booker (1975) obtained the following expressions for $(\overline{\Delta\phi})^2$ and $(\overline{\Delta A}/A)^2$ for weak scattering. The relations are in terms of $Z = \pi L^2/\lambda$, which is referred to as the Fresnel distance. [Following Eq. (2.53), we designated $z = L^2/\lambda$ as the Fresnel distance.]

$$\overline{(\Delta\phi)^2} = 4\, r_e^2 \lambda^2\, \overline{(\Delta N)^2}\, LD\, \sec\chi\, \frac{1 + 1/2\,(\frac{h\sec\chi}{Z})^2}{1 + (\frac{h\sec\chi}{Z})^2} \tag{2.60}$$

$$\overline{(\frac{\Delta A}{A})^2} = 4\, r_e^2 \lambda^2 \overline{(\Delta N)^2}\, LD\, \sec\chi\, \frac{1/2\,(\frac{h\sec\chi}{Z})^2}{1 + (\frac{h\sec\chi}{Z})^2} \tag{2.61}$$

when $h\sec\chi >> Z$

$$\overline{(\Delta\phi)^2} = (\frac{\overline{\Delta A}}{A})^2 = 2 r_e^2 \lambda^2\, \overline{(\Delta N)^2}\, LD\, \sec\chi \tag{2.62}$$

when $h\sec\chi << Z$

$$\overline{(\Delta\phi)^2} = 4\, r_e^2\, \lambda^2\, \overline{(\Delta N)^2}\, LD\, \sec\chi \tag{2.63}$$

$$\overline{(\frac{\Delta A}{A})^2} = \frac{2}{\pi^2}\, r_e^2\, \lambda^4\, \overline{(\Delta N)^2}\, \frac{h^2}{L^3}\, D\sec^3\chi \tag{2.64}$$

These relations are said to explain weak mid-latitude scintillation for parameters in the order of $L = 800$ m, $D = 200$ km, and $h = 300$ km.

In the analysis outlined above, a layer of finite thickness is considered, but in other treatments the layer is replaced by an equivalent two-dimensional screen. Thus scintillation may be discussed in terms of a dif-

fracting screen model (Cronyn, 1970). For present purposes, we will not distinguish between scattering by a layer or a screen.

For the theory of weak scattering to apply, it has been assumed that the phase variation introduced by the ionosphere is restricted to about 1 radian. For this condition, the amplitude variations observed at the ground are considered to correspond to the pattern of irregularities in the ionosphere, for irregularities below a certain size. If the phase variation is greater than 1 radian, the correspondence breaks down (Lawrence, Little, and Chivers, 1974). The amplitude scintillation index tends to increase with distance below the ionospheric layer but remain less than unity for weak scattering. The amplitude scintillation index for strong scattering can reach a value of unity and saturates or limits at that value, whereas phase scintillation does not reach a saturation point but continues to increase if the intensity of scattering continues to increase. It has developed in more recent analyses that phase variations are commonly in excess of 1 radian even when amplitude scintillation is weak (Rino and Fremouw, 1977).

The total field intensity at the ground is the sum of an unperturbed component and the perturbations in field intensity due to the irregularities as in Fig. 2.15. The mechanisms by which the perturbations in field intensity are generated involves electrical currents that flow in the irregularities due to the incident field intensity. Because of these currents, having a density different than that of the surrounding ionosphere, the irregularities act as antennas having roughly conical radiation patterns as suggested in Fig. 2.14. The beamwidth of the conical beams is about λ/L, the larger the irregularity the narrower the beamwidth and vice versa. At an observing point at a distance d below the layer where $d \ll z = L^2/\lambda$, with z the Fresnel distance corresponding to the scale length L, only one beam is intercepted and only phase variations are recorded. For larger distances, the cones of radiation overlap and conditions for interference and consequent amplitude scintillation occur. A slight variation of this description is to say that the diffracting screen or layer produces an angular spectrum of plane waves and that interference between the plane waves produces amplitude scintillation (Coles, 1978).

Assuming weak scattering and a pattern of ionospheric irregularities drifting horizontally, the above discussion indicates qualitatively how amplitude scintillations develop. A further question, however, is under what conditions will the amplitude scintillations correspond to and allow determination of the sizes of the irregularities that are causing the scintillation. An additional requirement, beyond the conditions stated above, is that the irregularities must not be too large. In particular, the irregularities must not fill more than the first Fresnel zone. Radiation from the even Fresnel zones interferes with that from the odd zones (Appendix 2.1) and this condition introduces effects on the received signal amplitude that preclude the identification of irregularities having scale sizes larger than $\sqrt{\lambda z}$ [Eq. (2.52b)]. Phase scintillations, however, are not so limited and can detect irregularities over a large range of scale sizes. Also phase scintillations do not saturate as do amplitude scintillations but can cover a wide dynamic range. The process by which amplitude scintillations are rendered unresponsive to large scale sizes has been referred to as Fresnel filtering. (Rufenach, 1971).

The temporal and spatial fluctuations of phase and amplitude are related to the power spectrum and autocorrelation function of electron density variations, the power spectrum and autocorrelation function being Fourier transforms of each other (Beckmann, 1967). Early analyses assumed a Gaussian form for the power spectrum (Briggs and Parkin, 1963), but later treatments have assumed a power-law form (Rufenach, 1972). Illustrations of these forms for the one-dimensional case by Rufenach are reproduced below, Eq. (2.65) representing the Gaussian form and Eq. (2.66) illustrating the power-law form.

$$P_N(\kappa_x) = 3 \times 10^{16}\, e^{-\kappa_x^2/2\kappa_{2N}^2} \quad (\mathrm{el/m^3})^2/(\mathrm{wavenumber})_{\mathrm{km}^{-1}} \qquad (2.65)$$

with $\kappa_{2N} = 1.16\ \mathrm{km}^{-1}$

$$P_N(\kappa_x) = 1 \times 10^{16}\, \kappa_x^{-2.5} \quad (\mathrm{el/m^3})^2/(\mathrm{wavenumber})_{\mathrm{km}^{-1}} \qquad (2.66)$$

The $P_N(\kappa_x)$ are power spectra of electron density variations expressed in terms of wavenumber κ_x, which is related to irregularity size ℓ_x by $\kappa_x = 2\pi/\ell_x$. In the above expressions ℓ_x is expressed in units of km, and the units of the spectra are $[(el/m^3)^2 km]$. Rufenach determined that $P_N(\kappa_x)$ is proportional to $\kappa_x^{-\beta_H+1}$ where β_H varies from 3 to 4. It was by comparing expressions such as those shown with experimental data that it was concluded that the power-law form is applicable.

The relation between irregularity size ℓ_x and the corresponding frequency of temporal phase variation depends on the velocity of the moving pattern of irregularities. Assuming the pattern to be moving in the x direction with velocity v_x, $\ell_x = v_x T = v_x/f$ and $f = v_x/\ell_x$. The frequency f is that of the temporal variation in signal phase corresponding to a periodicity in electron density of ℓ_x, and T is the period of the temporal variation. The velocity of the moving pattern of irregularities can be determined by the use of three spaced receiving antennas when the direction of the velocity is originally unknown (Coles, 1978).

The model involving diffraction in an ionospheric screen or layer has been widely employed to analyze scintillation, but it has been asserted that it may not be suitable if the irregularities are not confined to a sufficiently thin layer and if amplitude variations already occur at the lower boundary of the layer. First-order perturbation solutions of the scalar wave equation, based on the Rytov approximation or the method of smooth perturbations presented by Tatarski, are said to provide a means of treating the general case (Jokipii, 1973; Woo and Ishimaru, 1973, 1974; Crane, 1977; Ishimaru, 1978). The Rytov approximation is based upon a solution of the scalar wave equation in the form

$$(\nabla^2 + k_o^2 n^2)\ U(\underset{\sim}{r}) = 0 \tag{2.67}$$

where U represents a component of electric field intensity, $k_o = 2\pi/\lambda_o$, and n is index of refraction. The scalar quantity U is shown as a function of the position vector r. A solution of the equation can be obtained by setting

$$U(\underset{\sim}{r}) = U_o(\underset{\sim}{r})\ e^{\Psi_1(\underset{\sim}{r})} \tag{2.68}$$

where

$$\psi_1(\underset{\sim}{r}) = \chi + jS_1 = \ln \frac{A}{A_0} + j\,(S-S_0) \qquad (2.69)$$

with χ corresponding the fluctuation of the logarithm of the amplitude and S_1 the phase fluctuation. As the solution is expressed in logarithmic functions, it is convenient to express amplitudes this way when analyzing scintillation data and using the Rytov-approximation approach. For treatments of the method of smooth perturbations or the Rytov approximation, the reader is referred to Tatarski (1961, 1971) and Ishimaru (1978). Woo and Ishimaru (1973, 1974) and Woo (1975) have applied the Rytov approximation to the study of the solar wind and planetary atmospheres.

The diffracting screen or layer model has been defended as being convenient and accurate for treating ionospheric scintillation (Bramley, 1977) and has been used by Rino (1979 a,b) in his recent analysis of scintillation. Some proponents of the Rytov approximation say that the diffracting screen or layer model is an approximate method that gives good results in some cases and not in others, whereas the Rytov approximation is applicable generally. Some proponents of the diffracting screen or layer model say that it gives good results, that it involves concepts equivalent to the use of a lumped-constant equivalent circuit for treating transmission problems, and that the Rytov approximation does not always correctly predict observed scintillation characteristics.

2.6.2 Effect of Source Size, Interplanetary Scintillations

Stars twinkle in visible light but, because of their larger angular size, planets do not. The same effect of size occurs for radio waves. The reduction in scintillation when the source has an angular width greater than a certain value is due to the fact that the diffraction pattern on the ground is the convolution of the point-source pattern and the brightness distribution of the source. For weak scattering, the angular width of the source, $\Delta\theta$, must be less than the angular width of the irregularities as seen from the ground if scintillation is to develop. The relation used by Lawrence, Little, and Chivers (1964) is that

$$\Delta\theta < \frac{L}{2\pi d} \qquad (2.70)$$

for scintillation to occur, where L is the scale size of the irregularities and d is the distance to the irregularities. For strong scattering, they take

$$\Delta\theta < \frac{L}{2\pi d\phi} \qquad (2.71)$$

for scintillation to be evident, where ϕ is the magnitude or the average phase change in radians and is greater than 1 radian. The effect of source size was recognized by Briggs (1961). Typically, radio sources must be smaller than about 6 to 10 minutes of arc if ionospheric scintillation is to develop.

In recording signals from radio sources of very small size along paths passing close by the Sun, Hewish, Scott, and Wills (1964) observed scintillations having short periods, typically around 1 s, which is small compared with the periods, typically around 30 s, that had been associated with ionospheric scintillations up to that time. For such short-period scintillations to be recorded, the sources must have angular widths of about 0.5 second of arc or less. (The angular extent of sources can be determined by interferometry techniques.) On the basis of the relations embodied in Eqs. (2.70) and (2.71) and taking into account that the signal paths passed through the solar wind close to the Sun, it was concluded that the scintillations were of interplanetary origin. An account of the early observations of interplanetary scintillations (IPS) has been provided by Cohen (1969). The use of IPS has become an important means for obtaining information about the solar wind (Woo, 1977).

Before IPS were recognized, it was noted that radio-star signals that passed near the sun experienced angular broadening (Hewish, 1955). What was actually observed was a decrease in signal amplitude. This decrease could not be explained on the basis of absorption or refraction but only on the basis of angular broadening due to scattering by electron density irregularities. Angular broadening has been vividly illustrated as such by two-dimensional displays produced by a radio heliograph operating at 80 MHz (Blesing and Dennison, 1972). The radioheliograph, having a beamwidth at the zenith of 3.9', produces a 2° square-area picture of the sky every second.

When Pioneer 6 having a stable monochromatic signal was occulted by the Sun, another effect, spectral broadening, was observed (Goldstein, 1969). To record spectral broadening, the sidebands of the spacecraft signal are eliminated by filtering and only the pure carrier signal is recorded. Spectral broadening causes the carrier which originally has an exceedingly narrow width in frequency to be broadened in frequency. The phenomenon may be caused by the Doppler shift of elements of radiation that are scattered from electron density irregularities or by amplitude scintillation or by a combination of both mechanisms.

2.6.4 Observed Characteristics of Scintillation

Scintillation tends to be most intense in equatorial, auroral, and polar latitudes and to have a general pattern of occurrence as shown in Fig. 2.13 (Aarons, Whitney, and Allen, 1971, CCIR, 1978). Table 2.3 gives examples of observed percentages of occurrence of scintillation at equatorial, sub-auroral, and auroral latitudes at frequencies of 137 and 254 MHz. The table includes K_p values, which are measures of magnetic activity, and shows that scintillation activity increases with K_p in sub-auroral and auroral latitudes.

The unexpected occurrence of scintillation at microwave frequencies at equatorial latitudes is illustrated for 6 GHz in Fig. 2.16 by Taur (1973), who presented further examples of the same type. Equatorial scintillation is often characterized by a sudden onset, and its occurrence varies considerably with location within the equatorial region. Basu et al. (1980) obtained data at 1.54 GHz at Huancayo, Peru for a 20-month period in 1976-1977 using the MARISAT satellite. Scintillation occurs after sunset and before midnight, with maximum intensities in roughly February - March and September - October (Fig. 2.17). The maximum scintillation observed was 8 dB, peak-to-peak. Aarons et al. (1981a) obtained data at 1.54 GHz during the peak of the sunspot cycle in 1979 and 1980 from Huancayo, Peru; Natal, Brazil; and Ascension Island. Peak-to-peak fading greater than 27 dB was recorded at Ascension Island, and 7-9 dB were recorded at Huancayo and Natal. The latter two locations are close to the magnetic equator in what can be described as the electrojet region. Ascension Island is at approximately 17°S dip latitude and is in what is known as the equatorial anomaly, namely the region from about 15° to 20° north and south of the magnetic dip equator where electron densities are higher than at the geomagnetic equator itself (Rishbeth and Garriott, 1969).

Table 2.3 Percentage of occurrence of scintillation (CCIR, 1978).

(a) > 10 dB peak to peak, equatorial latitudes

Site	Frequency	Day	Night
		(0400-1600 LT)	(1600-0400 LT)
Huancayo (Peru)	137 MHz	3	14
	254 MHz	2	7
		(0600-1800)	(1800-0600 LT)
Accra (Ghana)	137 Mhz	0.4	14

(b) > 12 dB peak to peak at 137 MHz, sub-auroral and auroral latitudes

Site	K_p	Day (0500-1700 LT)	Night (1700-0500 LT)
Sagamore Hill (Massachusetts)	0 to 3+	0	1.4
	> 3+	0.1	2
Goose Bay (Labrador)	0 to 3+	0.1	1.8
	> 3+	1.6	6.8
Narssarssuaq (Greenland)	0 to 3+	2.9	18
	> 3+	19	45

(c) > 10 dB peak to peak at 254 MHz, auroral latitudes

Site	K_p	Day (0600-1800 LT)	Night (1800-0600 LT)
Goose Bay (Labrador)	0 to 3+	0.1	0.1
	> 3+	0.3	1.2
Narssarssuaq (Greenland)	0 to 3+	0.1	0.9
	> 3+	2.6	8.4

LT: Local time.

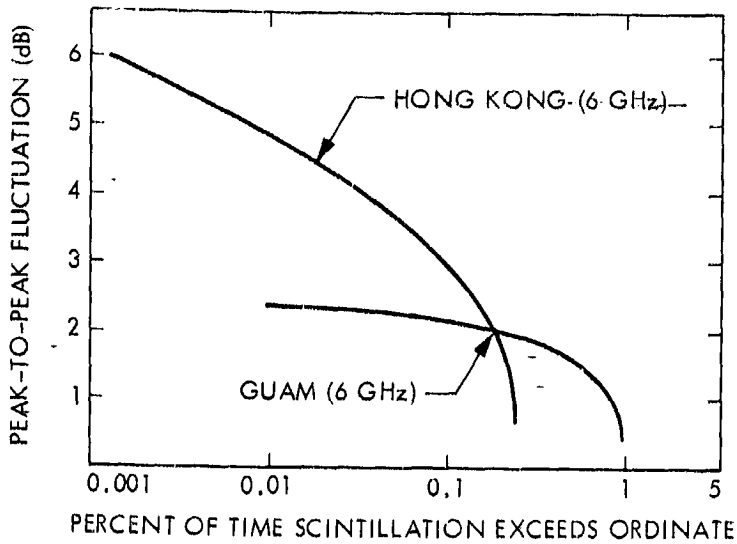

Figure 2.16. Scintillation, Guam and Hong Kong (Taur, 1973).

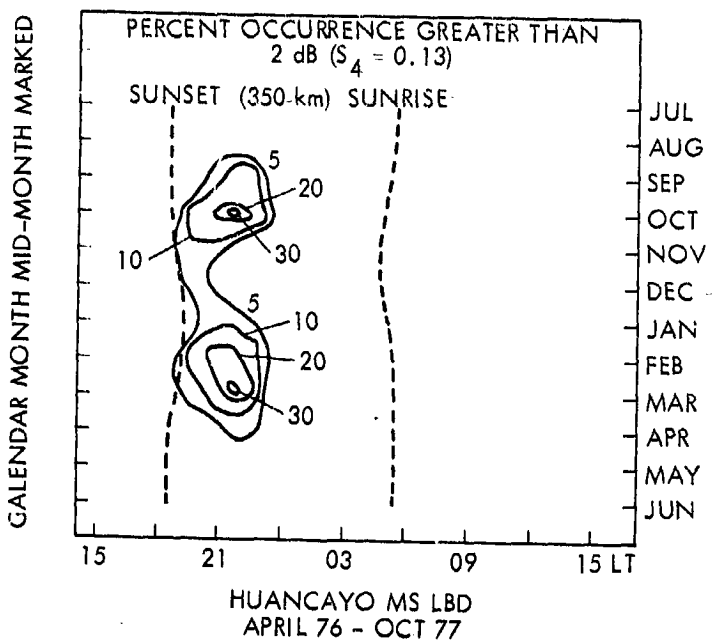

Figure 2.17. Monthly percentage occurrence of scintillations $\geq$ 2 dB, Huancayo, MARISAT, 1.54 GHz. (Basu et al., 1980).

Mid-latitude scintillation shows a well-established maximum near midnight corresponding to the occurrence of spread F. Scintillation increases at high latitudes compared to mid latitudes, the increase beginning near the region of the ionospheric trough. In the auroral oval, both discrete and diffuse aurora, as shown by Defense Meteorological Satellite program images, have been correlated with scintillations at 136-137 MHz (Martin and Aarons, 1977). Frihagen (1971), using 40 MHz transmissions, has reported two regions of peak scintillation activity at high latitude, one corresponding to the auroral oval and one above 80° geomagnetic latitude (over the polar cap). Aarons et al. (1981b) have prepared plots showing percentages of occurrence of scintillation greater than 10 dB in the polar cap at Thule, Greenland at a frequency of 250 MHz.

Measurements by Fremouw et al. (1978) employing 10 freqencies between 137 and 2891 MHz transmitted from a satellite in a high-inclination orbit and recorded at equatorial and auroral locations (Ancon, Peru; Kwajalein Island; and Fairbanks, Alaska) showed a $1/f^{1.5}$ variation of the intensity of amplitude scintillations with frequency for S_4 less than 0.4 and a $1/f$ variation of phase scintillation with frequency. Amplitude scintillations result in a reduction of signal-to-noise ratio. Phase scintillations may or may not be important depending on the type of system. For digital systems, phase scintillations are unimportant if the bit rate is much greater than the scintillation rate. Phase scintillations tend to be important for radionavigation systems such as the Global Positioning System and for synthetic-aperture radars. For positioning systems phase scintillation results in range jitter and consequent loss of accuracy in range (Rino, Gonzalez, and Hessing, 1981; Yeh and Liu, 1979) as increments of phase $\Delta\phi$ and corresponding changes in apparent range ΔR_ϕ are related by $\Delta\phi = 2\pi/\lambda_0 \, \Delta R_\phi$ [Eq. (2.47)]. Loss of signal coherence is another possible effect from scintillation (Rino, Gonzalez, and Hessing, 1981). Loss of coherence across a band as narrow as 11.5 MHz at UHF was observed by Fremouw et al. (1978).

Amplitude scintillations can be described quantitively by the use of power spectra, autocorrelation functions, cumulative probability distributions, fade-duration distributions, and plots showing message reliability (Whitney and Basu, 1977). Power spectra have been presented by a number of

authors including Rufenach (1972), Crane (1976), and Whitney and Basu (1977). Examples of power spectra and autocorrelation functions are shown in Figs. 2.18 and 2.19. Cumulative probability distributions show the percentage of time that signal amplitude exceeds specified dB values. The Nakagami-m distribution shows good agreement with observed distributions (Whitney and Basu, 1977; Fremouw et al., 1978; Panter, 1972). For the m of this distribution equal to one (not to be confused with the scintillation index m), the distribution is a Rayleigh distribution.

The power spectra, cumulative probability distributions, etc. contain detailed information about scintillation characteristics, but frequently one is primarily interested in certain parameters such as mean value, standard deviation, scintillation index, and coherence time. The index S_4 is the ratio of standard deviation to mean value. Coherence time τ_c can be obtained from plots of the autocorrelation function and is the time for this function to decrease from unity to some specified value such as 0.5 or 1/e. Whitney and Basu (1977) used 0.5 in their analysis of scintillation data. For predicting bit error rate, the form of the probability distribution function is needed.

In CCIR Report 263-4, values of the fading period of scintillation are given (CCIR, 1978). The period varies over a large range and can be as long as several minutes. The fading period of GHz scintillation varies from 2 to 15 seconds.

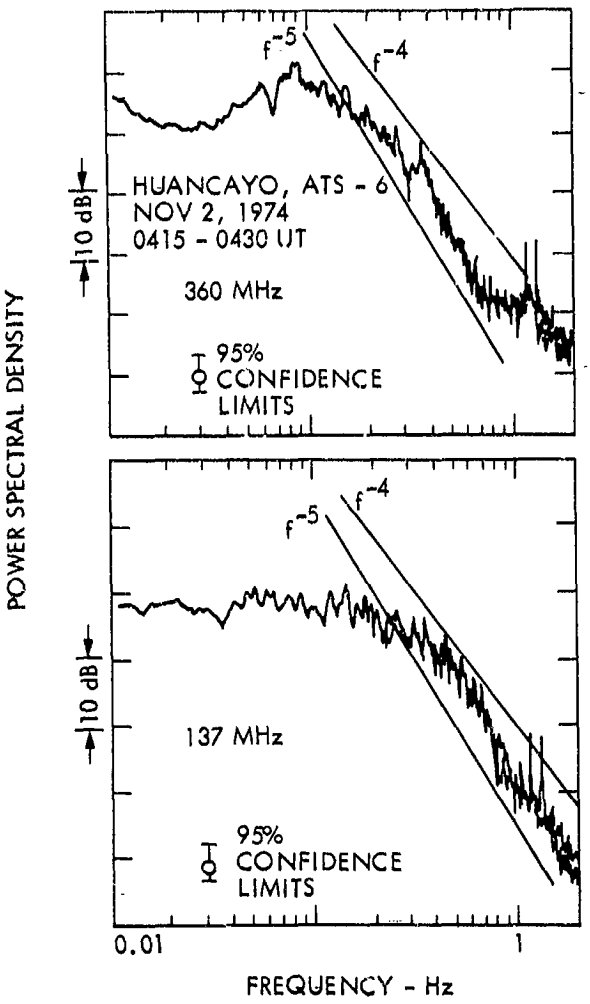

Figure 2.18. Typical power spectra for intense scintillations; S_4 = 0.94 at 137 MHz, S_4 = 0.78 at 360 MHz (Whitney and Basu, 1977).

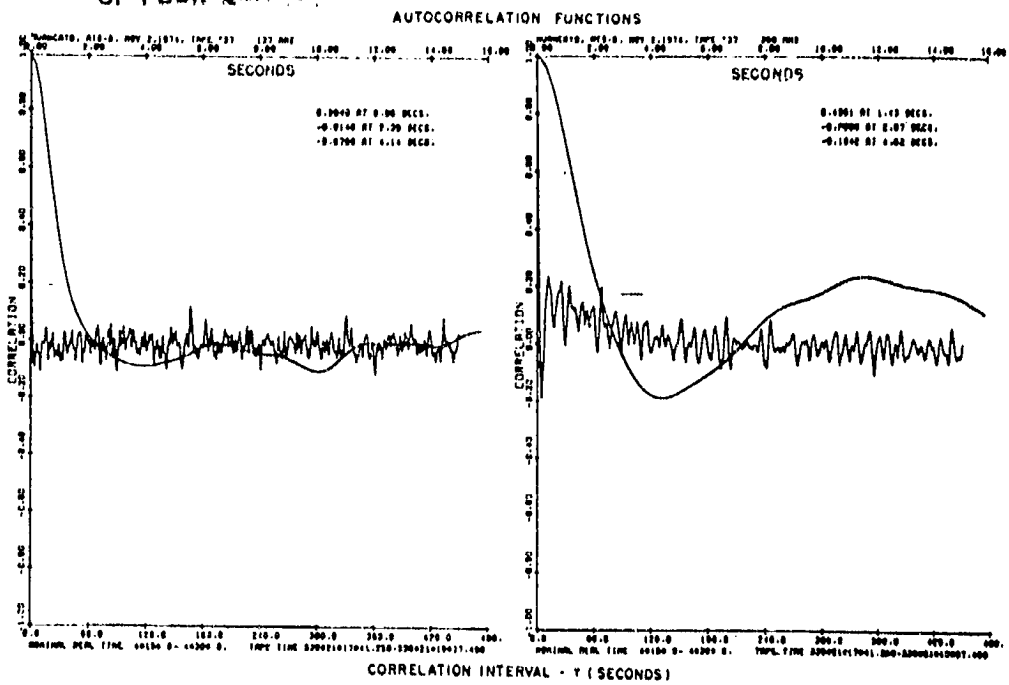

Figure 2.19. Typical autocorrelation data for intense scintillations; S_4 = 0.94 at 137 MHz, S_4 = 0.78 at 360 MHz (Whitney and Basu, 1977).

2.7 ABSORPTION

Attenuation was neglected in discussing the characteristic waves and Faraday rotation in previous sections, but waves propagating in the ionosphere tend to experience dissipative attenuation which becomes increasingly important with decreasing frequency. A principal mechanism of attenuation is collisions of free electrons with neutral atoms and molecules. An electromagnetic wave propagating in a plasma imparts an ordered component of velocity to the electrons but the electrons lose some of the associated energy in the collision process. Hence the electromagnetic wave is attenuated. The attenuation coefficient α, determining the rate of decrease of electric field intensity with distance in accordance with $e^{-\alpha z}$ for the left circularly polarized wave, is given, using conventional magneto-ionic theory, by

$$\alpha_\ell = \frac{Nq^2\nu}{2m\varepsilon_o n_{re} c[(\omega + \omega_B)^2 + \nu^2]} \text{ Nepers/m} \qquad (2.72)$$

where ν is the collision frequency. For the right circularly polarized wave, the corresponding expression is

$$\alpha_r = \frac{Nq^2\nu}{2m\varepsilon_o n_{re} c\,[\,(\omega-\omega_B)^2 + \nu^2\,]} \text{ Nepers/m} \qquad (2.73)$$

When attenuation is taken into account, the index of refraction becomes complex and is a function of collision frequency as well as electron density. The quantity n_{re} in Eqs. (2.72) and (2.73) stands for the real part of the complex index of refraction for the particular wave type considered. The value of n_{re} can be calculated precisely, based on assumed values of N and ν, but if losses are slight n_{re} has essentially the same value as for the lossless case. Note that ω appears in the denominator and that for $\omega >> \omega_B$ and $\omega >> \nu$, attenuation varies inversely with ω^2. The frequencies used for space communications are generally sufficiently high that attenuation does vary inversely with frequency squared and n_{re} does have the same value as in the lossless case. Furthermore n_{re} will approach unity as frequency increases. The quantity c is about 3×10^8 m/s.

For frequencies above about 30 MHz in particular, the attenuation coefficient varies inversely with frequency squared and takes the form of

$$\alpha = \frac{Nq^2\nu}{2m\varepsilon_o n_{re} c\omega^2} \text{ Nepers/m} \qquad (2.74)$$

To obtain attenuation in dB/m, the value of α in Nepers/m can be multiplied by 8.686. In the above expressions for α, all quantities are in SI units. For ionospheric work it may be convenient to express α in dB/km. A loss factor L_a in dB for ionospheric propagation is the integral of the attenuation coefficient α, expressed in dB/m or dB/km.

For oblique paths, total attenuation is proportional to sec χ/f^2, where χ is the zenith angle, for frequencies above 30 MHz (CCIR, 1978). Attenuation tends to be low at the frequencies used for space communications, the highest attenuations occurring under conditions of auroral and polar-cap absorption. It is for this reason that the subject of attenuation was deferred until these topics were introduced.

Table 2.4 shows values of auroral absorption at a frequency of 127 MHz as published in CCIR Report 263-4 (CCIR, 1978) but based upon extrapolations of 30 MHz riometer data in a supplement to CCIR Report 252-2. In a typical night of auroral activity, long quiet auroral areas appear to the north before midnight in the auroral zone. These progress southward and may reach close to the zenith by 23 h local time. One or two westward traveling folds or surges in the otherwise quiet areas may have been observed by this time. Between 23 h and 02 h the aurora forms become widespread and active in the sky, this phase being known as the auroral breakup. After the breakup, patchy, luminous forms appear in the sky. Quiet areas may then reappear as the opening phase of a second cycle of activity. Auroral absorption is usually greatest in the breakage and post-breakup periods.

Figure 2.20 shows illustrative hypothetical plots of absorption during a polar-cap absorption event at 30 MHz, as could be derived from riometer records. The top curve applies in the summer when sunlight occurs for 24 h a day. The other two curves for equal periods of day and night show a

Table 2.4 Auroral Absorption at 127 MHz, dB (CCIR, 1978).

Percentage of the time	Angle of elevation 20°	5°
0.1	1.5	2.9
1	0.9	1.7
2	0.7	1.4
5	0.6	1.1
50	0.2	0.4

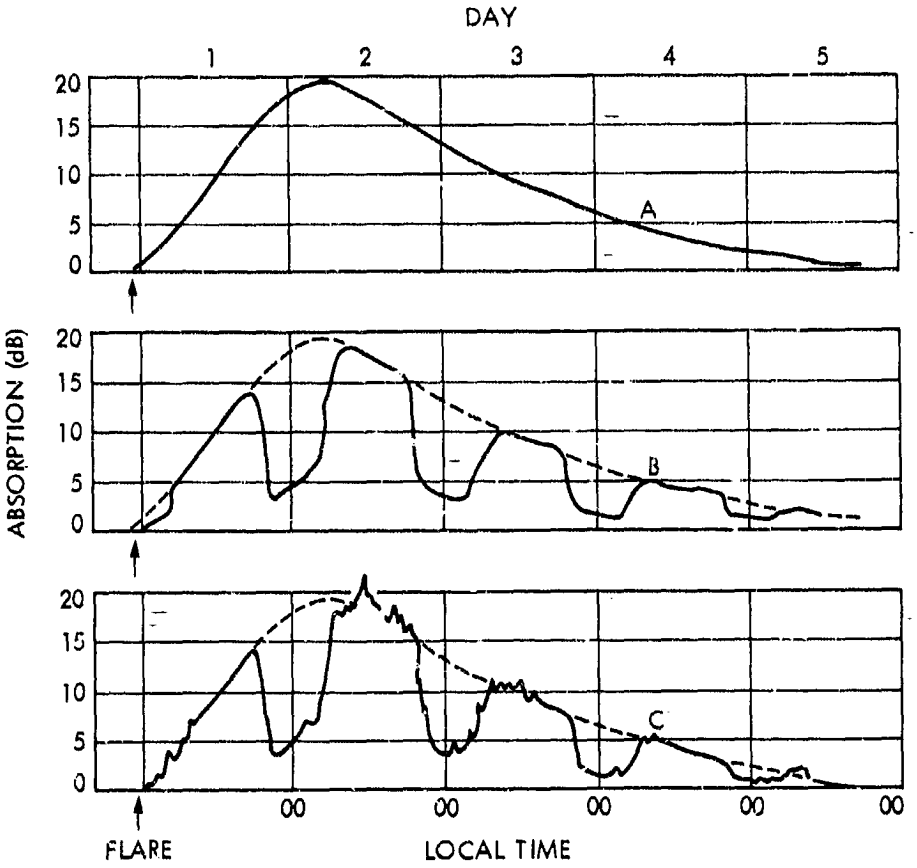

Figure 2.20. Hypothetical model showing polar cap absorption following a major solar flare as expected to be observed on riometers at approximately 30 MHz.

A: High latitudes - 24 hours of daylight.
B: High latitudes - equal periods of day and night.
C: Auroral Zone.

(CCIR, 1978).

pronounced diurnal variation in absorption. The decrease in absorption at night is due to the decreased equilibrium density of free electrons that occurs when solar electromagnetic radiation is absent.

2.8 TRANSIONOSPHERIC PROPAGATION PREDICTIONS AND CORRECTIONS

For some satellite systems advance estimates of atmospheric parameters, in the planning stage, is sufficient, but for other systems continuously updated long-term (e.g. monthly) or short-term (e.g. daily) predictions may be needed. Furthermore, real-time or near-real-time data on atmospheric characteristics may be required in some cases.

The problem of ionospheric predictions was considered in a conference devoted to solar-terrestrial predictions (Donnelly, 1978). Included in the proceedings of the conference are a report treating transionospheric propagation predictions (Klobuchar and members of Working Group, 1978) and other papers on this topic. It is stated in the working group report that monthly mean values of TEC can probably be predicted within ±20 percent for regions where a time history of TEC exists. However even if monthly mean values could be predicted perfectly accurately, short-term variations from the monthly mean values would still present a problem. Much of the difficulty arises from the ionospheric effects of geomagnetic storms. Theoretical capabilities are not presently capable of predicting storm-related TEC behavior, and prediction procedures based on morphological data are the only alternative. The report discusses the problem and possible remedies further.

Faraday-rotation data from linearly polarized 137-MHz beacons of the geosynchronous satellites ATS-1, SIR10, and Kiku-2 have been used by the Jet Propulsion Laboratory to measure TEC and determine ionospheric corrections to range and Doppler data used for Voyager spacecraft navigation (Royden, 1980). By taking the difference between TEC values determined by Faraday rotation and TEC values from dual-frequency transmissions from Voyager (2295 MHz in the S band and 8415 MHz in the X band), the electron content of the path beyond the ionosphere is also determined. The electron content beyond the ionosphere includes that of the plasmasphere and the solar plasma. In passing by the moon Io of Jupiter, furthermore, electrons in its atmosphere contributed to the total electron content along the path and made possible a

comparison of experimental results and theoretical models of the electron density surrounding Io.

A two-frequency technique involving time-delay measurements for determining TEC in order to correct for the time delay that it causes, has already been described in Sec. 2.3.1. The particular two-frequency technique used with Voyager, mentioned above, involves the difference in Doppler frequencies for the two down-link microwave frequencies.

Aarons, J., "Equatorial scintillations: a review," IEEE Trans. Antennas and Propagation, vol. AP-25, pp. 729-736, Sept. 1977.

Aarons, J. et al., "Seasonal and geomagnetic control of equatorial scintillations in two longitudinal sectors," J. Atmos. Terr. Phys., vol. 42, pp. 861-886, 1980.

Aarons, J., J. P. Mullen, and H. E. Whitney, "The dynamics of equatorial irregularity patch formation, motion, and decay," J. Geophys. Res., vol. 85, No. A1, pp. 139-149, Jan. 1, 1980.

Aarons, J., H. E. Whitney, and R. S. Allen, "Global morphology of ionospheric scintillations," Proc. IEEE, vol. 59, pp. 159-172, Feb. 1971.

Aarons, J., H. E. Whitney, E. Mackenzie, S. Basu, "Microwave equatorial scintillation intensity during solar maximum," Radio Science, vol. 10, pp. 939-945, Sept.-Oct. 1981a.

Aarons, J. et al., "VHF scintillation activity over polar latitudes," Geophys. Res. Lett., vol. 8, pp. 277-280, 1981b.

Akasofu, S. I., Polar and Magnetospheric Subsystems. New York: Springer-Verlag New York Inc., 1968.

Balsley, B. B., "Some characteristics of non-two-stream irregularities in the equatorial electrojet," J. Geophys. Res., vol. 74, pp. 2333-2347, May 1, 1969.

Baron, M. J., "Electron densities within aurorae and other auroral E-region characteristics," Radio Science, vol. 9, pp. 341-348, Feb. 1974.

Basu, S., D. Basu, J. P. Mullen, and A. Bushby, "Long-term 1.5 GHz amplitude scintillation measurements at the magnetic equator," Geophys. Res. Lett., vol. 7, pp. 259-262, April 1980.

Beckmann, P., Probability in Communication Engineering. New York: Harcourt, Brace & World, 1967.

Blesing, R. G. and P. A. Dennison, "Coronal broadening of the Crab Nebula 1969-1971: observations," Proc. Astron. Soc. Australia, vol. 2, pp. 84-46, March 1972.

Booker, H. G., "The role of the magnetosphere in satellite and radio-star scintillation," J. Atmos. Terr. Phys., vol. 37, pp. 1089-1098, Aug. 1975.

Booker, H. G., "The role of acoustic gravity waves in the generation of spread-F and ionospheric scintillation," J. Atmos. Terr. Phys., vol. 41, pp. 501-515, May 1979.

Bowhill, S. A., "Statistics of a radio wave diffracted by a random ionosphere," Journal of Research of NBS, vol. 65D, pp. 275-292, May-June 1961.

Bramley, E. N., "The accuracy of computing ionosphere radio-wave scintillation by the thin-phase-screen," J. Atmos. Terr. Phys., vol. 39, pp. 367-373, March 1977.

Briggs, B. H., "The correlation of radio star scintillations with geomagnetic disturbances," Geophysical Journal, vol. 5, pp. 306-317, Oct. 1961.

Briggs, B. H. and I. A. Parkin, "On the variation of radio star and satellite scintillations with zenith angle," J. Atmos. Terr. Phys., vol. 25, pp. 339-365, June 1963.

Callahan, P. S., "Columnar content measurements of the solar-wind turbulence near the sun," Astrophysical Journal, vol. 199, pp. 227-236, July 1, 1975.

CCIR, Report 263-4, Ionospheric Effects Upon Earth-space Propagation, in Volume VI, Propagation in Ionized Media, Recommendations and Reports of the CCIR, 1978, pp. 71-89. Geneva: International Telecommunications Union, 1978.

Cohen, M. H., "High-resolution observations of radio sources," Annual Review of Astronomy and Astrophysics, vol. 7, pp. 619-664, 1969.

Coles, W. A., "Interplanetary scintillation," Space Science Reviews, vol. 21, pp. 411-425, 1978.

Craft, H. D. and L. H. Westerlund, "Scintillations at 4 and 6 GHz caused by the ionosphere," AIAA 10th Aerospace Sciences Meeting, AIAA Paper No. 72-179, 1972. (Available as photocopy from AIAA Library, 750 3rd Ave., New York, NY 10012.)

Crain, C. M., H. G. Booker, and J. A. Gerguson, "Use of refractive scattering to explain SHF scintillations," Radio Science, vol. 14, pp. 125-134, Jan.-Feb. 1979.

Crane, R. K., "Spectra of ionospheric scintillations," J. Geophys. Res., vol. 81, pp. 2041-2050, May 1, 1976.

Crane, R. K., "Ionospheric scintillation," Proc. IEEE, vol. 65, pp. 180-199, Feb. 1977.

Cronyn, W. M., "The analysis of radio scattering and space-probe observations of small-scale structure in the interplanetary medium," Astrophysical Journal, vol. 161, pp. 755-763, Aug. 1970.

Davies, K., Ionospheric Radio Waves. Waltham, MA: Blaisdell Pub. Co., 1969.

Davies, K., G. K. Hartmann, and R. Leitinger, "A comparison of several methods of estimating the columnar electron content of the plasmasphere," J. Atmos. Terr. Phys., vol. 39, pp. 571-580, May 1977.

Davies, K., "Recent progress in satellite radio beacon studies with particular emphasis on the ATS-6 radio beacon experiment," Space Science Reviews, vol. 25, pp. 357-430, April 1980.

Donnelly, R. F. (ed.), Solar Terrestrial Predictions Proceedings, Volumes 1-4. Boulder, CO: Environmental Research Labs., NOAA, 1978.

Environmental Data Service, Values of Earth's Magnetic Field from Mathematical Models (Notice of Availability of Data Services), 1976. Contact National Oceanic and Atmospheric Admin., EDIS/NGSDC (D62), 325 Broadway, Boulder, CO 80303, Telephone: (303) 497-6478 FTS: 320-6478.

Evans, J. V., "Theory and practice of ionospheric study by Thomson scatter radar," Proc. IEEE, vol. 57, pp. 496-530, April 1969.

Farley, D. T., "A plasma instability resulting in field-aligned irregularities in the ionosphere," J. Geophys. Res., vol. 68, pp. 6083-6097, Nov. 15, 1963.

Flock, W. L., Electromagnetics and the Environment: Remote Sensing and Tele-Communications. Englewood Cliffs, NJ: Prentice-Hall, 1979.

Fremouw, E. J., R. L. Leadabrand, R. C. Livingston, M. D. Cousins, C. L. Rino, B. C. Fair, and R. A. Long, "Early results from the DNA wideband satellite experiment - complex-signal scintillation," Radio Science, vol. 13, pp. 167-187, Jan.-Feb. 1978.

Frighagen, J., "Occurrence of high latitude ionospheric irregularities giving rise to satellite scintillation," J. Atmos. Terr. Phys., vol. 33, pp. 21-30, 1971.

Goldstein, R. M., "Superior conjunction of Pioneer 6," Science, vol. 166, pp. 598-601, 31 Oct., 1969.

Hawkins, G. S. and J. A. Klobuchar, "Seasonal and diurnal variations in the total electron content of the ionosphere at invariant latitude 54 degrees," AFCRL-TR-74-0294. Bedford, MA: Air Force Cambridge Research Labs., 28 June, 1974.

Hay, J. S., S. J. Parsons, and J. W. Phillips, "Fluctuations in cosmic radiation at radio frequencies," Nature, vol. 158, p. 234, Aug. 17, 1946.

Heron, M. L., "Transequatorial propagation through equatorial plasma bubbles-discrete events," Radio Science, vol. 15, pp. 829-835, July-Aug. 1980.

Hewish, A., "The diffraction of galactic radio waves as a method of investigating the irregular structure of the ionosphere," Proc. Royal Society of London, Series A, vol. 214, pp. 494-514, 9 Oct., 1952.

Hewish, A., "The irregular structure of the outer regions of the solar corona," Proc. Royal Soc. of London, Series A, vol. 228, pp. 238-251, 22 Feb., 1955.

Hewish, A., P. F. Scott, and D. Wills, "Interplanetary scintillation of small diameter radio sources," Nature, vol. 203, pp. 1214-1217, Sept. 19, 1964.

Hines, C. O. et al., The Upper Atmosphere in Motion, Geophysical Monograph 18. Washington, D.C.: American Geophysical Union, 1974.

Hansucker, R. D., "Simultaneous riometer and incoherent scatter radar observations of the auroral D region," Radio Science, vol. 9, pp. 335-340, Feb. 1974.

Ishimaru, A., Wave Propagation and Scattering in Random Media, Vol. 2. New York: Academic Press, 1978.

Jenkins, F. A. and H. E. White, Fundamentals of Optics, Fourth Edition. New York: McGraw-Hill, 1976.

Jokipii, J. R., "Turbulence and scintillations in the interplanetary plasma," Annual Review of Astronomy and Astrophysics, vol. II, pp. 1-28, 1973.

Klobuchar, J. A., "Ionospheric effects on satellite navigation and air traffic control systems," in Recent Advances in Radio and Optical Propagation for Modern Communication, Navigation, and Detection Systems, AGARD Proceedings-LS-93, ISBN 92-835-1280-4. NTIS: Springfield, VA 22161, April 1978.

Klobuchar, J. A. (leader) and Working Group, "B. Trans-ionospheric-propagation predictions," in R. F. Donnelly (ed.), vol. 2. Working Group Reports and Reviews of Solar-Terrestrial Predictions Proceedings, pp. 217-245, Boulder, CO: Environmental Research Labs., NOAA, 1978.

Lawrence, R. S., C. G. Little, and H. J. A. Chivers, "A survey of ionospheric effects upon earth-space propagation," Proc. IEEE, vol. 52, pp. 4-47, Jan. 1964.

Leadabrand, R. L., M. J. Baron, J. Petriceks, and H. F. Bates, "Chatanika, Alaska, auroral-zone incoherent scatter facility," Radio Science, vol. 7, pp. 747-756, July 1972.

Little, C. G. and A. C. B. Lovell, "Origin of the fluctuations in the intensity of radio waves from galactic sources: Jodrell Bank observations," Nature, vol. 165, pp. 423-424, March 18, 1950.

Malin, S. R. C. and D. R. Barraclough, "An algorithm for synthesizing the geomagnetic field," Computers and Geosciences, vol. 7, No. 4, pp. 401-405, 1981.

Martin, E. and J. Aarons, "F layer scintillations and the aurora," J. Geophys. Res., vol. 82, pp. 2717-2722, July 1, 1977.

McClure, J. P., W. B. Hanson, and J. H. Hoffman, "Plasma bubbles and irregularities in the equatorial ionosphere," J. Geophys. Res., vol. 82, pp. 2650-2656, July 1, 1977.

Millman, G. H. and G. M. Reinsmith, "An analysis of the incoherent scatter-Faraday rotation technique for ionospheric propagation error correction," General Electric Technical Information Series R 74EMH2, Feb. 1974. (Available from HMES Technical Publications, Box 1122 (CSP4-24), Syracuse, NY 13201.)

Panter, P. F., Communication Systems Design. New York: McGraw-Hill, 1972.

Peddie, N. W., "International Geomagnetic Reference Field 1980," Geophysics, vol. 47, pp. 841, 842, May 1982.

Rino, C. L., "A power law phase screen model for ionospheric scintillation 1. Weak scatter," Radio Science, vol., 14, pp. 1135-1145, Nov.-Dec. 1979a.

Rino, C. L., "A power law phase screen model for ionospheric scintillation 2. Strong scatter," Radio Science, vol. 14, pp. 1147-1155, Nov.-Dec. 1979b.

Rino, C. L. and E. J. Fremouw, "The angle dependence of singly scattered wavefields," J. Atmos. Terr. Phys., vol. 39, pp. 859-868, Aug. 1977.

Rino, C. L., V. H. Gonzales, and A. R. Hessing, "Coherence bandwidth loss in transionospheric radio propagation," Radio Science, vol. 16. pp. 245-255, March-April 1981.

Rishbeth, H. and O. K. Garriott, Introduction to Ionospheric Physics. New York: Academic Press, 1969.

Royden, H. N., D. W. Green, and G. R. Walson, "Use of Faraday-rotation data from beacon satellites to determine ionospheric corrections for interplanetary spacecraft navigation," COSPAR/URSI Symposium on Scientific and Engineering Uses of Satellite Radio Beacons, Warsaw, Poland, May 19-23, 1980.

Rufenach, C. L., "A radio scintillation method of estimating the small-scale structure in the ionosphere," J. Atmos. Terr. Phys., vol. 33, pp. 1941-1951, 1971.

Rufenach. C. L., "Power-law wave number spectrum deduced from ionospheric scintillation observations," J. Geophys. Res., vol. 77, pp. 4761-4772, Sept. 1, 1972.

Smith, E. K., A Study of Ionospheric Scintillation as it affects Satellite Communication, Office of Telecommunications, U. S. Dept. of Commerce, Technical Memorandum 74-186, Nov., 1974.

Smith, E. K. and R. E. Edelson, "Radio propagation through solar and other extra-terrestrial ionized media," JPL Publication 79-117. Pasadena, CA: Jet Propulsion Laboratory, Jan. 15, 1980.

Smith, F. G., "Origin of the fluctuations in the intensity of radio waves from galactic sources: Cambridge observations," Nature, vol. 165, pp. 422-423, March 18, 1950.

Tatarski, V. E., Wave Propagation in a Turbulent Medium (translated from Russian by R. A. Silverman.) New York: McGraw-Hill, 1961. (Also published by Dover Publications, Inc., New York 1967.)

Tatarski, V. E., The Effects of the Turbulent Atmosphere on Wave Propagation (translated from Russian). Springfield, VA: National Technical Information Service, U. S. Department of Commerce, 1971.

Taur, R. R., "Ionospheric scintillation at 4 and 6 GHz," COMSAT Tech. Rev., vol. 3, pp. 145-163, Spring, 1973.

Whitney, H. E., J. Aarons, and C. Malik, "A proposed index for measuring ionospheric scintillation," Planet. Space Sci., vol. 7, pp. 1069-1073, 1969.

Whitney, H. E. and S. Basu, "The effect of ionospheric scintillation on VHF/UHF satellite communication," Radio Science, vol. 12, pp. 123-133, Jan.-Feb. 1977.

Woo, R. "Multifrequency techniques for studying interplanetary scintillations," Astrophysical Journal, vol. 201, pp. 238-248, Oct. 1, 1975.

Woo, R., "Measurements of the solar wind using spacecraft radio scattering observations," in Study of Travelling Interplanetary Phenomena 1977, Shea, M. A. and D. F. Smart (eds.), pp. 81-100. Dordrecht, Holland: Boston, D. Reidel Publishing Co., 1977.

Woo, R. and A. Ishimaru, "Remote sensing of the turbulence characteristics of a planetary atmosphere by radio occultation of a space probe," Radio Science, vol. 8, pp. 103-108, Feb. 1973.

Woo, R. and A. Ishimaru, "Effects of turbulence in a planetary atmosphere on radio occultation," IEEE Trans. on Antennas and Propagation, vol. AP-22, pp. 566-573, July 1974.

Woodman, R. F. and C. La Hoz, "Radar observations of F-region equatorial irregularities,"J. Geophys. Res., vol. 81, pp. 5447-5466, Nov. 1, 1976.

Yeh, K. C. and C. . Liu, "Ionospheric effects on radio communication and ranging pulses," IEEE Trans. on Antennas and Propagation, vol. AP-27, pp. 747-751, Nov. 1979.

Yeh, K. C. and G. W. Swenson, Jr., "F-region irregularities studies by scintillation of signals from satellites," Radio Science (Sec. D., Jour. of Research, National Bureau of Standards), vol. 68D, pp. 881-894, Aug. 1964.

APPENDIX 2.1

FRESNEL ZONES

To obtain expressions for the radii of the Fresnel zones, consider the two paths of Fig. A2.1. TPR is a direct path from a transmitter at T to a receiver at R, and path TSR is longer than TPR. If TSR = TPR + $\lambda/2$ where

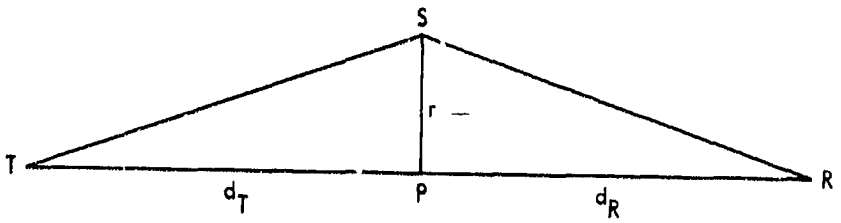

Figure A2.1 Geometry for consideration of Fresnel zones.

λ is wavelength, the region within the radius r of the direct path, at the distance d_T from T and d_R from R, is defined as the first Fresnel zone. Let this particular value of r be defined as F_1, the first Fresnel zone radius. Considering that the paths are such that TSP and RSP form good approximations to right triangles with $F_1 \ll d_T$ and $F_1 \ll d_R$,

$$TS = \sqrt{d_T^2 + F_1^2} = d_T \left[1 + \frac{F_1^2}{2d_T^2} \right] \tag{A2.1}$$

and

$$SR = \sqrt{d_R^2 + F_1^2} = d_R \left[1 + \frac{F_1^2}{2d_R^2} \right] \tag{A2.2}$$

Setting TPR + $\lambda/2$ = TSR gives

$$d_T + d_R + \lambda/2 = d_T + d_R + \frac{F_1^2}{2d_T} + \frac{F_1^2}{2d_R} \tag{A2.3}$$

from which

$$F_1^2 \left(\frac{1}{d_T} + \frac{1}{d_R}\right) = \lambda \qquad \text{(A2.4)}$$

and

$$F_1^2 \left(\frac{d_T + d_R}{d_T d_R}\right) = \lambda \qquad \text{(A2.5)}$$

so that

$$F_1 = \sqrt{\frac{\lambda d_T d_R}{d}} \qquad \text{(A2.6)}$$

where $d = d_T + d_R$. If TSR = TPR + $n\ \lambda/2$, then

$$F_n = \sqrt{n}\, F_1 \qquad \text{(A2.7)}$$

All the elements of radiation passing through the first Fresnel zone have components of field intensity that add constructively. Radiation passing through the second Fresnel zone (between $r = F_1$ and $r = F_2$) interferes destructively with that passing through the first zone, and radiation passing through the third zone adds with that through the first. This condition of alternating destructive and constructive interference continues, radiation from each zone being 180° out of phase with that from adjacent zones, but the amplitudes of the contributions decrease with increasing n.

CHAPTER 3
TROPOSPHERIC CLEAR-AIR EFFECTS

3.1 INDEX OF REFRACTION PROFILE

Propagation in the troposphere is influenced, and in some cases strongly affected, by the variation of the index of refraction with height. By definition, the index of refraction n of a particular type of wave in a given medium is the ratio of c, 2.9979×10^8, to v_p, the phase velocity of the wave in the medium. The index of refraction of the troposphere at radio frequencies is a function of pressure, temperature, and water vapor content as indicated by

$$N = (n - 1)10^6 = \frac{77.6\, p_d}{T} + \frac{72\, e}{T} + \frac{3.75 \times 10^5 e}{T^2} \qquad (3.1)$$

where P_d is the pressure of dry nonpolar air in mb (millibars), e is water vapor pressure in mb, and T is absolute temperature in kelvins (Smith and Weintraub, 1953). Because the index n is only slightly greater than 1, the usual practice is to use N units for convenience, with N defined as in Eq. (3.1). N, sometimes referred to as refractivity, is seen to vary inversely with temperature and to be strongly dependent on the water vapor pressure. The water vapor pressure e, the saturation water vapor pressure e_s, which is a function of temperature (Table 3.1), and the relative humidity R.H., are related by $e = e_s$ (R.H.). If Eq. (3.1) is expressed in terms of p, the total pressure, where $p = p_d + e$, it becomes

$$N = \frac{77.6\, p}{T} - \frac{5.6\, e}{T} + \frac{3.75 \times 10^5\, e}{T^2} \qquad (3.2)$$

The last two terms can be combined to give, approximately,

$$N = \frac{77.6\, p}{T} + \frac{3.73 \times 10^5\, e}{T^2} \qquad (3.3)$$

The last form is widely used and gives values for N that are accurate within 0.5 percent for the ranges of atmospheric parameters normally encountered and for frequencies below 30 GHz (Crane, 1976). If one wishes to consider separately the effects of dry air and water vapor, however, letting $N = N_d +$

Table 3.1 Saturation Water Vapor Pressure e_s in mb [Adapted from Smithsonian Meteorological Tables, 1958 (List, 1958)].

T(°C)	e_s (mb)	T (°C)	e_s (mb)
-30	0.5	20	23.4
-20	1.3	22	26.4
-10	2.9	24	29.8
0	6.1	26	33.6
2	7.1	28	37.8
4	8.1	30	42.4
6	9.3	32	47.6
8	10.7	34	53.2
10	12.3	36	59.4
12	14.0	38	66.3
14	16.0	40	73.8
18	20.6		

N_w where N_d refers to dry air and N_w to water vapor, Eq. (3.1) should be used with

$$N_d = \frac{77.6\ p_d}{T} \tag{3.4}$$

and

$$N_w = \frac{72\ e}{T} + \frac{3.75 \times 10^5\ e}{T^2} \tag{3.5}$$

The absolute humidity or water vapor density in gm/m^3, ρ, and e in mb are related (Appendix 3.1) by

$$\rho = \frac{216.5\ e}{T} \tag{3.6}$$

The dew point is the temperature at which air is saturated with water vapor, and values of the dew point can be used to determine e_s, the saturation water vapor pressure, by use of Table 3.1. For example, the highest accepted weather-observatory dew point of 34° [recorded on the shore of the Persian Gulf at Sharjah, Saudi Arabia (U.S. Standard Atmosphere, 1976)] corresponds to a vapor pressure of 53.2 mb and an absolute humidity of 37.5 gm/m^3.

Although an increase in temperature would cause a decrease in N if water vapor pressure were held constant, the saturation water vapor pressure increases rapidly with temperature and the highest values of N therefore occur for high temperatures (and high relative humidities).

The value of N corresponding to the value of e of 53.2 mb at a temperature of 34°C, for example, is 467. In nearby inland desert areas of Saudi Arabia where the relative humidity might approach 0, however, the value of N could approach 256, the value of dry air at the sea level pressure of 1013 mb and the temperature of 34°C or 307 K. The lowest surface values of N tend to occur in high, dry areas where both ρ and e are low. At a height of 3000 m, for example, assuming the pressure for a standard atmosphere but a temperature of 273 K, N is 230 with 100 percent relative humidity and 199 with 0 percent humidity. The values of N mentioned above are extreme. Monthly mean values of N at sea level vary between about 290 and 400 within ±25° of latitude from the equator, with a somewhat smaller variation elsewhere, and are typically 320 in the winter and 340 in the summer in the UK (Hall, 1979). In the United States, winter values vary from about 285 to 345 and summer values range from about 275 to 385 (Bean and Dutton, 1966).

Pressure, temperature, and water vapor content all decrease with height above the Earth's surface in the troposphere on the average, but temperature increases with height in temperature inversion layers. Pressure drops off approximately exponentially with height, and the decrease or change of e with height is variable but may be approximately exponential. The refractivity N may also decrease with height in a variable manner, but on the average tends to decrease exponentially as described by

$$N = N_S e^{-h/H} \qquad (3.7)$$

where N is the refractivity at the height h above the level where the refractivity is N_S. H is the appropriate "scale height." The change in N in the first km of height above the surface, ΔN, is a parameter of significance. In the average atmosphere as defined by the CCIR, N_S has the value of 315 and ΔN the value of -40, consistent with

$$N = 315\ e^{-h/7.36} \tag{3.8}$$

with h in km and 7.36 km the scale height H. Values of N_S and ΔN have been compiled, with N_S in some cases reduced to sea level values N_0, and charts showing these quantities, probability distributions of N_S, the water vapor density ρ, etc. have been provided by Bean, Horn, and Ozanich (1960), Bean et al. (1966), and the CCIR (1978a). Figure 3.1 shows annual cycles of N_S for several climatic types.

The exponential model is widely applicable but any reliable data on actual refractivity profiles should be used when available. Such data can be acquired by use of radiosondes or microwave refractometers and often display significant departures from the exponential form. A common cause of non-exponential refractivity profiles is the occurence of temperature-inversion layers. In an inversion layer, the temperature increases with altitude and such a layer is highly stable (Sec. 1.3). All vertical motions are strongly inhibited in an inversion layer, and pollution and water vapor existing below the layer tend to be confined below it. Temperature inversions may develop when the loss of heat from the surface of the Earth is not compensated by inputs of heat, the ground being a more efficient radiator than air and therefore cooling more rapidly. Surface and low-level inversions tend to develop at night and in the arctic and subarctic in winter and in locations such as the San Joaquin Valley of California where fog forms under the inversion and prevents surface heating in the winter. Inversions may form also when warm air blows over a cool surface such as an ocean and when the cold air of a cold front extends beneath warm air.

Inversions are also caused by subsiding air, and this type of inversion is of common occurrence because in portions of developing or semipermanent

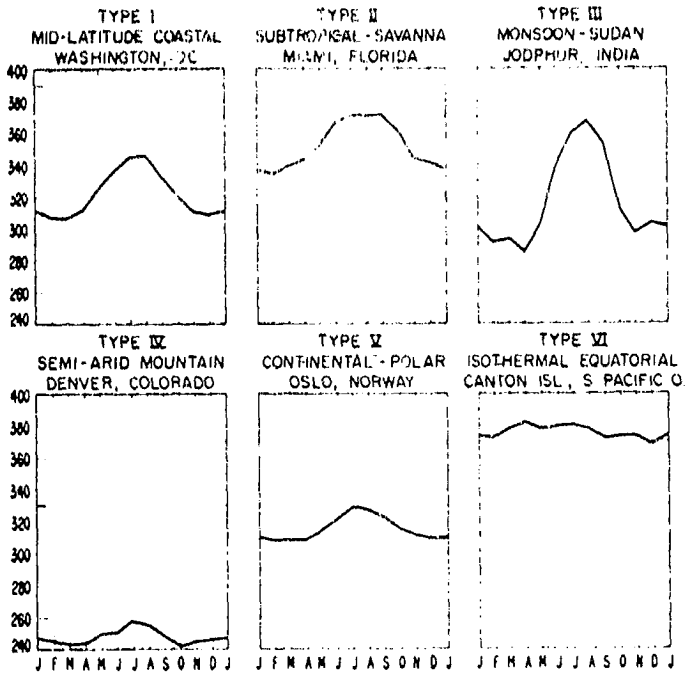

Figure 3.1. Annual cycles of N_s by climatic type (from Bean, Horn, and Ozanich, 1960).

anticyclones the air between about 500 and 5000 m descends at a rate typically around 1000 m/day (Scorer, 1968). The Pacific coast of the United States lies along the eastern edge of a semipermanent anticyclone that forms in the Pacific, and the persistent temperature inversion of the Los Angeles area is caused by subsiding air. This air is heated in a process of adiabatic compression but the movement and heating cannot extend to the ground itself, and a temperature inversion is thus formed at or near the surface.

The occurrence of a high water vapor content underneath an inversion layer may be accompanied by a rapid decrease in water vapor content through the inversion layer. The corresponding N value is also high beneath the layer and drops abruptly through the layer in such a case.

3.2 REFRACTION AND FADING

A practical consequence of the variation of the index of refraction of the troposphere with height is that electromagnetic waves do not travel in straight lines in the troposphere, but experience refraction or bending. To treat this phenomenon, one can consider ray paths which represent paths along which energy is transmitted. An important characteristic of an element of a ray-path is its curvature C, defined as $1/\rho$ where ρ is the radius of curvature. It can be shown (Bean and Dutton, 1966; Flock, 1979) that a ray path is a spherically stratified atmosphere having a curvature given by

$$C = -\frac{1}{n}\frac{dn}{dh}\cos\beta \tag{3.9}$$

where β is the angle of the ray measured from the horizontal. In the troposphere $n \approx 1$, and for rays having an angle β that is near 0, the expression for C simplifies to

$$C = -\frac{dn}{dh} \tag{3.10}$$

The latter form is usually suitable for terrestrial line-of-sight paths.

The change in direction or the amount of bending τ along a ray path can be determined by taking $\tau = \int C\, ds$ or $\tau = \Sigma C\, \Delta s$ where ds is an infinitesmal element of length and Δs is a finite element of length along the path. For an

infinitesmal length ds the corresponding bending $d\tau$ is given, from Eq. (3.9), by

$$d\tau = -\frac{1}{n}\frac{dn}{dh}\cos\beta\, ds \tag{3.11}$$

But as $dh = \sin\beta\, ds$

$$d\tau = -\frac{dn}{n\tan\beta} \tag{3.12}$$

This form can be used for ray tracing for any arbitrary index of refraction profile and for a path at any angle (Weisbrod and Anderson, 1959; Flock, 1979).

Very low-angle satellite paths may experience much the same effects as terrestrial line-of-sight paths. To illustrate these effects, it is convenient to use the simple form, $C = -dn/dh$, to consider propagation over a spherical earth. In this case the difference in curvature between a ray path and the Earth's surface is given by

$$\frac{1}{r_o} - C = \frac{1}{r_o} + \frac{dn}{dh} \tag{3.13}$$

where r_o is the Earth's radius and $1/r_o$ is the curvature of the Earth's surface. To analyze propagation, one can use a geometric transformation such that ray paths become straight lines and the Earth has an effective radius of k times the true radius r_o. This result is accomplished by setting

$$\frac{1}{r_o} + \frac{dn}{dh} = \frac{1}{kr_o} + 0 \tag{3.14}$$

thus maintaining the same relative curvature as that of Eq. (3.13). The 0 has been included on the right-hand side of Eq. (3.14) to emphasize that it applies to the case that $dn/dh = 0$, for which ray paths are straight lines. In terms of N units the relation becomes

$$\frac{1}{kr_o} = \left(157 + \frac{dN}{dh}\right) \times 10^{-6} \tag{3.15}$$

Table 3.2 lists corresponding values of k and dN/dh.

Table 3.2 Corresponding Values of dN/dh and k.

$\frac{dN}{dh}$ (N/km)	k
157	0.5
78	2/3
0	1
-40	4/3
-100	2.75
-157	∞
-200	-3.65
-300	-1.09

Typically, dN/dh = -40 and k = 4/3, and graphs prepared for k = 4/3 have been commonly used for plotting terrestrial microwave paths. However, k can vary over a range of values, and this type of graphical procedure has the shortcoming that a different graph is needed for each k value.

A more efficient procedure is to use a transformation which makes the Earth flat and allows plotting paths for various k values on the same chart. Such plots are made by calculating h' of Fig. 3.2 in accordance with

$$h' = \frac{d_1 d_2}{12.75\ k} \tag{3.16}$$

where d_1 and d_2 are the distances from the two ends of the path (GTE, 1972). The units of Eq. (3.16) are km for d_1 and d_2 and m for h'.

The basis for Eq. (3.16) is that $h' = h_{max} - h$ where h_{max} and h are calculated with respect to the center of the path by using, for h for example,

$$h = \frac{\ell^2}{12.75\ k} \tag{3.17}$$

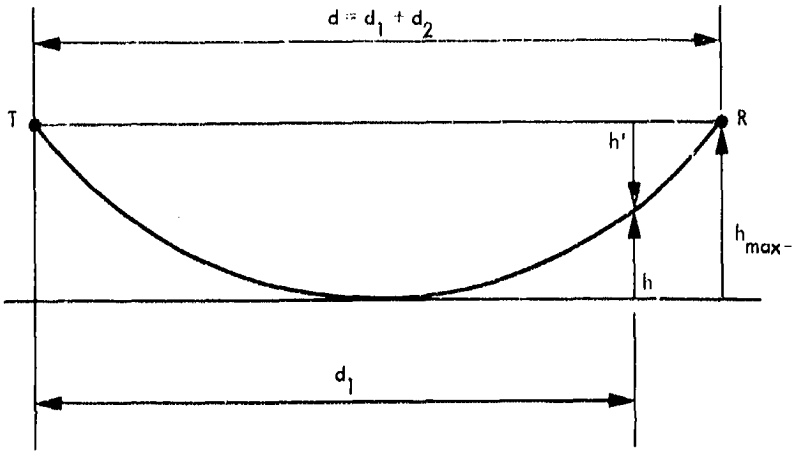

Figure 3.2. Quantities referred to for flat-earth plot.

where ℓ is the horizonal distance from the center of the path, at which point the path is horizontal. The distance ℓ is in km and h is in m in Eq. (3.17). This expression follows from the construction of Fig. 3.3 where, in contrast to Fig 3.2, the ray path is straight and the Earth is curved. Here ℓ, r_o, and r_o+h form the three sides of a right triangle. For $h << r_o$, it can be determined that

$$h = \frac{\ell^2}{2r_o} \tag{3.18}$$

with all quantities in identical units. For a finite value of dN/dh, however, r_o is replaced by kr_o, and the form of Eq. (3.17) results when ℓ is in km and h is in m.

The effect of the various k values is illustrated in exaggerated form in Figs. 3.4 and 3.5. In Fig 3.4 all the rays are horizontal at the common point. In Fig. 3.5 ray paths are shown which allow signals from a common transmitter to reach a common receiving location.

It is evident from the above discussion that tropospheric refraction may cause errors in the measurement of elevation angle and variations in angle of

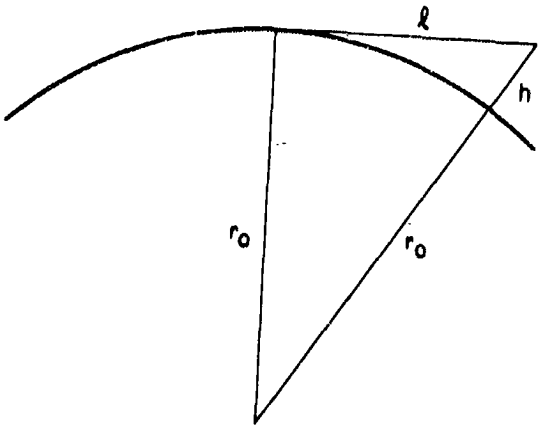

Figure 3.3. Geometry for determining h for initially horizontal ray.

arrival which can cause a reduction of signal amplitude for narrow-beam antennas. Also some degree of beam spreading or defocusing may occur and cause an attenuation of up to about 0.4 dB (Hall, 1979). To visualize how such defocusing occurs, consider a family of relatively closely spaced rays within an antenna beamwidth. The closer the spacing of the rays, the greater the signal intensity is. Defocusing involves a distortion of the ray paths such that the rays are more widely spaced then normally in the region of the receiving antenna.

Various programs for calculating bending have been devised. A simple procedure for calculating bending and elevation angle errors was presented by Weisbrod and Anderson (1959). Bending angles have been calculated by Crane (1976) for different elevation angles and for the 1966 U.S. Standard Atmosphere and an assumed humidity profile. His values are given in Table 3.3. The ray paths extend to the heights shown, and the heights correspond to the ranges or path lengths shown. The exact values of the bending angles will vary depending on atmospheric conditions, but the values of Table 3.3 are representative. Also included are values of range error or excess range,

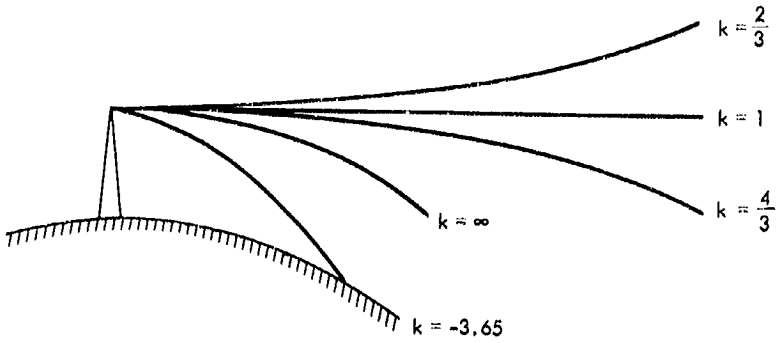

Figure 3.4. Ray paths for several values of k for initially horizontal rays (exaggerated and illustrative only).

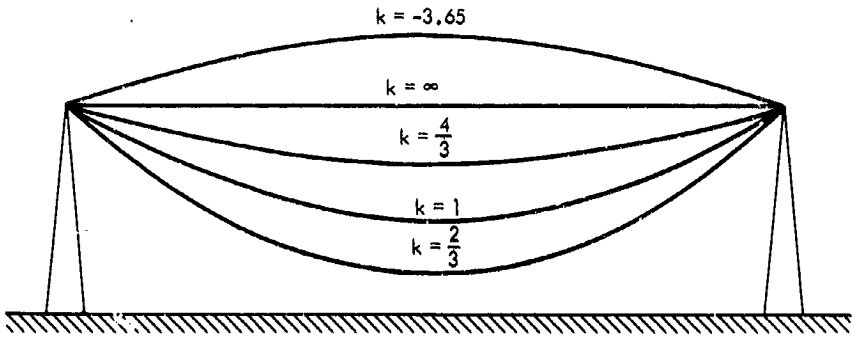

Figure 3.5. Ray paths from a transmitter T to a receiver R for various values of k (exaggerated and illustrative only).

which is discussed in Sec. 3.7. For transmitters or radar targets in the troposphere, the total bending and elevation angle errors are not the same; for astronomical sources and geosynchronous satellites, the total bending and elevation error angles are identical. Bending takes place largely in the lower troposphere and Crane (1976) has shown that the total bending τ is related to surface refractivity N_s by $\tau = a + b N_s$, where the coefficients a and b vary with elevation angle and have been tabulated in his paper for Albany, New York. Nearly the same values are said to apply in other circumstances.

A phenomenon of major importance in tropospheric propagation at small angles from the horizontal, especially in the presence of temperature inversions, is the occurrence of severe fading due to multipath propagation. Propagation over more than one path may involve reflection from land and water surfaces and from manmade structures. This type of multipath is considered in Chap. 6. Multipath propagation involving the atmosphere alone, such as suggested in Fig. 3.6, however, also occurs. In terrestrial line-of-sight links, a fading allowance of 30 to 45 dB is commonly assigned for multipath fading. Such paths are often essentially horizontal or at only a slight angle from the horizontal, whereas earth-space paths are usually at rather large angles above the horizontal for which tropospheric fading is much less severe. It is often considered that about 5° or 10° is the smallest elevation angle that should be employed for earth-satellite paths, but there are circumstances for which it may be necessary to operate at lower angles, as at high latitudes. Then atmospheric multipath fading may prove to be as serious as on terrestrial paths.

Table 3.3 Ray Parameters for a Standard Atmosphere [a,b].

Initial Elevation Angle (deg)	Height (km)	Range (km)	Bending (mdeg)	Elevation-Angle Error (mdeg)	Range Error (m)
0.0	0.1	41.2	97.2	48.5	12.6
	1.0	131.1	297.9	152.8	38.79
	5.0	289.3	551.2	310.1	74.17
	25.0	623.2	719.5	498.4	101.1
	80.0	1081.1	725.4	594.2	103.8
5.0	0.1	1.1	2.6	1.3	0.34
	2.0	11.4	25.1	12.9	3.28
	5.0	55.2	91.7	52.4	12.51
	25.0	241.1	176.7	126.3	24.41
	80.0	609.0	181.0	159.0	24.96
50.0	0.1	0.1	0.2	0.1	0.04
	1.0	1.3	1.9	1.0	0.38
	5.0	6.5	7.0	4.0	1.47
	25.0	32.6	14.3	10.3	3.05
	80.0	104.0	14.8	13.4	3.13

[a] U.S. Standard Atmosphere Supplements, 1966, Environmental Sci. Serv. Administration, Dept. of Commerce, Washington, D.C. (1966)

[b] N. Sissenwine, D.D. Grantham, and H.A. Salmela, AFCRL-68-0556, Air Force Cambridge Res. Lab., Bedford, Massachusetts (October 1968)

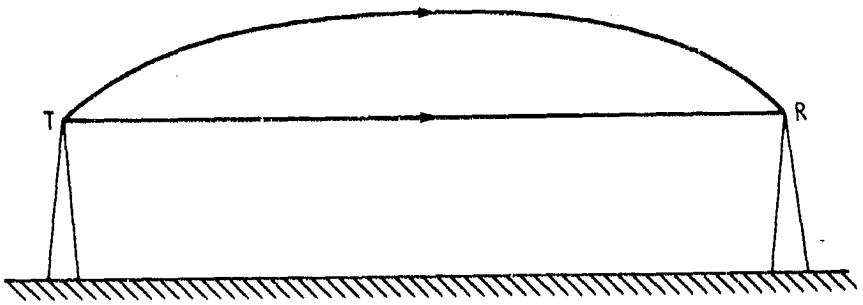

Figure 3.6. Concept of atmospheric multipath propagation. Energy reaches the receiver from the transmitter by two different paths. The relative phase of the two contributions varies, with the result that the two signals add constructively at one instant and interfere destructively an instant later.

3.3 DUCTING

Ducting is a strong refractive effect involving trapping of a wave in a duct, commonly a surface duct, and possibly propagation for an abnormally long distance. Ducting occurs frequently in some locations, but is not a reliable means of communication. It can, however, cause interference beyond the horizon, at a location that would otherwise be free from the interfering signal. On the other hand, it may prevent a signal from reaching the intended receiving location or cause severe fading.

A necessary condition for ducting to occur is that the refractivity decreases with height at a rate of 157 N units per km or greater. If $dN/dh = -157$, Eq. (3.15) shows that $1/kr_0 = 0$, corresponding to $k = \infty$ which condition corresponds to a flat earth. A ray that is launched horizontally under this condition remains horizontal and propagates at a constant height parallel to the surface of a spherical earth. If the rate of decrease of N is greater than 157 N/km, a ray may be bent downward to the surface of the Earth as for $k = -3.65$ in Fig. 3.4. Such a path may result in what is sometimes called blackout fading on a terrestrial path (Hautefeville et al., 1980).

In such a case, no signal reaches the receiving location and the use of space or frequency diversity may not improve the situation. The rays bent downward to the Earth's surface may be reflected upwards, however, and then refracted down to Earth again, etc., giving rise to ducting of the type illustrated in Fig. 3.7. A second condition for ducting is that the refractivity gradient of -157 N/km or greater be maintained over a height range of a number of wavelengths.

3.4 ATMOSPHERIC TURBULENCE

In addition to the variation of index of refraction with height, the index also exhibits variations associated with atmospheric turbulence. The theory of turbulence indicates that turbulence develops from wind shear, that

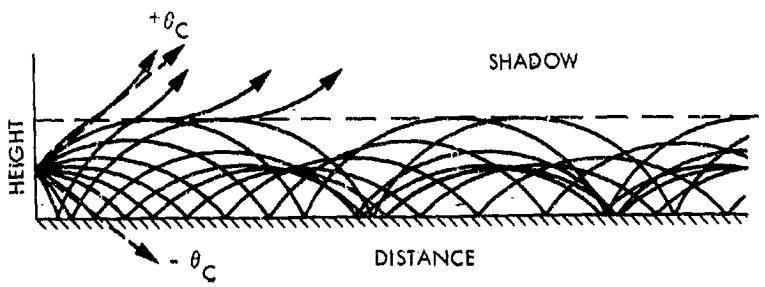

Figure 3.7. Example of ducting.

turbulence is introduced in the form of large turbulent eddies or blobs, and that energy is transferred from larger to smaller eddies throughout an inertial subrange corresponding to eddies of size ℓ where

$$L_0 > \ell > \ell_0$$

For eddies smaller than ℓ_0, viscous effects dominate and turbulent energy is dissipated. The process is suggested by Fig. 3.8.

Associated with the turbulent eddies or blobs is a corresponding time-variable structure of temperature, water-vapor density, and index of refraction. The quantity C_n^2 is a measure of the intensity of the index of refraction variations associated with the turbulence. In particular

$$C_n^2 = \overline{(n_1 - n_2)^2} \tag{3.19}$$

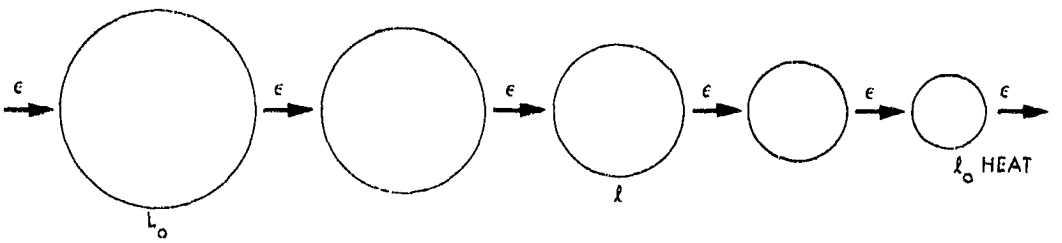

Figure 3.8. Illustration suggesting the transfer of energy at the rate ε from large eddies or blobs of characteristic size L_o to smaller blobs of characteristic size ℓ_o.

where n_1 and n_2 are values of the index of refraction at two locations a distance of 1 m apart. The overbar indicates an average value of the quantity below, namely $(n_1 - n_2)^2$. The atmosphere is normally turbulent to some degree, but the occurrence of turbulence is not uniform throughout the atmosphere. Turbulence tends to have a layered structure and may vary in the horizontal direction also.

The turbulent structure of the index of refraction of the troposphere is believed to be responsible for the scatter of electromagnetic waves that is the basis for troposcatter communication systems and radar clear-air echoes. Scatter of this type is known as Bragg scatter and is due to the structure of the index of refraction that has a periodicity of λ' where $\lambda' = \lambda/[2 \sin$

$(\theta/2)]$ where λ is the electromagnetic wavelength and θ is the scattering angle as shown in Fig. 3.9. The range of eddy size is large, and scatter from turbulence can be expected to occur over a wide range of frequencies and wavelengths.

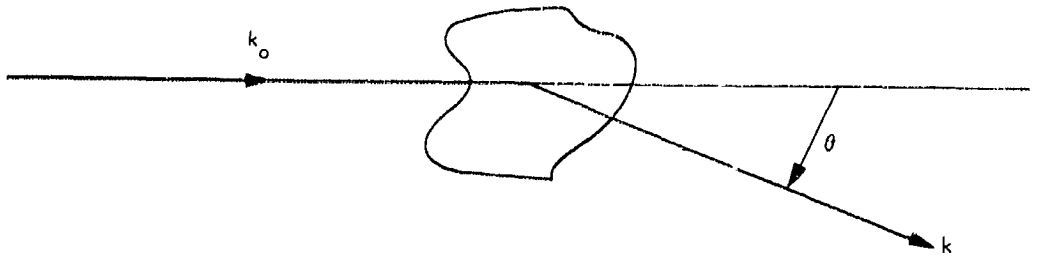

Figure 3.9. Scattering geometry.

For satellite communications, interest lies in the effect of turbulence on forward propagation through the turbulent region. The effects on forward propagation include amplitude fluctuations or scintillations, phase fluctuations, and angle-of-arrival variations.

3.5 AMPLITUDE VARIATIONS DUE TO REFRACTION AND TURBULENCE

It is not always easy to assess the relative importance of amplitude variations due to large-scale variations in refractivity and variations due to turbulence, either in advance planning or after the fact. Certain treatments of propagation emphasize one topic, and other studies deal with the other. In designing terrestrial line-of-sight links multipath fading associated with the refractivity profile receives attention, and effects or turbulence are largely ignored (GTE-Lenkurt, 1972). For earth-space paths the emphasis tends to be on effects due to turbulence (Theobold and Kaul, 1978).

The maximum amplitude variations due to turbulence are smaller in general than those due to multipath propagation, as discussed in Sec. 3.2, tend to occur more rapidly or at higher frequencies, and are commonly referred to as scintillation. Such scintillation increases in amplitude with frequency

(Thompson et al., 1975). (For brevity we will henceforth refer to refractive or multipath fading for effects due to large-scale variations in refractivity and to scintillation for effects due to turbulence.) Earth-space paths are at higher elevation angles than terrestrial paths. Even paths at what are considered to be low angles for satellite communications tend to be at larger angles than those of terrestrial paths, for which severe multipath fading may occur. Also multipath fading, while severe at certain times of the day and certain seasons in regions subject to strong temperature inversions, does not occur uniformly over all areas or at all times. Thus earth-space paths tend to experience scintillation associated with turbulence more than multipath fading, especially at larger elevation angles and higher frequencies.

Low-angle satellite paths, however, can encounter both scintillation and multipath fading, and refractive multipath effects may dominate at low angles. On a path in Hawaii at an elevation angle of 2.5° that simulated a low-angle, earth-space path at frequencies from 10 to 49 GHz, for example, Thompson et al. (1975) recorded both fades of more thn 20 dB and scintillations of several dB in amplitude.

Measurements of 4 and 6 GHz signals at the very small elevation angle of 1° at Eureka in the Canadian arctic, some of which are summarized in Table 3.4, show effects that are probably due primarily to refractive multipath fading.

Table 3.4 6 GHz Link Margins for Tropospheric Fading at Eureka, Canada, Elevation Angle ≈ 1 Degree (Strickland, et al., 1977).

Reliability Time Duration	90%	99%	99.9%
Worst two-hours	8.0 dB	18.0 dB	28.0 dB (Rayleigh)
Worst summer day	6.8 dB	15.5 dB	24.5 dB
Worst summer week (5 days)	5.4 dB	13.0 dB	22.0 dB
Worst month, July (15 days)	3.8 dB	10.8 dB	20.3 dB

Amplitude fluctuations and phase and angle-of-arrival variations due to turbulence are treated by Theobold and Kaul (1978), who include an example for a path at 28.56 GHz and an elevation angle of 10°. They predict a signal loss of 0.12 dB for clear weather, which is a small effect. Both the effects due to turbulence and the possibility of refractive fading would increase if the angle were decreased below 10°. As noted earlier, Thompson et al. (1975) recorded larger scintillations of several dB at an angle of 2.5° in Hawaii.

3.6 GASEOUS ATTENTUATION

A microwave absorption peak due to water vapor occurs at 22.235 GHz and peaks due to oxygen occur near 60 GHz and 118 GHz (CCIR, 1978b; Van Vleck, 1951; Waters, 1976). Below 10 GHz absorption caused by atmospheric gases is small. Vertical one-way attentuation values for frequencies above 1 GHz are shown in Fig. 3.10. Attentuation values for paths at elevation angles Θ above about 10° are equal to the vertical values divided by sin Θ, in a horizontally stratified atmosphere. Values of the attentuation constant due to oxygen and water vapor are shown in Fig. 3.11.

3.7 TROPOSPHERIC EFFECTS ON RANGE, PHASE, AND DOPPLER FREQUENCY

Range to a target is commonly determined by radar techniques by assuming that electromagnetic waves propagate with the velocity c (2.9979×10^8 m/s or approximately 3×10^8 m/s). The velocity of c corresponds to an index of refraction of unity. In the troposphere, however, the index of refraction, n, is slightly greater than unity with the result that the velocity of an electromagnetic wave is slightly less than c. A range error then results if the velocity c is assumed. The slight error in range is unimportant in many applications but may be important in other situations. In practice, when high accuracy in range is desired, it is anticipated that the range indicated by using the velocity c is greater than the true range and an effort is made to estimate as accurately as possible the excess range delay (the amount by which the indicated range exceeds the true range) in order to correct for it (Flock, Slobin, and Smith, 1982).

As for the case of the ionosphere (Sec. 2.3.1), the range error ΔR can be determined by taking $\int (n-1)\, d\ell$ along the path. For the troposphere, however,

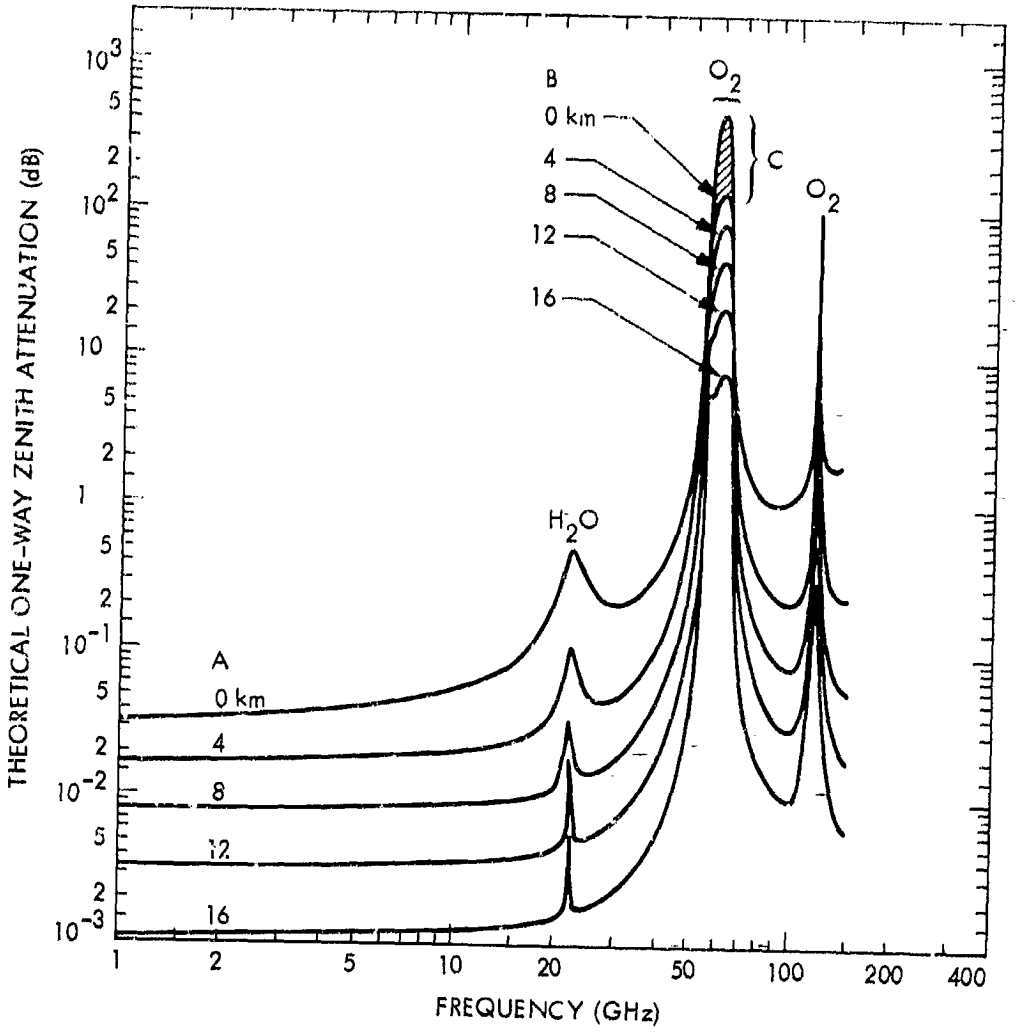

Figure 3.10. Theoretical vertical one-way attentuation from specified height to top of atmosphere for 7.5 g/m^3 of water vapor at the surface (CCIR, 1978b).

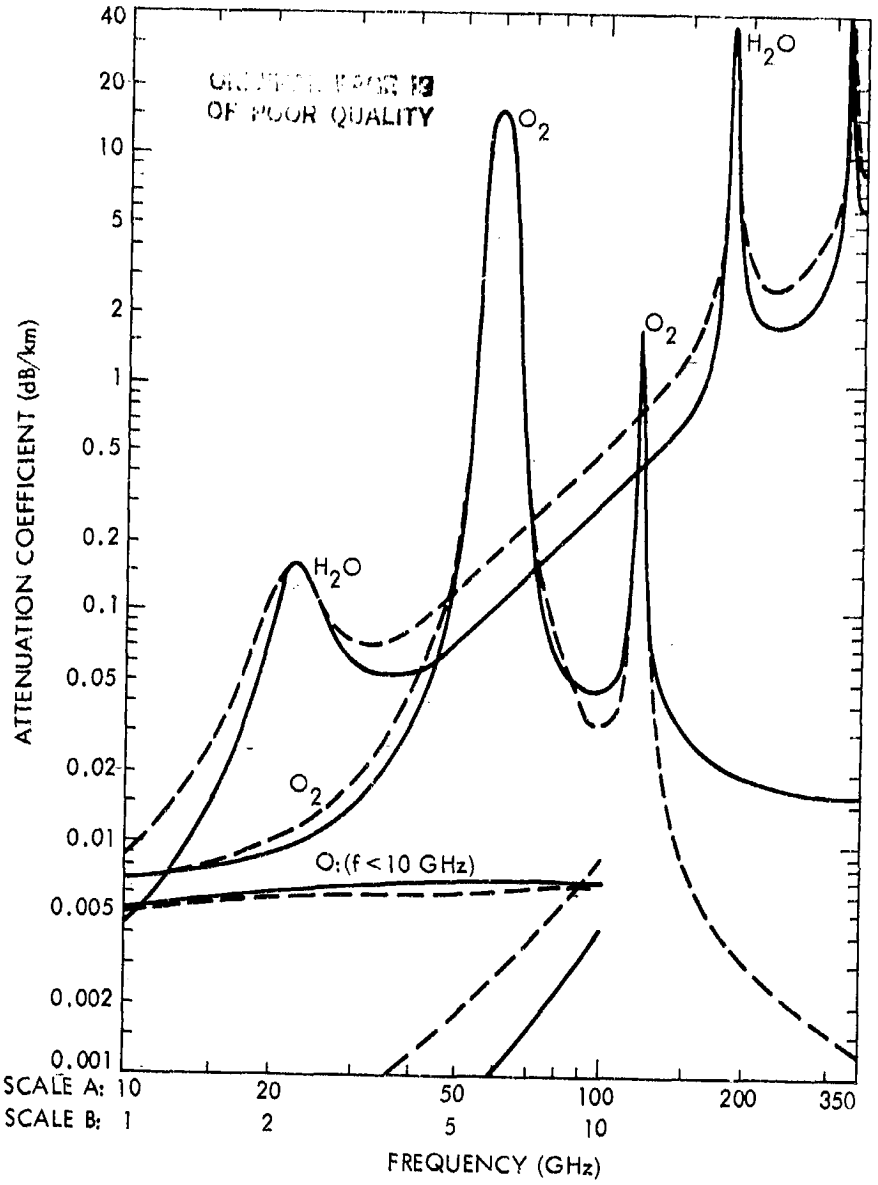

Figure 3.11. The attenuation constants due to oxygen and water vapor for a pressure of 1013.6 mb, a temperature of 20°C, and a water vapor density of 7.5 g/m^3. The solid curves are from CCIR Report 719, and the dotted curves represent recent results from a radiation transfer computer program developed by J.W. Waters of the Jet Propulsion Laboratory. Use Scale B for the curves for O_2 and H_2O below 10 GHz in the lower left-hand portion of the figure.

calculations are ... quantity $N = (n-1) \times 10^6$. (In the ionospheric analysis, N stands for an entirely different quantity, namely, electron density.) It is convenient to treat dry air and water vapor separately. For dry air, making use of Eq. (3.3) for a zenith path

$$\Delta R_d = 10^{-6} \int N_d \, d\ell = 10^{-6} \int_0^\infty \frac{77.6 \, p_d}{T} \, dh \qquad \text{m} \qquad (3.20)$$

with ΔR_d, the range delay due to dry air, in m. The pressure p_d is in mb, h is height in m, and T is temperature in kelvins. Pressure in the troposphere tends to decrease exponentially as indicated by $p = p_o e^{-h/H}$ (Eq. 1.18), where H is the scale height kT/mg or RT/Mg, k is Boltzmann's constant, g is the acceleration of gravity (about 9.8 m/s^2 at the earth's surface), R is the gas constant [8.3143×10^3 J/(K kg mol)], M is the mass of a kg mol, and m is the mass of an individual molecule. ($M/m = 6.025 \times 10^{26}$, which corresponds to Avogadro's number, but applies to a kg mol rather than to a gram mol.) Using the form of H involving R with M = 28.9665 kg from Table 3 of the U.S. Standard Atmosphere, 1976, treating T as if it were constant, and employing the value of g utilized by Hopfield (1971) corresponding to the height at 500 mb at 45 deg latitude (namely, 9.7877 m/s^2)

$$\int_0^\infty p_d \, dh = \int_0^\infty p_o \, e^{-h/H} \, dh = p_o H = \frac{p_o RT}{Mg} = p_o T \, 29.326$$

Substituting the value of the integral into Eq. (3.20) and identifying p_o as p_{o_d}, the surface pressure of dry air

$$\Delta R_d = 2.2757 \times 10^{-3} \, p_{o_d} \qquad (3.21)$$

with p_{o_d} in mb. If p_{o_d} is 1000 mb, for example, ΔR has the value of 2.28 m. The delay is directly proportional to surface pressure and independent of the temperature profile. Hopfield (1971) has examined the applicability of this relation and has concluded that it allows determining the range error due to dry air on a zenith path to an accuracy of 0.2 percent, or about 0.5 cm.

As H is a function of temperature and temperature varies with height, the exponential form $p_d\ e^{-h/H}$ with H a constant should only be assumed to apply over a limited height range. If account is to be taken of the variation of H with altitude, however, the integral of Eq. (3.20) can be represented as a summation of integrals over layers of limited thickness for which T can be treated as a constant. If this procedure is followed, T will cancel out of all the integrals and the same result will be obtained as shown by Eq. (3.21).

The delay caused by water vapor is considerably smaller than that for dry air, but total water vapor content along a path is variable and not predictable with high accuracy from the surface water vapor pressure or density. Therefore, water vapor is responsible for a larger error or uncertainty in range than in dry air. The expression for N_w, the contribution to refractivity of water vapor, is given by Eq. (3.5), but N_w can be expressed in terms of water vapor density ρ instead of water vapor pressure e, by using $e = \rho T/216.5$ (Eq. 3.6), and then takes the form

$$N_w = 0.3323\rho + \frac{1.731\rho}{T} \tag{3.22}$$

from which

$$\Delta R_w = 10^{-6} \int N_w\, d\ell \simeq 3.323 \times 10^{-7} \int \rho\, d\ell + 1.731 \times 10^{-3} \int (\rho/T)\, d\ell \quad m \tag{3.23}$$

Alternatively, the total excess range delay could be separated into ΔR_1 and ΔR_2 corresponding to the two terms of Eq. (3.3). Then

$$\Delta R_1 = 2.2757 \times 10^{-3}\ p_0 \qquad m \tag{3.24}$$

where p_0 is now the total surface pressure and

$$\Delta R_2 = 1.731 \times 10^{-3} \int (\rho/T)\, d\ell \qquad m \tag{3.25}$$

The value of the integral can be determined from radiosonde data if ρ and T vary only with height above the surface and not horizontally to a significant degree within the limits of the path.

Accumulation of sufficient data from radiosondes can provide a basis for a statistical description of the range error due to water vapor and for formulating models that may apply to particular locations. Radiosonde dat are available from only certain locations, however, and it may be impractical to use radiosondes regularly and routinely for determining range errors due to water vapor. Aircraft instrumented with microwave refractometers can provide more accurate data on ρ and T.

Another approach is to employ microwave radiometry to estimate the value of ΔR_2. This approach is based on the expression for the brightness temperature T_b observed when a source at a temperature of T_s is viewed through an absorbing medium having a variable temperature T. T_b is given by (Waters, 1976; Wu, 1977)

$$T_b = T_s e^{-\tau_\infty} + \int_0^\infty T \alpha e^{-\tau} d\ell \tag{3.26}$$

with $$\tau_\infty = \int_0^\infty \alpha d\ell$$

and $$\tau = \int_0^\ell \alpha d\ell$$

where α is the variable attentuation constant (scattering neglected) at the frequency employed. The expression for T_b takes a simpler, and perhaps more familiar, form when T is constant or when an effective value T_i can be employed. In this case

$$T_b = T_s e^{-\tau} + T_i (1 - e^{-\tau}) \tag{3.27}$$

A problem with the radiometer method is that oxygen and possibly liquid water contribute to α as well as water vapor. Use of a suitable pair of frequencies allows separating the effects of gaseous and liquid water to a reasonable degree, and the effect of oxygen can also be separated out (Staelin et al., 1977; Wu, 1977; Claflin, et al., 1978). Frequencies of 22.235 and 31.4 GHz have been used, 22.235 GHz being more sensitive to water vapor than liquid water by a factor of 2.5 and 31.4 GHz being more sensitive to liquid water than vapor by about a factor of 2.

By using Eq. (3.26) for the two different frequencies, and with the $T_s e^{-\tau_\infty}$ terms replaced by constants as T_s due to cosmic sources is small (2.7 K), the value of $\int_0^\infty W(\ell)\ \rho/T)\ d\ell$ is obtained where $W(\ell)$ can be regarded as a weighting function and has a nearly constant known value if a suitable pair of frequencies is employed (Wu, 1977).

Although there are limits to the accuracy to which ΔR_2 can be determined by the use of surface values, as mentioned earlier, Berman (1976) has nevertheless reported useful results for particular locations by using somewhat different day and night models, based on surface values of relative humidity and temperature.

The standard deviations or accuracies of the determinations of the range error due to water vapor that have been achieved are about 2.0 cm, and there is interest in reducing this value, particularly for VLBI and geodynamics experiments.

The exact value of ΔR_2 in a particular case depends on the value of the integral appearing in Eq. (3.25), but an indication of the magnitude of ΔR_2 can be obtained by assuming an exponential decrease of N_2 with a scale height H of 2 km. It is of interest that the value obtained in this way is the same as if N_2 were constant up to the height H and zero beyond. Assuming a vapor density of ρ of 7.5 gm/m^3 at the surface and a temperature of 280 K, the corresponding values of e and N_2 at the surface are 9.70 mb and 46.15 respectively. Then for a vertical path

$$\Delta R_2 = 10^{-6} \int_0^\infty 46.15\ e^{-h/2000}\ dh$$

$$= 10^{-6}\ (46.15)\ (2000) = 0.0923\ \text{m}$$

$$= 9.23\ \text{cm}$$

An extreme value of ΔR_2, corresponding to the highest accepted weather-observatory values of e and ρ of 53.2 mb and 37.5 gm/m^3 at the temperature of 34°C and assuming an exponential decrease of N_2 with a scale height of 2 km, is 42.1 cm, along a vertical path.

Once a ΔR value is known, a corresponding phase angle or phase error $\Delta\phi$ can be determined by

$$\Delta\phi = \Delta R\beta = \Delta R \frac{2\pi}{\lambda} \tag{3.28}$$

where β is the phase constant and is equal to 2π divided by the wavelength λ. The doppler frequency error f_D associated with the range and phase errors is given by

$$f_D = \frac{1}{2\pi} \frac{\Delta\phi}{\Delta t} \tag{3.29}$$

where the rate of change of phase with time is involved. Thus f_D involves the rate of change of refractivity along the path in question. The value given by Eq. (3.29) may also depend in practice to some extent on the interval of time Δt used to measure $\Delta\phi$.

For paths at elevation angle θ of about 10° or greater, the range delay equals the vertical or zenith value divided by $\sin\theta$. That is

$$\Delta R(\theta) = \frac{\Delta R}{\sin\theta} \tag{3.30}$$

Table 3.3 shows values of $\Delta R(\theta)$ or range error for elevation angles of 0°, 5°, and 50°, based on the 1966 Standard Atmosphere for 45°N latitude in July and including an assumed humidity-profile model. These values represent total delay due to both the dry component of the air and water vapor. Note the large values of the range error for 0° and 5°.

The widely used constants provided by Smith and Weintraub (1953) have been employed for calculating refractivity in this chapter. When extreme precision is important, reference can be made to values provided by Thayer (1974).

REFERENCES

Bean, B. R. and E. J. Dutton, Radio Meteorology. Washington, DC: Supt. of Documents, U.S. Government Printing Office, 1966.

Bean, B. R., J. D. Horn, and A. M. Ozanich, Climatic Charts and Data of the Radio Refractive Index for the United States and the World, National Bureau of Standards Monograph 22. Washington, DC: Supt. of Documents, U.S. Government Printing Office, Nov. 25, 1960.

Bean, B. R., B. A. Cahoon, C. A. Samson, and G. D. Thayer, A World Atlas of Atmospheric Radio Refractivity, ESSA Monograph 1. Washington, DC: Supt. of Documents, U.S. Government Printing Office, 1966.

Berman, A. L., The Prediction of Zenith Range Refraction from Surface Measurements of Meteorological Parameters. Technical Report 32-1602, Jet Propulsion Laboratory, Pasadena, CA, July 15, 1976.

CCIR, "Radiometeorological data," Report 563-1, Vol. V, Propagation in Non-ionized Media, Recommendations and Reports of the CCIR, 1978, pp. 69-89. Geneva: Int. Telecomm. Union, 1978a.

CCIR, "Attenuation by atmospheric gases," Report 719, Vol. V, Propagation in Non-ionized Media, Recommendations and Reports of the CCIR, 1978, pp. 97-102. Geneva: Int. Telecomm. Union, 1978b.

Claflin, E. S., S. C. Wu, and G. M. Resch, "Microwave radiometer measurement of water vapor path delay: data reduction techniques", in DSN Progress Report 42-48, Jet Propulsion Laboratory, Pasadena, CA, Sept. and Oct. 1978.

Crane, R. K., "Refraction effects in the neutral atmosphere," in Methods of Experimental Physics, Vol. 12, Astrophysics, Part B: Radio Telescopes (M. L. Meeks, ed.), pp. 186-200. New York: Academic Press, 1976.

Flock, W. L., Electromagnetics and the Environment: Remote Sensing and Telecommunications. Englewood Cliffs, NJ: Prentice-Hall, 1979.

Flock, W. L., S. D. Slobin, and E. K. Smith, "Propagation effects on radio range and noise in earth-space telecommunications", Radio Science, vol. 17, pp. 1411-1424, Nov.-Dec. 1982.

GTE Lenkurt, Engineering Considerations for Microwave Communication Systems. San Carlos, CA: GTE Lenkurt, Inc., 1972.

Hall, M.P.M., Effects of the Troposphere on Radio Communications. Stevenage, UK and New York: Peter Peregrinus (on behalf of Institution of Electrical Engineers), 1979.

Hautefeville, M., A. W. Boyle, A. G. W. Timmers, and J. D. Shannon, "Duct fading - is Senegal an isolated case?", Telecom. Jour., vol. 47, pp. 517-525, 1980.

Hopfield, H. S., "Tropospheric effect on electromagnetically measured range: prediction from surface weather data," Radio Science, vol. 6, pp. 357-367, March, 1971.

List, R. J., Smithsonian Meteorological Tables, Sixth Revised Edition. Washington, DC: Smithsonian Institution, 1958.

Scorer, R., Air Pollution. Elmsford, New York: Pergamon, 1968.

Smith, E. K. and S. Weintraub, "The constants in the equation for atmospheric refractive index at radio frequencies," Proc. IRE, vol. 41, pp. 1035-1037, August 1953.

Staelin, D. H. et al., "Microwave spectroscopic imagery of the earth," Science, vol. 197, pp. 991-993, Sept. 2,1977.

Strickland, J. I., R. I. Olsen, and H. L. Werstivk, "Measurements on low angle fading in the Canadian Arctic," Ann. Telecomm., vol. 32, pp. 530-535. 1977.

Thayer, G. D., "An improved equation for the radio refractive index of air," Radio Science, vol. 9, pp. 803-807, Oct. 1974.

Theobold, D. M. and R. Kaul, "Prediction of signal fluctuations and low angle fading on earth-space paths," in Prediction of Millimeter Wave Propagation Effects on Earth-Space Paths (10-100 GHz),, ORI, Inc., Section IV, Greenbelt, Maryland: NASA Goddard Space Flight Center, 1978.

Thompson, M. C., L. E. Wood, H. B. Janes, and D. Smith, "Phase and amplitude scintillations in the 10 to 40 GHz band," IEEE Trans. on Antennas and Propagation, vol. AP-23, pp. 792-797, Nov. 1975.

U.S. Standard Atmosphere, 1976, sponsored by NOAA, NASA, USAF. Washington, DC: Supt. of Documents, U.S. Government Printing Office, 1976.

VanVleck, J. H., "Theory of absorption by uncondensed gases", in Propagation of Short Radio Waves, Vol. 13, Radiation Laboratory Series (D. E. Kerr, ed.), pp. 646-664. New York: McGraw-Hill, 1951.

Waters, J. W., "Absorption and emission by atmospheric gases," in Methods of Experimental Physics, Vol. 12, Astrophysics, Part B: Radio Telescopes (M.L. Meeks, ed.), pp. 142-176. New York: Academic Press, 1976.

Weisbrod, S. and L. J. Anderson, "Simple methods for computing tropospheric and ionospheric refractive effects on radio waves," Proc. IRE, vol. 47, pp. 1770-1777, Oct. 1959.

Wu, S. C., "Frequency selection and calibration of a water vapor radiometer," in DSN Progress Report 42-43, Jet Propulsion Laboratory, Pasadena, CA, pp. 67-81, Nov. and Dec., 1977.

APPENDIX 3.1

RELATION BETWEEN WATER VAPOR PRESSURE AND DENSITY

The perfect gas law in the form applying to one molecular weight of gas is

$$pv = RT \tag{A 3.1}$$

where p is pressure, v is specific volume, R is the gas constant, and T is temperature in kelvins. To obtain density ρ in kg/m^3 use

$$\rho = \frac{M}{v} = \frac{pM}{RT} \tag{A 3.2}$$

where M is the mass of a kg mol. Using SI units throughout and setting p = e N/m^2 or Pa, M = 18 kg, and R = 8.3142×10^3 J/(K kg mol), one obtains

$$\rho = \frac{e\ 18}{8.3143 \times 10^3\ T} = \frac{2.165 \times 10^{-3}\ e}{T}\ kg/m^3 \tag{A 3.3}$$

If e is to be expressed in mb, however, rather than N/m^2 (Newtons/m^2)

$$\rho = \frac{e\ (18)\ (100)}{8.3143 \times 10^3\ T} = \frac{0.2165\ e}{T} \tag{A 3.4}$$

(Total level pressure in a standard atmosphere is 1013 mb or 1.013×10^5 N/m^2).

Finally for ρ in gm/m^3

$$\rho = \frac{216.5\ e}{T}\ gm/m^3 \tag{A 3.5}$$

In using SI units for M and R, we follow the usage of the U.S. Standard Atmosphere (1976), for example.

CHAPTER 4

ABSORPTION, SCATTER, AND CROSS POLARIZATION CAUSED BY PRECIPITATION

4.1 ATTENUATION BASED ON RAYLEIGH AND MIE SCATTERING

Raindrops cause attenuation of radio waves by both absorption and scatter. Absorption involves dissipation of some of the energy of an electromagnetic wave as heat. Scatter involves diversion of some of the energy of the wave into directions other than the forward direction. In the case of a beam of electromagnetic radiation, for example, it is said that energy is scattered out of the beam. The term extinction is applied to the sum of absorption and scatter. Attenuation constants can be defined for absorption, scatter, and extinction such that

$$\alpha_{ext} = \alpha_{abs} + \alpha_{sca} \tag{4.1}$$

where the α's are attentuation constants and can be identified by their subscripts.

Analysis of absorption and scatter by rain drops has often been based upon the assumption of a spherical drop shape. For drops that are small compared to wavelength, the theory of Rayleigh scattering tends to apply, and for drops that have sizes comparable to wavelength the more complicated Mie scattering theory, or refinements of it, must be used. The frequency range over which Rayleigh scattering applies is further restricted below what would be predicted on the basis of raindrop size alone by the lossy nature of raindrops which is responsible for absorption.

A further complication is that the shapes of the larger drops are not spherical. Drops with radii $\leq$ 170 μm are essentially spherical, whereas drops with radii between 170 and 500 μm are closely approximated by oblate spheroids. (An oblate spheroid is formed by rotating an ellipse about its shortest axis.) Between 500 and 2000 μm, drops are deformed into asymmetric oblate spheroids with increasingly flat bases, and drops $\geq$ 2000 μm develop a concave depression in the base which is more pronounced for larger drop sizes (Pruppacher and Pitter, 1971). The ratio of the minor to major axes of oblate

spheroidal drops is equal to 1-a, where a is the radius in cm of a spherical drop having the same volume. Figure 4.1 shows an example of the shape of a large drop.

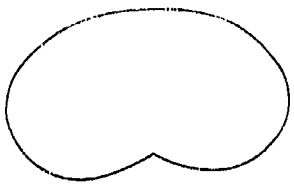

Figure 4.1. Form of a large raindrop (Pruppacher and Pitter, 1971).

The total or extinction power-density attentuation constant α_p for rain can be expressed as

$$\alpha_p = \int_a N(a)\, C_{ext}\left(n_c, \frac{a}{\lambda_o}\right) da \qquad (4.2)$$

where a is drop radius, n_c is the complex index of refraction of water (which varies with temperature), and λ_o is wavelength in air. C_{ext} is an extinction coefficient which is a function of n_c and a/λ_o. $N(a)\,da$ (having units of $1/m^3$) represents the number of drops per unit volume in the size interval da and is determined by the distribution of drop sizes which is a function of precipitation rate. Distributions of drop sizes have been determined empirically, the most widely used and tested distribution being the Laws and Parson (1943) distribution. The Marshall and Palmer (1948) distribution is also well known. The Laws and Parsons data (Table 4.1) obtained by collecting raindrops in pans of flour do not provide N(a) da, but M(a) da, the fraction of the total volume of water striking the ground due to drops of a given size. To determine N(a) da, one must use M(a) da and also v(a), the limiting terminal velocity of raindrops, in

$$N(a)\,da = \frac{M(a)\,da\,R}{v(a)\,a^3\,15.1} \tag{4.3}$$

Here R is the precipitation rate in mm/h, v(a) is in m/s, a is in cm, M(a) da is nondimensional, and N(a) da is the number of drops per m^3 in the size interval da. The Laws and Parsons data utilizes a finite value of da of 0.025 cm and Eq. (4.2) is evaluated in practice when using this distribution as a summation instead of as an integral. Values of v(a) are given in Fig. 4.2.

The Marshall and Palmer distribution made by making measurements of raindrops on dyed filter papers has the form of

$$N(R, a) = N_0\, e^{-Ca} \tag{4.4}$$

where R is rain rate and a is drop radius. N and N_0 are sometimes stated in units of cm^{-4}, corresponding to the number of drops per cm^3 in a size range of 1 cm in radius. In these units, N_0 has the value of 0.16. If a is in cm and R in mm/h

$$C = 82\, R^{-0.21} \tag{4.5}$$

The number of drops in a volume V, in units of cm^3, having radii between a and a + da is given by N da V. The Laws and Parsons distribution also can be approximated by an equation of the form of Eq. (4.4).

The determination of C_{ext} is usually based upon the Mie scattering theory for spherical drops (Kerr, 1951; Kerker, 1969; Zufferey, 1972). C_{ext} has the form of

$$C_{ext}\left(n_c,\ \frac{a}{\lambda_0}\right) = \frac{\lambda_0^2}{2\pi}\ \mathrm{Re} \sum_{n=1}^{\infty} (2n+1)\,(a_n + b_n) \tag{4.6}$$

where λ is wavelength in air and a_n and b_n are coefficients involving spherical Bessel and Hankel functions of complex arguments. C_{ext} and S_0, which gives the amplitude of the forward scattered wave, are related by

$$C_{ext}\left(n_c,\ \frac{a}{\lambda_0}\right) = \frac{4\pi}{\beta_0^2}\ \mathrm{Re}\ S_0\left(n_c,\ \frac{a}{\lambda_0}\right) \tag{4.7}$$

where β_0 is the phase constant $2\pi/\lambda_0$.

Table 4.1 Laws and Parsons Distribution Giving the Percent of Volume Reaching Ground Contributed by Drops of Various Sizes*.

Drop Radius Limits, a(mm)	Rain Rate, mm/h							
	0.25	1.25	2.5	12.5	25	50	100	150
0-0.125	1.0	0.5	0.3	0.1				
0.125-0.375	27.0	10.4	7.0	2.5	1.7	1.2	1.0	1.0
0.375-0.625	50.1	37.1	27.8	11.5	7.6	5.4	4.6	4.1
0.625-0.875	18.2	31.3	32.8	24.5	18.4	12.5	8.8	7.6
0.875-1.125	3.0	13.5	19.0	25.4	23.9	19.9	13.9	11.7
1.125-1.375	0.7	4.9	7.9	17.3	19.9	20.9	17.1	13.9
1.375-1.625		1.5	3.3	10.1	12.8	15.6	18.4	17.7
1.625-1.875		0.6	1.1	4.3	8.2	10.9	15.0	16.0
1.875-2.125		0.2	0.6	2.3	3.5	6.7	9.0	11.9
2.125-2.375			0.2	1.2	2.1	3.3	6.8	7.7
2.375-2.625				0.6	1.1	1.8	3.0	3.6
2.625-2.975				0.2	0.5	1.1	1.7	2.2
2.875-3.125					0.3	0.5	1.0	1.2
3.125-3.375						0.2	0.7	1.0

*Drop radius interval, da = 0.25 cm. Multiply percentage values by 0.01 to obtain M(a) da, e.g. for 50 mm/h and 1.125-1.375 mm M(a) da = 0.209.

After J.O. Laws and D.A. Parsons, "The Relation of Drop Size to Intensity," Transactions of the American Geophysical Union, pp. 452-460, 1943.

For frequncies of about 3 GHz and less, the "Rayleigh approximation" can be used instead of the Mie theory. For this case, C_{ext} takes the simple form of

$$C_{ext} = \frac{4\pi^2 a^3}{\lambda_o} \frac{6K_i}{(K_r + 2)^2 + K_i^2} \tag{4.8}$$

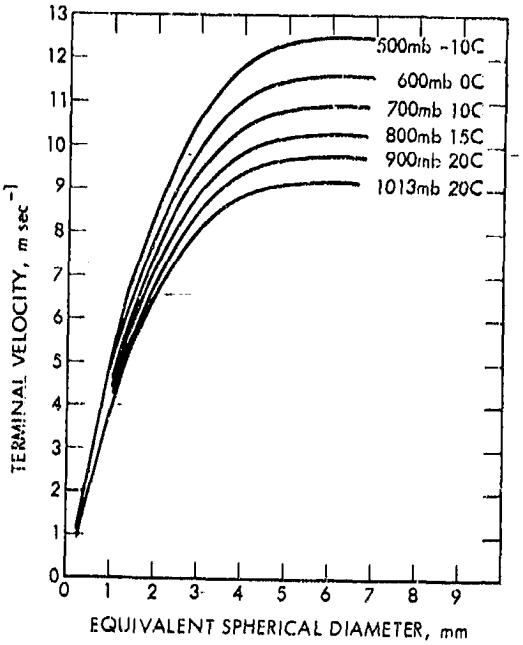

Figure 4.2. Terminal velocity of raindrops at six pressure levels in a summer atmosphere as a function of the equivalent spherical diameter. (From Beard, "Terminal Velocity and Shape of Cloud and Precipitation Drops Aloft," Journal of the Atmospheric Sciences, May 1976.) The pressures of 1013, 900, 800, 700, 600, and 500 mb correspond roughly to altitudes of 0, 975, 1950, 3000, 4200, and 5600 m of the U.S. Standard Atmosphere, 1976.

where a is drop radius, λ_0 is wavelength, K_i is the imaginary part of the relative dielectric constant of water, and K_r is the real part. As $n_c^2 = K_c$ where n_c is complex index of refraction and K_c is complex relative dielectric constant, values of K_r and K_i can be determined from knowledge of n_c. For λ_0 = 10 cm, K_r is 78.45 and K_i is 11.19 at 20°C.

Rather than calculating the attentuation constant by use of Eq. (4.2), an effective or bulk index of refraction m_c can be determined for a medium consisting of water drops in empty space (using m for the index of refraction of the medium to distinguish from n, the index of refraction of water). The index m_c is given in terms of the forward scattering function S_0 by

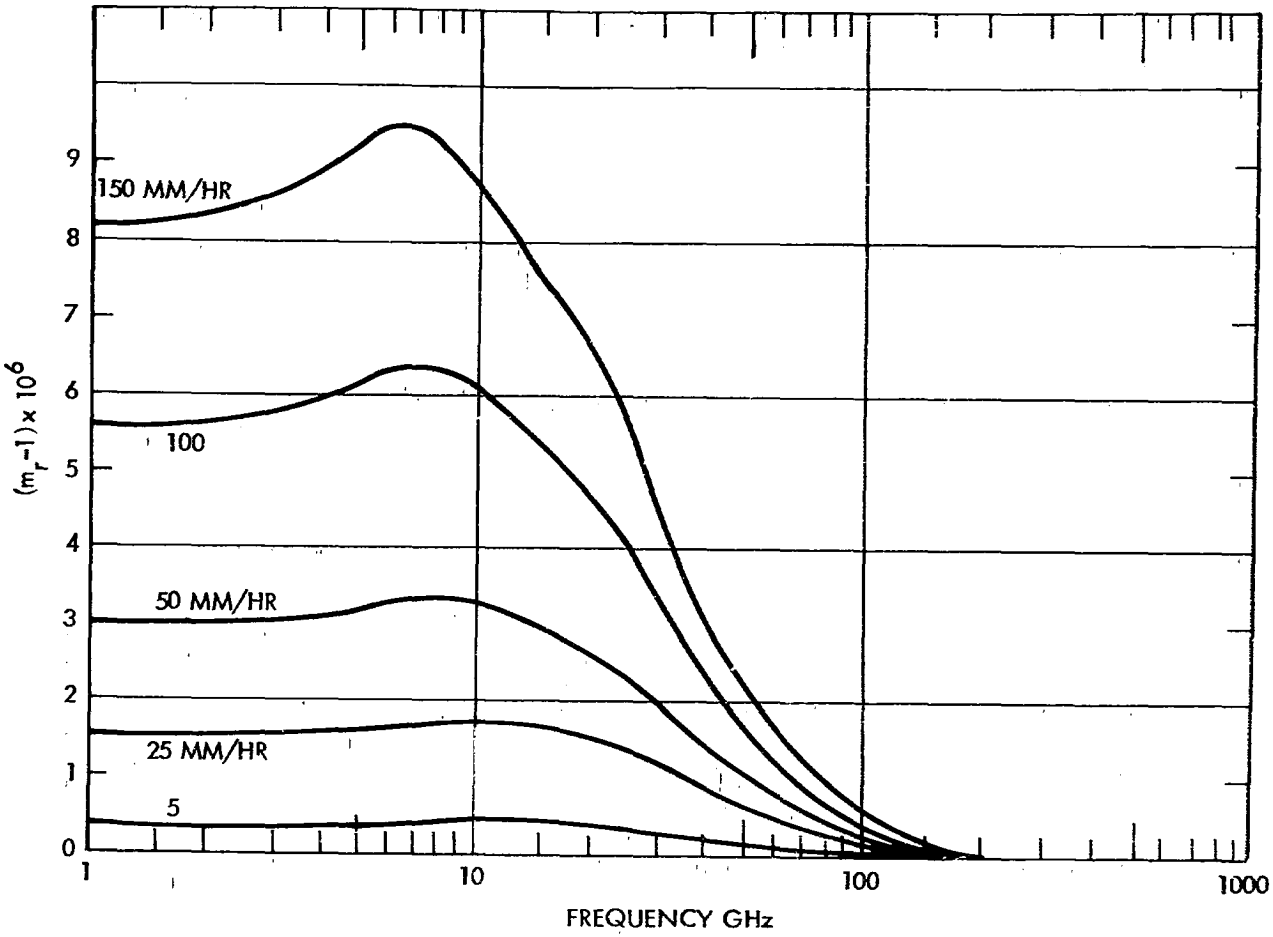

Figure 4.3a. The real part m_r minus unity of the complex index of refraction multiplied by 10^6 $[(m_r-1) \times 10^6]$, for a medium consisting of water drops in empty space for a temperature of 20°C and a Laws and Parsons distribution (Zufferey, 1972).

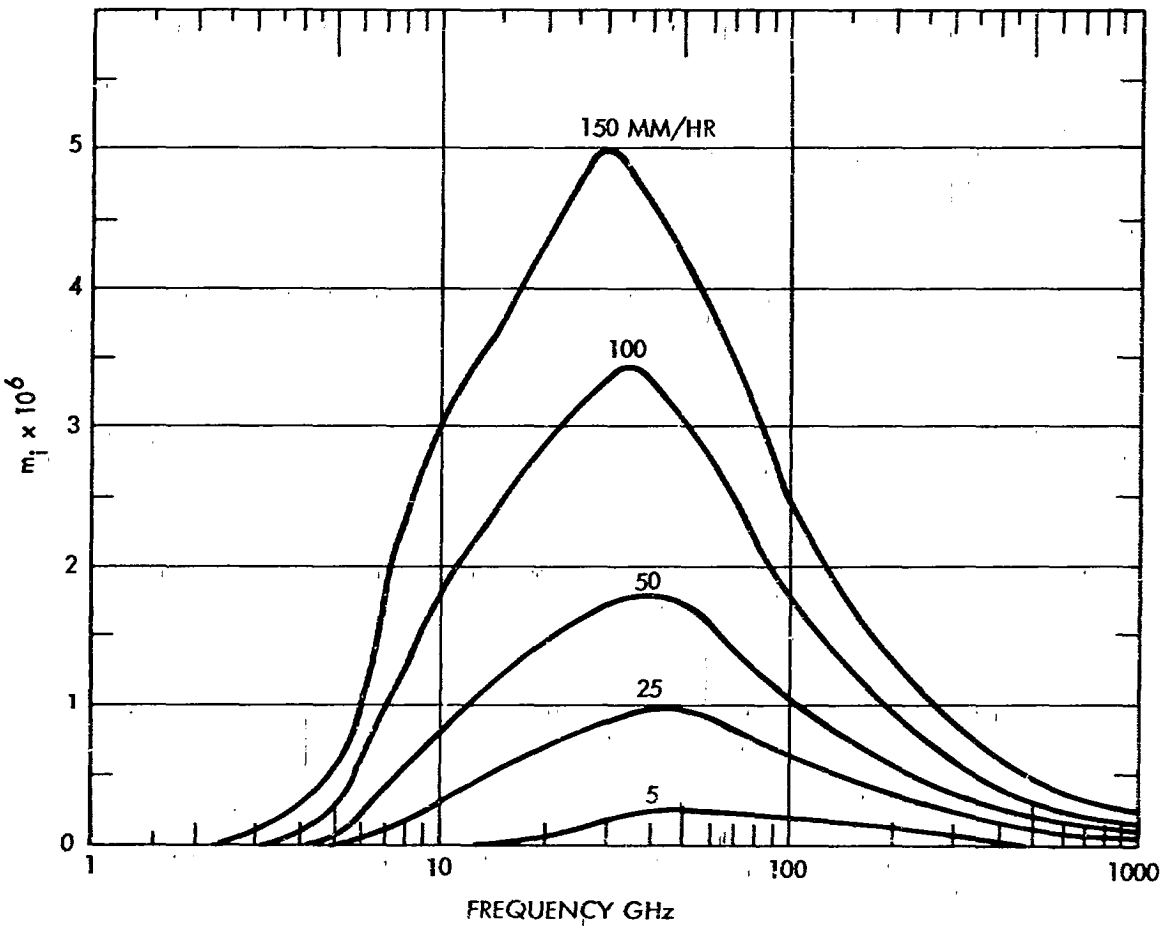

Figure 4.3b. The imaginary part m_i of the complex index of refraction multiplied by 10^6 ($m_i \times 10^6$) for the same medium (Zufferey, 1972).

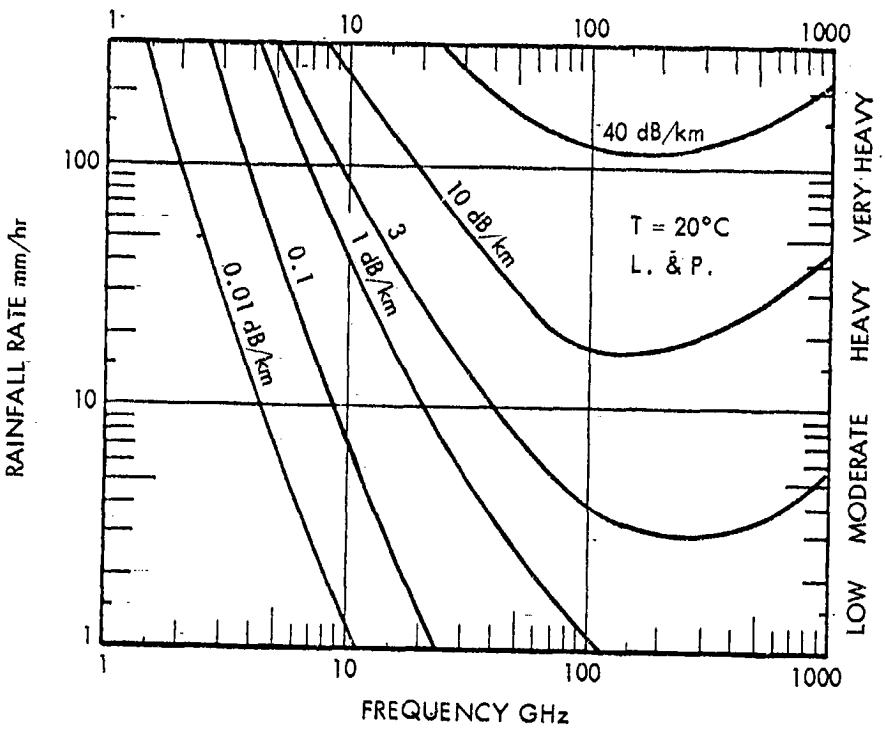

Figure 4.4. Rain rate versus frequency for specific values of attenuation constant (Zufferey, 1972).

$$m_c - 1 = j \frac{2\pi}{\beta_0^3} \int_a N(a)\, S_0\left(n_c, \frac{a}{\lambda_0}\right) da \qquad (4.9)$$

The approach using an effective index of refraction has been discussed by van de Hulst (1957) and Kerker (1969), but early consideration of the concept is attributed by Kerker to an 1899 paper by Rayleigh and 1890 and 1898 papers by Lorenz. The real part of the complex index determines the phase shift due to rainfall and the imaginary part of the index determines attenuation, the relation being that

$$\alpha = \beta_0 m_i \quad \text{Np/m} \qquad (4.10)$$

where α is the field-intensity attentuation constant in Nepers per m, β is $2\pi/\lambda_0$, and m_i is the imaginary part of the refractive index. To obtain the attentuation constant in dB/m multiply the value of α from Eq. (4.10) by 8.68 and to obtain the value in dB/km multiply also by 1000. (Alternatively, one can obtain a power-density attenuation coefficient by using $\alpha_p = 2\,\beta_0\, m_i$ and then multiplying by 4.34 to obtain attenuation in dB/m.)

Values of the real and imaginary parts of the complex index of refraction are shown in Fig. 4.3a and b. The values of m_i can be used to estimate the attenuation constant by use of Eq. (4.10). Plots of rainfall rate versus frequency for specific values of the attenuation constant are given in Fig. 4.4. These curves show that attenuation increases with rainfall rate and frequency, up to about 100 GHz or more.

4.2 EMPIRICAL RELATIONS BETWEEN RAIN RATE AND ATTENUATION

Values of the attenuation constant can be calculated as a function of frequency and rain rate by use of the Mie theory of the previous section, and empirical relations between rain rate and attenuation have also been developed. These relations have the form of

$$\alpha_p = a(f)\, R^{b(f)} \text{ dB/km} \qquad (4.11)$$

where a and b represent values which are a function of frequency, f, and R is rain rate. First observation of a relation of this type, but with b = 1, is credited to Ryde (1946). Values of a(f) and b(f) have since been determined by several workers including Zufferey (1972) who gave sets of values for light and heavy rain, the dividing line being taken as 10 mm/h. Olsen, Rogers, and Hodge (1978) have analyzed the relation thoroughly and derived tables of values of a(f) and b(f) for the Laws and Parsons and Marshall-Palmer distributions and for the drizzle and thunderstorm distributions of Joss. For the Laws and Parsons distributions they made separate determinations for the low rain rate values of 1.27, 2.54, 12.7, 25.4, and 50.8 mm/h (designating these values by LP_L) and for the high rain rates of 25.4, 50.8, 101.6, and 152.4 mm/h (designated by LP_H). The tables of Olsen, Rogers, and Hodge include the range from 1 to 1000 GHz for temperatures of 0^oC, 20^oC, and -10^oC. Values for frequencies of 15 GHz and lower for $T = 0^oC$ are given in Table 4.2 for the LP_L and LP_H rain rates.

Figure 4.5 shows values of attenuation constant as given in CCIR Report 721 (CCIR, 1978a) with credit to Olsen, Rogers, and Hodge. Values of a and b have also been provided by Crane (1966) on the basis of the Laws and Parsons distribution. His values for frequencies of 15 GHz and lower are given in Table 4.3.

In addition estimates of the attenuation constant for frequencies below 10 GHz can be taken from Fig. 4.4. For frequencies of 3 GHz or less values of the attenuation constant can be calculated by using Eq. (4.8) for C_{ext}.

Interest in attenuation due to rain tends to be concentrated at the higher frequencies above 10 GHz where the attenuation is the greatest, but the plots of Figs. 4.4 and 4.5 extend below 10 GHz as well. The values from the two figures are in general agreement, both showing that for frequencies of 10 GHz or less and rainfall rates of 100 mm/h or less, the attenuation constant has a value of about 3 dB/km or less. Attenuation constants of this order of magnitude, while less than for higher frequencies, may still be

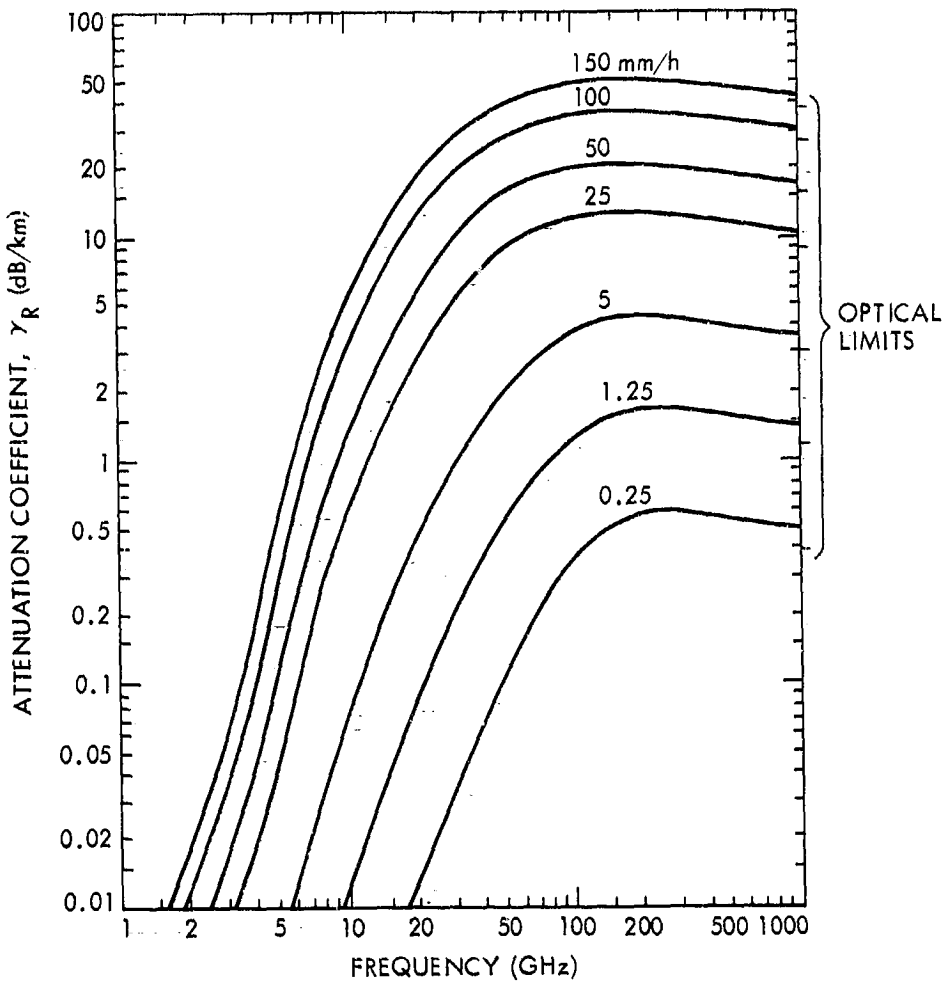

Figure 4.5. Attenuation constant as a function of rain rate and frequency (CCIR, 1978a).

Table 4.2 Values of a and b of Eq. (4.11) from Olsen, Rogers, and Hodge (1978) for T = 0°C and for Laws and Parsons Low and High Rain Rates.

Freq. (GHz)	a		b	
	LP_L	LP_H	LP_L	LP_H
1.0	6.41×10^{-5}	5.26×10^{-5}	0.891	0.947
1.5	1.45×10^{-4}	1.14×10^{-4}	0.908	0.976
2.0	2.61×10^{-4}	1.96×10^{-4}	0.930	1.012
2.5	4.16×10^{-4}	2.96×10^{-4}	0.955	1.054
3.0	6.15×10^{-4}	4.12×10^{-4}	0.984	1.100
3.5	8.61×10^{-4}	6.42×10^{-4}	1.015	1.150
4.0	1.16×10^{-3}	6.84×10^{-4}	1.049	1.202
5.0	1.94×10^{-3}	1.12×10^{-3}	1.113	1.274
6.0	3.05×10^{-3}	1.99×10^{-3}	1.158	1.285
7.0	4.55×10^{-3}	3.36×10^{-3}	1.180	1.270
8.0	6.49×10^{-3}	5.35×10^{-3}	1.187	1.245
9.0	8.88×10^{-3}	8.03×10^{-3}	1.185	1.216
10	1.17×10^{-2}	1.14×10^{-2}	1.178	1.189
11	1.50×10^{-2}	1.52×10^{-2}	1.171	1.167
12	1.86×10^{-2}	1.96×10^{-2}	1.162	1.150
15	3.21×10^{-2}	3.47×10^{-2}	1.142	1.119

Table 4.3 Parameters for Computing Attenuation Constant for 0°C, Laws and Parson Distribution (Crane, 1966).

f - GHz	a(f)	b(f)
1	0.00015	0.95
4	0.00080	1.17
5	0.00138	1.24
6	0.00250	1.28
7.5	0.00482	1.25
10	0.0125	1.18
12.5	0.0228	1.145
15	0.0357	1.12

serious, and concern about attenuation due to rain is thus not confined to the higher frequencies but includes all of the X-band (8-12 GHz). Attenuation in the S-band (2-4 GHz) is usually not a serious problem on earth-space paths unless the elevation angle is very small but may nevertheless need to be taken into account.

Attenuation due to rain increases the loss factor L, appearing in equations describing system performance and determining signal-to-noise ratio (Sec. 1.1). It should be kept in mind also that rain increases the system noise temperature, T_{sys}, as well. The increase in T_{sys} may play a more important role in reducing the signal-to-noise ratio than the increase in L for systems having low values of T_{sys}. This consideration is discussed further in Chap. 7.

4.3 STATISTICAL ANALYSIS OF ATTENUATION DUE TO RAINFALL

Procedures for calculating the attenuation constant for propagation through rain as a function of rain rate have been considered in previous sections. For describing the expected attenuation along an earth-space path, however, one needs to model the occurrence of rain along the path and needs to

know the length of path that is exposed to rain. Furthermore the data may be needed in statistical form. The statistical data are usually presented as plots showing the percentage of time that rainfall rates are exceeded.

4.3.1 Rainfall Data

A first step in developing an understanding of the effect of rainfall on propagation in a particular area may be to obtain raw data on the occurrence of rainfall there. When sufficient raw data have been accumulated, it can be put into statistical form.

Published data on rain are available for the United States from the National Climatic Center (Asheville, North Carolina 28801) of the National Weather Service. They supply Hourly Precipitation Data, issued monthly by state (including monthly maximum rainfalls for periods as short as 15 min for a number of stations in each state); Climatological Data, issued monthly by state (includes daily precipitation amounts); Climatological Data - National Summary, issued monthly (includes monthly rainfall and greatest rainfall in 24h); Climatological Data - Annual Summary (includes maximum rainfalls in periods ranging from 5 to 180 minutes); Local Climatological Data, issued monthly (includes hourly rainfall for individual weather stations); and Storm Data, published monthly for the United States. In Canada Monthly Records for Western Canada, Northern Canada, and Eastern Canada and a monthly Canadian Weather Review are available from Supply and Services Canada, Publishing Centre (Hull, Quebec KDA 059). Data for a number of other countries are on file at the National Weather Service Library, Room 816, Gramax Bldg., 13th Street, Silver Spring, MD.

Rain gauges are the means used for obtaining most of the National Weather Service rain data. A common type of gauge is supported in a vertical position and has a receiving area ten times the cross section of the measuring tube to facilitate precision in measurement. The amount of precipitation is determined by use of a hardwood measuring stick. Automatic tipping-bucket and universal weighing gauges are in use at National Weather Service stations that are manned by their own personnel (First Order Weather Stations), and chart records from these gauges can be obtained from the National Climatic Center.

If it is deemed advisable to obtain additional data on rainfall and/or attenuation due to rainfall because of a lack of detailed published data, a variety of options are available if sufficient support and time can be justified. One can set up their own rain gauges of the tipping bucket or weighing type. Radar can monitor precipitation over a wide area using the concepts discussed in Sec. 4.5 for bistatic scatter. For monostatic radar the distances R_1 and R_2 are the same, however, and the scattering volume V is proportional to R^2 for widespread rain, so the ratio of W_R/W_T is proportional to $1/R^2$ as shown in Eq. 4.12 (Flock, 1979).

$$\frac{W_R}{W_T} = \frac{G^2 \theta_{HP} \phi_{HP} c\tau \pi^3}{1024 (\ell n 2) R^2 \lambda^2} \left|\frac{K_c - 1}{K_c + 2}\right|^2 Z \qquad (4.12)$$

G is the radar antenna gain, θ_{HP} and ϕ_{HP} are the half-power beamwidths of the antenna, c is about 3×10^8 m/s, τ is the radar pulse length, λ is wavelength, and K_c is the complex relative dielectric constant of water. Z is $\Sigma\, d^6$ where d is drop diameter and is related to the rain rate R by $Z = 400\, R^{1.4}$ for the Laws and Parsons distribution and $Z = 200\, R^{1.6}$ for the Marshall and Palmer distribution. See Sec. 4.5 for further discussion of the basis for this relation that allows estimating R over the radar coverage area.

Another approach to measuring attenuation due to rain on earth-space paths is to use radiometer techniques. One procedure of this type involves using the Sun as a source. When a source having an effective temperature T_s is viewed through an absorbing medium having an effective temperature of T_i, the observed brightness temperature T_b is given by

$$T_b = T_s e^{-\tau} + T_i (1 - e^{-\tau}) \qquad (4.13)$$

where τ is referred to as optical depth and is the integral of the power-density attenuation coefficient along the path ($\int \alpha_p \, d\ell$). The temperatures of Eq. (4.13) are measures of power, as $k T_b B$, where k is the Boltzmann constant and B is bandwidth, is power. The first term on the right-hand side of Eq. (4.13) represents the power from the Sun attenuated by the Earth's atmosphere, and the second term represents thermal noise emitted by the Earth's atmos-

phere. The Sun subtends an angle of 0.5° viewed from the Earth, and if the antenna of the radiometer is perfectly aligned with the Sun and the Sun fills the beam, T_s is the effective brightness temperature of the Sun. Otherwise T_s is the average brightness temperature within the antenna beamwidth, as determined by the temperature of the Sun itself and the low background level of about 2.7 K.

The object of using Eq. (4.13) is to determine τ due to rain. This can be accomplished by first using the Sun as a source and then switching away from the Sun. The difference between the two values of T_b obtained in this way is $T_s\, e^{-\tau}$ and if T_s is known then τ is known. The temperature T_s can be determined by using the Sun as a source when no rain is present. (Some attenuation due to the gaseous constituents of the atmosphere may need to be taken into account as well.)

If the value of T_i of Eq. (4.13) can be determined then it is not necessary to use the Sun as a source. Instead one can point away from the Sun and record

$$T_b = T_i\,(1 - e^{-\tau}) \tag{4.14}$$

from which τ can be determined. T_i can be determined originally from measurements utilizing the Sun. T_i is in general less than the physical temperature of the volume of the sky where rain is falling because total attenuation is due to scattering as well as absorption. Eq. (4.14) can only be used with T_i equal to actual temperature when attenuation is due to absorption alone.

Data on attenuation due to rain, rather than on rain rate, have been obtained by several means. An advantageous procedure for obtaining data on earth-space paths is to use beacon signals on satellites. NASA has sponsored an extensive program of study of attenuation due to rain by this means, mostly at frequencies above 10 GHz (Bostian et al., 1979; Ippolito, 1978; Kaul, Rogers, and Bremer, 1977; Vogel, 1979). The Bell Laboratories (Hogg and Chu, 1975, Cox et al., 1980), COMSAT (Harris and Hyde, 1975) and other agencies have been active as well. CCIR Report 564-1 includes a summary of measurements using ATS satellites (CCIR, 1978b).

4.3.2 Effective Path Length

Two considerations about the length of the path through rain on earth-space links are as follows:

1. The average rain rate R along a path through a region where rain is falling tends to differ from the instantaneous point rain rate R_p, and this difference should be taken into account in estimating total attenuation along a path. One approach is to set $R = r R_p$ where R and R_p have the same probability of occurrence and r is an effective path average factor which must be determined empirically. Based largely upon modeling of data for the C, D, and E rain rate regions of Figs. 4.8 and 4.9, an expression for r, apparently applicable primarily to those regions, has been developed (CCIR, 1978c). The expression has the form of

$$r = \gamma(D)\, R_p^{-\delta(D)} \tag{4.15}$$

where D is the horizontal projection of the path through rain. Application of Eq. (4.15), using values of $\gamma(D)$ and $\delta(D)$ determined empirically, yields the plots of Fig. 4.6. The horizontal projection D is related to path length L through the rain by $D = L \cos\theta$ where θ is the elevation angle of the path. The product Lr can be regarded as an effective path length. Also R can be regarded as an average rain rate, and the process of determining r can be referred to as path averaging.

2. Temperature decreases with height and above the 0°C isotherm precipitation tends to occur as snow rather than rain. Snow causes considerably less attenuation than rain, and it is the length of the path up to the 0°C isotherm that largely determines attenuation due to precipitation. (Liquid drops are more strictly confined below the 0°C isotherm for light rains than for heavy rains). For $\theta \geq 10°$ the path length L can be taken to be equal to the height H of the 0°C isotherm above the surface divided by the sine of the elevation angle or

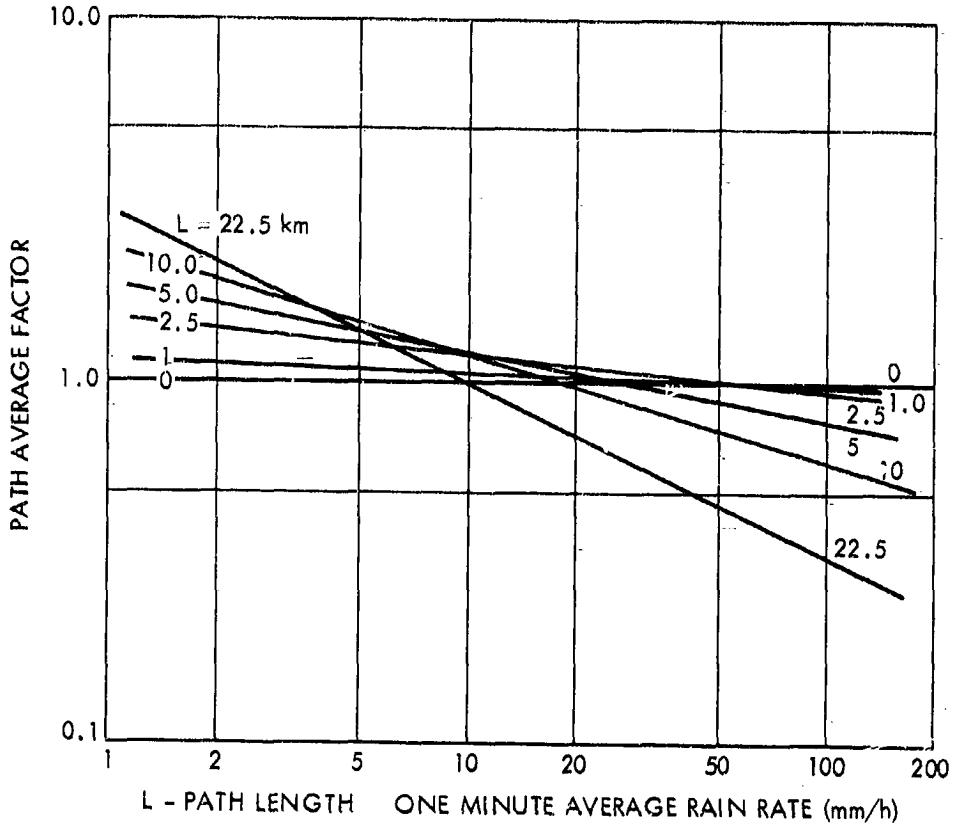

Figure 4.6. Effective path average factor for different path lengths and rain rates (CCIR, 1978c).

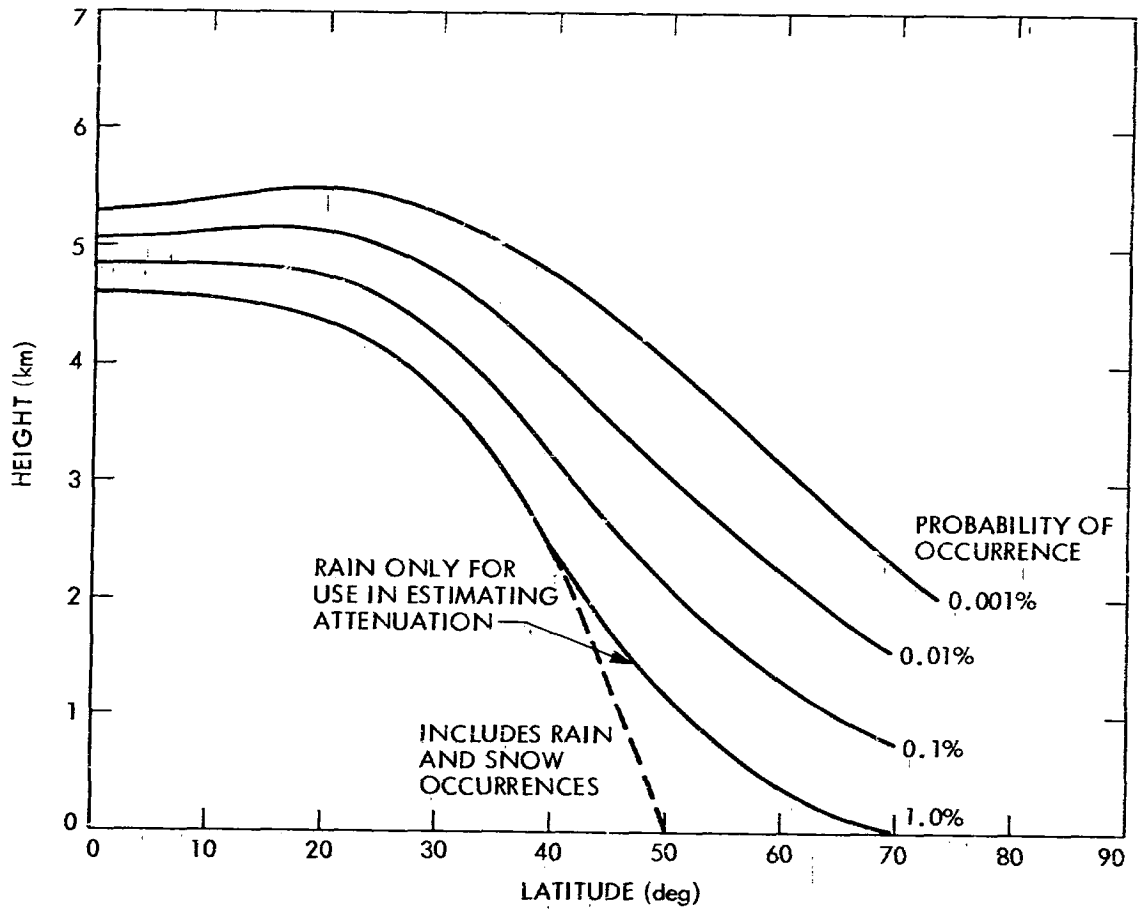

Figure 4.7. Heights of 0°C isotherms (Crane, 1980). See Fig. 9.11 and the related discussion (Step 3 of Sec. 9.4.2.1) for a proposed modification for latitudes below 40°.

$$L = \frac{H}{\sin \theta} = \frac{H_0 - H_g}{\sin \theta} \qquad (4.16)$$

where H_0 is the height of the 0°C isotherm and H_g is the height of the surface. The height of the 0°C isotherm H_0 varies with latitude and meteorological conditions. Figure 4.7 shows values of H_0 as a function of latitude and probability of occurrence.

A variety of procedures or methods have been used for determining an effective path length. In comparing the various approaches, Kaul, Wallace, and Kinal (1980) have determined that, for an elevation angle of 45° and a latitude of 40°N, an effective path length between 4 and 5 km is reasonable.

4.3.3 Models of Attenuation Due to Rain

Several statistical models of attenuation due to rain have been developed and refined and updated from time to time. The goal of the models is to provide statistical descriptions of attenuation but for this purpose one can use data on rainfall or attenuation or a combination of both. When data on rainfall are used as the data base, values of attenuation can be calculated from the rainfall data.

For locations of First Order Weather Stations in the United States and for locations having similar records elsewhere, data are available to provide reasonably satisfactory statistical descriptions of rainfall. Earth stations, however, may be located elsewhere than where weather stations are found, and it is thus desirable to divide the Earth into regions having similar rainfall characteristics and to attempt to obtain statistical descriptions of these characteristics. Selection of regions can be done on a large scale in rough accordance with the natural regions of the Earth (Sec. 1.4). A number of variations of such classifications exist. They agree generally on principal features but may disagree on detail and terminology. It has been suggested, however, that classifications made from biological, geographical, or agricultural viewpoints may need some modifications for telecommunications purposes (Segal, 1980). Figure 4.8 and 4.9 show the regions used in the Crane (1980) global model, and Fig. 4.10 shows the regions used in Canada.

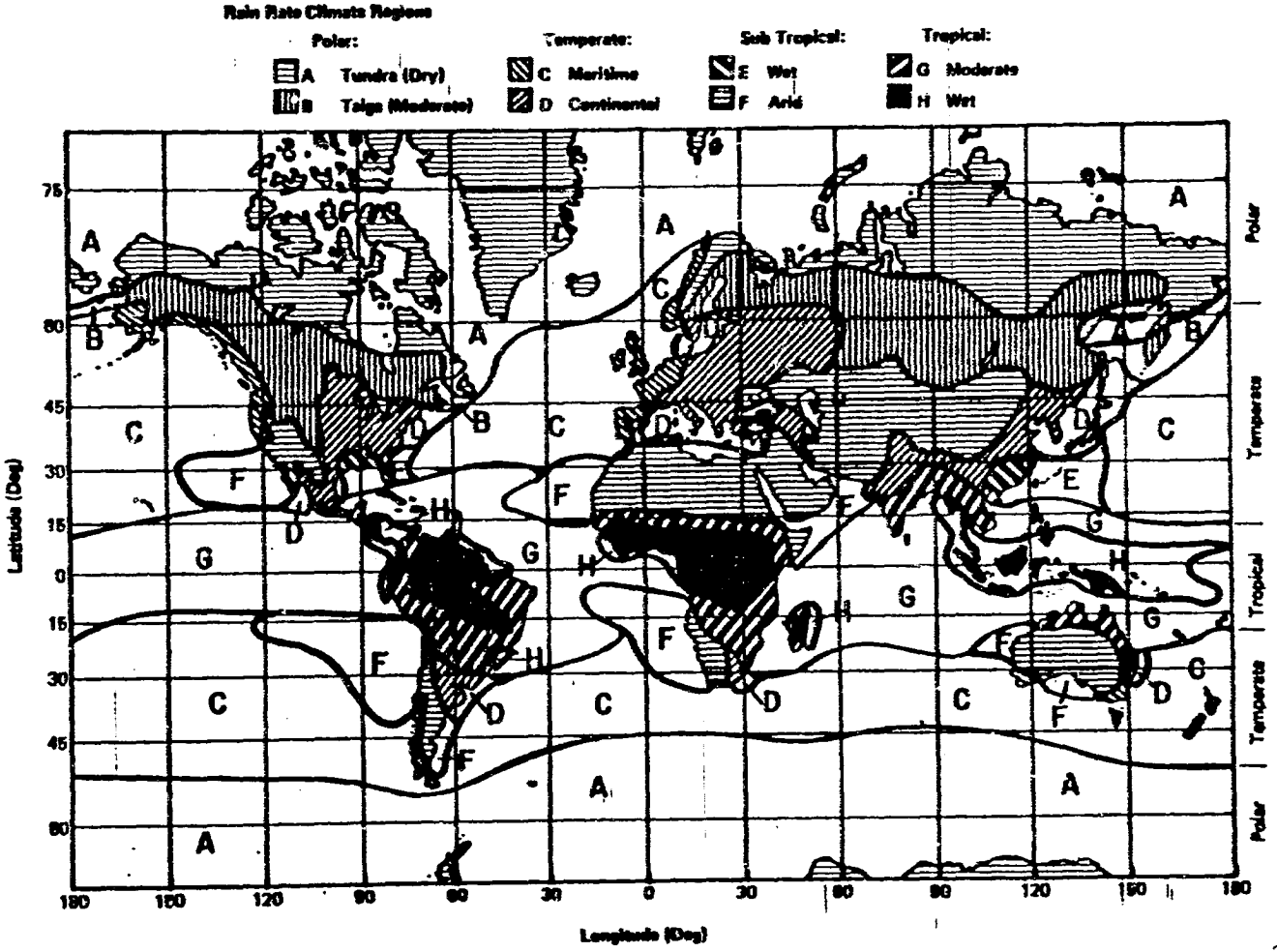

Figure 4.8. Global rain rate regions (Crane, 1980).

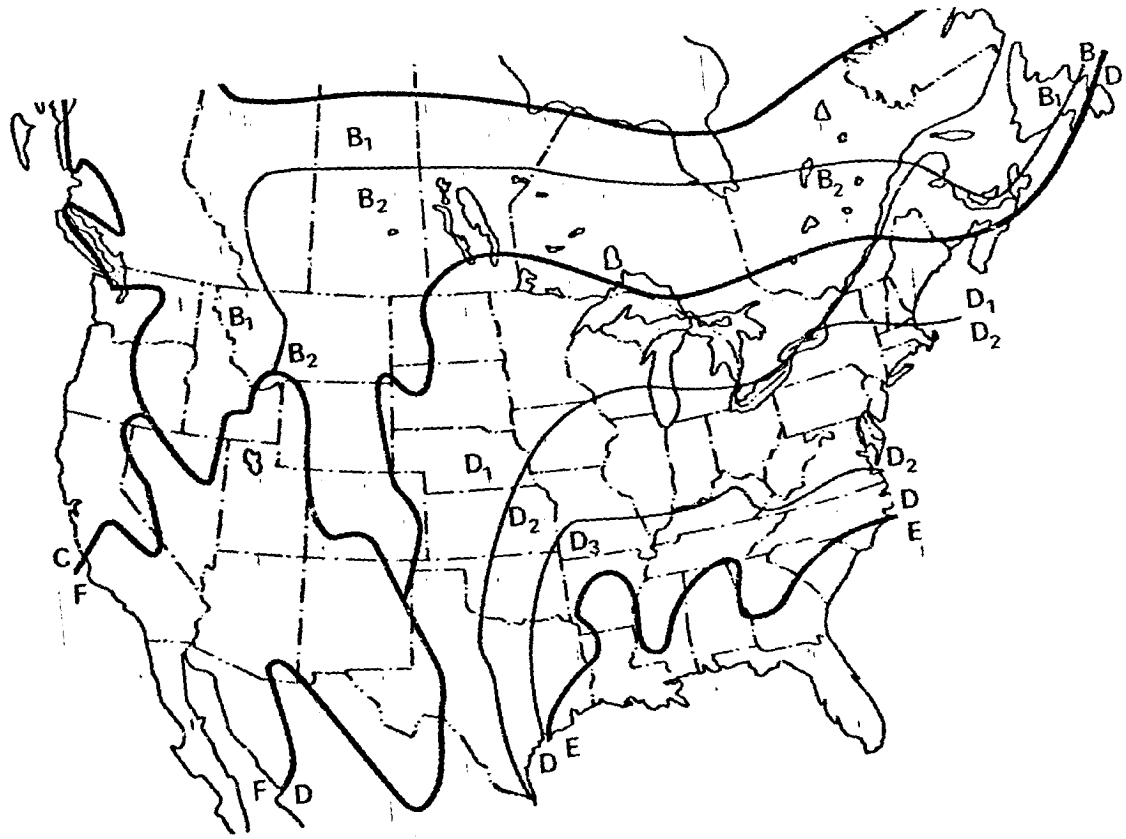

Figure 4.9. Rain rate regions of United States, as used in global model (Crane, 1980).

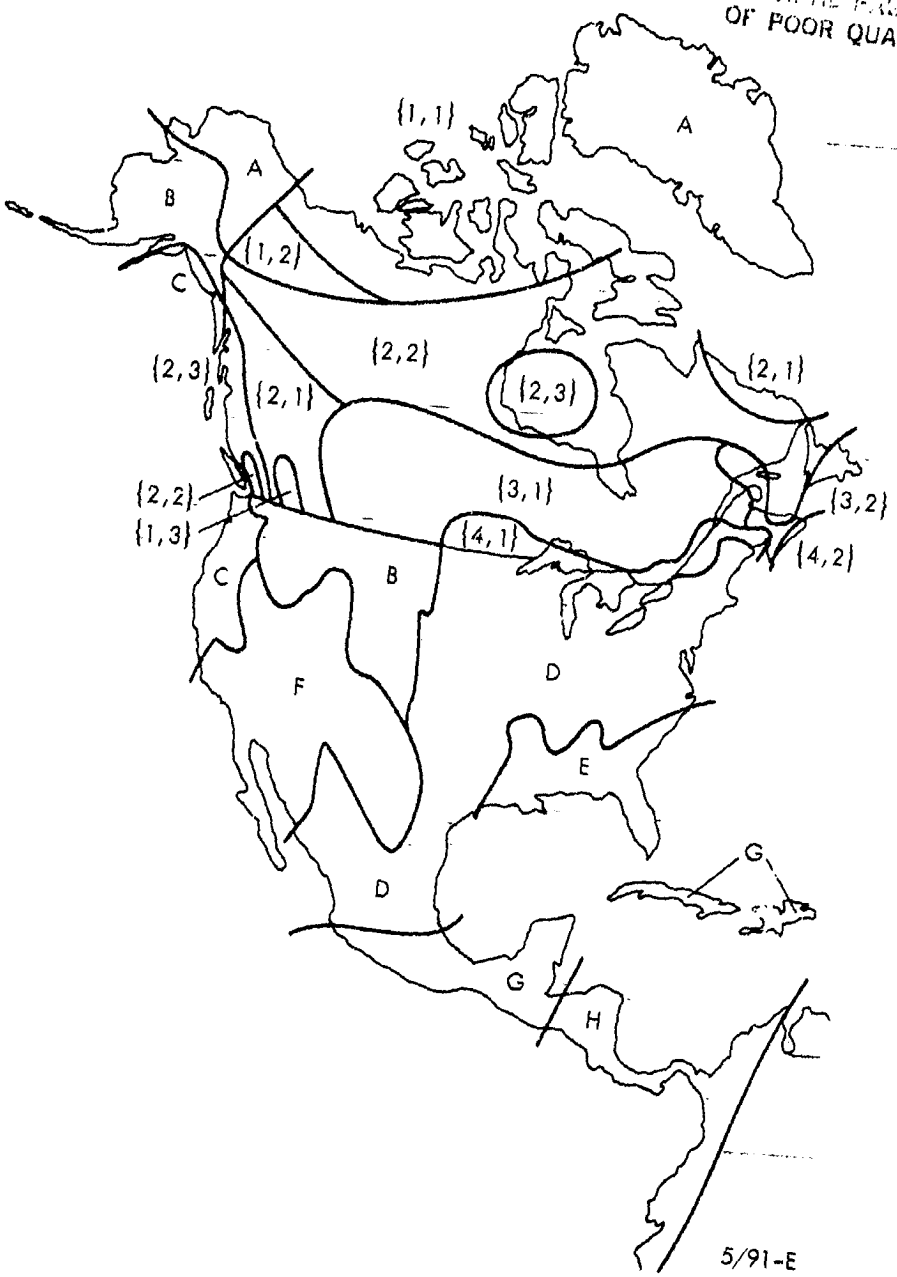

Figure 4.10. Rain rate regions of North and Central America. The regions are those of the Crane 1980 global model, except for Canada where the Canadian rain rate regions are shown. From CCIR Study Group report 5/91-E concerning Report 563-1, 1980.

The 8 rain-rate regions of Fig. 4.8 correspond to the natural regions introduced in Chap. 1, Table 1.3 fairly well. The rain rate regions are identified by letters in Fig. 4.8, and these letters are included in Table 1.3 when there is a clear correspondence. The largest discrepancy between Table 1.3 and the rain rate regions of Fig. 4.8 occurs with respect to regions 6, 8, and 9 of the table (grasslands and steppes, desert, and regions of Mediterranean climate) and rain rate region F of Fig. 4.8. Region F tends to include all 3 natural regions - 6, 8, and 9 - except that some of the grasslands of the Great Plains of the United States appear to be included in rain rate region D of Fig. 4.9. Regions 6, 8, and 9 of Table 1.3 are quite distinct from each other and from natural regions 3, 4, and 5 (rain rate regions C, D, and E). Southern California (region 9), for example, has long completely dry summers, winter rains, and very little thunderstorm activity near the coast, while the Great Plains (region 6) have maximum precipitation and frequent thunderstorms in the summer. The desert in Arizona (region 8) also has maximum precipitation and some severe thunderstorms in summer. It appears that further study of the telecommunications characteristics of regions 6, 8, and 9 (region F) is needed.

In areas where sufficient data are available, such as portions of Europe and North America, more detailed divisions than can be shown on worldwide or continental maps may be desirable. A variety of such subdivisions could be formulated. It should be taken into account that in mountainous areas of western North America and elsewhere, any broad general scheme of classification has its limitations. Quite detailed rainfall maps, perhaps for individual states, would be advantageous in such cases.

Regardless of what divisions or subdivisions are selected or whether one only uses data from a particular weather station, plots such as those of Fig. 4.11 can provide a basis for system design. Published rainfall data for the United States are available for periods as short as 5 minutes, and chart records may provide estimates for shorter periods. It is the Climatological Data - Annual Summaries that include maximum rainfalls for 5-minute periods and also for periods up to 180 minutes.

Characteristics of some of the models and analyses of attenuation due to rainfall that have been developed will now be described briefly.

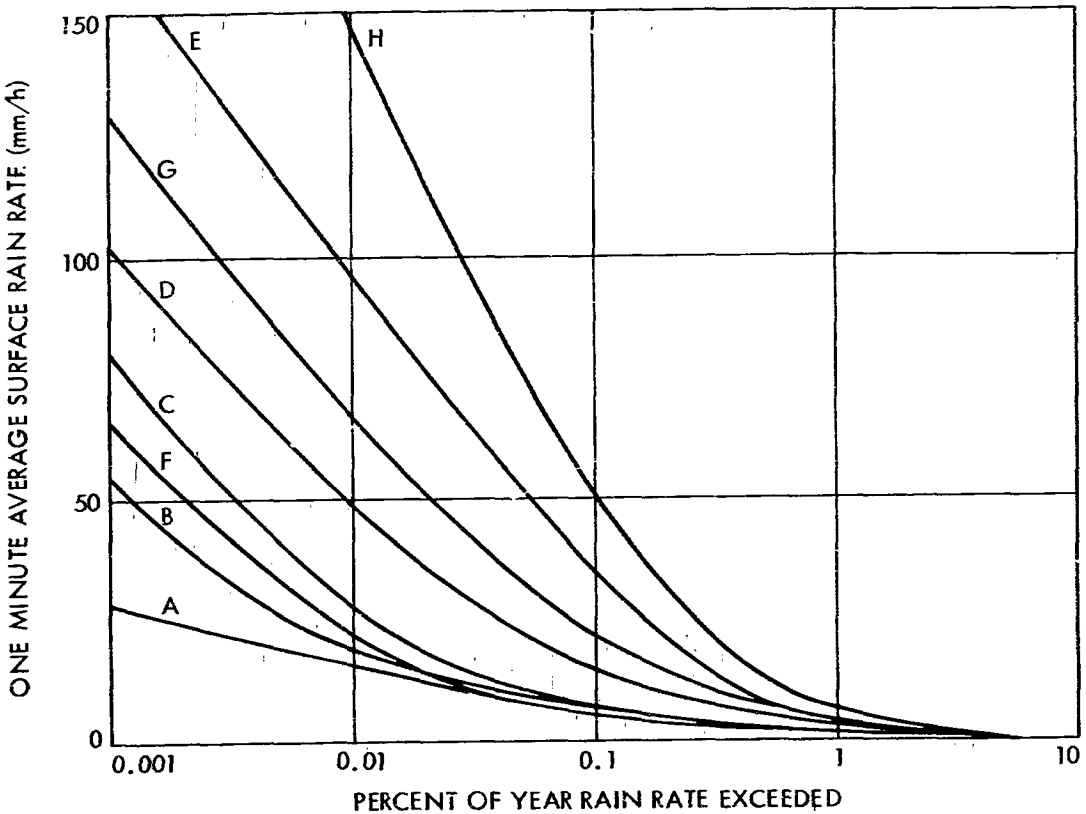

Figure 4.11. Rain rates as a function of a percent of year exceeded (CCIR, 1978c).

1. Rice-Holmberg Model

Using a variety of meteorological data, Rice and Holmberg (1973) formulated a model which predicts distributions of t-minute point rainfall rates. The model gives the cumulative number of hours in a year that the rain rate may be expected to exceed a specified value during t-minute periods, e.g. 1-minute periods, 5-minute periods, etc. The model involves the use of 3 basic parameters which are M, the annual rainfall in mm; β, the average annual ratio of thunderstorm rain to total rain; and D, the average number of days for which the precipitation equals or exceeds 0.25 mm. M and D are determined directly from recorded data, and β is derived from data on the greatest monthly precipitation values in mm and the average annual number of days with thunderstorms. In considering this model one can set $M = M_1 + M_2$ where M_1 represents thunderstorm or convective rain and M_2 represents stratiform rain which tends to be of relatively wide extent and long duration. Convective rain tends to involve high rain rates but for only comparatively short periods. The parameter β represents the ratio M_1/M.

2. Dutton-Dougherty Model, Modified Rice-Holmberg Model

The Dutton-Dougherty model predicts total attenuation from precipitation, clouds, and the clear air. For attenuation caused by rain it uses a modified Rice-Holmberg model (Dutton, 1977). An incentive for modifying the Rice-Holmberg model is that while the original model provides P(R), the percent of time that rainfall rate R is exceeded, given values of R, it is difficult to invert to obtain R, given P(R). That is, if one wishes to determine the rain rate R that is exceeded 0.01 percent of the time, for example, it is difficult to do so by using the original Rice-Holmberg model. The modified Rice-Holmberg model overcomes this problem. Like the original model it uses the 3 parameters, M, β, and D. Stratiform rain is assumed to be uniform up to the rain-cloud base and to decrease to zero at the storm top height, while convective rain is assumed to increase slightly, in terms of liquid water content, up to the rain-cloud base and to then decrease to zero at the storm top height.

The modified Rice-Holmberg model is available as a computer program from E. J. Dutton of the Boulder Laboratory facilities of NTIA/ITS (303 497-3646). Some results of interest, obtained by use of this computer program, have been published for Europe (Dougherty and Dutton, 1978) and the United States (Dutton and Dougherty, 1979). The papers provide maps of Europe and the United States that show contours of constant 1-minute rainfall rates in mm/h, corresponding to values equaled or exceeded for 1, 0.1, and 0.01 percent of the time. A percentage of 1 represents 87.7 h/yr, 0.1 percent corresponds to 8.77 h/yr, and 0.01 percent is equivalent to about 53 min/yr. The papers also include contours of the standard deviation in mm/h of annual rainfall rates corresponding to the percentages of 1, 0.1, and 0.01. Data for 30 yrs were used for the United States.

3. Lin and Lee Models

Lin (1977) and Lee (1979) describe and analyze procedures for obtaining rainfall statistics from data published by the National Climatic Center for the United States. Lin provides an empirical relation for computing attenuation as follows:

$$A(R, L) = \alpha(R) \frac{L}{1 + \frac{L}{\bar{L}(R)}} \quad \text{dB} \tag{4.17}$$

where A is total attenuation expressed as a function of rainfall rate R and path length L. The parameter α_p is the attenuation constant and has the form of aR^b, L is actual length, and $\bar{L}(R)$ is a characteristic path length given by

$$\bar{L}(R) = \frac{2636}{R - 6.2} \text{ km for } R > 10 \text{ mm/h} \tag{4.18}$$

Slightly different values can be used for a and b for vertically and horizontally polarized waves in the expression for α_p at 11 GHz, based on analysis by Chu (1974).

4. Piecewise Uniform Rain Rate Model

The piecework uniform model (Persinger et al., 1980) is a quasi-physical model developed to eliminate the need for effective path lengths. It involves the assumptions that the spatial rain rate distribution is uniform for low rain rates but becomes increasingly nonuniform as the peak rain rate increases. Total attenuation A is determined from

$$A = \frac{L}{N} \sum_{i=1}^{N} \alpha(R_i) \quad \text{dB} \tag{4.19}$$

where L is the path length which is divided into N equal intervals, α is the attenuation constant corresponding to rain rate R_i of the ith division or cell. A two level model has been developed for which

$$R_{\ell} = \begin{cases} R_1 & \text{for } 0 \leq \ell \leq CL \\ R_x & \text{for } CL \leq \ell \leq L \end{cases} \tag{4.20}$$

where

$$R_x = \begin{cases} R_1 & R_1 \leq 10 \text{ mm/h} \\ R_1 \left[\frac{R_1}{10}\right]^x & R_1 \geq 10 \text{ mm/h} \end{cases} \tag{4.21}$$

In terms of these quantities, the expression for A can be written as

$$A = \left[C\,\alpha(R_1) + (1 - C)\,\alpha(R_x) \right] L \quad \text{dB} \tag{4.22}$$

Based on experimental evidence for the eastern United States, C is taken to be 0.2 and x is taken to be -0.66. Path length L is found by using a height extent of rain H and a basal length B with

$$H = \begin{cases} 3.5 \text{ km, high latitude, above } 40° \\ 4.0 \text{ km, mid latitude} \\ 4.5 \text{ km, low latitude, below } 33° \end{cases} \tag{4.23}$$

and B = 10.5 km. then

$$L = \begin{cases} H/\sin\theta & \theta \geq \theta_0 \\ B/\cos\theta & \theta \leq \theta_0 \end{cases} \tag{4.24}$$

with $\theta_0 = \tan^{-1} H/B$ and θ the elevation angle.

It is stated that as a larger data base becomes available the two-level model could be expanded to multiple levels and to include climatic zone dependence.

5. Goldhirsh and Katz Analyses

Goldhirsh and Katz (1979) and Goldhirsh (1979) have used radar and disdrometer data as aids in analyzing and predicting attenuation due to rain. Radar, by recording the intensity of rainfall along a path and the height range over which echoes are received, can provide prediction of effective path length. The disdrometer is an instrument for measuring drop size distributions. The relations used for calculating attenuation are

$$A_R(t) = \sum_{i=1}^{N} \alpha_i \, \Delta r \tag{4.25}$$

with α_i the power-attenuation constant for the ith range bin and Δr the radar range resolution. The constant α_i is related to radar reflectivity Z by

$$\alpha_i = a \, Z_i^b \tag{4.25}$$

Z is determined experimentally by use of an equation of the form of Eq. (4.12), and a and b are determined empirically to make the values of α_1 agree with the values of α_p given by Eq. (4.2), based on Mie scattering theory utilizing the drop size distribution given by the disdrometer.

6. CCIR Report 563 of 1978

The Earth is divided in this report into 5 regions and curves are provided giving the percentage of an average year that rainfall rates are exceeded for the 5 regions. The curves giving the rain rates exceeded as a function of percentage of time extend at the low end to 0.001 percent, corresponding to about 5.3 min/yr.

7. CCIR Study Group Doc. P/105-E.

A document written for the Special Preparatory Meeting for WARC-79 (CCIR, 1978c) uses the rain rate regions of Fig. 4.8, Fig. 4.11, or Table 4.4 for determining the rain rates exceeded as a function of percentage of time, and the procedure for determining path length that has already been described in Sec. 4.3.2. This model, utilizing 8 rain rate regions, was developed in recognition of the shortcomings of the 5 rain rate regions of Report 563 of 1978. The model of 1978 and this study group model are forms of what have been referred to as global models. The equation for the total attenuation A along a path, according to the working group model, has the form of

$$A = \frac{H}{\sin\theta}\,\gamma(D)\,R_p^{-\delta(D)}\,a\,R_p^b \qquad (4.27)$$

where quantities are as defined in Sec. 4.3.2. The procedures of this model are easy to grasp and apply, assuming sufficient data for the determination of

$$r = \gamma(D)\,R_p^{-\delta(D)}.$$

8. 1980 Global Model

This form of global model by Crane (1980) uses a somewhat more complex procedure for estimating attenuation than that of the CCIR Study Group but is otherwise very similar. The number of rain rate regions is 8, and the same 8

regions are used as in the Study Group Model (Fig. 4.8). The United States is covered by 5 regions with one region, D, divided into 3 subdivisions as in Fig. 4.9. Figure 4.11 or Table 4.4, giving rain rates as a function of time exceeded for the 8 regions, are utilized. The model is based entirely upon rain rate data and utilizes the empirical relation $\alpha_p = \alpha R^{\beta}$ (same as aR^b) for converting rain rate to attenuation. Table 4.5 gives rain rates as a function of time exceeded for the regions of Canada. In the discussion of the model, it is stated that Eq. (4.15) produces the desired relationship between rain rate at a point and that averaged over a path but that because the attenuation constant is a nonlinear function of rain rate the form of Eq. (4.27) of the CCIR Study Group Model is not adequate for estimation of total attenuation. Numerical differentiation involving Eq. (4.15) has been carried out and has led to relative path rain-rate profiles which show that when high point rain rates occur, the most intense rain is found close to the sampling location. When rain rates are low at the sampling location, however, higher rain rates are likely at distances in excess of 6 km away. Approximation of the profiles by exponential functions leads to an expression for attenuation along a horizontal path of length D that involves 3 such functions as follows.

$$A(R_p, D) = \alpha R_p^{\beta} \left[\frac{e^{\mu\beta d} - 1}{\mu\beta} - \frac{b^{\beta} e^{c\beta d}}{c\beta} + \frac{b^{\beta} e^{c\beta D}}{c\beta} \right] \quad d \leq D \leq 22.5 \text{ km} \qquad (4.28)$$

$$A(R_p, D) = \alpha R_p^{\beta} \left[\frac{e^{\mu\beta D} - 1}{\mu\beta} \right] \quad 0 < D < d \qquad (4.29)$$

with A in dB, R_p in mm/h,

$$\mu = \frac{\ln\left[be^{cd} \right]}{d} \quad (d \text{ in km})$$

$$b = 2.3 R_p^{0.17} \quad (R_p \text{ in mm/h})$$

$$c = 0.026 - 0.03 \ln R_p$$

$$d = 3.8 - 0.6 \ln R_p$$

Table 4.4 Rain Rates as a Function of Percent of Year Exceeded for 1980 Global Model. From CCIR Study Group 5 Document 5/91-E for Report 563-1, 1990. (A separate table has been prepared for Europe.)

Link Reliability (Percent)	Percent of year rain rate is exceeded	Rain Rate R_p for Rain Rate Regions (mm/h)								OUTAGE TIME	
		A	B	C	D	E	F	G	H	Minutes Per Year	Hours Per Year
99.999	.001	29	58	78	108	165	66	185	253	5.3	0.09
99.997	.003	17	36	52	78	132	43	141	202	15.8	0.26
99.99	.01	10	20	28	49	98	23	94	147	53	0.88
99.97	.03	6	11	14	29	66	11	60	103	158	2.62
99.9	.1	3	5	7	15	35	5	32	64	526	8.77
99.7	.3	1	2	4	7	15	2	17	34	1580	26.3
99.0	1.	0.5	1	2	3	6	0.1	3	12	5260	87.66

Table 4.5 Rain Rates as a Function of Percent of Year Exceeded for Rain-rate Regions of Canada (see Fig. 4.10). From CCIR Study Group 5 Document 5/91-E for Report 563-1, 1980.

Link Reliability (Percent)	Percent of year rain rate is exceeded	Rain Rate R_p for Various Rain Climate Regions (mm/h)										OUTAGE TIME	
		1,1	1,2	1,3	2,1	2,2	2,3	3,1	3,2	4,1	4,1	Minutes Per Year	Hours Per Year
99.999	0.001	22	22	22	42	42	42	79	79	150	150	5.3	0.009
99.997	0.003	12	14	15	23	26	28	43	49	81	92	15.8	0.26
99.99	0.01	6.1	8.0	9.9	12	15	19	22	29	41	54	53	0.88
99.97	0.03	3.3	4.9	6.7	6.3	9.3	13	12	18	23	33	158	2.62
99.9	0.1	1.7	3.0	4.4	3.2	5.5	8.3	6.1	10	12	20	526	8.77
99.7	0.3	0.9	1.8	3.0	1.8	3.4	5.7	3.4	6.4	6.4	12	1580	26.3
99.0	1.0	-	1.1	2.0	.9	2.0	3.7	1.8	3.8	3.3	7.2	5260	87.66

For elevation angles θ greater than 10°, D is given by

$$D = \frac{H_0 - H_g}{\tan \theta} \tag{4.30}$$

where H_0 is the height of the 0°C isotherm from Fig. 4.7 and H_g is the height of the surface [consistent with Eq. (4.16)]. Attenuation A_s along a path of length L is given by

$$A_s = \frac{L\ A(R_p, 0)}{D} = \frac{A(R_p, 0)}{\cos \theta} \tag{4.31}$$

for $\theta \geq 10°$. For elevation angles less than 10 °, see Appendix 4.1.

It is reported that the mean deviations between model predictions and measurements in particular situations are smaller than 14 percent. The model applies to percentages of occurrence as small as 0.001 percent, and it is asserted that the model provides good results for the low percentages of 0.001 and 0.01 whereas other models fail for these low percentages.

9. 1982 CCIR Model

The rain-rate regions of the 1982 CCIR model are shown in Figs. 4.12-4.14, and the rain-rate values for these regions are given in Table 4.6. In addition, contours of constant rain rate exceeded for 0.01 percent of the time are provided in Figs. 9.8-9.10. Path length L is determined as in Sec. 4.3.2, except that the curves of Fig. 4.7 are now considered by the CCIR working group involved to give heights that are too great at low latitudes. Figure 9.11 shows the same curves (Method 2) as in Fig. 4.7 and also a new Method 1 curve for maritime climates, with a modification of the latter for low latitudes. This modification of CCIR IWP 5/2 is shown by the dashed curved in the figure and is also described by

$$H = \rho_p \left\{ 5.1 - 2.15 \log \left[1 + 10 \left(\frac{\phi - 27}{25} \right) \right] \right\} \tag{4.32}$$

where ϕ is latitude and ρ_p is an empirical height reduction factor given by

$$\rho_p = 0.6 \qquad \phi \leq 20°$$

$$\rho_p = 0.6 + 0.02(\phi - 20°) \qquad 20° \leq \phi \leq 40°$$

$$\rho_p = 1.0 \qquad \phi \geq 40°$$

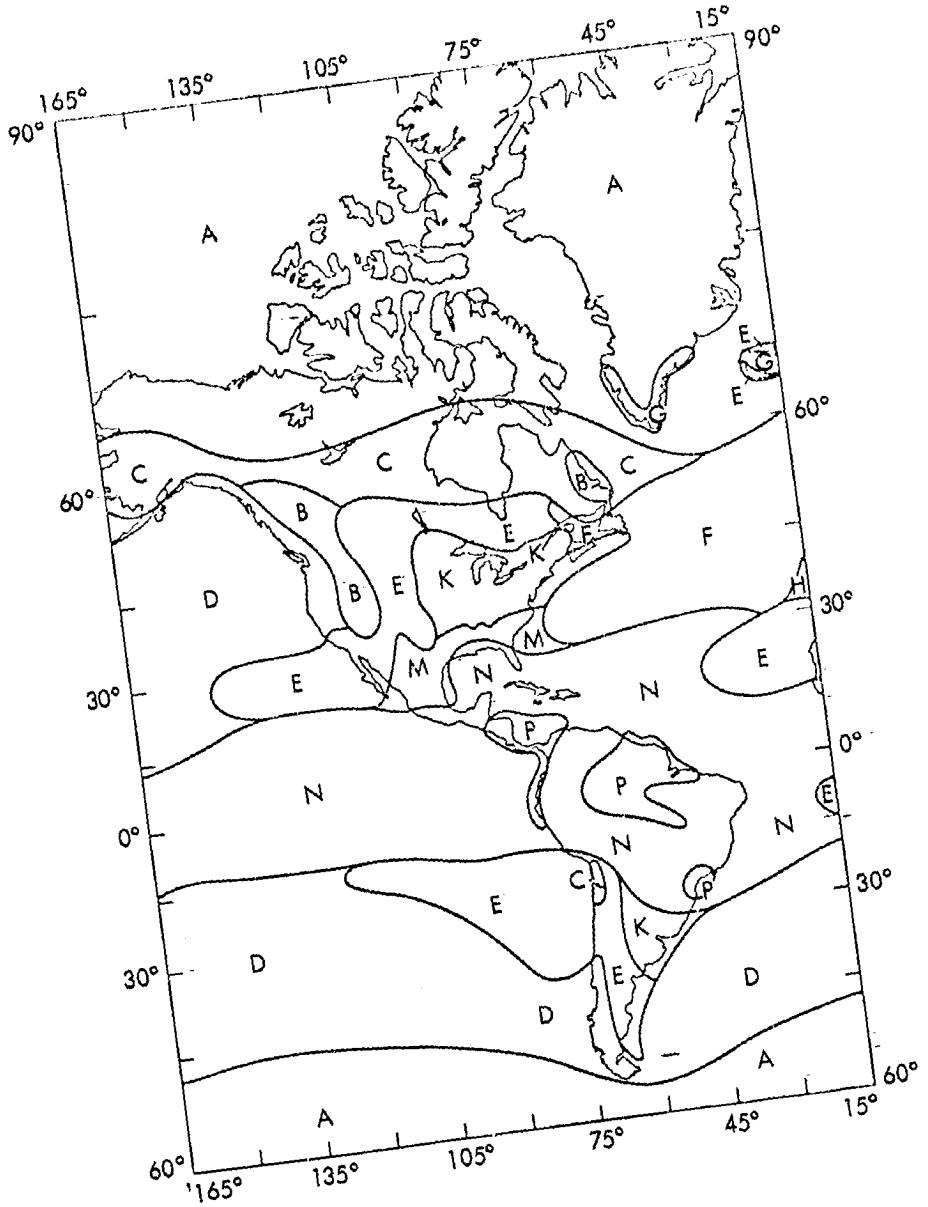

Figure 4.12. Rain-rate regions of the Americas (CCIR, 1982).

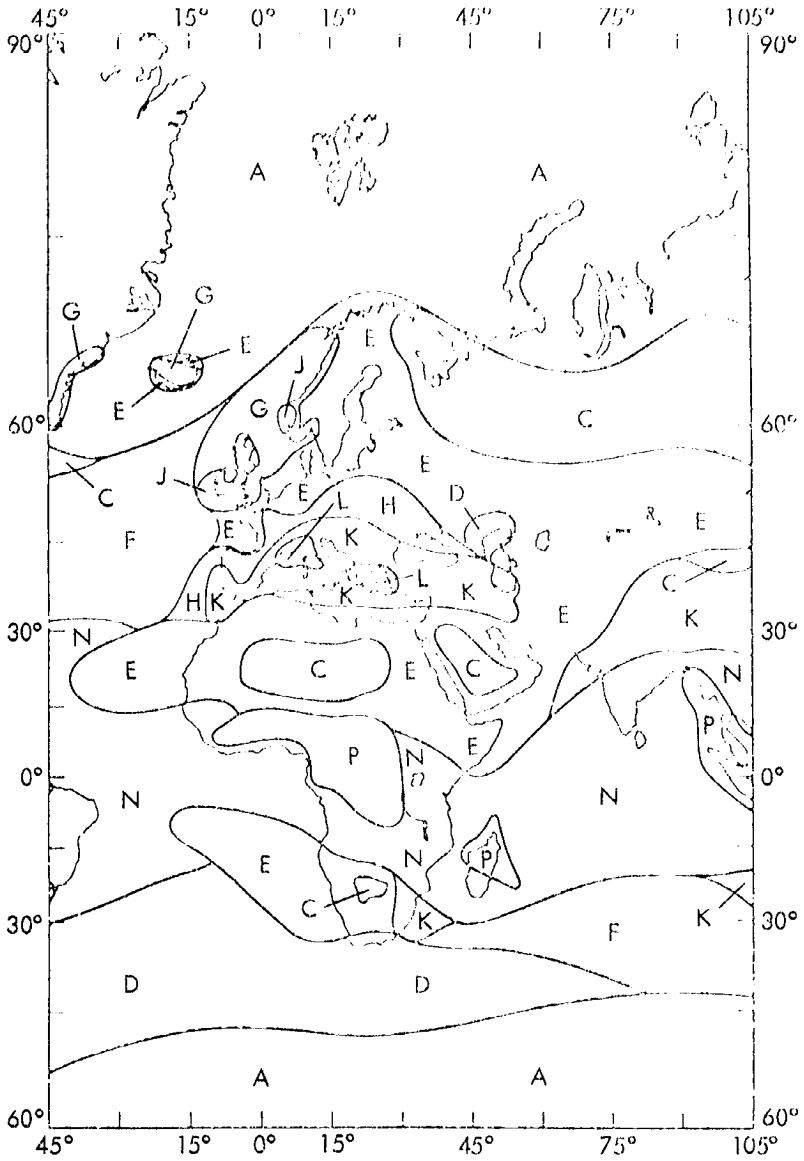

Figure 4.13. Rain-rate regions of Europe and Africa (CCIR, 1982).

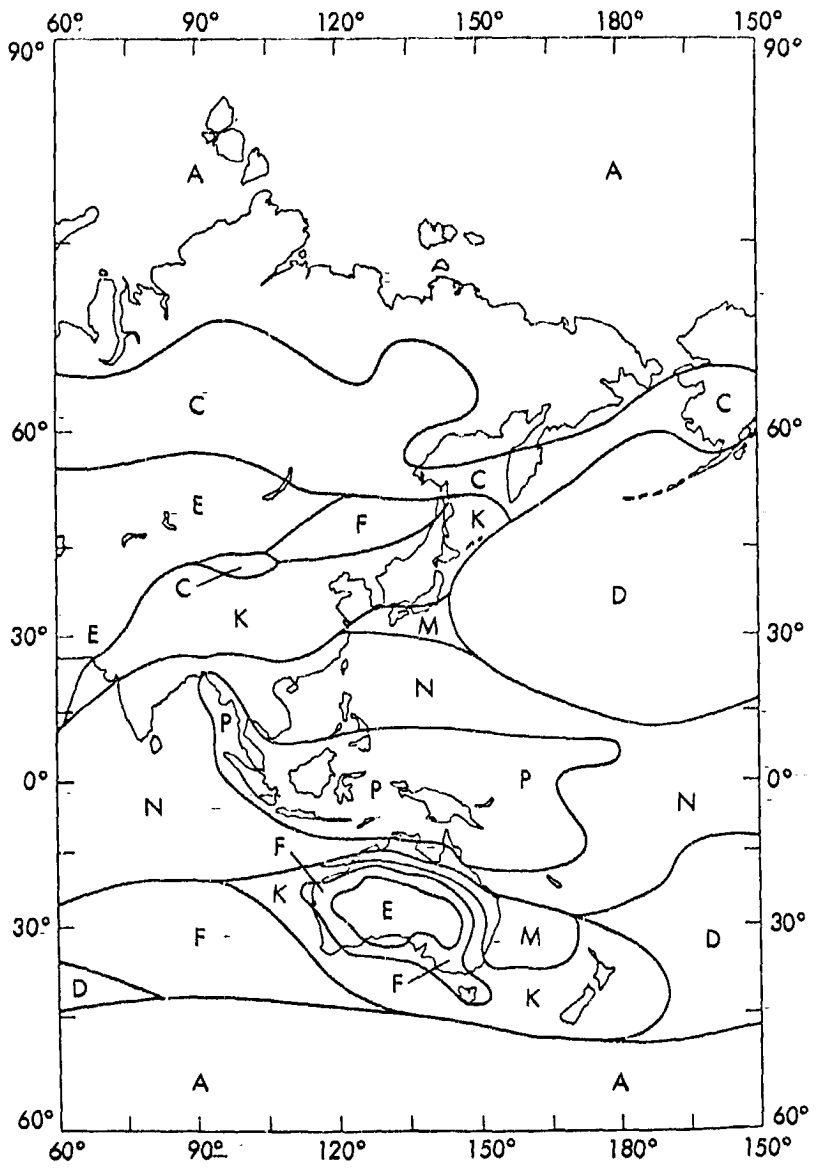

Figure 4.14. Rain-rate regions of Asia and Oceania (CCIR, 1982).

Table 4.6 Rain Intensities Exceeded (mm/h)
(CCIR, 1982).

% Time	A	B	C	D	E	F	G	H	J	K	L	M	N	P
1.0	-	1	-	3	1	2				2		4	5	12
0.3	1	2	3	5	3	4	7	4	13	5	7	11	15	34
0.1	2	3	5	8	6	8	12	10	20	12	15	22	35	65
0.03	5	6	9	13	12	15	20	18	28	23	33	40	65	105
0.01	8	12	15	19	22	28	30	32	35	42	60	63	95	145
0.003	14	21	26	29	41	54	45	55	45	70	105	95	140	200
0.001	22	32	42	42	70	78	65	83	55	100	150	120	180	250

Note that for latitudes less than 20° the height H is reduced by a factor of 0.6.

In using the model, a path reduction factor r_p is introduced such that

$$A = \alpha_p L r_p \quad \text{dB} \tag{4.33}$$

where A is attentuation in dB, L is path length, and r_p is the path reduction factor. The value of r_p is determined from

$$r_p = \frac{90}{90 + C_p D} \tag{4.34}$$

where D is the horizontal projection of L and C_p is given by Table 4.7 for continental climates. (C_p is 4 for a probability of occurrence of 0.01).

Table 4.7 Coefficient C_p for Determining Reduction Factor r_p for Continental Climates.

Percent of Year	0.001	0.01	0.1	1.0
C_p	9	4	0.5	0

4.4 DEPOLARIZATION DUE TO PRECIPITATION

The term depolarization refers to a degradation or change in polarization, as from purely vertical linear polarization to linear polarization at an angle slightly different from vertical. This latter condition is equivalent to a combination of vertical polarization, of a wave having an amplitude close to the orignal amplitude, and horizontal polarization, of a wave having a small but finite amplitude. Precipitation can cause such an effect.

The possibility of using two orthogonal linear or circular polarizations simultaneously on the same path is of much interest, but the ability to do so is limited to some degree by antenna characteristics and depolarization caused by precipitation or other phenomena. The two orthogonal linear polarizations are generally referred to as vertical and horizontal, but for earth-space paths, the polarizations tend to be rotated somewhat from the local vertical and horizontal axes (Dougherty, 1980). The two orthogonal circular polarizations are right and left circular polarization (Sec 2.1.1). Two orthogonal polarizations are sometimes referred to as cross polarizations, and, especially, a wave of the opposite or orthogonal polarization that is produced by a process of depolarization is known as a cross-polarized wave. The production of a cross-polarized wave can result in interference between orthogonally polarized channels of the same path.

In considering questions of wave polarization in transmission through rain, the ratio of the power of a wanted or copolarized wave to the power of an unwanted or cross-polarized wave is often pertinent. A copolarized wave has the same polarization as the transmitted wave, or the wave incident upon a region of rainfall, and the cross-polarized wave has the opposite or orthogonal polarization. Letting E_{11} and E_{22} represent electric field intensities of copolarized or wanted waves and E_{12} and E_{21} represent field intensities of cross-polarized or unwanted waves and expressing the power ratio in dB, the ratio may take the form of $20 \log E_{11}/E_{12}$, for example. The first subscript represents either a reference or original polarization, and the second subscript represents an actual (resulting or final) polarization. Thus, E_{12} is a field intensity having polarization 2. It may have been derived from a wave of original polarization 1, or polarization 1 may merely be the reference polarization of the system in question. A ratio of the above type is commonly referred to by the term cross polarization discrimination (XPD). For the example considered,

$$XPD = 20 \log E_{11}/E_{12} \tag{4.35}$$

The use of the term discrimination is pertinent in some cases, but the notation XPD has been used also to describe the polarization of a wave whether a process of discrimination is involved or not. For example, if a receiving

system has a linear, horizontally polarized antenna but an incident wave is linearly polarized at an angle τ with respect to the horizontal, it may be said that

$$XPD = 20 \log \cot \tau \tag{4.36}$$

as $E_{11} = E_0 \cos \tau$ and $E_{12} = E_0 \sin \tau$, where E_0 is the total field intensity of the wave and E_{11} and E_{12} are components along horizontal and vertical axes.

In the above illustrations of XPD, it is seen to be a value in dB representing the ratio of copolarized or wanted power to cross-polarized or unwanted power. Note that the cross-polarized power would be interfering power if it was desired to use polarization 2 for a second signal channel. A related quantity, cross-polarization isolation or XPI, can be illustrated by

$$XPI = 20 \log E_{11}/E_{21} \tag{4.37}$$

XPI is also a value in dB and represents the ratio of copolarized power to interfering power (taking E_{21} to be a field intensity having polarization 1 that may have been produced from a wave that originally had only polarization 2 and that in any case is unwanted). XPI has the advantage of being a direct measure of interference, but XPD is easier to determine experimentally (by receiving singly polarized satellite signals with a single antenna having orthogonally-polarized feeds). Theoretically, the two quantities XPD and XPI should have the same value.

Depolarization due to precipitation is caused by the nonspherical shape of raindrops and ice crystals; spherical raindrops do not cause depolarization. Depolarization would not occur in the case of spheroidal raindrops either if the electric field intensity vector of a linearly polarized wave were to lie strictly parallel to either the long or short axes of the raindrops (although the attenuation for the two cases would be different). In the general case, however, the roughly spheroidal drops tend to be tilted or canted with respect to the electric field intensity vectors of incident vertically or horizontally polarized waves as well. Wind contributes to canting and, even in the case of apparently vertical fall, the drops normally exhibit a distribution of canting angles.

Differential attenuation and phase shift of field components parallel to the long and short axes of symmetry of raindrops are what produces depolarization. The effect of differential attenuation on a linearly polarized wave is shown in a qualitative way in Fig. 4.12, where the elliptical cross-section of a canted oblate spheroidal raindrop is depicted. A circularly polarized wave is equivalent to the combination of two linearly polarized waves that differ by 90° in both spatial configuration and electrical phase, and depolarization occurs for circularly polarized waves also. Indeed, it develops that the degradation of XPD due to rain is worse for circularly polarized than linearly polarized waves (Chu, 1974).

Taur (1974) has reported experimental results showing a degradation of XPD to about 12 dB for 4-GHz circularly polarized transmissions from INTELSAT IV to the COMSAT Laboratories near Washington, D.C. He compared these results with prediction based on differential attenuation A and differential phase shift B as indicated by

$$XPD = 20 \log \frac{1 + e^{A+jB}}{1 - e^{A+jB}} \tag{4.38}$$

The observed values of XPD were somewhat lower than the predicted values.

Quantitative analysis has provided numerical values of differential attenuation and phase for waves that have field intensities along two orthogonal axes symmetrically oriented with respect to oblate-spheroidal and Pruppacher-Pitter raindrops (Morrison, Cross, and Chu, 1973; Hogg and Chu, 1975; Oguchi, 1977; Kaul, Wallace, and Kinal, 1980). Further analysis of cross-polarization has led to a relation between XPD, attenuation of the copolarized or original wave A, elevation angle θ, and polarization tilt angle with respect to the horizontal τ (Nowland, Olsen, and Shkarofsky, 1977; CCIR, 1978b). The expression used by the CCIR in Report 564-1 is

$$XPD = 30 \log f_{GHz} - 40 \log (\cos \theta) - 20 \log (\sin 2\tau) - 20 \log A \tag{4.39}$$

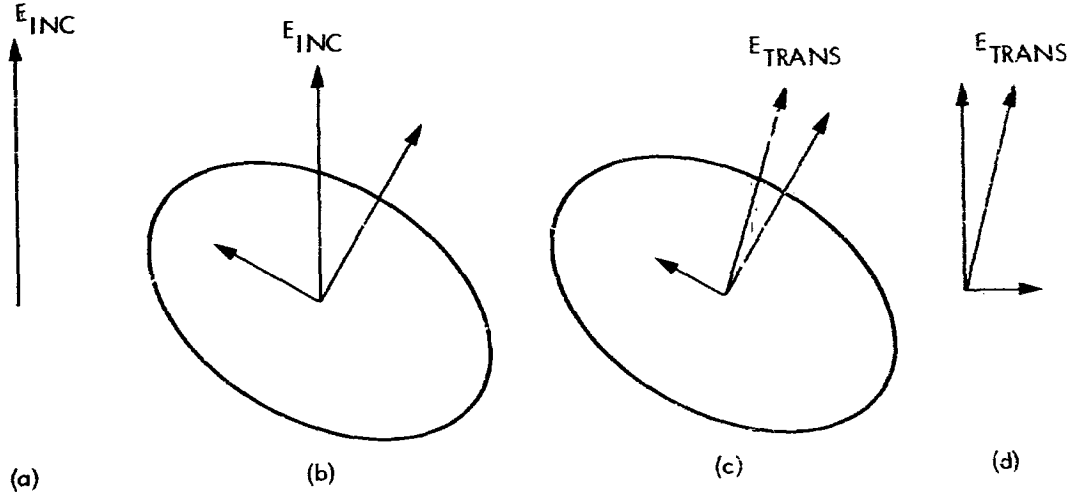

Figure 4.15. Illustration of the role of differential attenuation in producing depolarization. The incident wave on a region of precipitation has strictly vertical linear polarization as shown in (a), where the electric field intensity of the wave is designated as E_{inc}. In (b) the components of E_{inc} that are parallel to the major and minor axes of the spheroidal raindrops are shown. The component parallel to the major axis encounters more liquid water than the other component and is attenuated more strongly. Thus upon emerging from the region of rainfall, the total electric field intensity E_{trans} is no longer vertical. Components of E_{trans} parallel to the ellipse axes are shown in (c), and the horizontal and vertical components of E_{trans} are shown in (d).

For a fixed value of A, the XPD increases with frequency, which would indicate that XPD would be low (poor) for low frequencies. Attenuation, however, increases with frequency. Equation (4.39) is considered to be valid for

$$1 \text{ dB} \leq A \leq 15 \text{ dB}$$

$$10 \text{ dB} \leq XPD \leq 40 \text{ dB}$$

$$8 \text{ GHz} \leq f \leq 40 \text{ GHz}$$

$$10° \leq \tau \leq 80°$$

$$10° \leq \theta \leq 60°$$

The relation is provisional and should be used with caution. It has the form of

$$XPD = a - b \log A \qquad (4.40)$$

One approach to depolarization studies has been to empirically determine values of a and b for particular situations and to analyze how the values of a and b vary with frequency and elevation angle. Some results for a and b for 11.7 GHz, not far above 10 GHz, that have been obtained at Virginia Polytechnic Institute and State University (VPI & SU) and the University of Texas (UT), are shown in Table 4.7.

Occurrences of low values of XPD when attenuation is low have been attributed to ice crystals, which cause small attenuation but can significantly degrade XPD. Relations between XPD and attenuation that are developed for rain should not be extended to low values of attenuation for this reason (Bostian and Allnut, 1979).

Data on rain depolarization at 4 GHz have been obtained by Yamada et al. (1977). For such relatively low frequencies attenuation values are low and are not useful for predicting XPD either. Depolarization at such low frequencies is considered further in Sec. 9.4.3.

Table 4.7 11.7 GHz XPD Data. In the Case of the UT-Values, XPD Exceeded the Values Shown for the Percentages of Time Indicated. [Table is a Preliminary Version Assembled from Data in Kaul, Wallace, and Kinal, 1980.]

Source	XPD	θ	Applicability
VPI & SU	44.7-22.6 log A	33°	Aug. 1977
VPI & SU	36.3-16.2 log A	33°	1978
UT	42.9-17.5 log A	50°	10% Occurrence
UT	35.0-13.4 log A	50°	50% Occurrence
UT	31.5-12.6 log A	50°	90% Occurrence

As with atmospheric effects in general, attenuation and degradation in XPD due to rain are most severe on low-elevation-angle paths. Lin (1974) describes the occurrence of a squall line of heavy rain that produced 7 dB of attenuation and a degradation of XPD from 27 dB down to 9 dB on a 42-km 4 GHz path. The path length through rain of 42 km is considerably greater than for most earth-space paths, and some of the depolarization may have been caused by multipath propagation (Hogg and Chu, 1975).

4.5 BISTATIC SCATTER FROM RAIN

In considering the propagation of signals through a region of rainfall, interest commonly centers on the degree of attenuation of signals propagating in the forward direction. Another effect, however, is that rain scatters energy into all directions, with a resulting potential for interference with earth-satellite or terrestrial line-of-sight telecommunication systems. Such scatter can be referred to as bistatic scatter, using the term bistatic as for radar operations in which the transmitter and receiver are at different locations.

The process of bistatic scatter can be described as follows. The power density P in W/m^2 at a distance R_1 from a transmitter having a power output of W_T watts and an antenna gain of G_T is given by

$$P = \frac{W_T G_T}{4\pi R_1^2} \tag{4.41}$$

At the location where the power density is P, consider a target having a radar cross section of ηV m^2 where η is the cross section per unit volume and V is the total volume taking part in the scattering process. In the present case V is the common volume of the transmitting and receiving antennas as shown in Fig. 4.16.

Considering the common scattering volume to be small such that the distance from the transmitter to any part of it is R_1 and the distance from the receiver to any part of the volume is R_2, the common volume is presumed to radiate isotropically the power incident upon it so that the received power W_R, intercepted by an antenna with an effective area of A_R at the distance of R_2, is given by

$$W_R = \frac{W_T G_T \eta V A_R}{(4\pi)^2 R_1^2 R_2^2} \tag{4.42}$$

Making use of the relation between gain G and effective area A, namely $G = 4\pi A/\lambda^2$, the equation can be put into the form

$$\frac{W_R}{W_T} = \frac{G_T G_R \eta V \lambda^2}{(4\pi)^3 R_1^2 R_2^2 L} \tag{4.43}$$

where a factor L has been added to take account of attenuation of the incident and scattered waves and any polarization mismatch. Assuming for simplicity that Rayleigh scattering applies, the cross section per unit volume η is given by

$$\eta = \frac{\pi^5}{\lambda^4} \left| \frac{K_c - 1}{K_c + 2} \right|^2 \sum d^6 \quad m^2/m^3 \tag{4.44}$$

where K_c is the complex index of refraction of water at the frequency in question and summation is shown over all of the drop diameters d within a unit volume. This summation is commonly represented by the symbol Z so that

$$\eta = \frac{\pi^5}{\lambda^4} \left| \frac{K_c - 1}{K_c + 2} \right|^2 Z \quad m^2/m^3 \tag{4.45}$$

Empirical relations have been derived between Z and rain rate R. For the Laws and Parsons drop-size distribution

$$Z = 400\, R^{1.4} \tag{4.46}$$

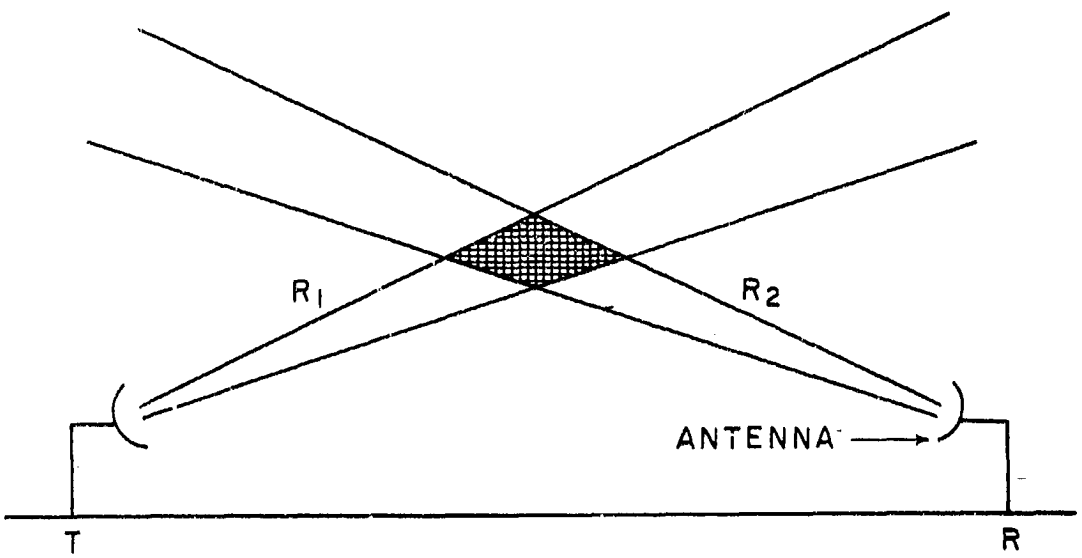

Figure 4.16.—The cross-hatched area is a two-dimensional representation of the common volume of the transmitting and receiving antennas.

with Z in mm^6/m^3 and R in mm/h. Another form of the relation between Z and R, which is a slight revision of the relation proposed by Marshall and Palmer and is based on their drop-size distribution is

$$Z = 200\ R^{1.6} \tag{4.47}$$

In monostatic radar observations of rainfall η can be determined from Eq. (4.43) and Z can then be determined from Eq. (4.45) except that for monostatic radar R_1 and R_2 are the same and V is proportional to distance squared so that W_R/W_T varies inversely with distance squared if rain fills the radar antenna beam-width. In Eqs. (4.44) and (4.45) all lengths are in m. To convert from Z in m^6/m^3 to mm^6/m^3 for use in Eqs. (4.46) and (4.47) multiply by 10^{18}.

For calculation of interfering signal levels one can assume rain rates R and calculate Z and η for insertion into Eq. (4.43).

4.6 CONCLUSION

Much of the interest in effects of precipitation on telecommunications has been directed to frequencies above 10 GHz, but the various models of attenuation due to rain are applicable to frequencies below 10 GHz as well. Attenuation and noise due to precipitation may be important for frequencies as low as 8 GHz or lower and need to be taken into account for frequencies as low as 4 GHz. Depolarization, the production of cross polarized components that have polarizations orthogonal to the original polarizations, increases with attenuation for frequencies above 8 GHz. For lower frequencies, differential phase shift rather than differential attenuation tends to make the major contribution to depolarization, and significant depolarization may take place at frequencies as low as 4 GHz (Taur, 1974; Sec. 9.4.3). Backscatter from precipitation is important in radar observations at frequencies as low as those of the L band (near 1300 MHz), and bistatic scatter from rain is a potential source of interference for telecommunication system operations at frequencies this low as well as at higher frequencies.

Water in the form of a thin layer of film over a radome or reflector and as the tiny drops of clouds or fog, as well as in the form of the larger drops of rain, can affect the performance of telecommunication systems. It has been pointed out that a given water content integrated along a path causes more attenuation when the water is in the form of a thin slab than when it occurs as fog or rain. Hogg and Chu (1975) used the water content of a slab 1 mm in thickness, corresponding to a rain of 25 mm/h over a 1-km path or fog of 0.1 g/m^3 over a 10-km path, to illustrate this point. Avoiding the use of radomes and using blowers to eliminate water films are means for minimizing system degradation due to water films.

Effects of clouds are considered in the following Chap. 5. Among the effects are a slight range delay, above that due to the gaseous constituents of the atmosphere. The same effect occurs for rain, for which the excess range (or time) delay can be determined from the real part of the complex index of refraction m_c of Sec. 4.1 by taking $\int R_e\,(m_c-1)\,d\ell$ namely the integral of the real part of m_c minus unity over the path. Further consideration of range delay due to liquid water, whether of the tiny drops of fog or the larger drops of rain, can be found in Sec. 5.1.

REFERENCES

Bostian, C. W., et al., A Depolarization and Attenuation Experiment Using the COMSTAR and CTS Satellites, Virg. Poly. Inst. and State Univ., Annual Report, NASA Cont. NAS5-22577, 1979.

Bostian, C. W. and J. E. Allnut, "Ice crystal depolarization on satellite-earth microwave radio paths," Proc. IEEE, vol. 126, p. 951, 1979.

CCIR, "Attenuation and scattering by precipitation and other atmospheric particles," Report 721, in Vol. V, Propagation in Non-ionized Media, Recommendations and Reports of the CCIR, 1978, pp. 107-115. Geneva: Int. Telecomm. Union, 1978a.

CCIR, "Propagation data required for space telecommunication systems," Report 561-1, in Vol. V, Propagation in Non-ionized Media, Recommendations and Reports of the CCIR, 1978, pp. 219-239. Geneva: Int. Telecomm. Union, 1978b.

CCIR, "Rain attenuation prediction," CCIR Study Groups Special Preparatory Meeting (WARC-79), Doc. P/105-E. Geneva: Int. Telecomm. Union, 1978c.

CCIR, "Radiometeorological data," Report 563-1, in Vol. V, Propagation in Non-ionized Media, Recommendations and Reports of the CCIR, 1982. Geneva: Int. Telecomm. Union, 1982.

Chu, T. S., "Rain induced cross-polarization at centimeter and millimeter wavelengths," Bell System Tech. Jour., vol. 53, pp. 1557-1579, Oct. 1974.

Cox, D. C., H. W. Arnold, H. H. Hoffman, and R. P. Leck, "Properties of attenuating and depolarizing atmospheric hydrometeors measured on a 19-GHz earth-space radiopath," Radio Science, vol. 15, pp. 855-865, July-Aug. 1980.

Crane, R. K., Microwave Scattering Parameters for New England Rain, Lincoln Laboratory Report 426, 1966.

Crane, R. K., "Prediction of attenuation by rain," IEEE Trans. on Communications, vol. COM-28, pp. 1717-1733, Sept. 1980.

Dougherty, H. T. and E. J. Dutton, "Estimating year-to-year variability of rainfall for microwave applications," IEEE Trans. on Communications, vol. COM-26, pp. 1321-1324, Aug. 1978.

Dougherty, H. T., A Consolidated Model for UHF/SHF Telecommunication Links between Earth and Synchronous Satellites, NTIA Report 80-45, U. S. Dept. of Commerce, National Telecommunications and Information Administration, August 1980.

Dutton, E. J., Earth-space Attenuation Prediction Procedures at 4 to 16 GHz, OT Report 77-123, May 1977. (Accession No. PB269-228/AS, NTIS, Springfield, VA).

Dutton, E. J. and H. T. Dougherty, "Year-to-year variability of rainfall for microwave applications in the U.S.A.," IEEE Trans. on Communications, vol. COM-27, pp. 829-832, May 1979.

Flock, W. L., Electromagnetics and the Environment: Remote Sensing and Telecommunications, Englewood Cliffs, NJ: Prentice-Hall, 1979.

Goldhirsh, J., "Predictive methods for rain attenuation using radar and in-situ measurements tested against the 28-GHz Comstar beacon signal," IEEE Trans. on Antennas and Propagation vol. AP-27, pp. 398-406, May 1979.

Goldhirsh, J. and I. Katz, "Useful experimental results for earth-satellite rain attenuation modeling," IEEE Trans. on Antennas and Propagation, vol. AP-27, pp. 413-415, May 1979.

Harris, J. M. and G. Hyde, "Preliminary results of COMSTAR 19/29 GHz beacon measurements at Clarksburg, Maryland," COMSAT Tech. Rev., vol. 7, pp. 599-623, 1977.

Hogg, D. C. and T. S. Chu, "The role of rain in satellite communications," Proc. IEEE, vol. 63, pp. 1308-1331, Sept. 1975.

Ippolito, L. J., 11.7 GHz Attenuation and Rain Rate Measurements with the Communications Technology Satellite (CTS), NASA Tech. Memo. 80283, Greenbelt, MD: NASA, 1978.

Kaul, R., D. Rogers, and J. Bremer, A Compendium of Millimeter Wave Propagation Studies Performed by NASA, ORI Tech. Report, NASA Contract NAS5-24252, 1977.

Kaul, R., R. Wallace, and G. Kinal, A Propagation Effects Handbook for Satellite Systems Design, A Summary of Propagation Impairments on 10-100 GHz Satellite Links with Techniques for System Design. Washington, D.C.: NASA Communications Division, NASA Headquarters, March 1980.

Kerker, M., The Scattering of Light and Other Electromagnetic Radiation. New York: Academic Press, 1969.

Kerr, D. E. (ed.), Propagation of Short Radio Waves, Vol. 13, Padiation Laboratory Series. New York: McGraw-Hill, 1951.

Laws, J. O. and D. A. Parsons, "The relation of drop size to intensity," Trans. of AGU, pp. 452-460, 1943.

Lee, W. C. Y., "An approximate method for obtaining rain rate statistics for use in signal attenuation estimating," IEEE Trans. on Antennas and Propagation, vol. AP-27, pp. 407-413, May 1979.

Lin, S. H., "An occurrence of very heavy rain on a 42-km path," IEEE Trans. on Communications, vol. COM-22, pp. 709-710, May 1974.

Lin, S. H., "Nationwide long-term rain rate statistics and empirical calculation of 11-GHz microwave rain attenuation," Bell System Tech. Jour., vol. 56, pp. 1581-1604, Nov. 1977.

Marshall, J. S. and W. M. Palmer, "The distribution of raindrops with size," Jour. Meteorology, vol. 5, pp. 165-166, Aug. 1948.

Morrison, J. A., M. J. Cross, and T. S. Chu, "Rain-induced differential attenuation and differential phase shift at microwave frequencies," Bell System Tech. Jour., vol. 52, pp. 599-604, April 1973.

Nowland, W. L., R. L. Olsen, and I. P. Shkarofsky, "Theoretical relationship between rain depolarization and attenuation," Electronics Letters, vol. 13, pp. 676-678, 27 Oct. 1977.

Oguchi, T., "Scattering properties of Pruppacher-and-Pitter form raindrops and cross-polarization due to rain: Calculations at 11, 13, 19.3, and 34.8 GHz," Radio Science, vol. 12, pp. 41-51, Jan.-Feb. 1977.

Olsen, R. L., D. V. Rogers, and D. B. Hodge, "The aR^b relation in the calculation of rain attenuation," IEEE Trans. on Antennas and propagation, vol. AP-26, pp. 318-329. March 1978.

Persinger, R. R., W. L. Stutzman, R. E. Castle, and C. W. Bostian, "Millimeter wave attenuation prediction using a piecewise uniform rain rate model," IEEE Trans. on Antennas and Propagation, vol. AP-28, pp. 149-153, March 1980.

Pruppacher, H. R. and R. L. Pitter, "A semi-empirical determination of the shape of cloud and rain drops," J. Atmos. Sci., vol. 28 pp. 86-94, Jan. 1971.

Rice, P. L. and N. R. Holmberg, "Cumulative time statistics of surface-point rainfall rates," IEEE Trans. on Communications, vol. COM-21, pp. 1131-1136, Oct. 1973.

Ryde, J. W., "The attenuation and radar echoes produced at centimetre wavelengths by various meteorological phenomena," in Meteorolgical Factors in Radio-Wave Propagation, Report of a Conference held on 8 April 1946 at the Royal Institution, pp. 169-189. London: The Physical Society, 1946.

Segal, B., "A new procedure for the determination and classification of rainfall rate climatic zones," URSI Commission F Open Symposium, Preprints of papers, Lennoxville, Quebec, Canada, 26-30 May 1980.

Taur, R. R., "Rain depolarization: theory and experiment," COMSAT Tech. Rev., vol. 4, pp. 187-190, Spring, 1974.

Van de Hulst, H. C., Light Scattering by Small Particles. New York: Wiley, 1957.

Vogel, W. J., CTS Attenuation and Cross-Polarization Measurements at 11.7 GHz, U. of Texas, Austin Final Report, NASA Contract NAS5-22576, 1979.

Yamada, M. A. Ogawa, O. Furuta, and H. Yuki, "Rain depolarization measurement by using INTELSAT-IV satellite in 4-GHz band at low elevation angle," URSI Commission F Symposium Proceedings, pp. 409-419, LaBaule, France, 1977.

Zufferey, C. H., "A Study of Rain Effects on Electromagnetic Waves in the 1 - 600 GHz Range," M. S. thesis. Boulder, CO: Department of Electrical Engineering, U. of Colorado, 1972 (reprinted in 1979).

APPENDIX 4.1
1980 GLOBAL MODEL

For elevation angles θ less than or equal to 10° in the 1980 Global Model, Crane (1980) states that D is given by

$$D = E\psi \tag{A 4.1}$$

with

$$\psi = \sin^{-1}\left\{\frac{\cos\theta}{H_o + E}\left[(H_g + E)^2 \sin^2\theta + 2E(H_o - H_g) + H_o^2 + H_G^2\right]^{1/2} - (H_g + E)\sin\theta\right\} \tag{A 4.2}$$

E is the effective earth radius and the value of 8500 km, corresponding to k = 4/3 (Sec. 3.2, Table 3.2) is suggested. H_o is the height of the 0°C isotherm, and H_g is the height of the ground (height of station).

Also for $\theta \leq 10°$

$$L = \left[(E + H_g)^2 + (E + H_o)^2 - 2(E + H_g)(E + H_o)\cos\psi\right]^{1/2} \tag{A 4.3}$$

CHAPTER 5
EFFECTS OF SMALL PARTICLES AND BIOLOGICAL MATTER

5.1 CLOUDS AND FOG

5.1.1 Introduction

Clouds, dust, and vegetation and their effects on propagation are the principal topics considered in this chapter. Clouds and fog are both composed of minute water droplets or ice crystals suspended in air. Fog forms near the Earth's surface, and clouds occur at higher levels. Both clouds and fog form through cooling, clouds when air cools adiabatically while rising—for example and fog by contact and mixing. Fog also sometimes forms by increase of water content. Clouds are of three basic types - cirrus, cumulus, and stratus (Donn, 1975).

Cirrus clouds are high, thin, separated or detached clouds. They usually form above about 9 km (about 30,000 ft) and consist of thin crystals or needles of ice rather than liquid water. Cumulus clouds are the majestic billowing white clouds of summer and fair weather generally. Their base is typically flat and they have considerable vertical extent. Stratus clouds have a large horizontal extent covering all or most of the sky and showing little structure. They tend to have a uniform grey color. If a cumulus or stratus cloud occurs above its normal level, the term alto precedes the name. If a cloud is associated with rain, the term nimbus may be added to the basic name. Thus, nimbo stratus clouds are rain or snow clouds, and cumulonimbus clouds, which develop from cumulus clouds, are the clouds of thunderstorms. Clouds combining the characteristics of two of the basic types have names such as stratocumulus and cirrostratus.

Drop sizes and liquid water contents in cumulonimbus clouds are given in Table 5.1, adapted from Ludlam (1980). The table shows values of drop concentration N, mass density ρ, and mean radius r for particular cumulonimbus clouds, which have relatively large values of liquid water content. The entries are arranged in groups or classes.

Table 5.1

Parameters of Cumulonimbus Clouds
(adapted from Ludlam, 1980).

Class	N/cm^3	$\rho(g/m^3)$	$r(\mu m)$
a	290	0.05	3.45
	590	0.13	3.74
	281	0.65	8.2
b	30	0.03	6.2
	41	0.025	5.26
	85	0.06	5.52
c	229	0.60	8.55
	182	0.95	10.76
	285	0.66	8.21
	220	0.51	8.21
	119	0.70	11.2
d	195	1.6	12.5
	99	5.0	22.9

Fog has four principal categories - radiation fog, advection fog, frontal fog, and upslope fog. Radiation fog forms when the Earth, and consequently the air immediately above it, cools on clear nights. Advection refers to horizontal movement, and advection fog forms when cold air passes over a warm sea surface and when warm moist air passes over a cold surface. The latter mechanism is responsible for about 4/5ths of all maritime fogs (Donn, 1975). Frontal fog is important over the continents and results at a front where warm air moves over cold air. Clouds form in the warm air, and if rain falls from the clouds it will add moisture to the cold air underneath which may already have been humid and near the dew point. The result is the formation of fog in the cold air. Upslope fog forms when humid air ascends a gradually sloping plain as in the interior plains of the United States. Ice fog forms at low temperatures in the order of -34°C (-30°F) and lower and is aggravated by man-made pollution. Ice fog is a problem ir winter in Fairbanks, Alaska (Benson, 1965, 1970).

The discovery that radar echoes can be received from clouds at frequencies of 3 GHz and lower suggests that clouds have a degree of structure that causes partially coherent backscatter echoes (Gossard, 1979). The contribution to coherent backscatter from water vapor in the cloud is believed to be much more important than the contribution from water droplets.

5.1.2 Attenuation

Attenuation of radio waves by clouds can be calculated on the basis of Rayleigh scattering theory, as the droplet sizes of clouds are small compared to wavelength. The power attenuation constant α_p for propagation in clouds is proportional to liquid water content ρ_ℓ as shown by

$$\alpha_p = K_\ell \rho_\ell \qquad \text{dB/km} \tag{5.1}$$

where K_ℓ is a proportionality factor that is dependent on frequency as shown in Fig. 5.1. Attenuation values for frequencies of 10 GHz and lower are small. The factor K_ℓ has a maximum value of about 0.1 in this frequency range, and 5 g/m^3 is a quite extreme value for ρ_ℓ. Thus the attenuation due to clouds or fog at 10 GHz is unlikely to be more than 0.5 dB/km, and attenuation values decrease as frequency decreases. Even higher values of density from 6 to 10 g/m^3 have been reported (Valley, 1965), but dense clouds more commonly have a density of only about 1 g/m^3.

For the low frequencies of this handbook, for which Fig. 5.1 cannot be read accurately, numerical values of the attenuation constant can be obtained by using

$$\alpha_p = \left[0.4343 \frac{6\pi}{\lambda} \ \mathrm{Im}\left(-\frac{K_c - 1}{K_c + 2}\right)\right] \rho_\ell \qquad \text{dB/km} \tag{5.2}$$

where λ is wavelength in cm, Im indicates the imaginary part of, K_c is the complex relative dielectric constant of water, and ρ_ℓ is water content in g/m^3. The constant K_c is a function of temperature and frequency. It has the value of 78.45-j 11.19 for T = 20°C and λ = 10 cm. Table 5.2 shows values of the imaginary part of $-(K_c-1/(K_c+2) = -R$, adapted from Battan (1973) and originally provided by Gunn and East (1954). Equation (5.2) can be used for ice as well as water clouds if the density of ice is taken as 1. See Battan

for justification for this step. The equation is based upon the theory of Rayleigh scattering which can be applied to particles which are sufficiently small compared to wavelength.

An alternative expression for attenuation in a cloud for frequencies from 1 to 50 GHz that does not require knowledge of K_c has the following form (Staelin, 1967).

$$\alpha_p = \frac{(4.343)\rho_\ell \, 10^{0.0122\,(291-T)-1}(1.16)}{\lambda^2} \quad \text{dB/km} \qquad (5.3)$$

T is temperature in kelvins and equals 273 plus the temperature in °C, λ is wavelength in cm, and ρ_ℓ is water content in g/m^3.

Values for total attenuation at frequencies of 2.3, 8.5, 10, and 32 GHz as calculated by Slobin (1981) are included in Table 5.3. The model utilized for calculations includes cloud layers having combined thickness as shown and also includes the small contributions to attenuation due to water vapor and oxygen as well as the larger contribution due to clouds. Values for the combined effect of water vapor and oxygen in a clear atmosphere are also shown for reference (the entry for $\rho_\ell = 0$). The condition $\rho_\ell = 1\ g/m^3$ and a total cloud thickness of 4 km is referred to as a worst case, but it is possible for values of ρ_ℓ as great as 6 g/m^3 or more to occur. See Table 7.1 for a more complete listing, Fig. 9.15 for a map of cloud regions of the United States, and Slobin (1982) for further information.

5.1.3 Noise

The contributions to system noise temperature due to clouds, water vapor and oxygen (primarily due to clouds) are shown in Table 5.3 also. For considering these values, Eq. (3.25) is repeated below,

$$T_b = T_s e^{-\tau} + T_i\,(1-e^{-\tau}) \qquad (3.25)$$

The equation applies to the brightness temperature T_b when a source at a temperature of T_s is viewed through an absorbing region having an effective temperature of T_i. The parameter τ represents optical depth, namely $\int \alpha_p dl$, the integral of the power density attenuation constant along the path. In the

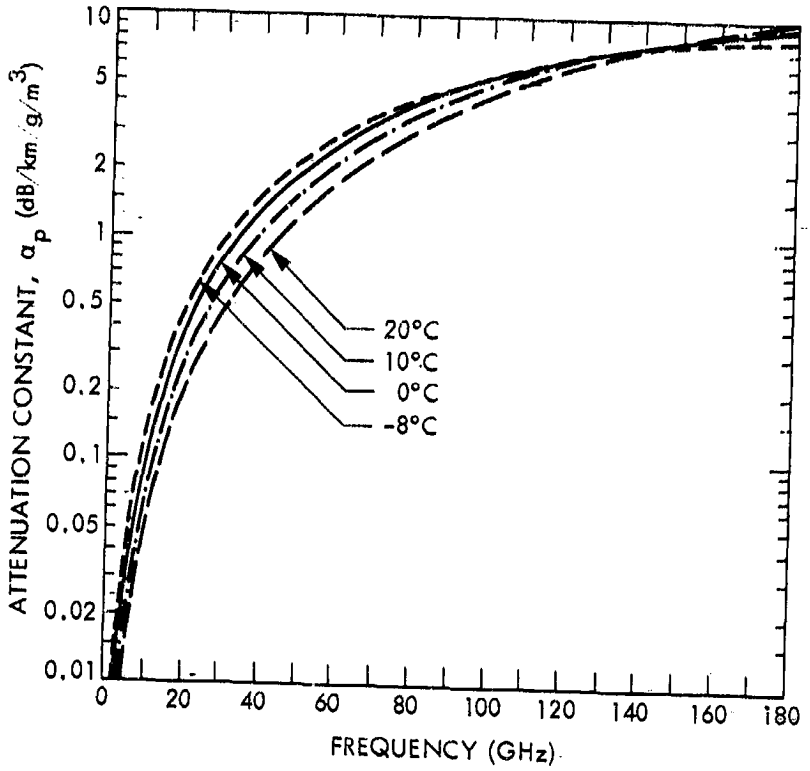

Figure 5.1. Theoretical attenuation by water cloud at various temperatures as a function of frequency (CCIR, 1978a).

C-3

Table 5.2 Im (-R), adapted from Battan (1973).—

Substance	T(°C)	Im (-R), λ = 10 cm	Im (-R), λ = 3.21
Water	20°	0.00474	0.01883
	10°	0.00688	0.0247
	0°	0.01102	0.0335
Ice	0°	9.6×10^{-4}	9.6×10^{-4}
	-10°	3.2×10^{-4}	3.2×10^{-4}
	-20°	2.2×10^{-4}	2.2×10^{-4}

$R = (K_c-1)/K_c+2)$, where K_c is the complex relative dielectric constant.

Table 5.3 Values of Attenuation and Contributions to System Noise Temperature of Cloud Models.

ρℓ	Total Thick-ness	S-Band (2.3 GHz) Zenith		X-band (8.5 GHz) Zenith		X-band (10 GHz) Zenith		K_a-Band 32 (GHz) Zenith	
		T(K)	A(dB)	T	A	T	A	T	A
0.5	2	2.43	0.040	6.55	0.105	8.25	.133	61.00	1.083
0.7	2	2.54	0.042	8.04	0.130	10.31	.166	77.16	1.425
1.0	2	2.70	0.044	10.27	0.166	13.55	.216	99.05	1.939
1.0	3	3.06	0.050	14.89	0.245	19.66	.326	137.50	3.060
1.0	4	3.47	0.057	20.20	0.340	26.84	.457	171.38	4.407
.0	0	2.15	0.035	2.78	0.045	3.05	.049	14.29	0.228

case considered here, the first term has a small value and may possibly be neglected or considered a constant, and the major contribution to T_b comes from the second term. The temperature T_b can be measured, and if τ is known or can be estimated and the first term can be estimated or ignored then a value for T_f can be determined from Eq. (3.25). Conversely, if values for T_f and τ are known or can be assumed, then T_b can be determined. Values for T_f generally range from about 260 K to 280 K.

To illustrate the latter procedures, let us assume an attenuation of 1 dB and a value of 273 K for T_f. Then using

$$A_{dB} = 10 \log L = 10 \tau \log_{10} e = 4.343 \tau \qquad (5.4)$$

where A is attenuation and $L = 1/e^{-\tau}$ and is a loss factor, $\tau = 1/4.343$, $e^{-\tau} = 0.794$, and $T_b = 56$ K [neglecting the first term of Eq. (3.25)]. An attenuation of only 1 dB is seen to be associated with a fairly large contribution to system noise temperature. The subject of noise is treated more fully in Chap. 7.

Attenuation and noise due to clouds are modest but not insignificant at frequencies of 10 GHz and lower. Table 5.3 includes entries for 32 GHz which illustrate the fact that the effects of clouds are more serious at higher frequencies.

5.1.4 Range Delay

In Sec. 3.7, the range or group delay due to dry air and water vapor were considered. Liquid water in the form of clouds and the larger drops of rain may also make a contribution to range delay.

Under the influence of the sinusoidally time-varying electric field of an incident electromagnetic wave, the small spherical droplets of clouds act as tiny antennas having an electric dipole moment p_1. By application of Laplace's equation (Ramo, Whinnery and Van Duzer, 1965, for example), it can be shown that, when the drop diameter is small compared to wavelength, p_1 is given by

$$p_1 = 3V\left(\frac{n^2-1}{n^2+2}\right)\varepsilon_o E_o \tag{5.5}$$

where V is the volume of the spherical particle and n is now the index of refraction of water at the frequency in question. The quantity ε_o is the electric permittivity of empty space (8.854×10^{-12} farads/m) and E_o is the electric field intensity of the incident wave in volts/m. In a region containing N such particles per unit volume

$$P = Np_1 = 3NV\left(\frac{n^2-1}{n^2+2}\right)\varepsilon_o E_o \tag{5.6}$$

where P is the electric dipole moment or electric polarization per unit volume (considering only the effect of the spherical water particles and neglecting all other possible contributions to P). The basic relations, by definition, between E, D (electric flux density), and P for an isotropic medium are that

$$D = \varepsilon_o E + P = \varepsilon_o (1+\chi)E = \varepsilon_o KE \tag{5.7}$$

where K is relative dielectric constant and χ is electric susceptibility. The relative dielectric constant K (commonly designated by ε_r) is equal to $\varepsilon/\varepsilon_o$, where ε is the electric permittivity of the medium. D and P have units of coulombs/m^2. From Eq. (5.7)

$$K = 1 + \chi \tag{5.8}$$

where K is an effective relative dielectric constant of a medium consisting of small spherical water droplets in empty space.

The excess range delay in the medium is proportional to the index of refraction of the medium minus unity. As n has already been used for the index of refraction of water, however, we will use m for the index of refraction of the medium. Index of refraction squared equals relative dielectric constant. Thus

$$m^2 = K \tag{5.9}$$

Then as in general $(1+a)^{1/2} = 1+a/2$ for $a<<1$ and in this case χ is much less than 1

$$m = 1 + \chi/2 \tag{5.10}$$

By comparison of Eqs. (5.6) and (5.7)

$$\chi = 3NV \left(\frac{n^2-1}{n^2+2}\right) \tag{5.11}$$

and

$$m - 1 = \frac{\chi}{2} = \frac{3NV}{2} \left(\frac{n^2-1}{n^2+2}\right) \tag{5.12}$$

The relation for determining the excess range delay ΔR due to the liquid water content of the troposphere is

$$\Delta R = \int \mathrm{Re}\,(m-1)\, dl \tag{5.13}$$

The expression indicates that the real part of m-1 should be used. This notation is needed because the index of refraction of water is complex and m is therefore complex also. The real part of m determines the phase shift and range delay, and the imaginary part determines attenuation. In deriving Eq. (5.12), no mention was made of the lossy nature of the droplets, but relations derived for a lossless medium can be applied to the lossy case by merely utilizing the proper complex value in place of the real value. Whereas the index of refraction of dry air and water vapor are independent of frequency in the radio frequency range up to about 50 GHz the index of refraction of liquid water is a function of frequency and temperature.

To illustrate the range delay due to water droplets in a cloud, consider the range delay for a zenith path through a dense cloud 1 km thick and having a water content of 1 g/m^3. For a frequency f = 3 GHz and temperature T = 20°C, it can be determined from curves given by Zufferey (1972) that $n = 8.88 - j0.63$. As water has a density of 1 g/cm^3, the water content of 1 g/m^3 fills only 10^{-6} of a cubic meter. Then NV of Eq. (5.12) is 10^{-6} and it develops that

$$\text{Re}\,(m-1) = 3/2\,(0.967)\,(10^{-6}) = 1.45 \times 10^{-6}$$

As a region of uniform water content and a thickness of 1 km is assumed, the integral of Eq. (5.13) simplifies to become the product of Re (m-1) and 10^3 m so that $\Delta R_2 = 1.45 \times 10^{-6}\,(10^{-3}) = 1.45 \times 10^{-3}$ m = 0.145 cm. For f = 10 GHz, n = 8.2-j1.8 and the value of ΔR is 0.144 cm, while for f = 30 GHz, n = 6-j2.8 but ΔR is still about 0.144 cm. The excess range delay in this case is quite insensitive to the value of n, which condition might be anticipated by noting that n^2 appears in both the numerator and denominator of Eq. (5.12). The excess delay is therefore insensitive to frequency as well. The water content of 1 g/m^3 assumed in the above example is that of a rather dense cloud, but it has been reported that the maximum water content of clouds lies between 6 and 10 g/m^3.

Raindrops are considerably larger than the small droplets of clouds, and to analyze the effects of raindrops one must generally use the Mie scattering theory or refinements of it. The technique of deriving an equivalent index of refraction can nevertheless be employed for rain; this approach has been utilized most extensively for determining the attenuation constant for propagation through rain. If $m = m_r - jm_i$, the field intensity attenuation constant α is given by

$$\alpha = \beta_0 m_i \qquad \text{Neper/m} \tag{5.14}$$

where $\beta_0 = 2\pi/\lambda_0$ is the phase constant and λ_0 is wavelength for propagation in empty space. (One Neper equals 8.68 dB.) The phase constant β for propagation through a region of rain is given by

$$\beta = \beta_0 m_r \qquad \text{radian/m} \tag{5.15}$$

For calculating the excess range delay ΔR due to rain, one can use

$$\Delta R = \int \text{Re}\,(m-1)\,dl = \int (m_r - 1)\,dl \tag{5.16}$$

Tables giving values of m_r-1 have been provided by Setzer (1970), and Zufferey (1972) has presented these values in graphical form. Setzer's value for m_r-1 for a rain of 25 mm/h at a frequency of 3 GHz, for example, is 1.8 X 10^{-6}. The excess range delay in a 1 km path of uniform rain of that rate is (1.8 X 10^{-6}) (10^3) = (10^3) = 0.18 cm, a value comparable to that for a zenith path through a cloud 1 km thick. For heavy rain of 150 mm/h the delay would be 0.92 cm in 1 km.

For estimating total excess range delay due to rain, one needs an estimate of effective path length through rain. This topic of effective path length has been considered with respect to estimating attenuation due to rain (Sec. 4.3.2). Effective path lengths through rain tend to be in the order of 4 or 5 km for an elevation angle of 45° at a latitude of 40°N and these figures can be used as a rough guide. In contrast with attenuation in rain which increases with frequency up to about 150 GHz, excess range delay decreases above 10 GHz and stays nearly constant below 10 GHz to 1 GHz or lower but has modest maxima in the 6 to 10 GHz range, depending on rain rate (Fig. 4.3a). It appears that the excess range delay due to rain may be of significance in some heavy rainstorms.

5.2 SAND, DUST, AND OTHER PARTICULATES

Sand and dust storms may reduce visibility to 10 m or less, reach a height of 1 km or more, and extend for hundreds of kilometers over the Earth's surface. Based on extrapolation of laboratory measurements at 10 GHz by Ahmed and Auchterlonie (1975), it has been estimated that the attenuation constant for a particulate density of 10 g/m^3 is less than 0.1 dB/km for sand and 0.4 dB/km for clay (CCIR, 1978a). It was concluded that total attenuation along an earth-space path should be less than 1 dB.

An analysis by Bashir, Dissanayake, and McEwan (1980) for 9.4 GHz has included the case of moist sandstorms and, assuming oblate spheroidal particles, has provided different values of attenuation for horizontal and vertical polarizations. Values for attenuation for moist sandstorms were as high as 1.83 dB/km for horizontal polarization. For dry sand the values were about 0.27 dB/km. Values for particulate density per m^3 of air were not given, but information on particle volumes was included. If the particles themselves

have densities of 1 g/cm^3, the particulate densities or loading in air would be about 1 g/m^3. Thus, particulate densities in the order of 1 to 10 g/m^3 have been assumed for obtaining estimates of attenuation in the cases cited here. Bashir et al (1980) concluded that attenuation in sandstorms could be a problem for domestic-satellite services in desert areas if sandstorms were encountered at both of two earth stations that were communicating via satellite. The possibility of depolarization and interference due to scatter in undesired directions were also considered. The effect of sand storms on microwave propagation has also been analyzed by Chu (1979) and Ghobrial (1980), and Goldhirsh (1982) has presented a unified, quantitative treatment of the effect of dust storms over desert regions on radar operations. The attenuation constant for propagation through dust or sand storms at centimeter wavelengths, as presented by Ghobrial and repeated by Goldhirsh is

$$\alpha = \frac{1.029 \times 10^6 \, K_{im} \, N_T}{[(K_r + 2)^2 + K_{im}^2]\lambda} \sum P_i \, r_i^3 \qquad \text{dB/km} \qquad (5.17)$$

where K_r and K_{im} are the real and imaginary parts of the complex relative dielectric constant of the dust or sand particles, N_T is the total number of particles per m^3, λ is the wavelength, and P_i is the probability that the particle radius lies between r_i and $r_i + \Delta r_i$. The quantity $K_{im}/[(K_r + 2)^2 + K_{im}^2]$ represents Im $[-(K_c - 1)/(K_c + 2)]$ as in Eq. (5.2) except that Eq. (5.2) refers to water drops. The effects of dust and sand on radar performance tend to be more serious than for earth-space communications because of the longer paths through dust or sand storms and two-way propagation over such paths.

Many aerosols of natural and manmade origin occur in the Earth's atmosphere and might occasionally have a slight effect on telecommunications on a local scale. Two sources of information on aerosols (particulate matter of the atmosphere) are Clouds and Storms by Ludlam (1980) and Man's Impact on the Global Environment (SCEP, 1970). Most interest in such particulate matter is related to air pollution or scientific considerations. Clearly visible clouds of pollen are given off by some trees, e.g. pine trees, during spring windstorms, and pollen from various plants is a source of hay-fever. Measurements in the plume of the Mt. St. Helens eruption of May 18, 1980 showed that particle number densities about 9.3 km downwind in the 0.01 to 10 μm diameter

range were from 4 to 1000 times the number density in the ambient air. For particles <2 μm in diameter the mass loading was about 9.5×10^{-5} g/m^3 compared with less than 10^{-7} g/m^3 in the ambient air (Hobbs et al, 1981). Even interplanetary space is not completely empty but is permeated by the solar wind and has a dust content of around 10^{-17} or 10^{-18} g/m^3 (Berman, 1979; Halliday and McIntosh, 1980).

5.3 BIOLOGICAL MATTER

Vegetation can have important effects on radio wave propagation, especially in the case of mobile communications. Flocks of birds are essentially large blobs of water as far as effects on radio waves are concerned and they can attenuate and scatter incident waves. Insects as well as birds are readily detectable by radar means and can have an effect on propagation when they occur in large concentrations, as in the case of swarms of locusts in Africa. The effects of these various forms of biological matter on propagation are considered briefly in this section. Vegetation is attached to but not part of the ground, except for roots, and is therefore included in this chapter, whereas phenomena of the solid or liquid Earth are considered in Chap. 6.

Propagation through the vegetation of dense forests and jungles has been treated by considering the forest to be a lossy dielectric having a complex relative dielectric constant ε_c and a complex index of refraction $n_c = n_r - jn_i$. In such a case, an electromagnetic wave is attenuated by a factor $e^{-\alpha d} = e^{-\beta_0 n_i d}$ where $\beta_0 = 2\pi/\lambda_0$ and is the free-space propagation constant, n_i is the magnitude of the imaginary part of the complex index, and d is distance. The attenuation due to this factor is the excess loss above that due to spreading. Using the form $\varepsilon_c = \varepsilon (1 - j \tan \delta)$ for the complex relative dielectric constant, Tamir (1974) has reported that measured values of ε range from 1.01 to 1.1 and $\tan \delta$ values range from 0.01 to 0.15. The quantities ε_c and n_c are related by $\varepsilon_c = n_c^2$.

In addition to a direct path through a section of forest, there may be additional paths as shown in Fig. 5.2. In this model TR is the direct path. Rays incident upon the upper boundary at angles equal to or greater than the critical angle θ_c, measured from perpendicular to the boundary, experience

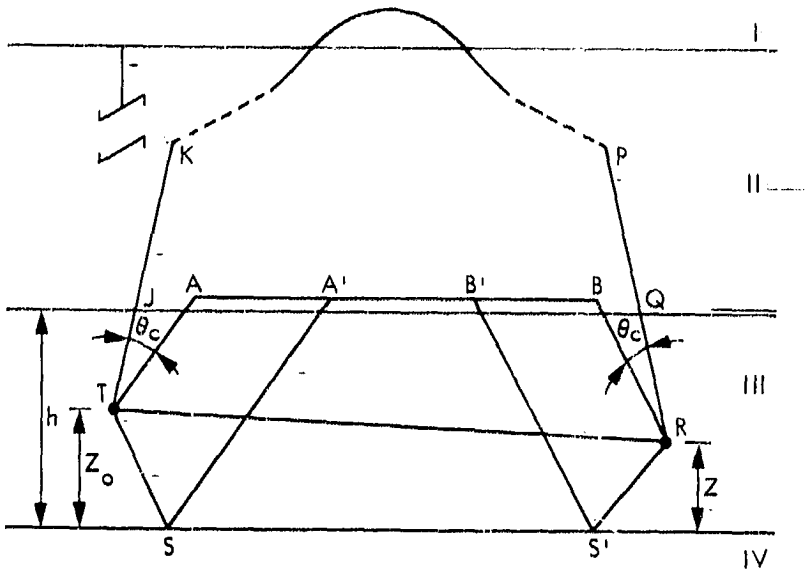

Figure 5.2. Ray paths in an idealized forest environment (Tāmir, 1974; CCIR, 1978b).

total reflection and energy may thus reach the receiver by a path such as TABR, for example.

Waves which skim over the tree tops following a path like TABR have been referred to as lateral waves (Tamir, 1974). Some energy may also be reflected from the ground as at S and S' and eventually reach the receiver location. Attenuation on direct paths like TR and reflected paths is very high, and for other than short paths propagation is said to be by lateral waves, or by a sky wave for lower frequencies.

Using data from several sources in the frequency range from 100 MHz to 3.3 GHz, LaGrone (1960) found an average excess attenuation constant α of $1.3 \times 10^{-3} f_{MHz}^{0.77}$ dB/m for propagation through woodland. Other data for propagation through woodland in the frequency range from 30 MHz to 2 GHz are summarized in Fig. 5.3 (CCIR, 1978b). For propagation over a grove of trees when transmitting and receiving antennas are sufficiently far from the trees,

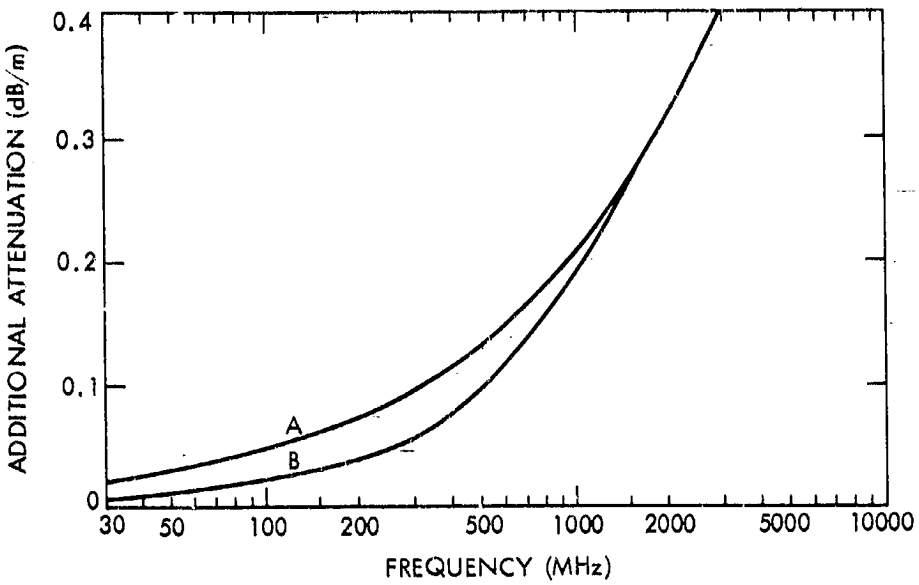

Figure 5.3. Excess attenuation in propagation through woodland (CCIR, 1978b).

transmission has been found to be primarily by diffraction (LaGrone, 1977). When the antennas are closer to small groves of trees less than 400 m in extent, Weissberger (1980) found the attenuation A in dB for a particular set of data to be given by $A = 0.197\ f_{MHz}^{0.284}\ d^{0.588}$ where f is frequency in MHz and d is distance in m.

Because of the highly variable nature of forests and vegetation as regards density, species, habits of growth, moisture content, how recently it has rained, and topography, it is very difficult to estimate attenuation in advance. Any expression or curve such as those given should be used only to obtain a very rough idea of possible effects. The proceedings of a workshop on radio systems in forested and/or vegetated environments contain considerable discussion about propagation in such environments (Wait, Ott, and Telfer, 1974). The paper by Tamir (1974) on lateral waves and a quite comprehensive though brief paper by Hagn (1974) are included in the proceedings of this workshop. All information reported here is for terrestrial paths but should apply to some degree for earth-space paths.

Effects of birds and insects on telecommunications can be expected to be localized. In the near vicinities of breeding and wintering colonies of birds and along major migration routes in the spring and fall, concentrations of birds could disrupt communications momentarily or increase the bit error rate for digital communications. Concentrations of sea birds occur in summer in arctic and subarctic areas, including the Aleutian and Pribilof Islands and Bering Strait of Alaska, Baffin Island of Canada, etc. Wintering areas of waterfowl and cranes in North America include the Gulf Coast, southern New Mexico, and interior valleys of California. The areas of bird concentration are frequently in or near wildlife refuges operated by federal agencies (Butcher, 1955), and contact with personnel of the wildlife agencies, the U. S. Fish and Wildlife Service in the United States, and the Canadian Wildlife Service in Canada, would be advisable if consideration is being given to installations near wildlife refuges or other areas of bird concentration. Concentrations of blackbirds and starlings are sometimes a problem in towns and cities. In addition to causing attenuation of transmissions, large flocks of birds scatter incident electromagnetic radiation and make good radar targets (Eastwood, 1967; Flock, 1974). Thus they have the potential to cause interference between two or more telecommunications or radar systems.

The pollen introduced into the atmosphere by trees and other plants falls under the heading of biological matter. Airborne cottonwood seeds are plentiful in certain areas (e.g. Boulder, Colorado) in the spring. As they are detectable by radar they have some potential for causing interference also.

REFERENCES

Ahmed, I. Y. and L. J. Auchterlonie, "Microwave measurements on dust using an open resonator," Electronics Letters, vol. 12, pp. 445, 446, 19 Aug. 1979.

Bashir, S. O., A. W. Dissanayake, and N. J. McEwan, "Prediction of forward scattering and cross polarization due to dry and moist haboob and sandstorms in Sudan in the 9.4 GHz band," Telecom. J., vol. 47, pp. 462-467, July, 1980.

Battan, L. J., Radar Observation of the Atmosphere, Chicago: U. of Chicago Press, 1973.

Benson, C. S., Ice Fog: Low Temperature Air Pollution. Report UAG R-173, Geophysical Institute, U. of Alaska, Fairbanks, AK, 1965.

Benson, C. S., "Ice fog," Weather, vol. 25, pp. 9-18, Jan. 1970.

Berman, A. L., "A Unified Observational Theory for Solar Wind Columnar Turbulence," DSN Progress Report 42-50, pp. 124-131, Jan. and Feb. 1979.

Butcher, D., Seeing America's Wildlife, New York: Devin Adair Co., 1955.

CCIR, "Attenuation and scattering by precipitation and other atmospheric particles," Report 721 in vol. V, Propagation in Non-ionized Media, Recommendations and Reports of the CCIR, 1978, pp. 107-115. Geneva: Int. Telecomm. Union, 1978a.

CCIR, "Influence of terrain irregularities and vegetation on tropospheric propagation," Report 236-4 in vol. V, Propagation in Non-ionized Media Recommendations and Reports of the CCIR, 1978, pp. 52-56. Geneva: Int. Telecomm. Union, 1978b.

Chu, T. S., "Effects of sandstorms on microwave propagation," Bell Syst. Tech. J., vol. 58, pp. 549-555, Feb. 1979.

Donn, W. L., Meteorology, New York: McGraw-Hill, 1975.

Eastwood, E., Radar Ornithology. London: Methuen, 1967.

Flock, W. L. and J. L. Green, "The detection and identification of birds in flight using coherent and noncoherent radars," Proc. IEEE, vol. 62, pp. 745-753, June 1974.

Ghobrial, S. F., "The effect of sandstorms on microwave propagation," Proc. Nat. Telecomm. Conf., Houston, TX, vol. 2, pp. 43.5.1-43.5.4, 1980.

Goldhirsh, J., "A parameter review and assessment of attenuation and backscatter properties associated with dust storms over desert regions in the frequency range of 1 to 10 GHz," IEEE Trans. Antennas on Propagation, vol. AP-30, pp. 1121-1127, Nov. 1982.

Gunn, K. L. S. and T. W. R. East, "The microwave properties of precipitation particles," Quart. J. Roy. Meteor. Soc., vol. 80, pp. 522-545, 1954.

Hagn, G. H., "Electrical properties of forested media," in Workshop on Radio Systems in Forested and/or Vegetated Environments, Wait, J. P., R. H. Ott, and T. Telfer (eds.), pp. I-C-1 to I-C-15, Technical Report No. ACC-ACO-I-74, U. S. Army Communications Command, Fort Huachuca, AZ, Feb. 1974 (distributed by NTIS, Springfield, VA).

Halliday, I. and B. A. McIntosh (eds.), Solid Particles in the Solar System, Symposium No. 90, IAU, Ottawa, Canada, Aug. 27-30, 1979. Dordrecht, Holland; Boston: D. Reidel Pub. Co., 1980.

Hobbs, P. W., L. F. Radke, M. W. Eltgroth, D. A. Hegg, "Airborne studies of emissions from the volcanic eruptions of Mount St. Helens," Science, vol. 211, pp. 816-818, 20 Feb. 1981.

LaGrone, A. H., "Forecasting television service fields," Proc. IRE, vol. 48, pp. 1011, June, 1960.

Ludlam, F. H., Clouds and Storms, University Park: Pennsylvania State U. Press, 1980.

Ramo, S., J. R. Whinnery, and T. Van Duzer, Fields and Waves in Communication Electronics. New York: Wiley, 1965.

SCEP (Study of Critical Environmental Problems), Man's Impact on the Global Environment, Cambridge, MA; M.I.T. Press, 1970.

Setzer, D. E., "Computed transmission through rain at microwave and visible frequencies," Bell System Tech. Jour., Vol. 49, pp. 1873-1892, Oct. 1970.

Slobin, S. D., Microwave Noise Temperature and Attenuation of Clouds at Frequencies Below 50 GHz, JPL Publication 81-46, Pasadena, CA: Jet Propulsion Lab., 1981.

Slobin, S. D., "Microwave noise temperature and attenuation of clouds: statistics of these effects at various sites in the United States, Alaska, and Hawaii", Radio Science, vol. 17, pp. 1443-1454, Nov.-Dec. 1982.

Smith, E. K. and Re. E. Edelson, Radio Propagation through Solar and other Extraterrestrial Ionized Media, JPL Publication 79-117, Pasadena, CA: Jet Propulsion Laboratory, Jan. 15, 1980.

Staelin, D. H., "Measurements and interpretation of the microwave spectrum of the terrestrial atmosphere near 1-centimeter wavelength," J. Geophys. Res., vol. 71, pp. 2975-2881, 1966.

Tamir, T., "Lateral wave applications to radio systems," in Workshop on Radio Systems in Forested and/or Vegetated Environments, Wait, J. R., R. H. Ott, and T. Telfer (eds.), pp. I-B-1 to I-B-7, Technical Report No. ACC-ACO-I-74, U. S. Army Communications Command, Fort Huachuca, AZ, Feb. 1974 (distributed by NTIS, Springfield, VA).

Valley, S. L. (ed.), Handbook of Geophysics and Space Environments, New York; McGraw-Hill, 1965.

Wait, J. R., R. H. Ott, and T. Telfer (eds.), Workshop on Radio Systems in Forested and/or Vegetated Environments, Technical Report No. ACC-ACO-I-74, U. S. Army Communications Command, Fort Huachuca, AZ, Feb. 1974, (distributed by NTIS, Springfield, VA).

Weissberger, M. and J. Hauber, "Modeling the increase in loss caused by propagation through a grove of trees," North American Radio Science Meeting, Quebec, June, 1980.

Zufferey, C. H., "A Study of Rain Effects on Electromagnetic Waves in the 1-600 GHz Range," M. S. thesis. Boulder, CO: Department of Electrical Engineering, University of Colorado, 1972 (reprinted in 1979).

CHAPTER 6
TERRAIN EFFECTS AND MULTIPATH PROPAGATION

6.1 GROUND WAVES AND EFFECTS OF TERRAIN

Previous chapters have dealt largely wth atmospheric effects on radio-wave propagation, but terrestrial telecommunication links and earth-space transmissions at small elevation angles or between satellites and mobile receivers may be influenced by the electrical properties of the Earth's surface and by features of terrain. Reflections from the solid Earth, manmade structures, and bodies of water may result in multipath propagation which is characterized by fading. This topic is treated in Sec. 6.2. A brief treatment of other effects of the Earth's surface on radio-wave propagation is given in this section. In Secs. 6.3-6.5, the three classes of mobile-satellite services--land-mobile, marine-mobile, and aeronautical-mobile--are considered.

6.1.1 Ground Waves

One means by which radio waves propagate from one location to another is by ground waves. In analyzing propagation near the Earth's surface what are referred to as ground waves are often separated into space waves and surface waves. A space wave consists of the direct wave from transmitter to receiver and the reflected wave, if any that reaches the receiver after reflection from the Earth's surface. It is the surface wave that is most strongly affected by the electrical properties of the Earth. The attenuation of the surface wave is high and surface wave propagation is limited to short distances for high frequencies. The surface wave is the principal component of the ground wave for frequencies of a few MHz, is of secondary importance at VHF (30-300 MHz), and can be neglected for frequencies greater than 300 MHz (Bullington, 1977).

An approximate expression for the attenuation or loss factor L_s for a surface wave is

$$L_s = \frac{-1}{1 - j\, 2\pi d/\lambda (\sin\theta + z)^2} \qquad (6.1)$$

where

$$z = \left(K - j \frac{\sigma}{\omega \varepsilon_0} - \cos^2 \theta\right)^{1/2}$$

for horizontal polarization and

$$z = \frac{\left(K - j \frac{\sigma}{\omega \varepsilon_0} - \cos^2 \theta\right)^{1/2}}{K - j \frac{\sigma}{\omega \varepsilon_0}}$$

for vertical polarization. L_s has a maximum value of unity. The expression is most accurate for $L_s \leq 0.1$ and within 2 dB in amplitude in any case but in error in phase by 180^0 as $L_s \to 1$ (Bullington, 1977). In the above expressions $\sigma/\omega\varepsilon_0$ can be replaced by its approximate equivalent $60\sigma\lambda$. The conductivity σ is in mhos/m, θ is the elevation angle, $\omega = 2\pi f$ where f is frequency, ε_0 is the electric permittivity of empty space (8.854×10^{-12} F/m), and K is the relative dielectric constant. If using $60\sigma\lambda$, λ is in m. Surface waves are most important at frequencies below the 100 MHz lower limit of this handbook and in a region within a few wavelengths of the ground. They can be neglected in most applications of microwave mobile communications (Jakes, 1974, where the microwave range is treated as from about 450 MHz to 10 or 20 GHz). A more thorough treatment of surface waves can be found in Jordan and Balmain (1968). Ground-wave propagation at frequencies from 10 kHz to 30 MHz is considered in CCIR Recommendation 368-3 (CCIR, 1978a).

6.1.2 Effects of Obstructions

Obstructions along a path in the form of hills and buildings introduce loss with respect to free-space propagation, and the loss varies with time because tropospheric refraction varies with time. For considering the effect of obstructions, the concept of Fresnel zones is useful. To introduce this topic consider Fig. 6.1 which shows two paths TPR and TSR between a transmitter T and a receiver R. TPR is a direct path, and TSR is longer than TPR. If TSR = TPR + $\lambda/2$ where λ is wavelength, the region within the radius r (in the plane perpendicular to TR), at the distance d_T from T and d_R from R, is defined as the first Fresnel zone. The particular value of r in this case

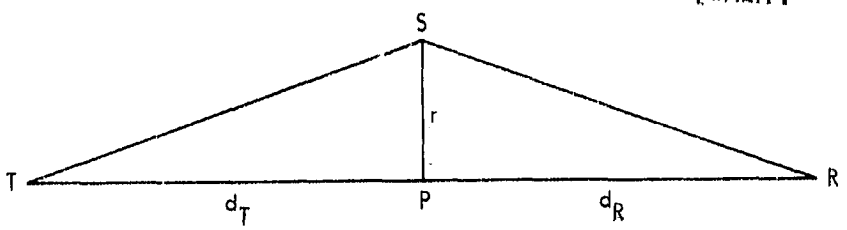

Figure 6.1. Geometry for consideration of Fresnel zones.

is the first Fresnel zone radius and is designated here by F_1. The above concept can be extended to the case when TSR = TPR + $n\lambda/2$, for which the corresponding Fresnel zone radius can be designated as F_n. The significance of the first Fresnel zone is that all the elements of radiation passing through this zone have components of electric field intensity that add constructively. Radiation passing through the second Fresnel zone (values of r between F_1 and F_2), however, interferes destructively with radiation passing through the first Fresnel zone, that passing through the third Fresnel zone adds constructively with that in the first zone but makes a smaller contribution, etc. The process can be understood in terms of Huygen's principle which states that every elementary area of a wavefront can be regarded as a source of secondary spherical waves. When r is small compared to d_T and d_R, it can be determined that

$$F_1 = \sqrt{\frac{\lambda d_T d_R}{d}} \quad \text{m} \tag{6.2}$$

where $d = d_T + d_R$ and all lengths are in meters or that

$$F_1 = 17.3 \sqrt{\frac{d_T d_R}{fd}} \quad \text{m} \tag{6.3}$$

if distances are in km, f is measured in GHz, and F_1 is in meters. For the situation where d_T is approximately equal to d the expression for F_1 corresponding to Eq. (6.2) is

$$F_1 = \sqrt{\lambda d_R} \quad \text{m} \tag{6.4}$$

The value of F_n is related to that for F_1 by

$$F_n = \sqrt{n}\, F_1 \tag{6.5}$$

One might think that a satisfactory signal amplitude would result on a telecommunications link as long as a direct line of sight from the transmitter to the receiver is provided, but consideration of Huygen's principle suggests that having a direct line of sight may not be sufficient. The analysis of the effect of an obstruction approximating a knife edge is given in texts on optics, for example that by Jenkins and White (1976), and in Jordan and Balmain (1968). The results are conveniently expressed in terms of the ratio h_c/F_1 of path clearance h_c to the first Fresnel zone radius F_1, as in Fig. 6.2. If the edge of the knife-edge obstruction is at the direct line of sight, a loss of 6 db is encountered. To avoid attenuation a clearance of about 0.6 F_1 is required. Note that the Fresnel zone analysis is in terms of field intensity. For zero clearance the total field intensity at the receiver location is reduced to 0.5 of the value for a completely unobstructed path. A reduction of field intensity to 0.5 corresponds to a reduction of power to 0.25 and therefore to the loss of 6 dB. In analyses of diffraction a parameter v equal to $\sqrt{2}\, h_c/F_1$ may be utilized and resulting values of attenuation may be plotted as a function of v instead of h_c/F_1. The parameter v is used, for example, in CCIR Report 715 (CCIR, 1978b) and in Jordan and Balmain (1968).

The field intensity beyond an obstacle is dependent upon the form of the obstacle. Whereas the loss due to a knife-edge obstacle at grazing incidence is 6 dB, the corresponding value for a smooth spherical earth is about 20 dB (Bullington, 1977). Formulas and nomograms for determining the loss due to diffraction by a smooth spherical earth are given in CCIR Report 715. This same report and CCIR Report 236-4 discuss propagation over irregular terrain, and Hall (1979) also treats this difficult topic. Multiple knife-edge diffraction is the subject of a paper by Deygout (1966). His approach is to first determine which knife-edge obstacle causes the greatest loss and to

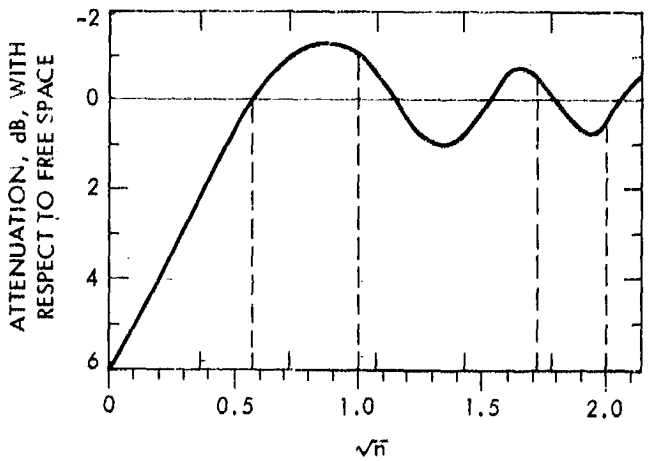

Figure 6.2. Attenuation due to knife-edge diffraction, with relation to free space, as a function of $h_c/F_1 = \sqrt{n}$ (Hall, 1979).

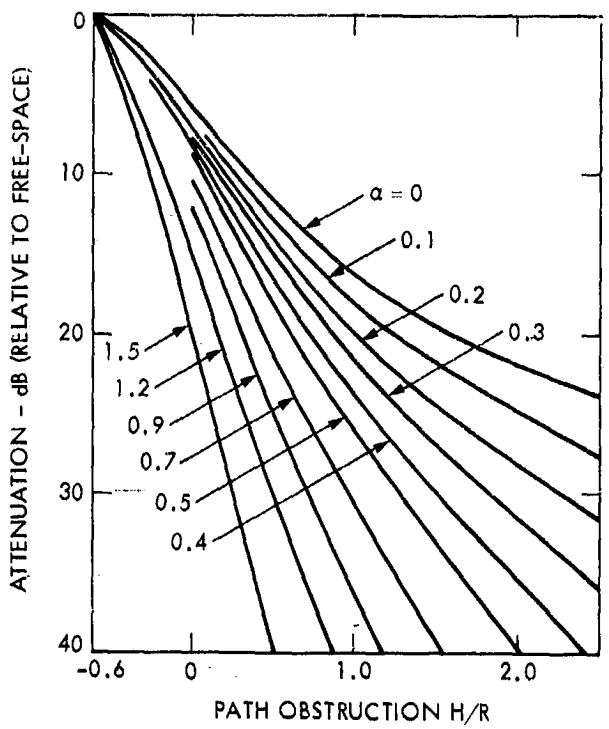

Figure 6.3. Attenuation due to diffraction over obstacles, with relation to free space, as a function of the parameter of α and $H/R = H/F_1$ with H the height of the obstacle above a direct unobstructed path (Assis, 1971).

determine this loss. Then locations and additional losses are calculated for the other knife-edge obstacles. Assis (1971), noting that the assumption of a knife-edge often gives overly optimistic results, employs the approach of Deygout but applies it to the case of rounded obstacles. He provides a set of curves (Fig. 6.3) which give loss as a function of H/F_1, where H is the height of the obstacle above a direct unobstructed path from transmitter to receiver, and the parameter α where

$$\alpha = \lambda^{2/3} r^{1/3}/F_1 \tag{6.6}$$

with λ the wavelength, r the radius of curvature, and F_1 the first Fresnel zone radius. Note that the condition $H/F_1 = -0.6$ corresponds to $h_c/F_1 = 0.6$ and to free-space propagation. Also $H/F = 0$ and $\alpha = 0$ is the condition for the loss of 6 dB mentioned for knife-edge diffraction, and $H/F_1 = 0$ and $\alpha = 1.5$ corresponds roughly to the loss of 20 dB mentioned earlier as well. For positive values of H/F_1, corresponding to obstructions extending above direct unobstructed paths, losses are shown to increase above those for $H/F_1 = 0$. An alternative approach to propagation over irregular terrain uses the theory of integral equations (Ott, 1971) instead of diffraction theory.

It is possible for the signal beyond an obstacle, such as a mountain, to be larger than if the obstacle was not present. This condition occurs due to diffraction alone in the case of a knife-edge obstacle as in Fig. 6.2, but in this case the enhancement in signal level occurs when there is a direct line-of-sight path, with an obstacle below the direct path. More commonly the term obstacle gain is applied when there is no line-of-sight path. In this case obstacle gain involves multipath propagation as in Fig. 6.4, for example, where four paths exist between a transmitter and a receiver on the opposite side of an obstacle. Obstacle gain depends upon the occurrence of favorable

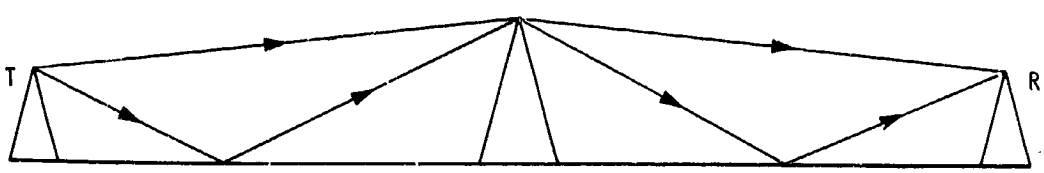

Figure 6.4. Possible ray paths contributing to obstacle gain.

phase relations between the signals arriving over the different paths. It can be destroyed by meteorological variations and thus may be subjet to fading but can be used to advantage in certain circumstances (Kirby et al., 1955; Hall, 1979).

The losses associated with the occurrence of obstacles on mobile communication systems are commonly referred to as shadowing losses.

6.2 MULTIPATH PROPAGATION

6.2.1 Introduction

The term multipath refers to a condition in which energy reaches the receiver of a telecommunications system by more than one path. Multipath operation tends to be undesirable, because the signals arriving over the different paths tend to arrive with variable relative phase, with the result that they alternately reinforce each other and interfere destructively. The total signal is then characterized by fading involving repeated minima, and the danger exists that the minima will fall below the acceptable signal level. The signals arriving over the different paths also have different time delays which can result in intersymbol interference in digital systems. Multipath propagation may result from reflections from land and water surfaces and man-made structures. Multipath propagation may also arise from atmospheric effects alone, in the absence of reflections from surface features.

Reflections from a plane surface and the total electric field intensity which results when field intensities arriving over two paths are summed can be considered with the aid of Fig. 6.5. The figure shows direct and reflected rays reaching a receiver at a height h_R above a flat, smooth surface at $h = 0$. The transmitter is assumed to be so far away that the two rays can be considered to be parallel at an elevation angle of θ from the horizontal. Assuming also a perfectly conducting surface and horizontal polarization, a 180^0 phase shift will occur upon reflection so that at $h = 0$ $E_r = -E_i$, where E_r is the field intensity of the reflected wave and E_i is the field of the incident wave of path 2 of Fig. 6.5. The difference in length of paths 1 and 2, $\Delta\ell$, is $2h_R \sin\theta$. If $\Delta\ell = \lambda/2$ (or $n\lambda/2$ with n odd), maximum total signal intensity will be recorded as the combination of the -180^0 phase shift on

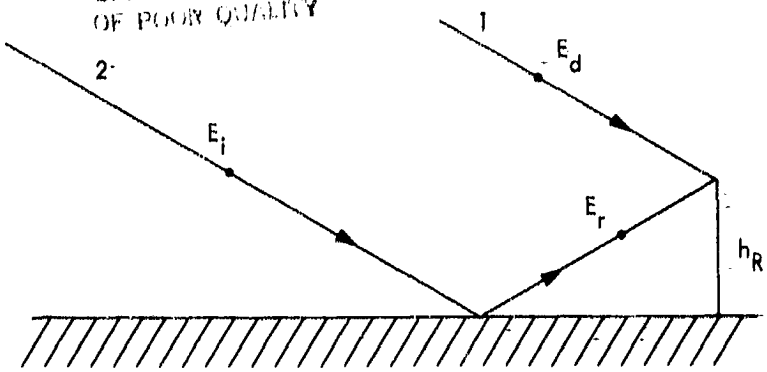

Figure 6.5. Direct and reflected rays for space-earth path employing horizontal polarization (electric-field intensity vectors perpendicular to the plane of the drawing).

reflection and the phase shift of 180^0 corresponding to $\Delta\ell = \lambda/2$ results in signal reinforcement. If $\Delta\ell = \lambda$ (or $n\lambda/2$ with n even), destructive interference between the two rays occurs as they then differ in phase by 180^0. It might seem that satisfactory operation is assured if h_R is chosen so that $\Delta\ell = n\lambda/2$ with n odd. The discussion to this point, however, has neglected the atmosphere. In the Earth's atmosphere the ray paths will be curved to some degree and variable with time so that destructive and constructive interference may take place alternately even for a fixed receiver location and height. In mobile operations, furthermore, the receiver position with respect to reflecting surfaces will vary and the height will not necessarily be optimum at any particular location.

The phase shift ϕ corresponding to the difference in path length $\Delta\ell = 2h_R \sin\theta$ is given by

$$\phi = \frac{4\pi h_R \sin\theta}{\lambda} \qquad (6.7)$$

where λ is wavelength. If the field intensities E_1 and E_2 of rays arriving over the two paths of Fig. 6.5 have the same amplitude E_0, the total field intensity can be found to be given, with the aid of Fig. 6.6, by

$$|E| = \left|2E_0 \sin\left(\frac{2\pi h_R \sin\theta}{\lambda}\right)\right| \approx \left|2E_0 \sin\frac{\phi}{2}\right| \qquad (6.8)$$

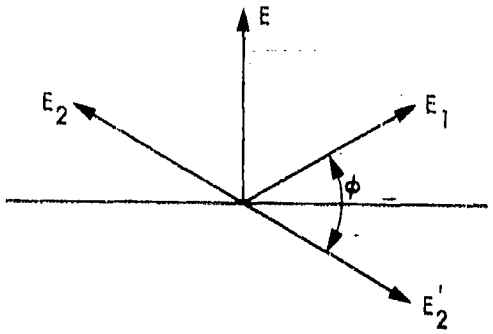

Figure 6.6. Phasor diagram illustrating how field intensities of direct and reflected rays (E_1 and E_2) add to give total electric field intensity E.

The two phasors E_1 and E_2 represent field intensities arriving over paths 1 and 2 at the receiver location of Fig. 6.5. In the absence of the phase reversal of 180° upon reflection, E_2 would have the direction of E_2'. Taking account of the phase reversal, the components of E_1 and E_2 along the vertical axis add so that $E = 2E_0 \sin \phi/2$.

For terrestrial paths, the analysis of how direct and reflected waves combine to reinforce or interfere destructively can be analyzed with the help of Fig. 6.7. For the case that $d \gg h_R$ and $d \gg h_T$ and for propagation over a flat earth $\Delta\ell = r_2 - r_1 = 2\pi h_T h_R/d$. The corresponding phase difference

$$\phi = \frac{2\pi}{\lambda}(r_2 - r_1) = \frac{4\pi h_T h_R}{\lambda d} \qquad (6.9)$$

For a perfectly conducting surface and assuming equal field intensities E_0 for the two paths it develops that after taking account of the reversal of phase on reflection

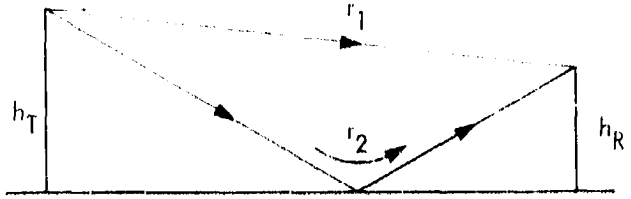

Figure 6.7. Direct and reflected rays for terrestrial path.

$$|E| = \left|2\, E_0 \sin\left(\frac{2\pi h_T h_R}{\lambda d}\right)\right| = \left|\, 2E_0 \sin\frac{\varphi}{2}\,\right| \qquad (6.10)$$

The relations for the terrestrial path have been included for comparison with those for a path from space to earth. Equation (6.8) can be obtained from Eq. (6.10) by replacing h_T/d by $\sin\theta$.

The approaches shown for earth-space and terrestrial paths can be modified to take account of earth curvature when necessary (Beckmann and Spizzichino, 1963; Flock, 1979). Earth curvature affects the phase relation between direct reflected rays and may also result in a decrease in the magnitude of the reflected ray. The latter condition tends to be most important for aeronautical-mobile systems and is mentioned further in Sec. 6.5.

The different time delays of the signal arriving over the different paths when multipath propagation occurs also tend to be of most importance for aeronautical-mobile systems, for which the differences tend to be greatest. The time delays tend also to be of greater importance for digital systems than for systems employing analog signals.

6.2.2 Reflection Coefficient for Specular Reflection

The complex electric field intensity E_r of the reflected wave on path 2 at $h = 0$ has an amplitude and phase angle that is given by the product of E_i, the electric field intensity of the incident wave at $h = 0$, and the reflection coefficient ρ (Fig. 6.5). Thus, at $h = 0$, $E_r = \rho E_i$ or

$$\rho = E_r/E_i \qquad (6.11)$$

where all 3 quantities may be complex. It is evident that the reflection coefficient determines the amplitude and phase of the reflected wave, with respect to the incident wave. The greater the magnitude of ρ, the greater is the potential for harmful fading.

The reflection coefficient for a smooth surface is a function of the relative dielectric constant K, conductivity σ (mhos/m), elevation angle θ, and angular frequency $\omega = 2\pi f$. For a horizontally polarized incident wave the reflection coefficient ρ_h is given by

$$\rho_h = \frac{\sin\theta - \sqrt{K - j\,\sigma/\omega\varepsilon_0 - \cos^2\theta}}{\sin\theta + \sqrt{K - j\,\sigma/\omega\varepsilon_0 - \cos^2\theta}} \qquad (6.12)$$

The angle θ is measured from the horizontal. The symbol ε_0 represents the electric permittivity of empty space, 8.854×10^{-12} F/m.

The usual form for ρ_v the reflection coefficient for vertical polarization, or for the electric field intensity vectors in the plane of incidence (the plane of the drawing as shown in Fig. 6.8), is

$$\rho_v = \frac{[K - j\sigma/\omega\varepsilon_0]\sin\theta - \sqrt{K - j\,\sigma/\omega\varepsilon_0 - \cos^2\theta}}{[K - j\sigma/\omega\varepsilon_0]\sin\theta + \sqrt{K - j\,\sigma/\omega\varepsilon_0 - \cos^2\theta}} \qquad (6.13)$$

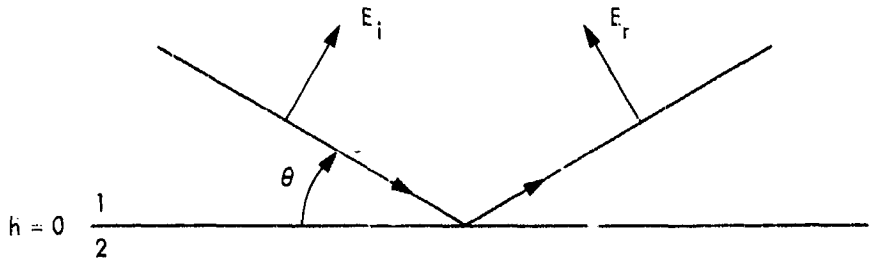

Figure 6.8. Electric field intensity vectors for vertically polarized wave.

Note that [illegible] wave and E_r, the field intensity of the reflected wave, are not strictly vertical unless $\theta = 0^0$. On the contrary E_i and E_r have horizontal components, and the relation between these horizontal components at $h = 0$ is determined by the boundary conditions which apply at this surface. Consistent with Fig. 6.8 it has been assumed in advance that the horizontal components are oppositely directed. Thus for a perfectly conducting surface $\rho_v = +1$, consistent with the horizontal components of E_1 and E_r being equal and opposite so that the total tangential field intensity is zero at the surface of a perfect conductor. But for $\theta = 90^0$ where horizontal and "vertical" polarizations are indistinguishable, $\rho_h = -1$. The reason for this discrepancy is that different initial assumptions are made about the directions of E_i and E_r for the two polarizations. For horizontal polarization E_i and E_r are assumed to be in the same direction whereas they are assumed to be in opposite directions for vertical polarization. As two vectors pointing in the same direction but 180^0 out of phase are equivalent to two vectors pointing in opposite directions but in phase, the two results are actually compatible. It would seem more logical to treat the two polarizations in the same way so that ρ_v would equal -1 for $\theta = 90^0$ and $\sigma = \infty$. Then the discrepancy referred to above would not occur, and it would not be necessary to provide an explanation of it. The form of Eq. (6.13), however, is widely used, as in Jordan and Balmain (1968) for example. Plots of ρ_h and ρ_v are given in Fig. 6.9.

An interesting characteristic of the reflection coefficient for vertical polarization is that when both media are lossless and a wave is incident from medium 1 to medium 2, ρ_v goes to zero for a particular elevation angle θ_p defined by

$$\theta_p = \tan^{-1} \sqrt{\frac{K_1}{K_2}} \tag{6.14}$$

This angle is referred to as the Brewster angle. If medium 1 is air

$$\theta_p = \tan^{-1} \sqrt{\frac{1}{K_2}} \tag{6.15}$$

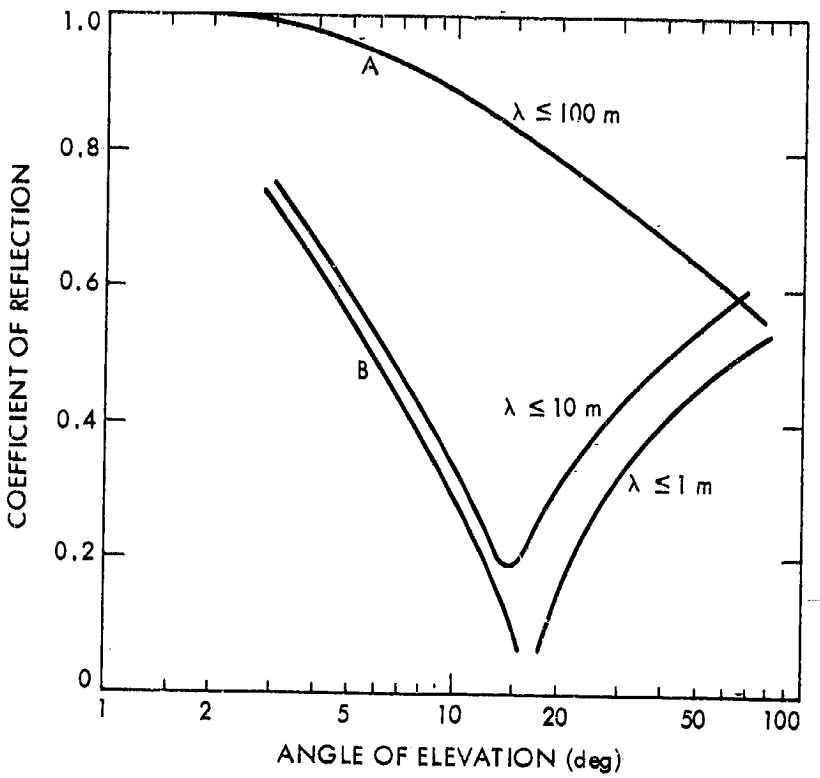

Figure 6.9. Reflection coefficients for plane average ground. A: horizontal polarization; B: vertical polarization (CCIR, 1978c).

For $\sigma \neq 0$, a minimum $|\rho_v|$ still tends to occur, and as it is $\sigma/\omega\varepsilon_0$ that appears in Eq. (6.13) the minimum tends to be quite pronounced for large values of ω.

6.2.3 Surface Roughness

The discussion of reflection in Secs. 6.2.1 and 6.2.2 assumed a perfectly smooth reflecting surface, consistent with reflection in the forward direction only. If a surface is rough, however, energy is reflected or scattered in other directions as well, with the result that the magnitude of the forward reflection coefficient is reduced. A commonly accepted criterion for roughness is the Rayleigh criterion, which can be explained with the help of Fig. 6.10. Consider two rays A and B such that ray A follows a path that is longer than that of ray B by π rad, the two rays being reflected from locations that differ in height by Δh. As the two rays differ in phase by π rad (assuming the same phase angle for their forward reflection coefficients) they interfere destructively for forward reflection. Therefore it can be argued that some of the incident energy is scattered in other than the forward direction. The amount $\Delta\ell$ by which the path length of ray A exceeds that of ray B is given by

$$\Delta\ell = 2\Delta h \sin\theta \tag{6.16}$$

and the corresponding phase difference $\Delta\phi$ is set equal to π so that

$$\Delta\phi = \frac{4\pi}{\lambda}\,\Delta h \sin\theta = \pi \tag{6.17}$$

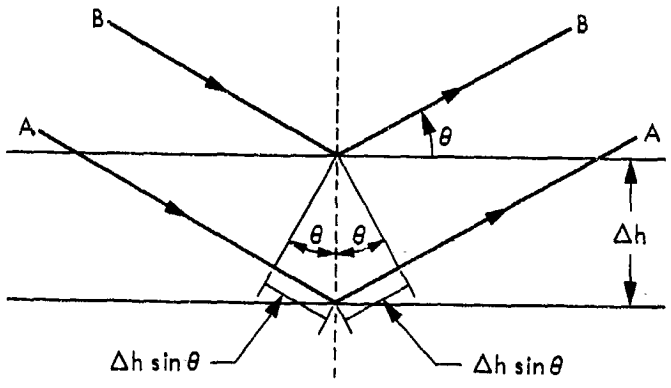

Figure 6.10. Basis for Rayleigh criterion.

from which

$$\Delta h > \frac{\lambda}{4 \sin \theta} \tag{6.18}$$

can be taken as the criterion for roughness. If it is desired to have a criterion for smoothness, one might use

$$\Delta h < \frac{\lambda}{8 \sin \theta} \tag{6.19}$$

The integer in the denominator is arbitrary and may be larger than 8 (16, for example). Note that we have allowed a range of Δh for which the surface is not defined as either rough or smooth.

As large reflection coefficients for forward reflection tend to be undesirable, the occurrence of high degrees of surface roughness of possibly reflecting surfaces can generally be looked upon with favor. In the case of reflection from a rough surface some degree of specular reflection may still occur and diffuse scattering takes place as well. Specular reflection is of the same type as that from a smooth surface. It is directional, coherent in phase, and tends to have small fluctuations in amplitude. Diffuse scattering exhibits little directivity, is incoherent in phase, and in mobile communications tends to exhibit large fluctuations which are Rayleigh distributed (Beckmann and Spizzichino, 1963). The following section treats the Rayleigh probability density function.

6.2.4 Statistical Characteristics of Multipath Signals

In considering the statistics of multipath signals received by moving mobile receivers, a distinction can be made between the rather rapid fluctuations that occur over short distances of a few tens of wavelengths when the mean signal is essentially constant and the slower variations in mean signal level that occur as the vehicle moves over large distances and experiences shadowing losses (Jakes, 1974). For analyzing the rapid variations, it can be assumed that the received field intensity E can be expressed as the sum of two components that are separated by 90° in phase such that

$$E = x(t) \cos \omega t + y(t) \sin \omega t \tag{6.20}$$

The quantities x(t) and y(t) represent the amplitudes of the two orthogonal terms, and both are assumed to have normal or Gaussian distributions with zero means and the same variance σ^2 such that

$$p(x) = \frac{1}{\sqrt{2\pi}\,\sigma} \; e^{-\frac{x^2}{2\sigma^2}} \tag{6.21}$$

and

$$p(y) = \frac{1}{\sqrt{2\pi}\,\sigma} \; e^{-\frac{y^2}{2\sigma^2}} \tag{6.22}$$

where p(x) and p(y) represent probability densities. Assuming that p(x) and p(y) are statistically independent, their joint probability p(x,y) is given by

$$p(x,y) = p(x)\,p(y) = \frac{1}{2\pi\sigma^2} \; e^{-\frac{x^2+y^2}{2\sigma^2}} \tag{6.23}$$

It is desirable to know the probability density of the total field intensity amplitude which will now be designated by r. The relation between r, x, and y is

$$r^2 = x^2 + y^2$$

To determine p(r) one can begin by using the relation (Beckmann, 1967)

$$p(r,\phi) = p(x,y)J \tag{6.24}$$

where J is the Jacobian defined by

$$J = \begin{vmatrix} \frac{\partial x}{\partial r} & \frac{\partial y}{\partial r} \\ \frac{\partial x}{\partial \phi} & \frac{\partial y}{\partial \phi} \end{vmatrix} \tag{6.25}$$

The derivatives can be evaluated by noting that

$$x = r\cos\phi \tag{6.26}$$

and

$$y = r \sin \phi \tag{6.27}$$

from which

$$J = \begin{vmatrix} \cos \phi & \sin \phi \\ -r \sin \phi & r \cos \phi \end{vmatrix}$$

$$= r(\cos^2 \phi + \sin^2 \phi) = r$$

so that

$$p(r,\phi) = \frac{r}{2\pi\sigma^2} e^{-\frac{r^2}{2\sigma^2}} \tag{6.28}$$

To obtain $p(r)$ one can integrate with respect to ϕ from 0 to 2π with the result that

$$p(r) = \frac{r}{\sigma^2} e^{-\frac{r^2}{2\sigma^2}} = \frac{2r}{\alpha} e^{-\frac{r^2}{\alpha}} \tag{6.29}$$

where $\alpha = 2\sigma^2$ is the mean square value of $p(r)$. This function is known as the Rayleigh probability density function. The forms of the Rayleigh and normal density functions are shown in Fig. 6.11.

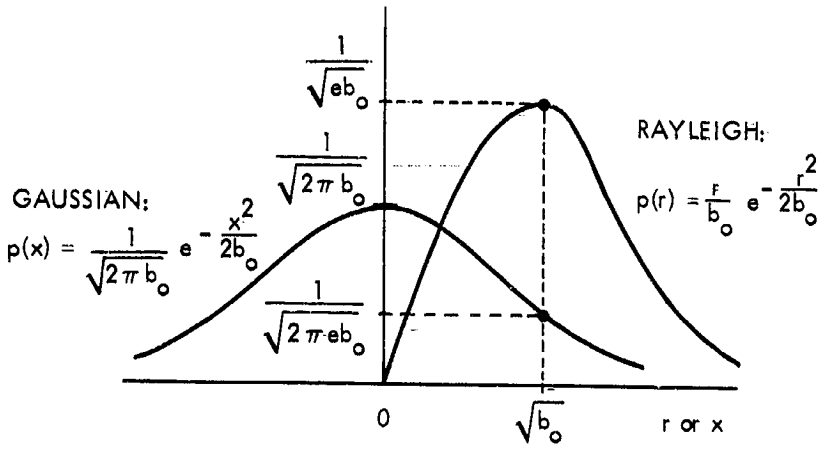

Figure 6.11. Normal or Gaussian and Rayleigh probability density functions (Jakes, 1974).

The probability density in this case for phase, $p(\phi)$, is uniform with $p(\phi) = 1/2\pi$ for $0 \leq \phi \leq 2\pi$. Considerable experimental evidence exists to the effect that the signal received by a land mobile receiver (in ground-to-ground service) is Rayleigh distributed on a local scale. A good approximation to a Rayleigh distribution tends to occur for as few as four to six multipath components (Schwartz, et al., 1966). In cases when the number of rays is very small, however, the Rayleigh distribution may not be applicable. The Rayleigh distribution can be considered to be a special case of more general distributions including the m distribution (Panter, 1972) and the Weibull distribution (Beckmann, 1967; Shepherd, 1972), and forms of these distributions may be applicable when the Rayleigh distribution is not.

When expressed in dB, the slower variations in mean signal level tend to follow the normal or Gaussian distribution and to have a probability density of the form of

$$p(x) = \frac{1}{\sqrt{2\pi}\ \sigma} \quad e^{-\frac{(x-x_0)^2}{2\sigma^2}} \tag{6.30}$$

where now $x = \ln y$ with y representing field intensity and $x_0 = \ln y_0$ with y_0 the mean field intensity. [Values in dB represent $20 \log_{10} (y/y_0)$ but our interest is not in dB values as such, and the natural logarithmic relationship is sufficient and convenient for present purposes.] To obtain the probability density of field intensity one can use

$$p(x)\, dx = p(y)\, dy$$

and note that as $x = \ln y$, $dx = dy/y$ so that $p(y) = p(x)/y$ and thus

$$p(y) = \frac{1}{\sqrt{2\pi}\ \sigma\ y} \quad e^{-\frac{[\ln(y/y_0)]^2}{2\sigma^2}} \tag{6.31}$$

This probability density is known as the lognormal probability density function.

The probability distribution for combined Rayleigh and lognormal fading has been analyzed by Hansen and Meno (1977). The probability density of a constant vector and a signal following the Rayleigh distribution is the Rice or Rice-Nakagami density function described by

$$(p(r) = \frac{2r}{\alpha} e^{-\frac{(r^2+c^2)}{\alpha}} I_0 \quad (=\frac{2cr}{\alpha}) \tag{6.32}$$

where r is the total electric field intensity, c is the peak field intensity of the constant line-of-sight component, α is the mean-square value appearing in the Rayleigh distribution [Eq. (6.29)], and I_0 is the modified Bessel function of the first kind and zero order (Norton et al., 1955; Beckmann and Spizzichino, 1963; Beckmann, 1967).

6.3 LAND-MOBILE SATELLITE CHANNELS

Any earth-space path may experience reflections and resulting multipath fading, but fixed earth stations can be designed to minimize multipath problems. Mobile satellite services are especially vulnerable to multipath fading for two principal reasons. One is that they must operate in a large variety of locations which in general cannot be selected or prepared in advance. The major factor contributing to fading, however, is the movement of the vehicle. No matter how reliable the signal may be when the vehicle is stationary and in a favorable location, fading becomes a potential problem for a moving vehicle.

Certain measures can be taken to minimize multipath fading. The use of directional antennas which discriminate against reflected rays is one important means. This approach is most effective in the case of satellites at rather high elevation angles, as contrasted to terrestrial services and low-angle satellites. Circular polarization has the favorable feature that reflected rays above the Brewster angle tend to have the orthogonal circular polarization from that which is transmitted. As receiving antennas are designed for the transmitted polarization, they are insensitive to the orthogonal polarization of the reflected ray. Thus multipath fading, resulting from interference between direct and reflected rays, is minimized.

Measurements have been made of signal intensities of transmissions from the ATS-6 satellite to mobile receivers at 860 MHz and 1550 MHz in a number of cities in the United States (Hess, 1980). The data reported are primarily from Denver. The excess path loss for 90 percent spatial coverage for 90 percent of the time for urban areas is about 25 dB and quite insensitive to frequency. The statement is made that the comparable value for suburban/rural areas is under 10 dB. The probability density of signal intensity is found to be different from that of the Rayleigh distribution.

Another study (Brisken et al., 1979) using the ATS-1 and ATS-3 satellites determined that ground-reflection multipath and ignition noise affected satellite communications less than terrestrial mobile communications. Position determinations of a less precise nature than planned for the GPS satellites (Sec. 6.6) were made by measuring the transit times of coded transmissions from the two satellites to the mobile vehicle and back. Measurements were made mostly in the Washington, DC area and in southwestern states, especially Colorado, Arizona, and California.

The planned Land Mobile Satellite Service (LMSS) is intended to provide narrowband, primarily voice, communications via satellite between land mobile vehicles, generally in rural areas, and earth stations (Knouse, 1980). The coverage area of LMSS will include the continental United States, Alaska, Canada, and possibly Hawaii. The satellite-to-mobile uplink and downlink frequencies will be in the 806-890 MHz band and the satellite-to-earth station frequencies will be in the 2550-2690 MHz portion of the S band. A downlink frequency of 868 MHz and an uplink frequency of 823 MHz have been used for uplink and downlink analyses, respectively, in the UHF band. A large LMSS satellite antenna will provide multiple, spot beams. Although LMSS is intended primarily for rural areas, it is planned that LMSS will be compatible with urban cellular mobile phone service. It has been planned to employ a 5 dB margin for multipath fading and to not provide additional margin for shadowing. The decision to not attempt to compensate for shadowing involves, among other factors, the concept that the service is intended mostly for rural areas where a line-of-sight path will be maintained for a large percentage of the time.

6.4 MARITIME-MOBILE SATELLITE CHANNELS

Maritime-mobile satellite systems encounter multipath effects which generally arise from reflection and scatter from the surface of the oceans and seas.

The electric field intensity at a maritime-mobile receiving antenna, due to signals transmitted from a satellite, is the vector sum of components associated with the direct wave from the satellite, a specularly or coherently reflected wave, and a diffusely or incoherently scattered wave. The field intensity of the diffuse wave normally has a Rayleigh distribution. The magnitude of the reflection coefficient for the specularly reflected wave is decreased below that for a smooth surface by surface roughness which can be characterized by the factor s, given by

$$s = \frac{h}{\lambda} \sin \theta \tag{6.33}$$

where h is the rms sea wave height, λ is wavelength, and θ is elevation angle (Beckmann and Spizzichino, 1963; CCIR, 1978c). If the first Fresnel zone contains a large number of scatterers, the reflection coefficient can be expressed as the product of the coefficient r_0 for a smooth surface and a factor k where

$$k = e^{-8\pi^2 s^2} \tag{6.34}$$

Values of the reflection coefficient for a smooth plane sea are shown in Fig. 6.12. In practice, with normal sea conditions in most areas, multipath reflections from the sea surface are said to be primarily diffuse (CCIR, 1978d).

The MARISAT maritime satellite communication system utilizes geostationary satellites over the Atlantic, Pacific, and Indian oceans and shore stations at Southbay, Connecticut; Santa Paula, California; and Fucino, Italy (Lipke et al., 1977). Each satellite receives transmissions at 6 GHz from shore stations and translates them to 1.5 GHz for transmission to ships. Transmissions from ships to satellites are at 1.6 GHz and those from the satellites to the shore stations are at 4 GHz. An allowance of 4 dB for short-term fading is provided for the L-band (1.5 and 1.6 GHz) links.

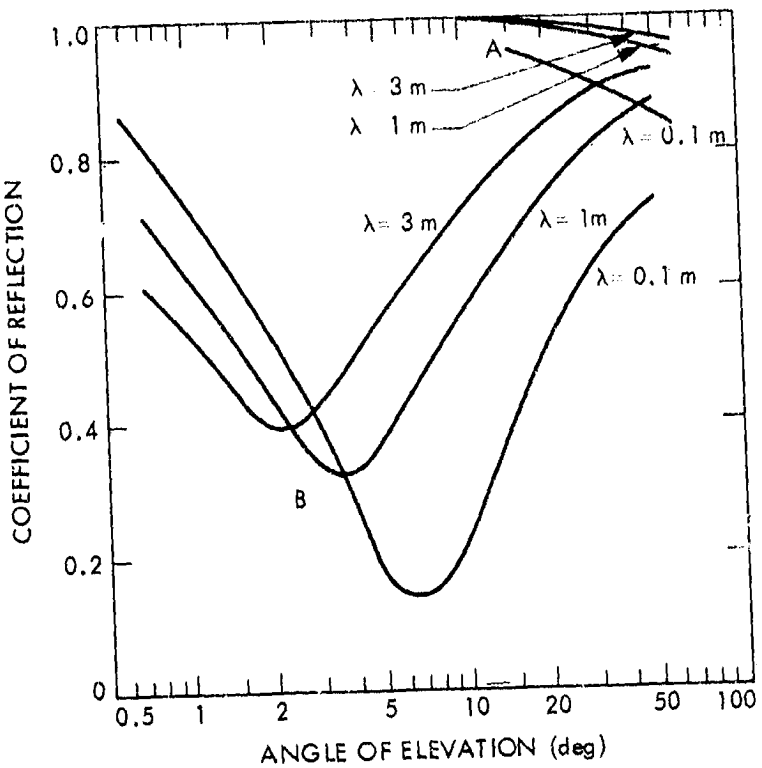

Figure 6.12. Reflection coefficients for smooth plane sea. A: horizontal polarization; B: vertical polarization (CCIR, 1978c).

6.5 AERONAUTICAL-MOBILE SATELLITE CHANNELS

Because of the heights at which aircraft fly, aeronautical-mobile satellite operations involve considerations that may not be important for vehicles and ships that are confined to the Earth's surface.

For surface operations, multipath propagation is of importance primarily because of the resulting fading. For aeronautical operations, however, time delays of the reflected rays, with respect to the direct rays, may be of importance as well. The time delay is greatest when an aircraft is directly beneath a satellite. For an aircraft at an altitude of 15 km, for example, the time delay of the reflected ray is 100 μs. For the north Atlantic air routes and a geostationary satellite at 30^{0} longitude, the delay times for aircraft between 8 and 17 km are between about 20 and 60 μs (CCIR, 1978d).

The problem of multipath time delays is treated in the CCIR references (Report 505-2) under the heading of modulation interference. The interference due to multipath propagation is also referred to as intersymbol interference. The time delays mentioned above do not cause significant garbling of voice signals. The effect on data transmissions depends on the relative magnitude of the time delay and the bit length. When the two periods are comparable, errors may arise unless remedial measures are taken. If the bit period is large compared to the propagation delay and sampling is done at the center of each bit period, problems are minimal.

For small elevation angles and aircraft heights above about 10 km, the reflection from a smooth surface is reduced by the Earth's curvature below the value for a plane earth. The factor by which the reflection coefficient is reduced is known as the divergence factor D (Beckmann and Spizzichino, 1963) and is illustrated in Fig. 6.13 for two different aircraft heights.

Aircraft can range over land and sea and also over areas of ice and snow such as the Greenland ice cap and Antarctica. Reflection coefficients for such surfaces, consisting of snow which gradually changes with depth to compact snow and finally to ice, are illustrated in Fig. 6.14.

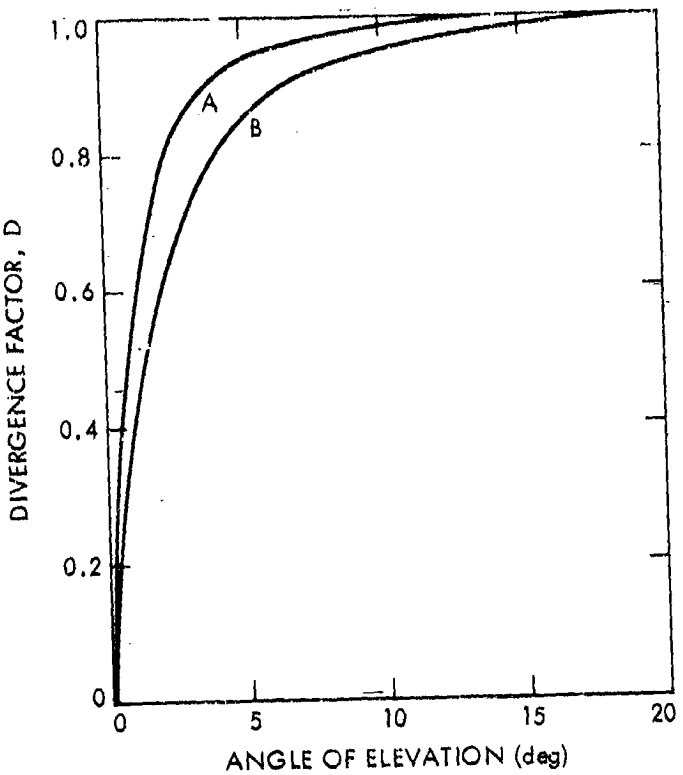

Figure 6.13. Divergence factors, D, for reflection from a smooth spherical earth. A: aircraft at 3,300m, B: aircraft at 10,000m (CCIR, 1978c).

Aircraft in flight pass through the maxima and minima of the interference pattern which tends to be set up by reflection, and they experience fading which is a function of the applicable reflection coefficients. The vertical separation, Δh_R, between maxima of the interference pattern can be found from Eq. (6.8), assuming reflection from a plane surface, by setting

$$\frac{2\pi\Delta h_R \sin \theta}{\lambda} = \pi.$$

from which

$$\Delta h_R = \frac{\lambda}{2 \sin \theta} \qquad (6.35)$$

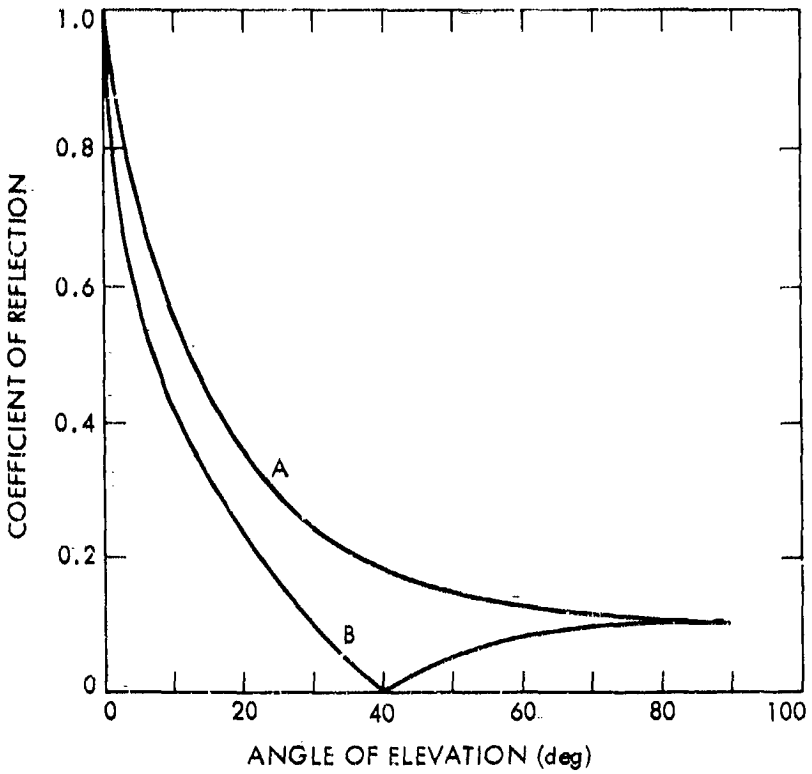

Figure 6.14. Field intensity reflection coefficients for ice caps such as those of Greenland and Antarctica. A: horizontal polarization, B: vertical polarization (CCIR, 1978c).

Table 6.1 lists values of Δh_R as determined from Eq. (6.35) for various elevation angles θ.

θ (deg)	Δh_R
2	14.3 λ
4	7.2 λ
8	3.6 λ
15	1.9 λ
30	1.0 λ
60	0.58 λ
90	0.5 λ

Table 6.1 Vertical separation between maxima of interference pattern.

Ascending and descending aircraft pass rapidly through the maxima and minima in the interference pattern. For the elevation angles of about 15° and greater even aircraft in nominally level flight experience the full range of fading because of the limited ability to maintain constant height.

In flight over water the Doppler spectrum of the sea-reflected signal introduces spectral spreading of the received signal, as a function of the elevation angle of the aircraft with respect to the origin of the reflected signal. Values of the measured Doppler bandwidth between points at 1/e of the peak amplitude for L-band transmissions from ATS-5 are shown in Fig. 6.15.

An AEROSAT satellite system specifically designed for aircraft communications has been proposed but never funded. Volume VIII, Mobile Services, Recommendations and Reports of the CCIR, 1978 includes a large number of reports that provide information pertinent to mobile communications, including satellite-mobile communications. The contents of Report 505-2 of this volume have been especially useful in the preparation of Sec. 6.5.

6.6 THE NAVSTAR GLOBAL POSITIONING SYSTEM

The three previous sections have involved consideration of multipath effects that may be of importance to the three categories of land, maritime, and aeronautical mobile communications services. In addition, the effects are pertinent to radionavigation systems, including the pending NAVSTAR Global

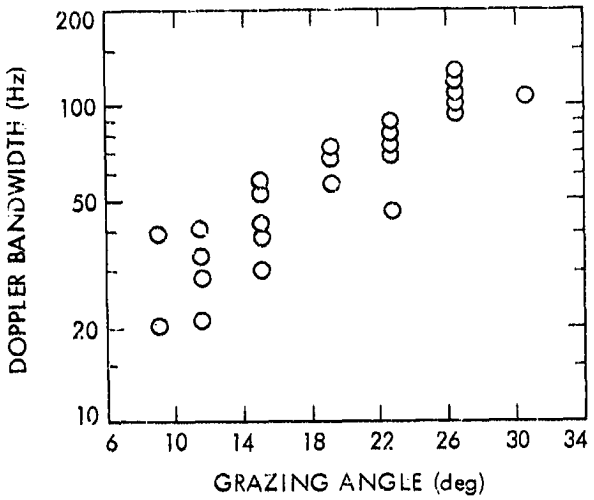

Figure 6.15. Doppler bandwidth as a function of elevation angle, based on 1550 MHz transmissions from the ATS-5 satellite to a 707-type aircraft (CCIR, 1978c).

Positioning System (GPS) (Milliken and Zoller, 1978). The system will provide three-dimensional position and velocity information to mobile or fixed receivers anywhere in the world whether on land or sea or in the air. Original plans called for 24 satellites in 12-hour orbits at an altitude of 20,183 km in 3 orthogonal planes (8 in each plane). Budgetary considerations have required a change to operation with a total of 18 satellites (Book, Brady, and Mazaika, 1980). Signals are transmitted at two L-band frequencies, 1227 and 1575 MHz, to permit correction for ionospheric time delay. The satellites carry precision clocks, and if the user has a precision clock signals from 3 satellites are sufficient to determine position. A fourth satellite is required for most users, however, who must have a clock of reasonable accuracy but will not have a precision clock. The fourth satellite provides the necessary correction for the offset of the user clock. Position determination involves the employment of two codes, the P code which provides precision measurement of time and the C/A code which provides easy lock-on to the signal. It is expected that multipath propagation will cause errors in position determination of 1.2 to 2.7 m. The overall error in range is expected to be 3.6 to 6.3 m.

REFERENCES

Assis, M. S., "A simplified solution to the problem of multiple diffraction over rounded obstacles," IEEE Trans. Antennas and Propagation, vol. AP-19, pp. 292-295, March 1971.

Beckmann, P., Probability in Communication Engineering. New York: Harcourt, Brace & World, 1967.

Beckmann, P. and A. Spizzichino, The Scattering of Electromagnetic Waves from Rough Surfaces. New York: Macmillan Co., 1963.

Book, S. A., W. F. Brady, and P. K. Mazaika, "The nonuniform GPS constellation," in IEEE 1980 Position Location and Navigation Symposium Record, pp. 1-8. New York: Institute of Electrical and Electronics Engineers, 1980.

Brisken, A. F., R. E. Anderson, R. L. Frey, and J. R. Lewis, "Land-mobile communications and position fixing using satellites," IEEE Trans. Vehicular Technology, vol. VT-28, pp. 153-170, Aug. 1979.

Bullington, K., "Radio propagation for vehicular communications," IEEE Trans. Vehicular Technology, vol. VT-26, pp. 295-308, Nov. 1977.

CCIR, "Ground-wave propagation curves for frequencies between 10 kHz and 30 MHz," Recommendation 368-3 in Vol. V, Propagation in Non-ionized Media, Recommendations and Reports of the CCIR, 1978, pp. 17-33. Geneva: Int. Telecomm. Union, 1978a.

CCIR, "Propagation by diffraction," Report 715 in Vol. V, Propagation in Non-ionized Media, Recommendations and Reports of the CCIR, 1978, pp. 36-46. Geneva: Int. Telecomm. Union, 1978b.

CCIR, "Multipath effects in aircraft-to-satellite communication and radio determination links," Report 505-2 in Vol. VIII, Mobile Services, Recommendations and Reports of the CCIR, 1978, pp. 507-530. Geneva: Int. Telecomm. Union, 1978c.

CCIR, "Link power budgets for a maritime mobile satellite service," Report 760 in Vol. VIII, Mobile Services, Recommendations and Reports of the CCIR, 1978, pp. 409-420. Geneva: Int. Telecomm. Union, 1978d.

Deygout, J., "Multiple knife-edge diffraction of microwaves," IEEE Trans. Antennas and Propagation, Vol. AP-14, pp. 480-489, July, 1966.

Flock, W. L., Electromagnetics and the Environment: Remote Sensing and Telecommunications. Englewood Cliffs, NJ: Prentice-Hall, 1979.

Hall, M. P. M., Effects of the Troposphere on Radio Communications. Stevenage, U. K. and New York: Peter Peregrinus (on behalf of Institution of Electrical Engineers), 1979.

Hansen, F. and F. I. Meno, "Mobile fading - Rayleigh and lognormal superimposed," IEEE Trans. Vehicular Technology, vol. VT-26, pp. 332-335, Nov. 1977.

Hess, G. C., "Land-mobile satellite excess path loss measurements," IEEE Trans. Vehicular Technology, vol. VT-29, pp. 290-297, May 1980.

Jakes, W. C., Microwave Mobile Communications. New York: Wiley, 1974.

Jenkins, F. A. and H. E. White, Fundamentals of Optics, Fourth Edition. New York: McGraw-Hill, 1976.

Jordan, E. C. and K. G. Balmain, Electromagnetic Waves and Radiating Systems. Englewood Cliffs, NJ: Prentice-Hall, 1968.

Kirby, R. S., H. T. Dougherty, and P. L. McQuate, "Obstacle gain measurements over Pikes Peak at 60 to 1,046 Mc," Proc. IRE, vol. 43, pp. 1467-1472, October 1955.

Knouse, G. H., "Terrestrial/land mobile satellite considerations, NASA plans, and critical issues," IEEE Trans. Vehicular Technology, vol. VT-29, pp. 370-374, Nov. 1980.

Lipke, D. W. et al., "MARISAT - a maritime satellite communication system," COMSAT Technical Review, vol. 7, pp. 351-392, Fall, 1977.

Milliken, R. J. and C. J. Zoller, "Principle of operation of NAVSTAR and system characteristics," Navigation, vol. 25, pp. 95-106, Summer, 1978.

Norton, K. A., P. L. Rice, and L. E. Vogler, "The use of angular distance in estimating transmission loss and fading range for propagation through a turbulent atmosphere over irregular terrain," Proc. IRE, vol. 43, pp. 1488-1526, Oct. 1955.

Ott, R. H., "An alternative integral equation for propagation over irregular terrain," Radio Science, vol. 6, pp. 429-435, 1971.

Panter, P. F., Communication Systems Design. New York: McGraw-Hill, 1972.

Schwartz, M., W. R. Bennett, and S. Stein, Communication Systems and Techniques. New York: McGraw-Hill, 1966.

Shepherd, N. H., "Radio wave loss deviation and shadow loss at 900 MHz," IEEE Trans. Vehicular Technology, vol. VT-26, pp. 309-313, Nov. 1977.

CHAPTER 7
RADIO NOISE

7.1 SYSTEM NOISE TEMPERATURE AND ANTENNA TEMPERATURE

7.1.1 Basic Concepts of Electrical Noise

Electrical noise is developed in resistors or conductors, due to the random motions of electrons. The available noise power p at the terminals of a resistor in a 1 Hz bandwidth at radio frequencies is independent of the value of the resistance and frequency and is given by

$$p = kT \qquad \text{W/Hz} \qquad (7.1)$$

where k is Boltzmann's constant (1.381×10^{-23} J/K) and T is temperature in kelvins (K). The noise power P in a bandwidth B in the radio frequency range is therefore given by

$$P = kTB \qquad \text{W} \qquad (7.2)$$

with B in Hz. The standard reference value, T_0 = 290 K, is normally used for T for noise power calculations.

If a receiver or amplifier has a resistive input impedance, the noise power at the output terminals of the receiver will be

$$P = gkT_0B + P_i \qquad \text{W} \qquad (7.3)$$

where g is the power gain of the amplifier and P_i is noise which is generated internally within the amplifier. The noise performance of an amplifier can be measured by use of a noise figure F where F is defined by the relation

$$F = \frac{P_{out}}{gP_{in}} \qquad (7.4)$$

with the subscripts representing output and input and with $P_{in} = kT_0B$. Alternatively, a noise temperature T_R can be used to describe the noise performance of the receiver such that

$$P_{out} = gk\,(T_0 + T_R)B \tag{7.5}$$

Making use of Eqs. 7.3-7.5, it can be established that

$$F = 1 + \frac{T_R}{T_0} \tag{7.6}$$

and

$$T_R = T_0\,(F-1) \tag{7.7}$$

An advantage of using T_R as a measure of the noise introduced by the receiver is that it refers to the input terminals of the receiver and is additive with respect to temperatures representing other noise sources that may be applied to the receiver input terminals, as in Eq. (7.5).

Consider next a resistive or dissipative attenuator at the temperature T_0. In many applications, one simply considers the power output of the attenuator to be the input power times the power "gain" g_a of the attenuator so that $P_{out} = P_{in}g_a$. It is convenient when working with attenuators, and with noise, to use a noise temperature in place of noise power itself. In that case

$$T_{out} = T_{in}\,g_a \tag{7.8}$$

A resistive attenuator, however, does more than attenuate. It adds noise as well, and it is advantageous to refer this noise to the input terminals of the attenuator in the same way that receiver noise was referred to the input terminals of the receiver. To carry out this procedure, it is necessary to determine the input temperature of an attenuator such that the temperature accounts for the noise generated by the attenuator and is consistent with Eq. (7.8). The advantage is, as with receivers, that this noise temperature is additive with respect to noise temperatures representing other sources of noise that may be applied to the input of the attenuator. Then one can use Eq. (7.8) for an attenuator with T_{in} representing either the attenuator by itself or the sum of the attenuator input noise temperature and a temperature

representing another noise source such as an antenna. (See Fig. 7.1.) It develops that for an attenuator by itself (no input)

$$T_{in} = (\ell_a - 1)\, T_0 \tag{7.9}$$

and

$$T_{out} = (1 - g_a)\, T_0 \tag{7.10}$$

with $\ell_a = 1/g_a$. If an antenna which introduces noise corresponding to the temperature T_A is connected to the input terminals of the attenuator then

$$T_{in} = T_A + (\ell_a - 1)\, T_0 \tag{7.11}$$

and

$$T_{out} = T_A\, g_a + (1 - g_a)\, T_0 \tag{7.12}$$

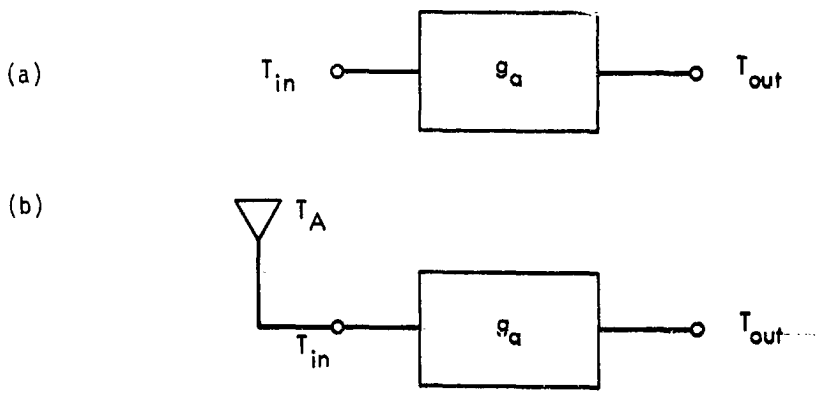

Figure 7.1. Concept of noise temperature of attenuator. For both systems $T_{out} = T_{in}\, g_a$. In Fig. 7.1a, no input is connected to the attenuator and $T_{in} = (\ell_a - 1)\, T_0$. In Fig. 7.1b, $T_{in} = T_A + (\ell_a - 1)\, T_0$, where T_A is the antenna noise temperature.

One additional basic relation is needed in order to define system noise temperature. Consider a system consisting of two separate parts connected in series as in Fig. 7.2.

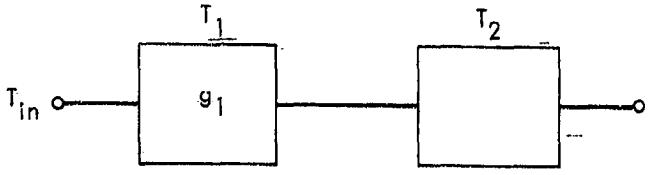

Figure 7.2. System of two parts connected in series and having temperatures of T_1 and T_2.

It develops that

$$T_{in} = T_1 + \frac{T_2}{g_1} \tag{7.13}$$

Thus, if g_1, the gain of the first part, is greater than unity, T_1 plays a greater role in determining T_{in} than T_2. Each of the two parts of the system may be an amplifier, attenuator, or combination of amplifiers and attenuators. The concept illustrated by Eq. (7.13) can be extended to additional stages. For example, for a system of three parts, $T_{in} = T_1 + T_2/g_1 + T_3/g_1g_2$.

7.1.2 System Noise Temperature

Following Kraus (1966), system noise temperature T_{sys} is defined with the aid of Fig. 7.3, suggesting a telecommunications receiving system including an

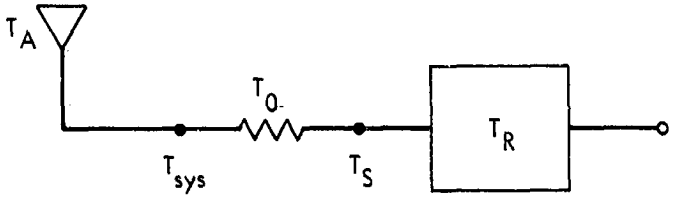

Figure 7.3. Locations where T_{sys} and T_s are defined.

antenna having a noise temperature of T_A, a dissipative transmission line which acts as an attenuator at a temperature of $T_a = T_0$, and a receiver having a noise temperature of T_R. T_{sys} is defined as referring to the antenna terminals and is given by

$$T_{sys} = T_A + (\ell_a - 1)\, T_0 + \ell_a T_R \tag{7.14}$$

Noise introduced by the antenna is accounted for by T_A. Then follows a term representing the input temperature of an attenuator at a temperature of T_0 [corresponding to T_1 of Eq. (7.13)]. Finally, $\ell_a T_R$ corresponds to T_2/g_1 of Eq. (7.13) when $T_2 = T_R$ and $1/g_a = \ell_a$.

Some analyses of telecommunications links make use of T_s, defined at the receiver terminals, rather than T_{sys}. It is simple to convert from T_{sys} to T_s by using

$$T_s = T_{sys}\, g_a \tag{7.15}$$

resulting in

$$T_s = T_A\, g_a + (1 - g_a)\, T_0 + T_R \tag{7.16}$$

Either T_{sys} or T_s can be used, if carrier power and noise power are defined at the same location, either the antenna terminals or the receiver terminals. Noise power X at the antenna terminals is given by

$$X = k\, T_{sys}\, B \tag{7.17}$$

and at the receiver terminals by

$$X = k\, T_s\, B \tag{7.18}$$

Note that if $g_a = \ell_a = 1$, corresponding to zero attenuation between the antenna and receiver.

$$T_{sys} = T_s = T_A + T_R \tag{7.19}$$

The effective noise temperature of the antenna T_A (not its physical temperature) accounts for all the noise appearing at the output terminals of the antenna, including sky noise and noise of terrestrial origin. The term sky noise includes noise emitted by the constituents of the Earth's atmosphere, namely gases, hydrometeors, and other matter such as dust. It also includes extraterrestrial noise emitted by the Sun, Moon, planets, and universe and the 2.7 K component which fills space. Terrestrial noise may be picked by the side lobes or as a result of antenna spillover and blockage, in the case of an earth-station antenna. The main lobe, however, of a satellite-borne antenna is usually pointed at the Earth and thus receives noise of terrestrial origin. Interfering signals also constitute noise whch contributes to T_A.

The system noise temperature can be decreased by placing a preamplifier at the antenna terminals. In that case, for a system otherwise the same as that of Fig. 7.3,

$$T_{sys} = T_A + T_{PRE} + \frac{(\ell_a - 1)\, T_0 + \ell_a T_R}{g_{PRE}} \tag{7.20}$$

For this procedure to be most effective, the noise temperature of the preamplifier, T_{PRE}, must be low and the gain of the preamplifier, g_{PRE}, should be high. In the above expressions ℓ_a and g_{PRE} are numerical values and not dB values.

The various contributions to T_A are considered in the following section.

7.2 ATMOSPHERIC CONTRIBUTIONS TO NOISE TEMPERATURE

The principal types of naturally occurring radio noise, generated externally from the receivers of telecommunications systems, are the noise of lightning discharges (commonly referred to as atmospheric noise), cosmic noise, thermal radiation from the atmosphere and nearby terrain and objects, and noise from the Sun, Moon, and distant planets. Noise from lightning predominates for frequencies below about 20 MHz, and cosmic noise tends to be most important between about 20 and 1000 MHz. Above 1000 MHz, atmospheric thermal noise tends to predominate, when the antenna points into space and not towards the Sun or some other strong discrete source. Noise from lightning

occurs mainly at frequencies below the range of this handbook and cosmic noise is considered in Sec. 7.3. Attention is directed in this section to atmospheric thermal radiation.

A basic relation concerning noise applies to the noise temperature T_b recorded when observing a noise source, represented by a temperature T_s, through an absorbing region. The relation for the zenith case is

$$T_b = T_s\, e^{-\tau_\infty} + \int_0^\infty T(h)\, \alpha(h) e^{-\tau}\, dh \qquad (7.21)$$

with

$$\tau_\infty = \int_0^\infty \alpha(h)\, dh$$

and

$$\tau = \int_0^h \alpha(h)\, dh$$

with $\alpha(h)$ the absorption constant expressed as a function of height h (Waters, 1976). When T(h) is a constant, a change of the variable of integration made by noting that $\alpha(h)\, dh$ equals $d\tau$ allows carrying out the integration and obtaining the simpler form (with $\tau = \tau_\infty$)

$$T_b = T_s\, e^{-\tau} + T_i\, (1-e^{-\tau}) \qquad (7.22)$$

The first term of Eq. (7.22) shows that the noise source beyond the absorbing region is attentuated by a factor $e^{-\tau}$. The second term represents atmospheric thermal noise which may be generated whether there is a noise source T_s beyond the absorbing region or not. (If τ is zero, corresponding to no absorption, the second term is zero.) If attenuation due to scattering occurs as well as absorption, Eq. (7.22) may need to be modified such that $\alpha(h)$ in the second term represents absorption only. However, Eq. (7.22) may still be used as it is with $\alpha(h)$ representing extinction, even when there is scattering, if an appropriate, effective temperature T_i can be determined. In this case, T_i will be less than the actual physical temperature of the absorbing region.

One procedure for determining T_f involves alternately pointing at the Sun and away from the Sun. The difference in the two values of T_b gives $T_s\ e^{-\tau}$ and, from $T_s\ e^{-\tau}$ and the two values of T_b, $T_f\ (1-e^{-\tau})$ can also be determined. By also recording T_b when pointing at the Sun with no absorbing region (no clouds or precipitation) in between and correcting for the rather small absorption due to gases, one can then determine T_s itself for the Sun. Knowing T_s then allows determining $e^{-\tau}$ when clouds or precipitation are present. Finally, as all the other quantities of Eq. (7.22) are known, T_f can be determined as well. In practice, this procedure is followed whether it is known that T(h) is actually a constant or not.

Extraterrestrial noise corresponding to a noise temperature of 2.7 K is always present as well but this value is small and can be accounted for or ignored, in the latter case resulting in

$$T_b \cong T_f\ (1-e^{-\tau}) \tag{7.23}$$

The value of the effective temperature T_f will be different at different times and locations, but taking it as 280 K appears to give generally good results in temperate regions. Wulfsberg and Altshuler (1972) found that 284 K was a suitable value for Hawaii. In other cases, where scattering becomes significant, lower temperatures such as 273 K or 260 K (CCIR, 1981) have been used.

Figure 7.4 shows the ratio of the extinction (total attenuation) constant to the absorption constant for a 12 mm/h rain model and for a cloud model. It can be seen that scattering is not important for clouds for frequencies below about 50 GHz, but is significant for a 12 mm/h rain for frequencies above about 5 GHz. Figure 7.5 shows a plot of Eq. (7.23) for T_f = 280 K and also shows the relations $T_b = 60\ A_{dB}$ which applies for sufficiently small values of absorption.

For low-noise systems, the decrease in signal-to-noise ratio (SNR) due to the accompanying increase in noise is larger than the decrease due to signal attenuation, for attentuation up to about 10 dB. This condition is illustrated by Fig. 7.6 which is based upon Eq. (7.23) with T_f = 280 K and upon

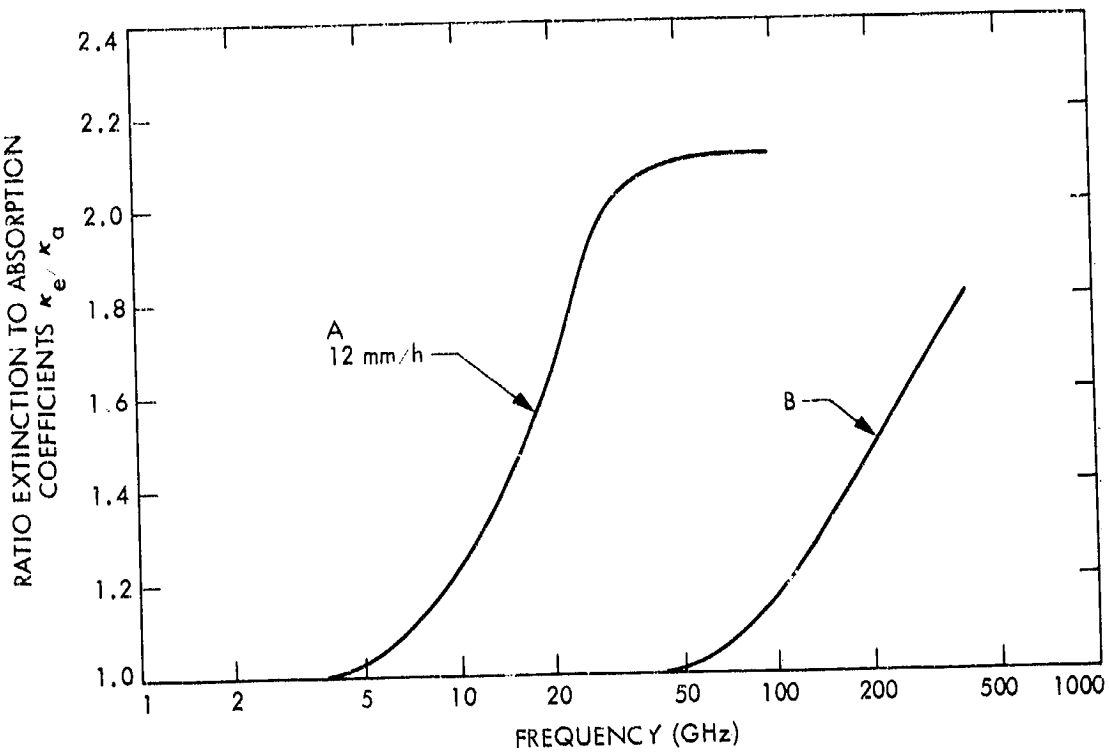

Figure 7.4. Ratio of extinction to absorption coefficients for a rain model (A) and a cloud model (B) (CCIR, 1981).

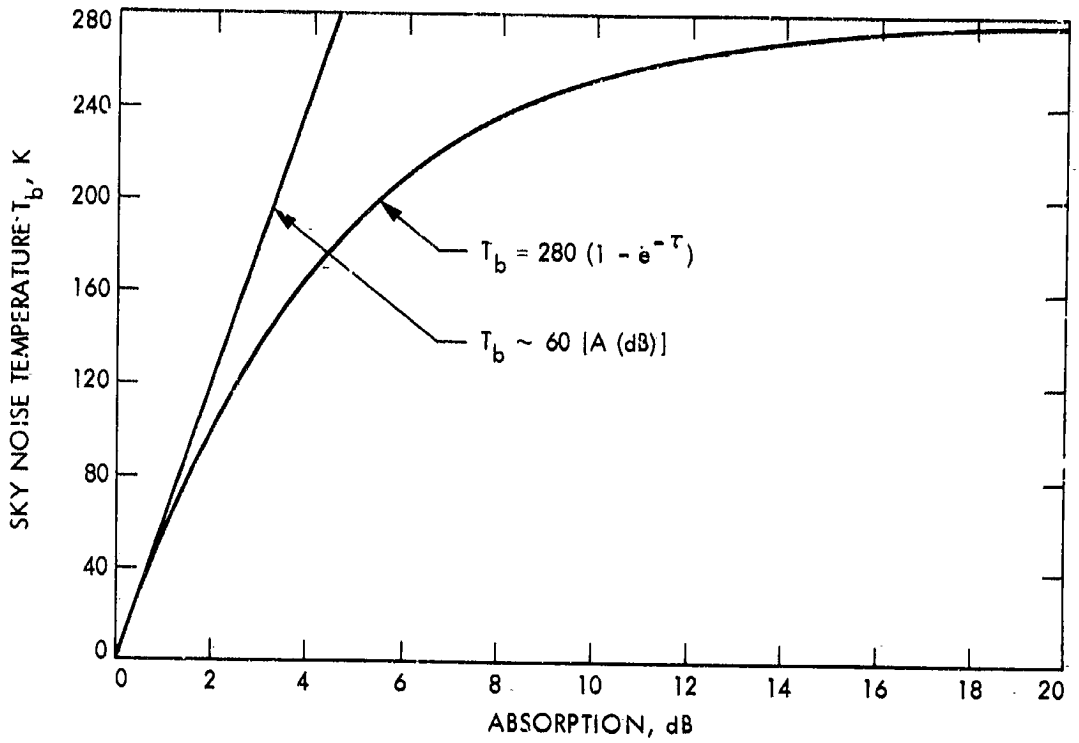

Figure 7.5. Sky noise temperature T_b due to absorbing region, assuming T_f = 280 K (CCIR, 1981).

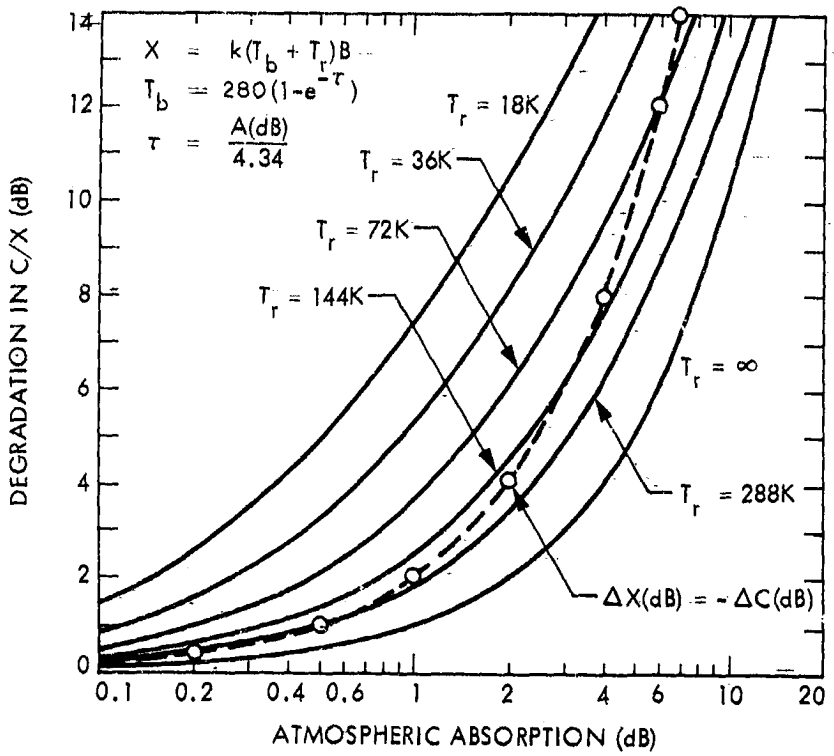

Figure 7.6. Degradation in signal-to-noise ratio (C/X) versus atmospheric absorption, for various values of T_1 (taking T_1 as equal to T_r).

$$SNR = C/X \tag{7.24}$$

with C reduced from the free space value by a factor of $e^{-\tau}$ and

$$X = k\,(T_b + T_1)B = kT_2B \tag{7.25}$$

where T_1 is the system noise temperature in the absence of the contribution T_b and $T_2 = T_b + T_1$ is the system noise temperature when T_b is included. As the optical depth τ is a power-density attenuation coefficient rather than a coefficient for field intensity,

$$4.34\tau = A_{dB} \tag{7.26}$$

where A is attenuation in dB.

The dotted line in Fig. 7.6 divides the figure into two regions. To the left and above this line, the decrease in SNR due to the increase in noise is greater than the decrease due to attenuation while the reverse is the case to the right and below the line. For example, if $T_1 = T_R = 18$ K as may occur in the NASA-JPL Deep Space Network, then atmospheric absorption of 1 dB will result in an increase of noise power of about 6.5 dB and a total decrease in SNR of 7.5 dB. Of the 7.5 dB decrease, about 87 percent is due to the increase in noise. For large earth stations of the type used for satellite communications, T_1 may be between 50 and 100 K, for which a 1 dB increase in absorption will result in a 2 to 3.3 dB increase in noise and a 3 to 4.3 dB decrease in SNR.

Attenuation due to the gases of the troposphere was illustrated in Sec. 3.6, and attenuation caused by rain was discussed in Chap. 4. Some values of attenuation and noise due to clouds were given in Sec. 5.1.3, and a more extensive set of such values is given in Table 7.1 (Slobin, 1981, 1982). For low noise systems, especially for frequencies above 10 GHz but also for frequencies as low as 8.5 GHz, clouds are an important source of noise. The values of Table 7.1 apply for zenith paths (elevation angle of 90°). Attenuation for elevation angles other than 90° can be obtained from

TABLE 7.1 Sample Cloud Models and S-, X-, K_A-Band Zenith Effects (Slobin, 1981, 1982).

Case	Lower Cloud				Upper Cloud				Remarks	S-Band (2.3 GHz) Zenith		X-Band (8.5 GHz) Zenith		X-Band (10 GHz) Zenith	
	Density g/m^3	Base km	Top km	Thick-ness km	Density g/m^3	Base km	Top km	Thick-ness km		T(K)	A(dB)	T(K)	A(dB)	T(K)	A(dB)
1	-	-	-	-	-	-	-	-	Clear Air	2.15	.035	2.78	0.45	3.05	.049
2	0.2	1.0	1.2	0.2	-	-	-	-	Thin Clouds	2.16	.036	2.90	.047	3.22	.052
3	-	-	-	-	0.2	3.0	3.2	0.2		2.16	.036	2.94	.048	3.28	.053
4	0.5	1.0	1.5	0.5	-	-	-	-		2.20	.036	3.55	.057	4.12	.066
5	-	-	-	-	0.5	3.0	3.5	0.5		2.22	.037	3.83	.062	4.50	.073
6	0.5	1.0	2.0	1.0	-	-	-	-	Medium Clouds	2.27	.037	4.38	.070	5.27	.084
7	-	-	-	-	0.5	3.0	4.0	1.0		2.31	.038	4.96	.081	6.06	.098
8	0.5	1.0	2.0	1.0	0.5	3.0	4.0	1.0	Heavy Clouds	2.43	.040	6.55	.105	8.25	.133
9	0.7	1.0	2.0	1.0	0.7	3.0	4.0	1.0		2.54	.042	8.04	.130	10.31	.166
10	1.0	1.0	2.0	1.0	1.0	3.0	4.0	1.0		2.70	.044	10.27	.166	13.35	.216
11	1.0	1.0	2.5	1.5	1.0	3.5	5.0	1.5	Very Heavy Clouds	3.06	.050	14.89	.245	19.66	.326
12	1.0	1.0	3.0	2.0	1.0	4.0	6.0	2.0		3.47	.057	20.20	.340	26.84	.457

Notes:

1) Clear and cloud models as described in text
2) Cases 2-12 are clear air and clouds combined
3) Antenna located at sea level
4) Heights are above ground
5) No cosmic background or ground contribution considered
6) T(K) is atmospheric noise temperature at zenith
7) A(dB) is atmospheric attenuation along vertical path from ground to 30 km above ground

$$A(\theta) = \frac{\text{zenith}}{\sin \theta} \quad \text{dB} \tag{7.27}$$

for values of θ above about 10°. For lower elevation angles, the following expression has been used.

$$A(\theta) = \frac{2\,A_{\text{zenith}}}{\sin^2 \theta + 0.00235 + \sin \theta} \quad \text{dB} \tag{7.28}$$

Figure 7.7 shows values of noise temperature for an atmosphere having a water vapor density of 10 g/m^3, according to CCIR Report 720 (1978) (solid-line curves) and according to a JPL program (various symbols) (Smith and Waters; Smith, 1982b). The noise temperatures from the JPL program are higher in the valleys between the peak temperatures than the CCIR curves. For a zenith path (elevation angle θ = 90°), the noise due to water vapor is small for frequencies of 10 GHz and lower. Note, however, that for values of θ of 10° and less, water vapor makes a rather large contribution to system noise. For θ = 0°, as for a terrestrial path, the noise temperature due to water vapor is about 140 K at 10 GHz.

7.3 EXTRATERRESTRIAL NOISE

7.3.1 Introduction

While studying atmospheric noise from thunderstorms, Jansky, an engineer with the Bell Telephone Laboratories, first identified radio noise of extraterrestrial origin (Jansky, 1932, 1933). The identification was made while conducting direction-finding observations at a frequency of 20.5 MHz. Three sources of noise were recorded--noise from nearby thunderstorms, noise from distant thunderstorms, and noise of cosmic or extraterrestrial origin. The cosmic noise came from a region having a right ascension angle near 18 h and a declination angle near -10 deg, which is the direction of the center of the Galaxy. Jansky noted that the extraterrestrial noise was often the limiting factor with respect to the detection of weak signals in the frequency range he was working in.

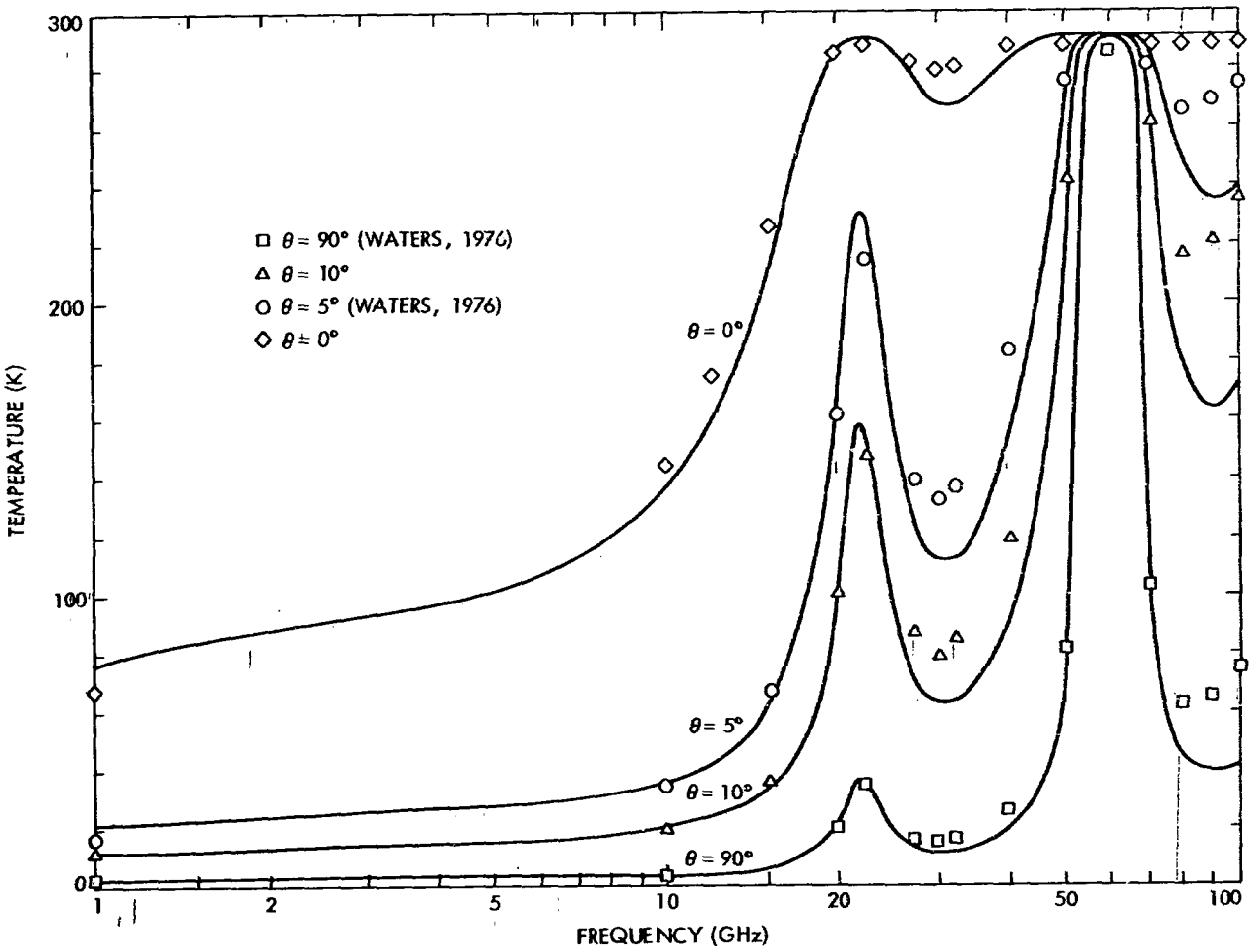

Figure 7.7. Comparison of sky noise temperature between the JPL program (various symbols) and CCIR Report 720 (1978) for a water vapor density of 10 g/m^3 and a surface temperature of 20°C, with θ the elevation angle.

Reber followed up on Jansky's work by constructing and operating a receiving system having a 9.5 m paraboloidal reflector in his backyard in Wheaton, Illinois. Utilizing a frequency of 160 MHz, he constructed the first radio map of the Milky Way (Reber, 1940). Later he investigated the intensity distribution of cosmic noise at 480 MHz (Reber, 1948).

The first recorded recognition of radio emission from the Sun was made in 1942 by Hey (1946), who was concerned with radio noise causing interference to 5-m radars in southern England during World War II. Jamming by German forces was suspected at first in a particular case in February 1942, but it was concluded that the noise was associated with a large sunspot. Later in the same year, Southworth (1945) of the Bell Telephone Laboratories observed thermal emission from the quiet Sun at centimeter wavelengths. Reber (1941) did not succeed in detecting the Sun by radio means until 1943-44, as at frequencies of a few hundreds of MHz the Milky Way appears brighter than the Sun when viewed with a broad-beam antenna.

The first observation of emission from a discrete radio source, Cygnus A, was made by Hey, Parsons, and Phillips (1946). The identification as a discrete source was originally made for the wrong reason, namely that emission from the source was thought to vary in amplitude as mentioned when introducing the subject of ionospheric scintillation (Sec. 2.6.1). Observations by Bolton and Stanley (1948), utilizing the resolution obtained by interference between direct and reflected rays at a location on a cliff overlooking the sea, however, showed that the source was indeed discrete, in fact confined to 8' of arc. Their observations were made mainly at 100 MHz, for which they reported that the source had an effective temperature of 4×10^6 K. In the same year, Ryle and Smith (1948), utilizing a frequency of 80 MHz, identified another strong discrete radio source, Cassiopeia A.

The brightness of the sky at radio frequencies does not correspond to that at optical frequencies, and it has been difficult to identify radio sources with visible objects. The first such identification was made by Bolton, Stanley, and Slee (1949), who identified the radio source Taurus A with the crab Nebula, the expanding shell of the supernova of 1054 A.D. The

prediction in 1945 by van de Hulst of emission by neutral hydrogen at 1421 MHz (Kraus, 1966) and the subsequent detection of such emission by Ewen and Purcell (1951) at Harvard was an important development. The emission by neutral hydrogen is due to a hyperfine transition between two states corresponding to the electron spin being parallel or antiparallel to the spin of the nucleus (the proton). The probability of spontaneous emission of this type is very low, but the extent of interstellar space is so vast that the total amount of emission by hydrogen in space is sufficient to be observable in our galaxy and also in nearby galaxies.

Since the early developments mentioned above many discrete sources of radio emission have been identified and much progress has been made in mapping and cataloguing the discrete sources and background radiation. Interesting histories of the radio observations of extraterrestrial sources have been given by Shklovsky (1960) and Hey (1971), and a valuable thorough account of radio astronomy has been prepared by Kraus (1966). Radio sources are useful for calibrating radio telescopes and, in discussing this topic, Wielebinski (1976) has presented a list of radio sources. The proceedings of IAU Symposium No. 74 include reports on a number of efforts in the mapping of radio sources (January, 1977), and recent treatments of radio sources have been presented by Fomalont (1981), Kellerman and Pauliny-Toth (1981), and Miley (1981).

The discovery by Penzias and Wilson (1965) of microwave background radiation corresponding to about 3 K in temperature was an important development which earned the Nobel Prize for them (Wilson, 1979). The radiation is believed to be relict radiation from the formation of the universe. It displays a high degree of isotropy, varying by only about 0.003 K in 24 hours. Shakeshaft and Webster (1968) analyzed the values of microwave flux at 12 different frequencies as reported by various observers. They concluded that the values were in agreement with blackbody radiation from matter at 2.68 K, and a value of 2.7 K is commonly assigned to microwave background radiation.

7.3.2 Thermal Emission

Radio noise may be due to thermal or non-thermal emission and may cover a continuum of frequencies or occur at a discrete line frequency.

Thermal emission from black bodies obeys the Rayleigh-Jeans law in the radio-frequency range so that the noise power density w received from a uniform source is given by

$$w = \frac{2kT}{\lambda^2} \Omega_s \qquad W/m^2/Hz \tag{7.29}$$

where k is Boltzmann's constant (1.38×10^{-23} J/K), T is temperature in kelvins, λ is wavelength in m, and Ω_s is the solid angle subtended by the source. It can be seen that w varies inversely with wavelength squared or with λ to the -2 power. The exponent, n, of λ, is known as a spectral index (Kraus, 1966). A hot blackbody emits thermal radiation and thus tends to be a strong emitter at infrared and optical frequencies but a weak emitter at radio frequencies.

Emission from neutral hydrogen is line emission (most prominently at the discrete frequency of 1421 MHz), but emission from ionized hydrogen, such as occurs near hot stars, is a form of thermal emission. The thermal radiation comes from free electrons experiencing acceleration, as when deflected in passing near a proton. The spectral index for ionized hydrogen can range from 0 to -2. Flux from a region of ionized hydrogen is as described by Eq.(7.29), but T can be either a constant for which n = -2 or can vary as wavelength squared for which n = 0. Recall that the brightness temperature T_b when viewing a region of intrinsic temperature T_i having an optical depth of τ is given by

$$T_b = T_i \ (1 - e^{-\tau}) \tag{7.30}$$

For a region containing free electrons τ is inversely proportional to frequency squared or directly proportional to wavelength squared, and for high frequencies (e.g. 3 GHz) for which τ is very small

$$T_b \cong = T_i \tau \propto T_i \lambda^2$$

Then the T of Eq.(7.29) becomes T_b and is proportional to wavelength squared so that n = 0. For lower frequencies for which τ is large $T_b \cong T_i$, w varies inversely as λ^2, and n = -2.

7.3.3 Non-thermal Emission

The mechanism believed to be responsible for most non-thermal radio emission is synchrotron radiation. The form of radiation occurs when high velocity electrons follow spiral paths in magnetic fields (Jackson, 1962; Kraus, 1966). The electrons may be cosmic ray particles having relativistic velocities. Alfven and Herlofson (1951) first suggested that the intense radio emission at low frequencies is due to synchrotron radiation. Consider a relativistic electron moving in a circular orbit. Under this condition, radiation from the electron is concentrated in a narrow cone of width θ which is pointed in the direction of the instantaneous velocity, as suggested in Fig. 7.8. An observer in this direction will observe a short burst of linearly polarized radiation, with its electric field intensity vector oriented as shown in the illustration. Such radiation has a broad frequency spectrum. The spectral index for synchrotron radiation derived from cosmic-ray particles tends to be around 0.75 so that the power density of the radiation, w, is proportional to $\lambda^{0.75}$. Note that unlike the case for thermal emission, the spectral index for non-thermal emission is positive. Table 7.2 gives flux densities, w, and spectral indices for a few of the strongest discrete sources of radio noise, at a frequency of 400 MHz.

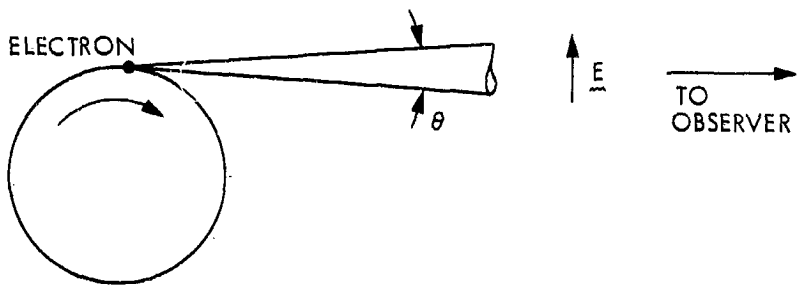

Figure 7.8. Beam of radiation from a very high velocity electron.

Line emission from neutral hydrogen is a form of nonthermal emission. It has provided a picture of the spiral structure of our galaxy.

TABLE 7.2

Flux Densities and Spectral Indices
For Some Nonthermal Radio Sources (Kraus, 1966).

Source	w at 400 MHz in Janskys (Jy) (multiples of 10^{-26} W/m^2/Hz)	Spectral Index
Cassiopeia A	6,100	0.77
Cygnus A	4,500	0.7 - 1.2
Taurus A	1,230	0.27
Virgo A	580	0.83
Hydra A	133	0.87

Cassiopeia A, in our galaxy, is the most intense discrete source of radio noise in the sky, other than the Sun. Cygnus A, the second most intense noise source other than the Sun, is external to our galaxy. It is actually a galaxy itself, and as it is an exceptionally intense source of radio waves it is known as a radio galaxy. Many radio galaxies radiating from 10 to 10^6 times more radiowave power than normal galaxies have been discovered. Both Cassiopeia A and Cygnus A are nonthermal sources.

7.3.4 The Sun, Moon, and Planets

The Sun emits as a blackbody with a temperature near 6000 K in the optical range, but at radio frequencies (below about 30 GHz) the emission from the quiet Sun is greater than that for a blackbody at this temperature and emission from the disturbed Sun is much greater yet at radio frequencies. Radiation at a particular frequency f, where $f \cong f_p$, comes mostly from a layer located just above a critical layer having a plasma angular frequency $\omega_p = 2\pi f_p$ given by

$$\omega_p^2 = \frac{Nq^2}{m\varepsilon_0}$$

where N is electron density, q is the electron charge, m is the electron mass, and ε_0 is the electric permittivity of empty space. As N decreases with alti-

tude, the lower frequencies are emitted from higher regions of the solar corona. The Sun appears larger and brighter at radio frequencies than for visible frequencies. The equivalent blackbody temperature for radio frequencies under disturbed conditions may be 10^{11} or higher (Kraus, 1966). Note that ω_p is the same quantity that appears in $K = 1 - \omega_p^2/\omega^2$, where $K = n^2$ is the relative dielectric constant for the ordinary wave in a plasma [see Eq. (2.9)].

Radio emission from the Sun can be classified into three components, that from the quiet Sun, a slowly varying component from bright regions, and bursts from transient disturbances such as flares (Kundu, 1965; Elgaroy, 1977). The slowly varying component is most prominent in the 3- to 60-cm wavelength range. Emission at 10.7 cm has been recorded for many years at Ottawa, Canada. Data from observatories recording radiation at 3, 10.7, 21, and 43 cm and 169 MHz are included in Solar-Geophysical Data reports issued by NOAA, Boulder, Colorado. Bursts are classified into centimeter bursts, decimeter bursts, and bursts at meter and decameter wavelengths. The latter are further divided into Types I, II, III, IV, and V.

Centimeter-wave bursts have a rapid rise in intensity and a slower decline and cover essentially a smooth continuum of frequencies. The more complex decimeter bursts show a great variety of fluctuations superimposed on the continuum. Type I or noise storm radiation consists of a slowly varying, broadband enhancement of the normal solar radiation on which a series of bursts near 5 MHz are superimposed. The enhanced radiations last from hours to days, and the bursts last from a fraction of a second to several seconds. The radiation is strongly circularly polarized. Type II and III bursts are intense events whose frequencies drift lower at rates of about 1 MHz/s and 20 MHz/s, respectively. Type IV bursts cover a smooth continuum of frequencies having wavelengths from centimeters to decameters and last from about 10 minutes to a few hours. Type V bursts are also continuum events but last only for seconds to minutes and are usually limited to meter wavelengths.

When the beam of a receiving antenna comes close to the Sun, the noise due to the Sun increases in a manner dependent upon the characteristics of the antenna pattern and the relative positions of the Sun and the antenna beam.

Figure 7.9 shows the recorded increase in system noise temperature for the 64-m, S-band antenna of the Deep Space Network of the Jet Propulsion Laboratory when tracking Pioneer 8 (Nov. 1968, near the solar maximum).

Radio emission from the Moon was first detected, at a wavelength of 1.25 cm, by Dicke and Beringer (1946). The mean brightness temperature of the Moon for the S and X bands if about 240 K (JPL, 1977), and the Moon has the rather large angular size of about 0.5°. The observed temperature at microwave frequencies varies slightly with the phase of the Moon, reaching a maximum about 3.5 days after full moon. As for the general case, the noise temperature of an antenna that is pointed at the Moon is the average temperature for the beam. If other sources of noise can be neglected, the average temperature is about

$$240(\Omega_{Moon}/\Omega_{antenna})$$

where Ω_{Moon}, the solid angle of the Moon is $(\pi/4)\theta^2_{Moon}$, with θ_{Moon} the angular width of the Moon and $\Omega_{antenna}$ the solid angle of the antenna (as a rough rule of thumb about $\frac{4}{3}\ \theta_{Hp}\phi_{Hp}$, where θ_{Hp} and ϕ_{Hp} are the half-power beamwidths).

Emission from the planets is of much interest from the viewpoint of radio science, the intense, sporadic, and fluctuating emission of decametric radiation from Jupiter being especially noteworthy. Equation (7.30) gives the relation used by JPL (1977) for estimating the increase, T_{pl}, in system noise temperature due to certain planets at the S and X bands, assuming the planets fall within the antenna beamwidth.

$$T_{Pl} = \frac{S_o \lambda^2}{8\pi k R^2}\, G\, e^{-2.77\ \theta^2/\theta^2_{HP}} \qquad (7.30)$$

In Eq. (7.30), S_o is the flux density in $W/m^2/Hz$ at a range of 1 AU (1.5×10^{11}m), R is the range of the planet in AU, k is Boltzmann's constant (1.38×10^{-23} J/K), λ is the radio wavelength, G is antenna gain modified to include atmospheric attenuation, θ is the planet-earth-probe angle in deg, and θ_{HP} is the half-power beamwidth of the antenna in deg. The flux densities S_o in Janskys (Jy) at 1 AU (1 Jy = 10^{-26} $W/m^2/Hz$) for some of the planets are given in Table 7.3.

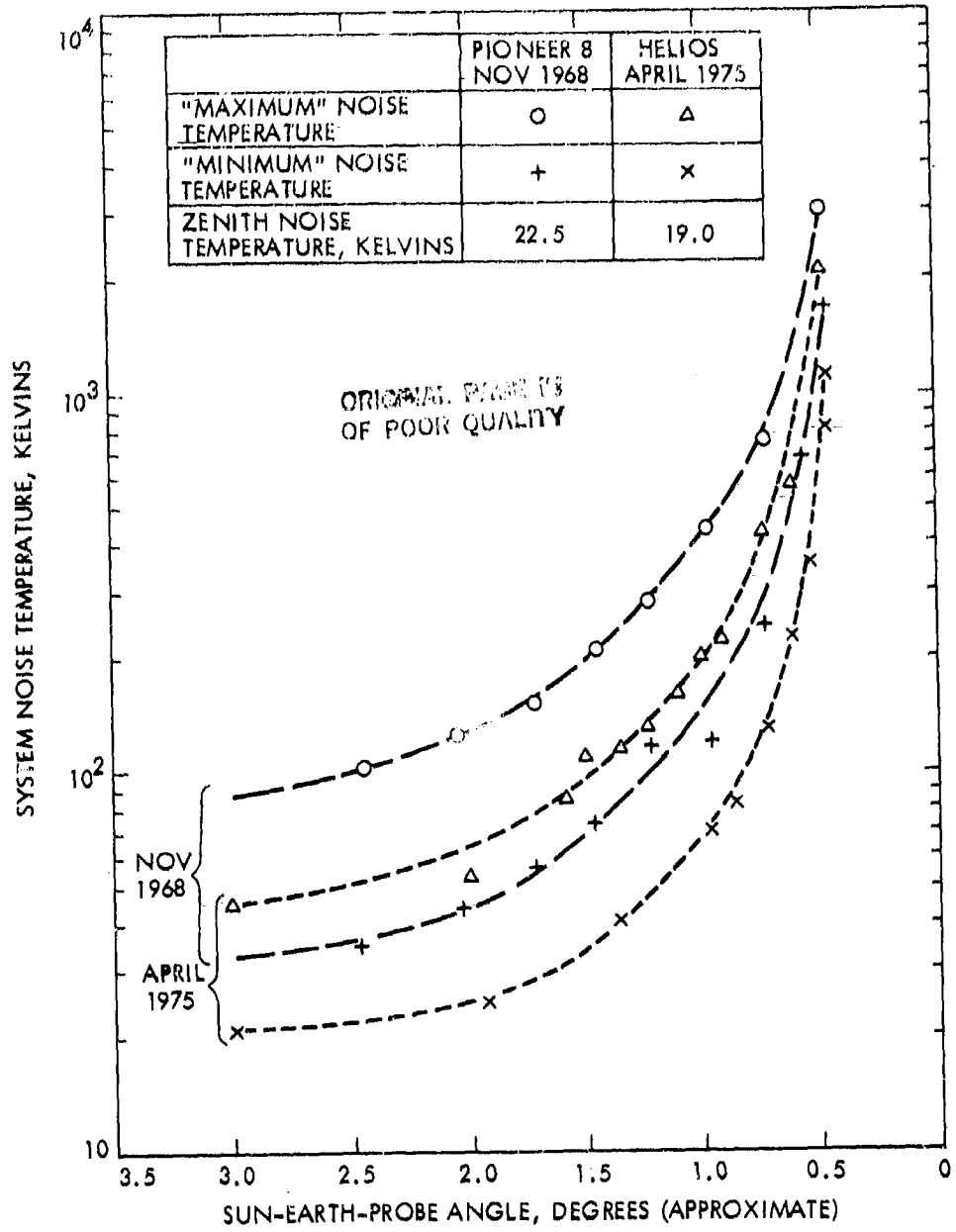

Figure 7.9. System noise temperature vs. sun-earth-probe angle at S-band for 64-meter antenna stations, from measured data (JPL, 1977).

TABLE 7.3

Flux Density S_o in Janskys (Jy)
at one AU (1 Jy = 10^{-26} W/m^2/Hz).

	S-band	X-band
Venus	0.53 Jy	7.4 Jy
Mars	0.050 Jy	0.68 Jy
Saturn	14 Jy	170 Jy
Jupiter	91-118 Jy	330 Jy

7.3.4 Satellite Operations

A radio map of our galaxy at a frequency of 200 MHz for a beamwidth of 17° is shown in Fig. 7.10. The plot is in galactic coordinates and is quite symmetrical with respect to the galactic equator. A noise temperature of 1200 K is shown for the center of the Galaxy. Figure 7.11 shows a similar plot, but for a frequency of 250 MHz and in celestial coordinates, with the zero declination line corresponding to the Earth's equator. For geostationary satellites the corresponding values of declination δ are restricted to about $\pm 8.7°$. (For an earth station at the highest possible latitude of about 81.3° for communicating with a geostationary satellite, $\delta \cong \sin^{-1} 6356/(35{,}785 + 6356) = 8.7°$ where 6356 is the polar radius and 35,785 km is the altitude of a geostationary satellite.)

The contours of Fig. 7.11 are in units of 6 K above 80 K, the value for the coldest parts of the sky. For an 18 h right ascension angle and 0° declination, for example, the value from Fig. 7.11 is 37 and the corresponding brightness temperature T_b is 6 x 37 + 80 = 302 K at 250 MHz. To estimate the brightness temperature at a higher frequency note that the brightness B at radio frequencies for a blackbody at a temperature T is given by the Rayleigh-Jeans radiation law

$$B = \frac{2kT}{\lambda^2} \qquad \text{W/m}^2\text{/Hz/rad}^2 \qquad (7.32)$$

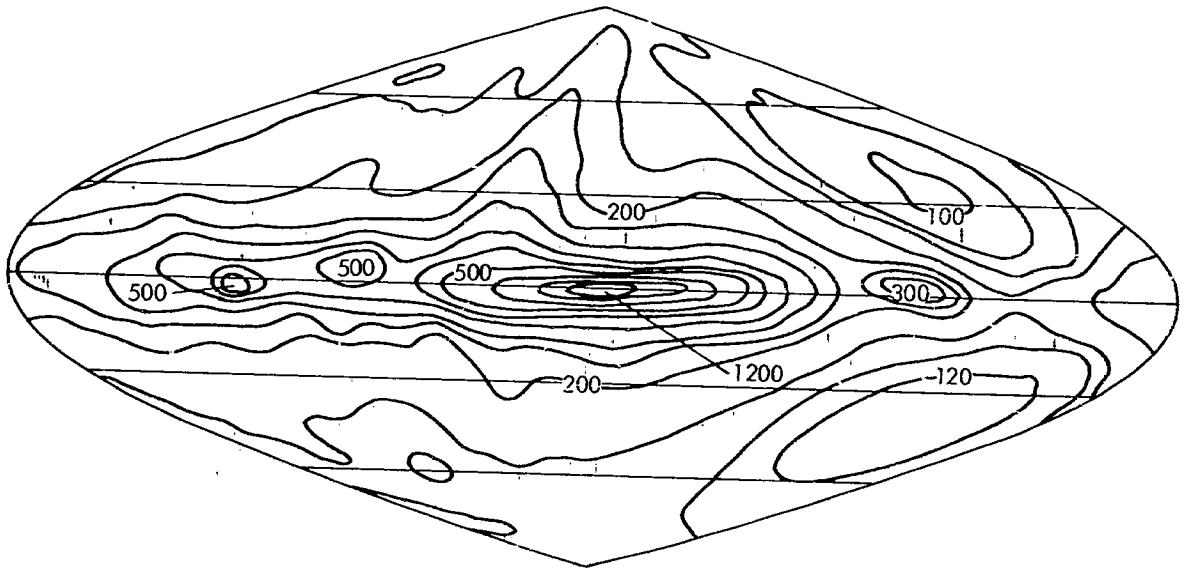

Figure 7.10. Radio map of the Galaxy at λ = 1.5 m obtained with a 17° beamwidth. The numbers on the contours are radio brightness temperature (K). The galactic centre lies at the centre of the map. The horizontal lines are marked at intervals of 30° of galactic latitude. (After Droge and Priester, 1956).

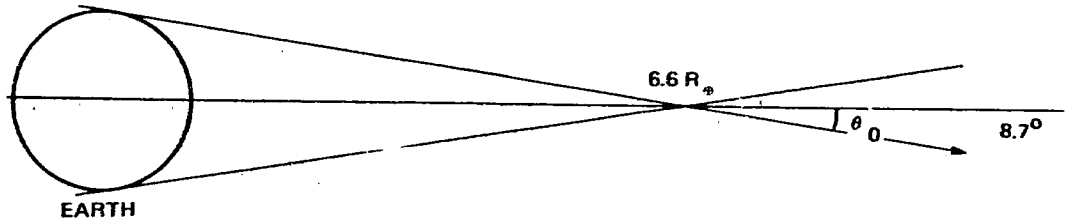

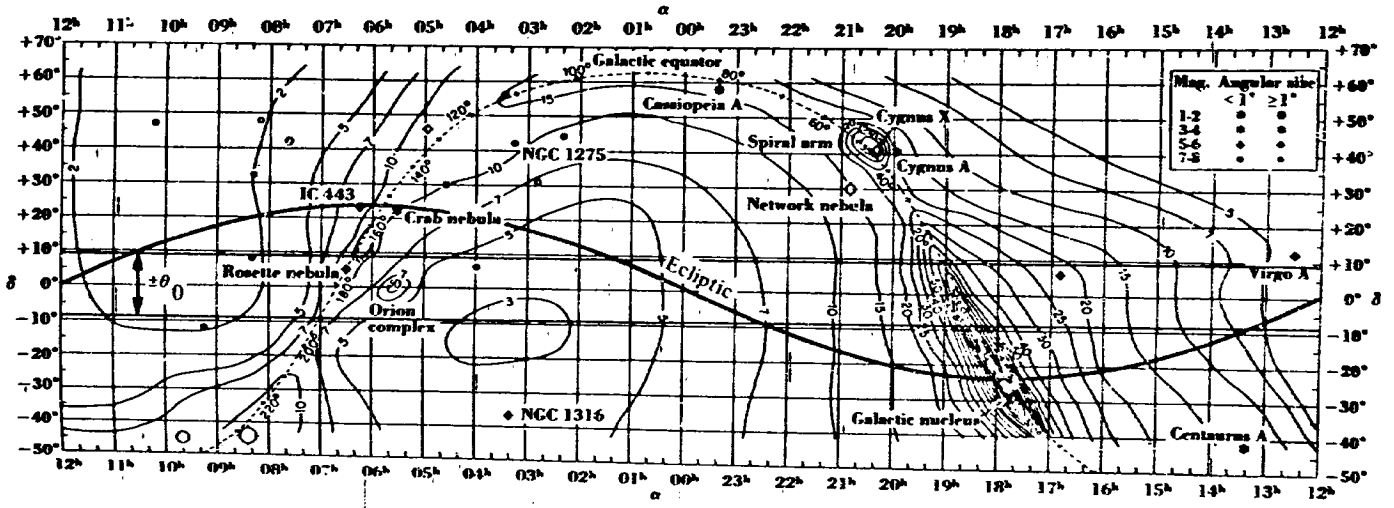

Figure 7.11. Radio sky at 250 MHz as a background for that part of the celestial sphere of interest in earth-satellite telecommunications using the geostationary orbit (CCIR, 1981; Kraus, 1966).

It can be shown (Flock, 1979) that an antenna receiving radiation from a blackbody, assuming that it fills the antenna beam, will receive the power per Hz, w, given by

$$w = kT \qquad \text{W/Hz} \tag{7.33}$$

For the case of nonthermal radiation, an equivalent blackbody temperature can be assigned even though blackbody-radiation theory does not apply. If the spectral index for nonthermal radiation is +0.75 and T of Eq. (7.32) is to be defined as an equivalent blackbody brightness temperature so that the Rayleigh-Jeans law can be utilized, then T must vary as $\lambda^{2.75}$ or $f^{-2.75}$ (Smith, 1982a). On this basis the total brightness temperature at a microwave frequency f_i can be determined from T for 250 MHz (referred to as f_o) by

$$T_b(f_i) = T_b(f_o)\left[\frac{f_i}{f_o}\right]^{-2.75} + 2.7 \text{ K} \tag{7.34}$$

For example, if f_i = 1 GHz,

$$T_b = 302(4)^{-2.75} + 2.7 = 9.4 \text{ K}$$

while for f_i = 4 GHz

$$T_b = 302(16)^{-2.75} + 2.7 = 2.8 \text{ K}$$

The quantity 2.7 K represents the microwave background radiation investigated by Penzias and Wilson (1965), and T_b for f_i = 4 GHz is close to this microwave background level. It can thus be noted that the brightness temperature T_b is a strong function of frequency and decreases to a very low value in the S band.

For frequencies above 2 GHz, the extraterrestrial sources of importance are the Sun and a few non-thermal sources such as Cassiopeia A, Cygnus A and X, and the Crab nebula (CCIR, 1981). Examination of Fig. 7.10, however, shows that the non-thermal sources mentioned are not of concern for geostationary-satellite operations as they fall outside the range of δ of $\pm$8.7°. For deep-

space missions, the value of δ can be near $\pm 23.5°$, corresponding to the ecliptic, or larger and somewhat larger values of noise may be encountered than for geostationary satellites.

7.4 NOISE OF TERRESTRIAL ORIGIN

The receiving antenna of an uplink to a satellite points at the Earth which has an effective temperature T_e that is commonly taken to be 290 K. The noise temperature of this antenna is the average temperature within the beam, as mentioned for the case of the Moon (Sec. 7.3.4). (If the Earth fills the beam the brightness temperature is T_e, and if the Earth fills only part of the beam the temperature will be less.) Work in progress (Smith, private communication) indicates that T_e actually has a value less than 290 K and probably less than 200 K for frequencies below 10 GHz.

If one wishes to examine noise of terrestrial origin more precisely, it can be noted that temperature over the Earth's surface varies with location and time and that the brightness temperature of an area is not the actual temperature but the true temperature multiplied by emissivity, which is less than 1. (Emissivity can approach but never exceed 1.) The variation in brightness temperature is the basis for certain passive remote sensing techniques. The scanning microwave spectrometer on Nimbus 6, for example, produced passive microwave spectral images of the Earth and maps showing temperatures of atmospheric layers as well (Staelin et al., 1977). The permanent ice and snow cover of Antarctica and Greenland, for example, showed as having low brightness temperatures ranging from 140 to 160 K at 31.65 GHz.

For the case of a downlink from a satellite, the sidelobes and backlobe of the earth-station receiving antenna pick up small amounts of radiation from the Earth. Thus the Earth provides at least a slight contribution to the noise temperature of even a very high-quality earth-station antenna. The magnitude of the contribution must usually be determined empirically. Any object in the field of view of an antenna contributes to antenna noise temperature unless it is a perfect conductor. In determining the level of microwave background radiation, Penzias and Wilson (1965) found in a particular case an antenna temperature of 6.7 K when the antenna was pointed to the zenith, of which 2.7 K was cosmic relict radiation, 2.3 K was of atmospheric origin, and

0.9 K was judged to be due to ohmic losses in the antenna and back-lobe response. The latter value is for a very high-efficiency horn antenna and can be considered to be an absolute minimum value.

Noise of terrestrial origin may be natural or man-made. Consideration of man-made radio noise is outside the scope of this handbook but a useful treatment has been provided by Skomal (1978). Chapters are included in his text about noise from automobiles, electric-power systems, and industrial, scientific, and medical sources. It is stated that unintentionally generated noise of metropolitan areas may arise within any portion of the radio spectrum between 30 Hz and 7 GHz. Line spectra, perhaps occurring as high-integer order harmonics of a fundamental signal, are often encountered below 500 MHz.

REFERENCES

Alfven, H. and N. Herlofson, "Cosmic radiation and radio stars," Phys. Rev., vol. 78, p. 616, 1950.

Bolton, J. G. and G. J. Stanley, "Variable source of radio frequency radiation in the constellation of Cygnus," Nature, vol. 161, pp. 312-313, Feb. 28, 1948.

Bolton, J. G., G. J. Stanley and O. B. Slee, "Positions of three discrete sources of galactic radio-frequency radiation," Nature, vol. 164, pp. 101-102, July 16, 1949.

CCIR, "Radio emission associated with absorption by atmospheric gases and precipitation," Report 720, Vol. V, Propagation in Nonionized Media, Recommendations, and Reports of the CCIR, 1978, pp. 103-106. Geneva: Int. Telecomm. Union, 1978.

CCIR, "Propagation data required for space telecommunication systems," Draft Revision of Report 564-1 (Mod. 1) of Vol. V, Propagation in Non-ionized Media, Recommendations and Reports of the CCIR, 1978. CCIR Study Group Doc. USSG-5/34, April 9, 1981.

Dicke, R. H. an R. Beringer, "Microwave radiation from the Sun and Moon," Astrophysics Journal, vol. 103, p. 375, 1946.

Droge, F. and W. Priester, "Durchmusterun der allgemeinen Radiofrequenz-Strahlung bei 200 MHz," Z. Astrophys. vol. 40, pp. 236-248, 1956.

Elgaroy, E. O., Solar Noise Storms. Oxford, New York: Pergamon Press, 1977.

Ewen, H. I. and E. M. Purcell, "Radiation from galactic hydrogen at 1420 Mc/s," Nature, vol. 168, pp. 356-357, Sept. 1, 1951.

Fomalont, E. B., "Extended radio sources," in Origin of Cosmic Rays, IAU Symposium, No. 94, Setti, G., G. Spada, and A. W. Wolfendale (eds.), pp. 111-128. Dordrecht, Holland: D. Reidel, 1981.

Hey, J. S., "Solar radiations in the 4 to 6 meter radio wavelength band," Nature, vol. 157, p. 47, 1946.

Hey, J. S., The Radio Universe, Oxford, New York: Pergamon Press, 1971.

Hey, J. S., S. J. Parsons, and J. W. Phillips, "Fluctuations in cosmic radiation at radio frequencies," Nature, vol. 158, p. 234, Aug. 17, 1946.

Jansky, K. G., "Directional studies of atmospherics at high frequencies," Proc. IRE, vol. 21, pp. 1387-1398, Oct. 1933.

Jansky, K. G., "Electrical disturbances apparently of extraterrestrial origin," Proc. IRE, vol. 21, pp. 1387-1398, Oct. 1933.

Jauncey, D. L. (ed.), Radio Astronomy and Cosmology, IAU Symposium No. 74, Dordrecht, Netherlands: Reidel, 1977.

JPL, Deep Space Network/Flight Project Interface Design Handbook, Document 810-5, Rev. D; Section TC1-40, DSN Telecommunications Interfaces, Atmospheric and Environmental Effects, Jet Propulsion Laboratory, Pasadena, CA, 15 Dec. 1977.

Kellerman, K. I. and I. I. K. Pauliny-Toth, "Compact radio sources," in Annual Review of Astronomy and Astrophysics, vol. 19, pp. 373-410. Palo Alto, CA: Annual Reviews, 1981.

Kraus, J. D., Radio Astronomy. New York: McGraw-Hill, 1966.

Miley, G., "The structure of extended extragalactic radio sources," in Ann. Rev. Astron. Astrophys., vol. 18, pp. 165-218. Palo Alto, CA: Annual Reviews, 1981

Penzias, A. A. and R. W. Wilson, "A measurement of excess antenna temperature at 4080 mc/s," Astrophys. J., vol. 142, pp. 419-421, 1965.

Reber, G., "Cosmic static," Proc. IRE, vol. 28, pp. 68-70, Feb. 1940.

Reber, G., "Cosmic static," Astrophys. J., vol. 100, pp. 279-287, Nov. 1944.

Reber, G., "Cosmic static," Proc. IRE, vol. 36, pp. 1215-1218, Oct. 1948.

Ryle, M. and F. G. Smith, "A new intense source of radio-frequency radiation in the constellation of Cassiopeia," Nature, vol. 162, pp. 462-463, Sept. 18, 1948.

Shakeshaft, J. R. and A. S. Webster, "Microwave background in a steady state universe," Nature, vol. 217, pp. 339, 340, Jan. 27, 1968.

Shklovsky, I.S., Cosmic Radio Waves, English translation by R. B. Rodman and C. M. Varsavsky. Cambridge, MA: Harvard U. Press, 1960.

Skomal, E. N., Man-Made Radio Noise, New York: Van Nostrand, 1978.

Slobin, S. D., Microwave Noise Temperature and Attenuation of Clouds at Frequencies Below 50 GHz, JPL Publications 81-46, Pasadena, CA: Jet Propulsion Lab., 1981.

Slobin, S. D., Microwave noise temperature and attenuation of clouds: statistics of these effects at various sites in the United States, Alaska, and Hawaii," Radio Science, vol. 17, pp. 1443-1454, Nov.-Dec. 1982.

Smith, E. K. and J. W. Waters, Microwave Attenuation and Brightness Temperature Due to the Gaseous Atmosphere, A Comparison of JPL and CCIR Values, JPL Publication 81-81, Pasadena, CA: Jet Propulsion Lab., 1981.

Smith, E. K., "The natural radio noise source environment," Proceedings of 1982 IEEE International Symposium on Electromagnetic Compatibility, Santa Clara, CA (Sept. 6-8, 1982). New York: The Institute of Electrical and Electronics Engineers, 1982a.

Smith E. K., "Centimeter and millimeter wave attenuation and brightness temperature due to atmospheric oxygen and water vapor," Radio Science, vol. 17, pp. 1455-1464, Nov.-Dec. 1982b.

Southworth, G. D., "Microwave radiation from the sun," J. Franklin Inst., vol. 239, p. 285, 1945.

Staelin, D. H., et al., "Microwave spectroscopic imagery of the earth," Science, vol. 197, pp. 991-993, Sept. 2, 1977.

Waters, J. W., "Absorption and emission by atmospheric gases," in Methods of Experimental Physics, vol. 12, Astrophysics, Part B: Radio Telescopes (M.L. Meeks, ed.), pp. 142-176. New York: Academic Press, 1976.

Wielebinski, R., "Antenna calibration," in Methods of Experimental Physics, vol. 12, Astrophysics, Part B: Radio Telescopes (M.L. Meeks, ed.), pp. 82-997. New york: Academic Press, 1976.

Wilson, R. W., "The cosmic microwave background," Rev. Mod. Phys., vol. 51, pp. 433-445, July 1979.

Wulfsberg, K. N. and E. E. Altshuler, "Rain attenuation at 15 and 35 GHz," IEEE Trans. on Antennas and Propagation, vol. AP-20, pp. 181-187, March 1982.

CHAPTER 8
PROPAGATION EFFECTS ON INTERFERENCE

8.1 INTRODUCTION

As a result of the congestion of the frequency spectrum and the geostationary orbit and the related widespread use of frequency sharing, consideration of interference has assumed an important role in earth-station siting and other aspects of telecommunication-system design. Interference may arise between terrestrial systems, between terrestrial and space systems, and between space systems. Attention is given here to interference involving space systems, whether between space systems or between space and terrestrial systems. Space-system earth stations, which normally transmit high power and have sensitive receiving systems, may cause interference to terrestrial systems when transmitting and may be interfered with by terrestrial systems when receiving. In addition, one earth station may interfere with another. Also, earth stations may receive interfering, unwanted transmissions, as well as wanted signals, from satellites. Likewise satellites may receive interfering transmissions from other than the intended earth station, and terrestrial systems may receive interference from space stations.

In Sec. 8.2, some basic considerations are presented concerning the signal-to-interference ratio for a single wanted or service transmission and a single interfering transmission arriving over a direct path.

In considering the problem of interference to or from an earth station, analysis may be separated into two stages. In the first, a coordination area surrounding the earth station is determined. This area, based on calculating coordination distances in all directions from the earth station, is defined such that terrestrial stations outside the area should experience or cause only a negligible amount of interference. To determine coordination distances information on transmitter powers, antenna gains, and permissible interference levels is needed. For the earth station, the gain towards the physical horizon on the azimuth considered is used. For terrestrial systems, the maximum antenna gain is used. When considering interference due to scatter from rain,

it is assumed that the beams of the two antenna systems intersect in a region where rain is falling. The coordination procedure is thus based on unfavorable assumptions with respect to mutual interference.

After the coordination area has been established, potential interference between the earth station and terrestrial stations within the coordination area can be analyzed in more detail. In this stage of analysis, the actual antenna gains of the terrestrial stations in the directions toward the earth station will be used. Also, it is determined whether the beams of the earth station and terrestrial station truly do intersect, in considering scatter from rain. Terrestrial stations within the coordination area may or may not be subject to or cause significant interference depending on the factors taken into account in the second stage of analysis.

Two propagation modes are considered for determining coordination area. One involves propagation over near-great-circle paths, and one involves scatter from rain. Coordination distances d_1 and d_2 are determined for the modes and the larger of the two values is used as the final coordination distance. Determination of the two distances is considered in Secs. 8.3 and 8.4. Interference between space stations and terrestrial systems is discussed in Sec. 8.5. Procedures for interference analysis are summarized in Sec. 8.6, and certain practical matters about the siting of earth stations are discussed in Sec. 8.7.

From the propagation viewpoint, interference between terrestrial systems and earth stations is concerned very much with transhorizon propagation. In the late 1950's and early 1960's, transhorizon propagation became of considerable interest as a means of communication over long distances. The rather weak but consistent troposcatter signals were and are utilized for this purpose, as the stronger but sporadic signals due to ducting and rain scatter do not occur for the high percentages of time needed for reliable communications. At the present time however, much interest in transhorizon propagation is related to interference. Ducting and rain scatter contribute to the higher levels of interfering signals that occur for smaller percentages of time, and they are highly important in interference analysis (Crane, 1981). The occurrence of ducting is vividly displayed on PPI radar screens showing ground-

clutter echoes. At times ducting causes ground clutter or other targets to appear at considerably greater ranges than normally. Actually there is no fixed normal appearance of the radar screen, as the maximum range at which ground-clutter echoes appear fluctuates continuously.

In this chapter, attention is given to propagation effects on interference and to determination of coordination area, with emphasis on basic concepts. Additional details, including some of the empirically derived expressions utilized for coordination analyses are given in appendices. CCIR Reports 569, 724, and 382 (CCIR, 1978a, b, c and 1982a, b, c) and Appendix 28 to Radio Regulations (ITU, 1982) treat these topics and have been utilized in the preparation of this chapter. Persons carrying out coordination analyses will wish to refer to these reports, especially to Appendix 28 for legal purposes; all of the charts, tables, and other details of the reports are not repeated here. Instead, an effort has been made to provide explanatory background material and summaries of procedures for use as an introduction and reference on interference analysis. The material in the CCIR reports is subject to a continuing process of revision and updating as a comparison of the reports for 1978 and 1982 indicates.

The procedure described in Appendix 28 of Radio Regulations must be followed in determining coordination area if legal requirements are to be met. The material of Appendix 28 concerning coordination area is essentially the same as that of CCIR Report 382 for 1978. Study Groups 4 (Fixed Service Using Communication Satellites) and 9 (Fixed Service Using Radio-Relay Systems) have primary responsibility for coordination area; Report 382 is in Volume 9, prepared by Study Group 9. Reports 569 and 724, prepared by Study Group 5, (Propagation in Non-ionized Media) represent its inputs to the coordination problem. As this handbook is concerned primarily with propagation effects, we describe the approaches of Reports 569 and 724 as well as the procedures of Report 382 and Appendix 28.

8.2 THE SIGNAL-TO-INTERFERENCE RATIO

The signal-to-noise ratio, C/X, of a telecommunications link was given in Chap. 1 in the form of

$$(C/X)_{dB} = (EIRP)_{dBW} - (L_{FS})_{dB} - L_{dB} + (G_R/T_{sys})_{dB} - k_{dBW} - B_{dB} \quad (8.1)$$

In this section, attention is given to a corresponding signal-to-interference ratio, C/I. For considering this ratio, first separate EIRP into P_T and G_T where EIRP stands for effective isotropic radiated power, P_T represents the transmitted power, and G_T represents transmitting antenna gain. Also, the loss factor L_{dB} can be separated into $A(p,\theta)$, the attenuation in dB, expressed as a function of percentage of occurrence p and elevation angle θ, and the factor $-20 \log \delta$ representing polarization mismatch (Dougherty, 1980). As δ varies from 0 to 1, $-20 \log \delta$ is a positive quantity. Separating $(EIRP)_{dBW}$ and L_{dB} as indicated, C_{dBW} alone becomes

$$C_{dBW} = (P_T)_{dBW} + (G_T)_{dB} + (G_R)_{dB} - (L_{FS})_{dB} - A(p,\theta) + 20 \log \delta \quad (8.2)$$

For I_{dBW}, the interfering power arriving over a direct path, a similar expression applies, namely

$$I_{dBW} = (P_{T_i})_{dBW} + (G_{T_i})_{dB} + (G_{R_i})_{dB} - (L_{FS_i})_{dB} - A_i(p,\theta) + 20 \log \delta_i \quad (8.3)$$

where the subscript i refers to the interfering signal. The quantity G_{T_i} represents the gain of the antenna of the interfering transmitter in the direction of the receiving system being interfered with, and a similar interpretation applies to the other terms. Interference due to scatter from precipitation will be considered in Sec. 8.3. On the basis of Eqs. (8.2) and (8.3), the $(C/I)_{dB}$ ratio may be expressed as:

$$(C/I)_{dB} = (P_T)_{dBW} - (P_{T_i})_{dBW} + (G_T)_{dB} - (G_{T_i})_{dB} + (G_R)_{dB} - (G_{R_i})_{dB} + 20 \log(d_i/d) + A_i(p,\theta) - A(p,\theta) + 20 \log \delta/\delta_i \quad (8.4)$$

The term $20 \log(d_i/d)$ arises from the L_{FS} free-space basic transmission loss terms which have the form of $(4\pi d/\lambda)^2$, where d is distance. In Eq. (8.4), d is the length of the path of the wanted signal and d_i is the length of the path of the interfering signal.

For analyzing transmissions from space to Earth or vice versa, the polarization mismatch factor δ equals cos θ where θ is a polarization mismatch angle to which there may be three contributions such that

$$\theta = \theta_o + \theta_i + \theta_r \tag{8.5}$$

The angle θ_o arises from geometrical considerations and can be determined from

$$\theta_o = \delta B - \alpha\delta A \tag{8.6}$$

With δB, the difference in back azimuths between the service path (to the intended earth station) and the interfering path (to the earth station being interfered with). The back azimuth is the angle to the earth station measured from the north-south meridian of the subsatellite point. The factor δA represents the difference in azimuths of the two earth stations, azimuth in this case being measured at the earth station as the angle from geographic north to the great circle path from the earth station to the subsatellite point (Fig. 8.1). The quantity α depends on the great circle distance Z between the earth stations. On this topic, we follow the treatment by Dougherty (1980) and reproduce two of his illustrations showing θ_o as a function of B and A (Fig. 8.2) and B and Z as a function of earth station latitude and longitude with respect to the subsatellite point (Fig. 8.3).

The angle θ_i represents the Faraday rotation of a linearly polarized wave that may take place in propagation through the ionosphere. The concept of Faraday rotation is not applicable to the propagation of circularly polarized waves. The relation for θ_i used by Dougherty (1980) is

$$\theta_i = 108°/f^2 \tag{8.7}$$

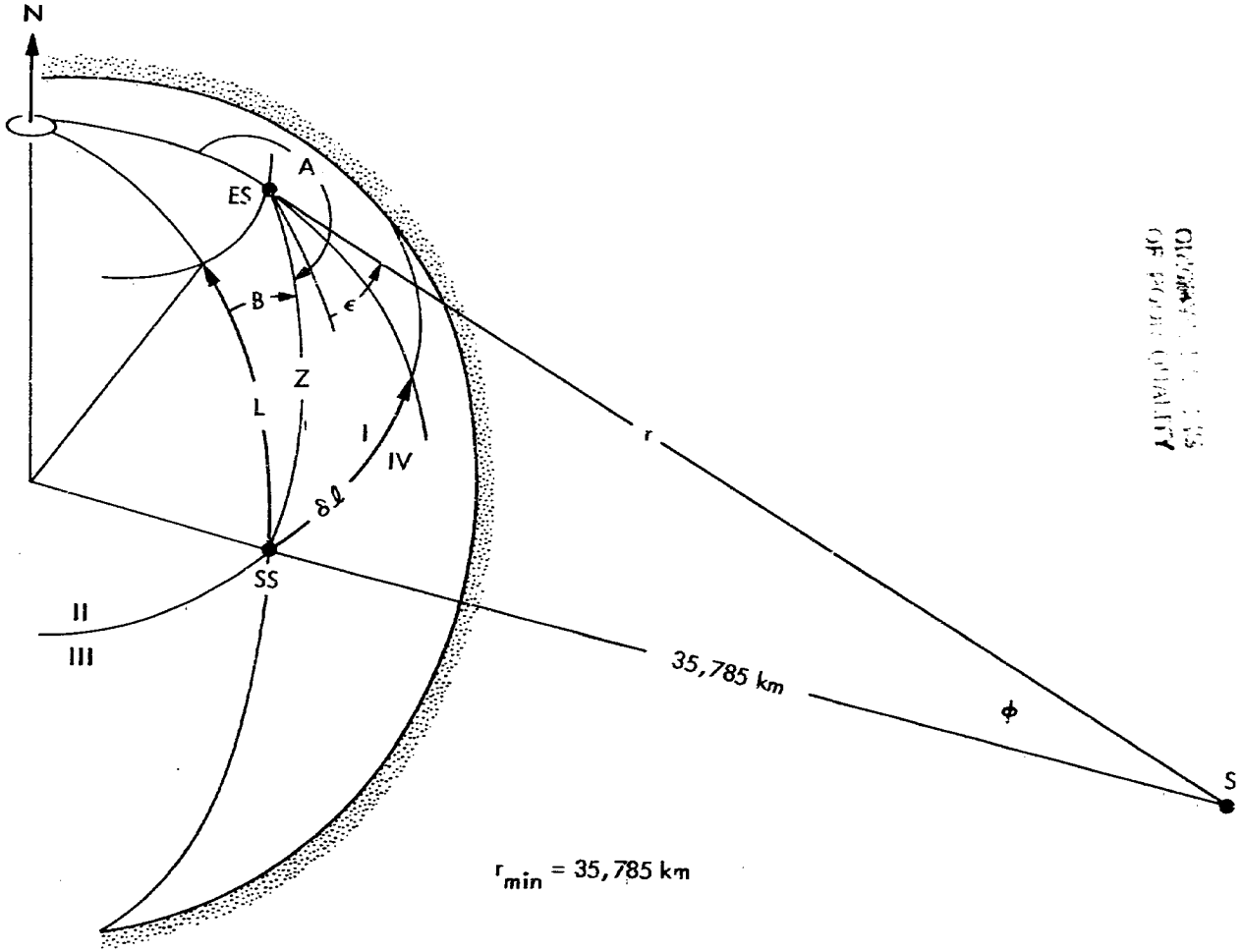

Figure 8.1. Synchronous satellite geometry (Dougherty, 1980).

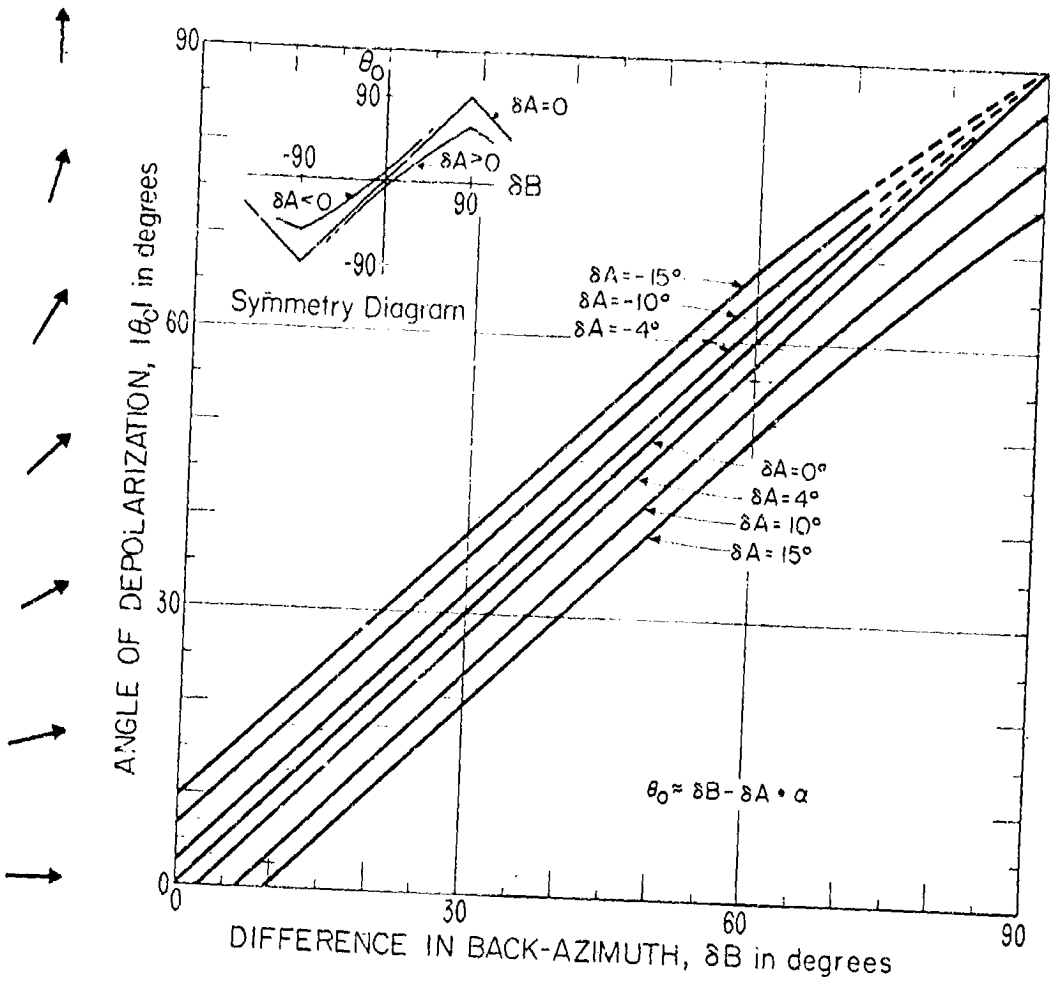

Figure 8.2. The depolarization angle for linear polarization for a potential interference situation (Dougherty, 1980).

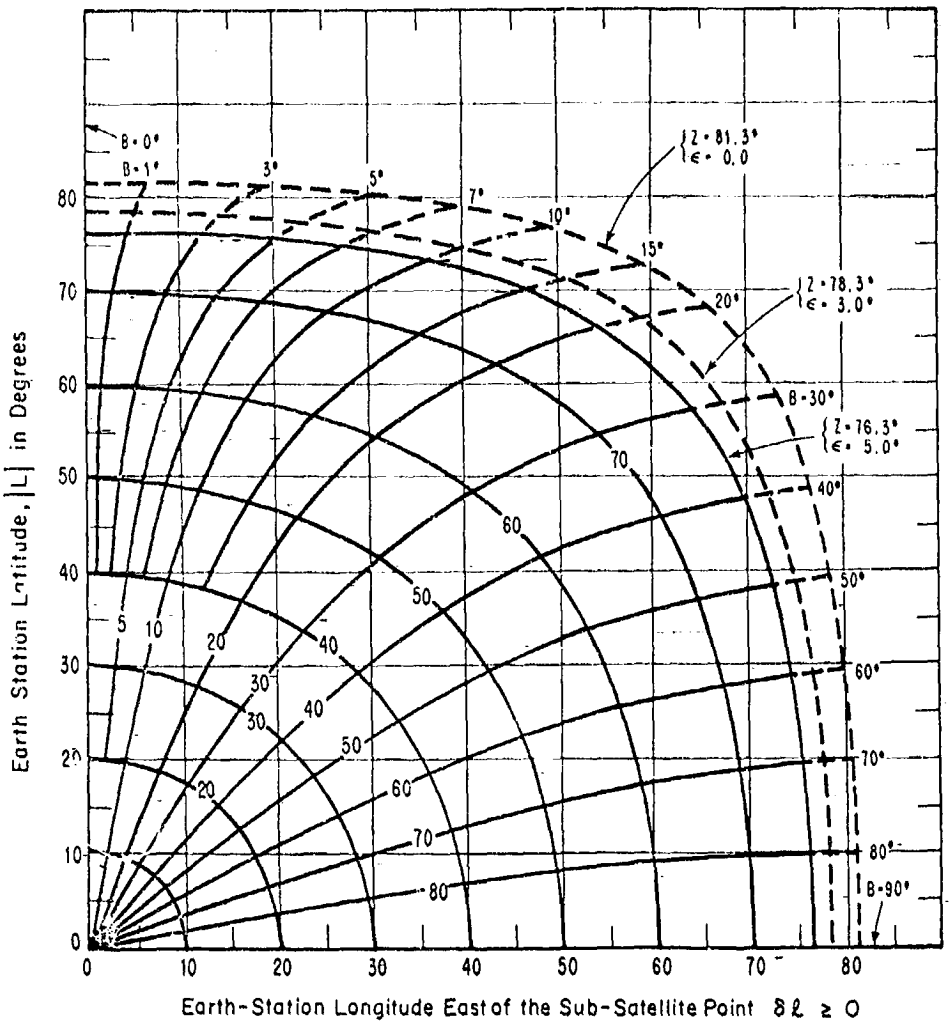

Figure 8.3. The great-circle arc (Z) and the back-azimuth (B, from SS to ES) as a function of the earth-station's (ES) north latitude L and degrees of longitude ($\delta\ell$) east of the sub-satellite point (SS) (Dougherty, 1980).

with f the frequency in GHz. (This value of θ_i corresponds to the maximum one-way effect of the ionosphere for an elevation angle of 30°.) The subject of Faraday rotation is treated in Sec. 2.2. The angle θ_r represents the possible rotation of the electric field intensity due to depolarization caused by precipitation. By definition, the cross polarization discrimination (XPD) is given by

$$XPD = 20 \log E_{11}/E_{12}$$

where E_{11} is the amplitude of the copolarized signal (having the original polarization and after taken account of any attenuation due to precipitation) and E_{12} is the amplitude of the orthogonally polarized signal produced by depolarization due to precipitation. The angle θ_r is $\tan^{-1} E_{11}/E_{12}$.

For determining the values of A (p, θ) and δ in Eqs. (8.2) and (8.3), one evaluates the service path under unfavorable conditions, using the loss occurring for a small percentage of the time, corresponding to p = 0.01 percent, for example. The interference path, however, is evaluated with the minor losses occurring for say 50 percent of the time. This practice takes into account such possibilities as the wanted signal propagating through an intense rain cell while the unwanted signal follows a path which misses the rain cell and encounters negligible attenuation.

8.3 COORDINATION AREA BASED ON GREAT CIRCLE PROPAGATION

8.3.1 Basic Concepts

For determining coordination areas, attenuation needs to be given in two modes of propagation of interfering signals (CCIR, 1982a, b, c). Propagation mode one (mode 1), referring to propagation over a direct near-great-circle path, occurs essentially all of the time. The second propagation mode (mode 2) is via scatter from hydrometers, principally rain, and may occur infrequently. In this section, some general considerations are presented, and propagation mode 1 is discussed. Scatter from rain (mode 2) is treated in Sec. 8.4.

In system planning, it is generally required to estimate the relatively intense interference level which is exceeded for some small percentage, p, of the time (e.g., p = 0.01 percent) and also perhaps the interference level exceeded for about 20 percent (p = 20 percent) of the time. Corresponding to high interference levels are low values of basic transmission loss L_b (Fig. 8.4). Note that in considering attenuation due to rain (Chap. 4) concern was directed to the small percentages of time for which maximum values of attenuation occurred. Here the concern is for the small percentages of time for which the highest interfering signal intensities occur.

The total loss factor, L_t, relating the interfering transmitted power, P_{T_i}, and the interfering received power, P_{R_i}, is defined by

$$L_t = P_{T_i}/P_{R_i} \tag{8.8}$$

An expression for the basic transmission loss, L_b, referred to above, can be obtained by a modification of Eq. (1.2), namely from $P_{R_i} = P_{T_i}G_TG_R/L_{FS}L$. Identifying $L_{FS}L$ as L_b

$$L_b = L_{FS}L = \frac{P_{T_i}G_TG_R}{P_{R_i}} \tag{8.9}$$

where L_{FS} is the free-space basic transmission loss and L represents other system losses. In decibel values referring to p percent of the time, Eq. (8.8) becomes

$$[L_t(p)]_{dB} = (P_{T_i})_{dBW} - [P_{R_i}(p)]_{dBW} \tag{8.10}$$

and Eq. (8.9) becomes

$$[L_b(p)]_{dB} = (P_{T_i})_{dBW} + (G_T)_{dB} + (G_R)_{dB} - [P_{R_i}(p)]_{dBW} \tag{8.11}$$

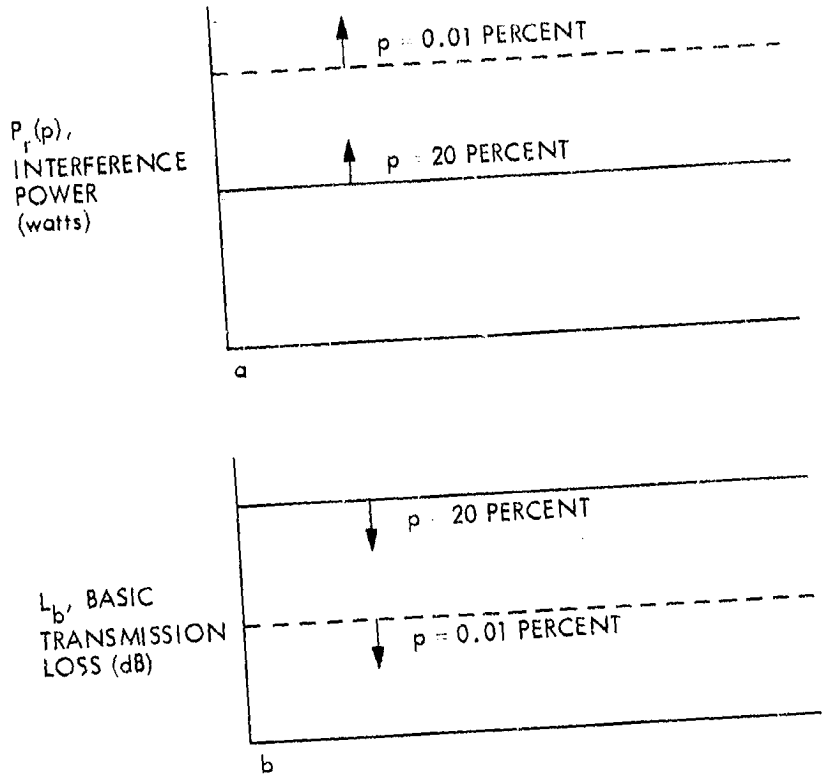

Figure 8.4. Correspondence between interference level and basic transmission loss. The interfering signal power will be above a certain level for 0.01 percent of the time, as suggested by the arrow extending upwards from the dotted line of Fig. 8.4a. The high interference level above the dotted line of Fig. 8.4a correspond to the low values of basic transmission loss below the dotted line of Fig. 8.4b. For 20 percent of the time, the interference level will be above the solid line of Fig. 8.4a, and the corresponding values of basic transmission loss will be below the solid line of Fig. 8.4b.

In Eqs. (8.10) and (8.11) ... permissible interference power level to be exceeded for no more than p percent of the time. Further information about permissible interference levels is given in Appendix 8.1. The gains G_T and G_R are the gains of the transmitting and receiving antennas. For determining coordination distance, the horizon gain at the azimuth considered is used for the earth-satellite station and the maximum gain is used for the terrestrial station. From Eq. (8.9), it can be seen that if $G_T = G_R = 1$, $L_b = P_{T_i}/P_{R_i}$. For this reason, L_b is said to be the loss that would occur between isotropic antennas.

The basic transmission loss L_b is seen to be the product of L_{FS} and L. For a line-of-sight path and for frequencies below 10 GHz, L_b will be roughly but not exactly equal to L_{FS}. In any case, L_{FS} makes a major contribution to L_b. The free-space basic transmission loss L_{FS} was introduced in Sec. 1.1.1 and defined there by

$$L_{FS} = (4\pi d/\lambda)^2 \tag{8.12}$$

where d is distance from the transmitting to receiving locations and λ is wavelength. At higher frequencies, the dissipative attenuation associated with water vapor and oxygen may make significant contributions to L_b. Dissipative attenuation of the interfering signal due to rain is not included in L_b for the low values of p normally considered in applying Eq. (8.11) as $L_b(p)$ then represents the low values of basic transmission loss that can be tolerated for only small percentages of time. When considering interfering signals, high values of L_b can be readily tolerated. It is the low values of L_b that are of concern.

In terms of decibel values, Eq. (8.12) can be written as

$$(L_{FS})_{dB} = 20 \log(4\pi) + 20 \log d - 20 \log \lambda \tag{8.13}$$

where d and λ are in meters. Commonly, however, L_{FS} is expressed in terms of frequency f rather than wavelength λ. By replacing λ by c/f where $c = 2.9979 \times 10^8$ m/s, one obtains

$$(L_{FS})_{dB} = -147.55 + 20 \log f + 20 \log d \qquad (8.14)$$

If f is expressed in GHz rather than Hz, a factor of 180 dB must be added to the right-hand side of Eq. (8.13) and if d is in km rather than m, an additional factor of 60 dB must also be included. The expression for $(L_{FS})_{dB}$ then takes the form of

$$(L_{FS})_{dB} = 92.45 + 20 \log f_{GHz} + 20 \log d_{km} \qquad (8.15)$$

8.3.2 Line-of-Sight Paths

Although L_b may equal L_{FS} approximately for frequencies below 10 GHz for a certain range of values of p, in the absence of horizon or obstacle effects, the actual received interfering signal on even a clear line-of-sight path fluctuates due to the effects of multipath propagation, scintillation, and defocusing and may be greater or less than that calculated from L_{FS} alone. Thus although factor L of Eq. (8.9) has been referred to as a loss factor, it must be able to assume values either greater than or less than unity if it is to be applicable to the situation considered here. The variation of the received level P_{R_i} with time provides the basis for specifying P_{R_i} as a function of p. For line-of-sight paths, L can be expressed as $A_o + A_D - G_p$ and L_b is given by

$$(L_b)_{dB} = (L_{FS})_{dB} + A_o + A_D - G_p \qquad (8.16)$$

where A_o is the attenuation in dB due to oxygen and water vapor. (See. Fig. 3.11 for attenuation caused by oxygen; that due to water vapor can be neglected below 15 GHz.) The coefficient A_D represents attenuation due to defocusing in dB, and G_p is an empirical factor in dB given by Table 8.1 for paths of 50 km or greater (CCIR, 1982a).

Table 8.1 G_p of Eq. (8.16) in dB (values which may be exceeded for p percent of the time).

p	0.001	0.01	0.1	1
G_p	8.5	7.0	6.0	4.5

For distances shorter than 50 km, the values of G_p can be proportionally reduced. To estimate the value exceeded for all but 20 percent of the time, CCIR Report 569 recommends adding 1.5 dB to the value of L_{FS} (thereby increasing L_b by 1.5 dB with respect to what it would be otherwise). The coefficient G_p can be taken as zero for p = 20 percent.

Attenuation due to defocusing results when the variation of refractivity with height dN/dh (Sec. 3.2) itself varies with height so that rays at different heights experience different amounts of bending. Rays traversing the region, rays which were originally essentially parallel for example, then became more widely separated than otherwise and signal intensity is consequently reduced. It develops that the variation of dN/dh with height h is proportional to ΔN, the decrease in refractivity N in the first km above the surface. Figure 8.5 shows attenuation due to defocusing as a function of ΔN and elevation angle θ (CCIR, 1982d).

A given path may be a clear line-of-sight path for certain values of dN/dh (Sec. 3.1) but may have part of the first Fresnel zone obstructed for other values of dN/dh. The effect of obstruction is taken into account in Sec. 8.3.3.

8.3.3 Transhorizon Paths

Major attention in the analysis of interference between terrestrial systems and the earth stations of space systems is directed to transhorizon propagation. The term transhorizon path refers to a path extending beyond the normal radio horizon for which diffraction is a relevant propagation

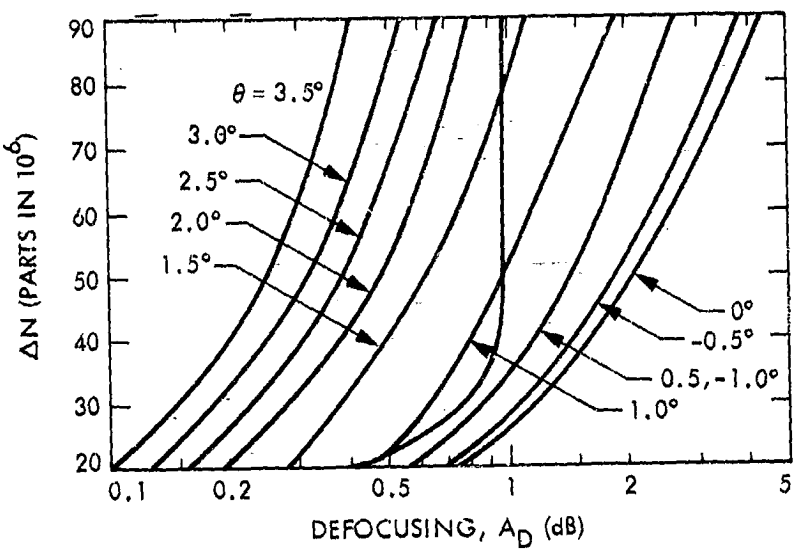

Figure 8.5. Defocusing on near-horizontal paths as a function of ΔN (the decrease in refractivity in the first km) for various values of grazing-angle θ (CCIR, 1982d).

mechanism, as distinguished from a clear line-of-sight path at one extreme and a strictly troposcatter path at an opposite extreme. For transhorizon paths, a diffraction loss term, A_s (dB) must be added to the free-space basic transmission loss L_{FS}. In addition, account must be taken of ducting and superrefraction which can be expected to occur for some percentages of the time.

When both the transmitting and receiving terminals of a link are immersed in a duct, the basic transmission loss L_b between the two terminals has been shown to be given by

$$(L_b)_{dB} \geq 92.45 + 20 \log f_{GHz} + 10 \log d_{km} + 0.03\, d_{km} + A_c \qquad (8.17)$$

where A_c(dB) is a coupling loss that takes account of the fact that not all of the rays leaving the transmitting antenna may be trapped within the duct. The distance d in the term 0.03 d is in km and 0.03 is the theoretical minimum value of a duct attenuation coefficient γ_d, having units of dB/km (Dougherty and Hart, 1979). Note that in the expression for $(L_{FS})_{dB}$ (Eq. 8.15), 20 log d appears rather than 10 log d. The basis for using 10 log d for a duct is that a wave in a duct is constrained in the vertical direction and spreads out only in the horizontal direction, whereas in free space a wave spreads in both directions. Because L_b for a duct includes the term 10 log d rather than 20 log d, L_b for propagation in a duct tends to be significantly less than L_{FS}.

In the general case γ_d in the equation for $(L_b)_{dB}$ for a transhorizon path [0.03 in Eq. (8.17)], depends on meteorological conditions, frequency, and percent of time and can be determined only by empirical means. For establishing the value of γ_d, the Earth has been divided into four zones in CCIR Report 569 (CCIR, 1982a). These zones are:

Zone A1: coastal areas, i.e., land with an altitude less than 100 m above sea level but not extending more than 50 km inland from Zones B or C.

Zone A2: All other land

Zone B: seas, oceans, and other substantial bodies of water (as a criterion, one which can encompass a circle of diameter 100 km) at latitudes greater than 23.5° N or S, but excepting the Black Sea and the Mediterranean.

Zone C: seas, oceans, and other substantial bodies of water (as a criterion, one which can encompass a circle of diameter 100 km) at latitudes less than 23.5° N or S and including the Black Sea and the Mediterranean.

Taking account of the diffraction loss and ducting, the basic transmission loss L_b for paths entirely in one zone is given by

$$(L_b)_{dB} = 92.45 + 20 \log f_{GHz} + 10 \log d_{km} + (\gamma_d + \gamma_o + \gamma_w) d_{km} + A_c + A_s \quad (8.18)$$

The attenuation constants γ_o and γ_w refer to oxygen and water vapor. The attenuation due to water vapor can be neglected for frequencies below 15 GHz. The attenuation constant for oxygen is shown in Fig. 3.11. In CCIR Report 569, values of γ_d are given as a function of frequency and percent p in graphical form for the 4 zones. These graphs are reproduced as Figs. 8.6 - 8.9. The value of A_c is given in the form of a table, reproduced here as Table 8.2.

Table 8.2 Values of Coupling Loss, A_c (dB).

	Percent of Time			
Zone	0.001	0.01	0.1	1
A2	9	10	11	14
A1,B,C	6	7	8	11

The value of A_s, the diffraction loss, is given in Report 569 as

$$A_s = 20 \log [1 + 6.3\, \theta\, (fd_h)^{1/2}] + 0.46\, \theta\, (fCr)^{1/3} \quad (8.19)$$

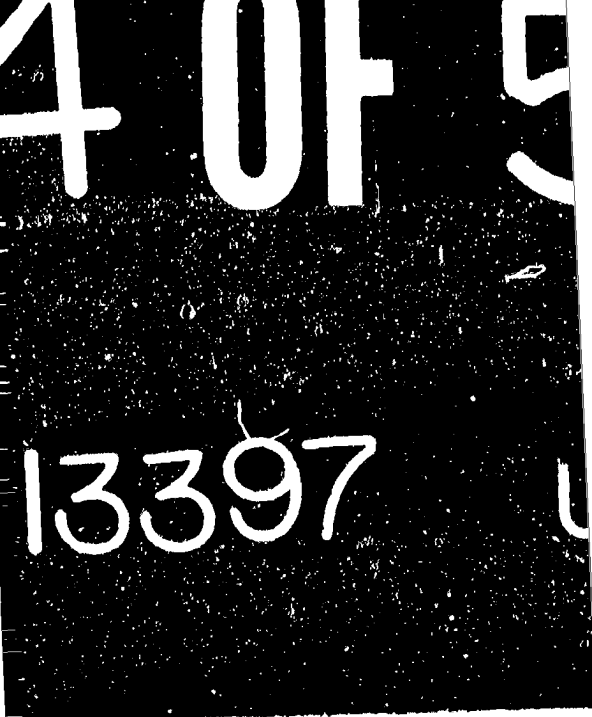

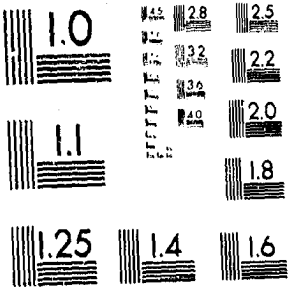

MICROCOPY RESOLUTION TEST CHART
NATIONAL BUREAU OF STANDARDS
STANDARD REFERENCE MATERIAL 1010a
(ANSI and ISO TEST CHART No. 2)

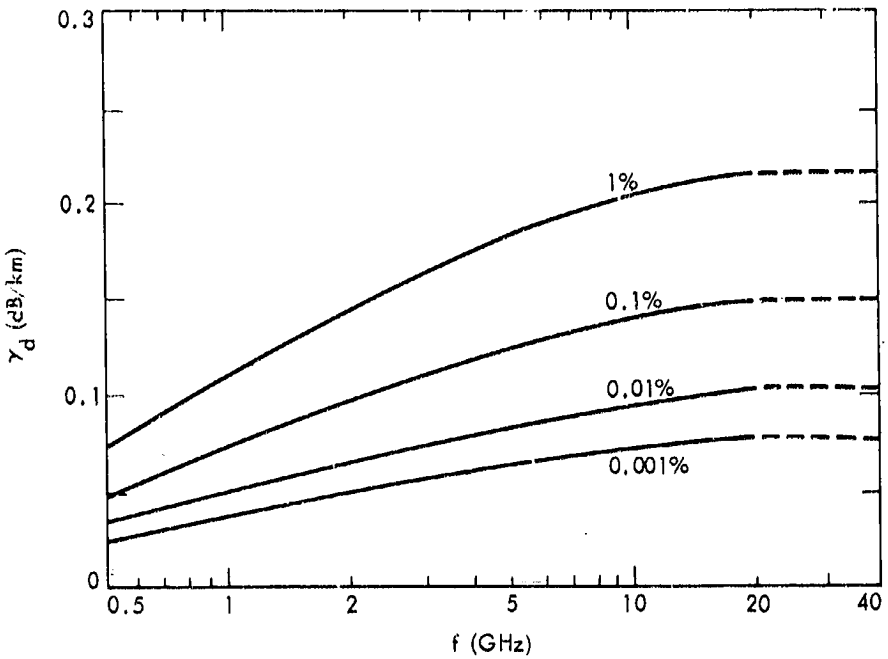

Figure 8.6. Attenuation constant for zone A1 (CCIR, 1982a).

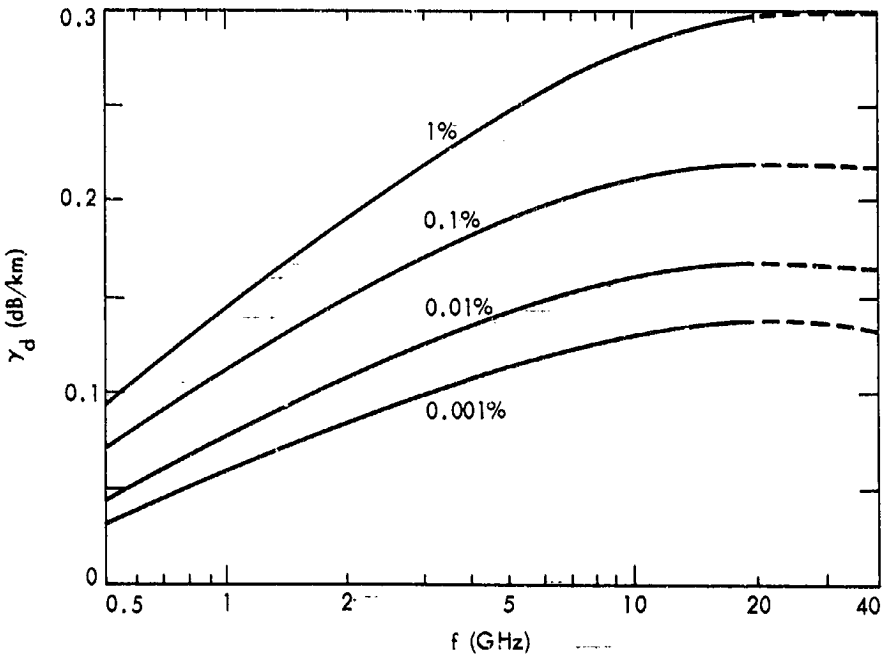

Figure 8.7. Attenuation constant for zone A2 (CCIR, 1982a).

C-4

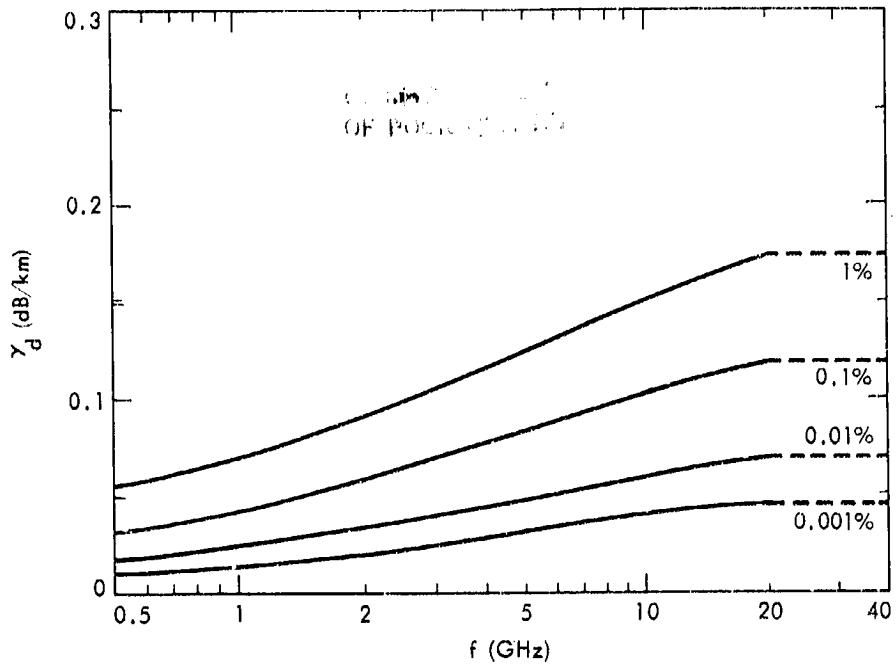

Figure 8.8. Attenuation constant for zone B (CCIR, 1982a).

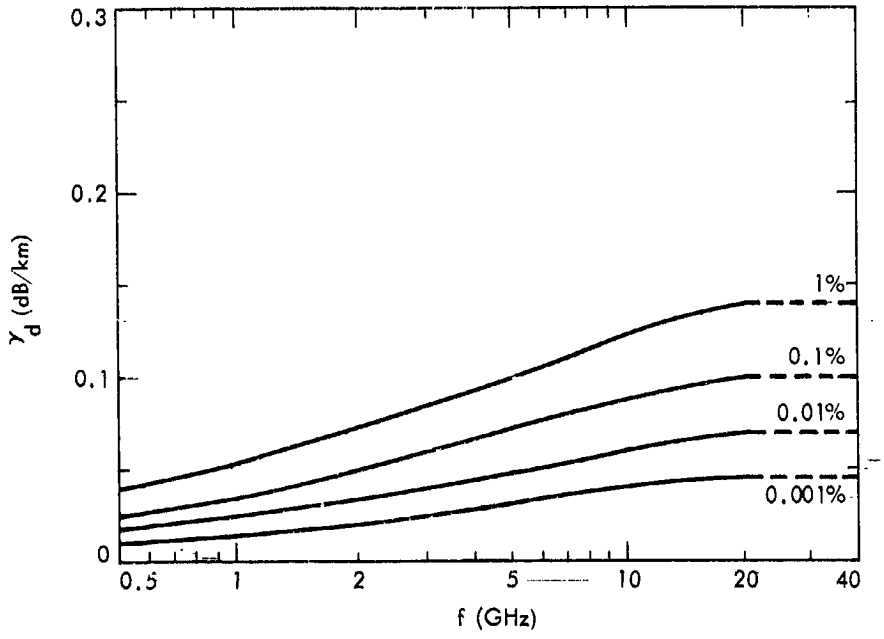

Figure 8.9. Attenuation constant for zone C (CCIR, 1982a).

where f is frequency in GHz, d_h is the horizon distance in km, θ is the horizon elevation angle in degrees, and Cr is the obstacle radius of curvature. Equation (8.18) can be solved for d by use of an interactive computer program, using the value of L_b which is the minimum acceptable value for a particular value of p.

The treatment of Report 724 is similar to that described above for Report 569, but in Report 724 only 3 zones A, B, and C are considered. Zone A is land, excluding the coastal strip extending 50 km inland. The coastal strips are included within Zones B and C which are otherwise the same as zones B and C of Report 569. In Report 724, γ_d is given by $\gamma_d = a(p) + b(p)g(f)$ where a, b, and g are empirically determined expressions which have different forms for the three zones. The expressions are shown in Table I of Report 724 and are reproduced in Appendix 8.2. The quantity A_s has a slightly different form in Report 724, corresponding to letting d_h = 0.5 km and Cr = 10 m in Eq. (8.19). [See Eq. (8.21).]

The treatments of Report 382 (CCIR, 1982c) and Appendix 28 of Radio Regulations (ITU, 1982) are similar to each other but Report 382 has received updating from the 1978 version which has not yet been included in Appendix 28. The 1982 versions of the three CCIR reports referrred to (569, 724, and 382) were all updated with respect to the 1978 versions, but it was felt that it was too early to propose corresponding changes in Appendix 28, which closely follows the 1978 version of Report 382.

Report 382 and Appendix 28 take account of essentially the same factors as Reports 569 and 724 but in place of the 10 log d, γ_d, and A_c terms of Eq. (8.18), which all relate to ducting, one empirically derived expression $\beta_Z d_1$ is employed such that the equation for L_b takes the form of

$$(L_b)_{dB} = 120 + 20 \log f + \beta d_1 + A_h \qquad (8.20)$$

where

$$\beta = \beta_Z + \beta_V + \beta_O$$

The factors β_V and β_O represent attenuation in dB/km due to water vapor and oxygen. It is $\beta_Z d_1$, where β_z is expressed as a function of f and p and has different forms for the 3 zones, that takes account of ducting and super-refraction. The 3 forms are included in Appendix 8.2. The term A_h is the same as A_s of Reports 569 and 724, with d_h = 0.5 km and Cr = 10 m as in Report 724. Making these substitutions result in

$$A_h = 20 \log (1 + 4.5\,0\, f^{1/2}) + 0 f^{1/3} \qquad (8.21)$$

Equation (8.20) can be solved for d_1, the coordination distance corresponding to the value of L_b which can be tolerated for p percent of the time.

Troposcatter signals, resulting predominantly from inhomogeneous scattering by random fluctuations of the index of refraction of the atmosphere, are normally weaker than the interfering signals due to ducting and super-refraction. However, the tropospheric scatter signals may be predominant for percentages of time between about 1 and 50 percent and for percentages less than one percent when high site shielding (A_h values of 30 dB and greater) is encountered.

8.4 COORDINATION AREA FOR SCATTERING BY RAIN

For considering interference due to scatter from rain, one can start with a slightly modified version of Eq. (4.43) which refers to bistatic scatter from rain. Inverting this relation to obtain a total loss factor L_t, using G_T, G_{ES}, R_T, and R_{ES} to refer to the gains of the terrestrial and earth-station antennas and their distances from the region of rain scatter, and replacing W_T and W_R by P_{T_i} and P_{R_i} results in

$$L_t = \frac{P_{T_i}}{P_{R_i}} = \frac{(4\pi)^3 R_T^2 R_{ES}^2 L}{G_T G_{ES} \eta V \lambda^2} \qquad (8.22)$$

In this exression, L is a loss factor (greater than unity if truly a loss), V is the common scattering volume, and η is the radar cross section per unit volume. For Rayleigh scattering η has the form of

$$\eta = \frac{\pi^5}{\lambda^4} \left| \frac{K_c - 1}{K_c + 2} \right|^2 Z \quad m^2/m^3 \tag{8.23}$$

where K_c is the complex dielectric constant of water and is a function of frequency and temperature. When expressed in mm^6/m^3, the quantity Z is related to rainfall rate R in mm/h for a Laws and Parsons distribution of drop sizes by the empirical expression

$$Z = 400\, R^{1.4} \tag{8.24}$$

Physically, Z represents $\sum d^6$ where d is the drop diameter and the summation is carried out for all of the drops in a unit volume. For frequencies higher than 10 GHz for which Rayleigh scattering does not apply, an effective or modified value of Z, designated as Z_e, is used for coordination distance calculations.

Usually the earth-station antenna has a smaller beamwidth than the terrestrial antenna. Assuming that such is the case and noting that the scattering volume V is defined by the antenna with the smallest beamwidth, V is given approximately by $V \approx (\pi/4)\theta^2 R_{ES}^2 D$ where θ is the beamwidth of the earth-station antenna, R_{ES} is in distance of the earth station from the common scattering volume V, and D is the extent of the common scattering volume along the path of the earth-station antenna beam. Noting that the beamwidth θ of an aperture-type antenna is given approximately by λ/d where d is the aperture dimension, assuming a circular aperture, and recalling that the gain G of an antenna is related to effective area A by $G = 4\pi A/\lambda^2$, it develops that $\theta^2 = \pi^2/G$ and $V = \pi^3 R_{ES}^2 D/(4\, G_{ES})$. In Eq. (8.23) for η, $|(K_C-1)/(K_C + 2)|^2$ has a value of about 0.93 (Battan, 1973), which is close to unity. Substituting for V and η and dropping numerical factors which affect the magnitude only slightly, the expression for the loss factor L_t becomes

$$L_t \approx \frac{R_T^2 \lambda^2 L}{Z D G_T} = \frac{R_T^2 c^2 L}{f^2 Z D G_T} \tag{8.25}$$

An important point about this relation is that it involves only the distance R_T of the scattering volume V from the terrestrial station rather than both distances as in Eq. (8.22).

To consider the application of Eq. (8.25) further, we convert to decibel values and utilize the presentations of CCIR Reports 569, 724, and 382 starting with the 1978 versions of Reports 569 and 724 which follow the basic form of Eq. (8.25) most closely. Replacing λ^2 of the original Eq. (8.25) by c^2/f^2 so that 20 log c - 20 log f = 169.54 - 20 log f replaces 20 log λ, the resulting expression in the 1978 version of Report 569, when applied to frequencies below 10 GHz, is

$$[L_t(p)]_{dB} = 199 + 20 \log (R_T)_{km} - 20 \log f_{GHz} - 10 \log M - 10 \log C + \gamma_o r_o + B - 10 \log Z - 10 \log D_{km} - 10 \log G_T \qquad (8.26)$$

The numerical value of 199 is obtained, approximately, by adding 60 dB to 169.54 because of expressing R_T in km rather than m and subtracting 30 dB because of expressing D in km also. In the equation, Z is in mm^6/m^3 rather than m^6/m^3 and use of these units introduces a factor of 180 dB, but expressing f in GHz rather than Hz introduces a factor of 180 dB of opposite sign and the two 180 dB factors cancel. The loss factor L of Eq. (8.25) is represented by -10 log M where M is a polarization mismatch factor (Sec. 8.2), by -10 log C which takes account of attenuation due to rain within the common scattering volume, by $\gamma_o r_o$ for the attenuation due to oxygen, and by B which is a terrain blocking factor. As M and C are less than unity, -10 log M and -10 log C are positive quantities. See Appendix 8.3 for the form of C and for discussion of B.

Considering the term -10 log Z where $Z = 400\ R^{1.4}$ for a Laws and Parson distribution, the rainfall rates R that are available are usually surface rates. In some treatments, as in the 1978 version of Report 382, it has been assumed that the reflectivity Z decreases with height at a rate of about 1 dB/km. To take account of this assumed decrease of Z with height when R is a surface rate, it is only necessary to subtract the height of the common scat-

tering volume in km. This height h can be determined from $h = \ell^2/2kr_0$ (Eq. 3.18 and following paragraphs), where ℓ in this case equals $R_T - R_{hor}$, namely the difference between the distance of the terrestrial transmitter from the scattering volume and the distance to the horizon of the terrestrial transmitter (Fig. 8.10). Letting $k = 4/3$ and taking r_0 as 6371 km and R_{hor} as 40 km (corresponding to an antenna height of 100 m) results in $2kr_0 = 17{,}000$ and $h = (R_T - 40)^2/17{,}000$. Thus

$$10 \log Z = 26 + 14 \log R - \frac{(R_T - 40)^2}{17{,}000} \tag{8.27}$$

In the 1982 versions of Reports 569, 724, and 382, however, Z is assumed to be constant with height so that $10 \log Z = 26 + 14 \log R$.

The 1978 version of Report 724 uses essentially the same relation as in the 1978 version of 569 but includes a table giving values of D, referring to it as rain cell diameter, as a function of rain rate and climatic region for 0.01 percent of the time. Both reports include the attenuation due to water vapor and a correction for the deviation from Rayleigh scattering, but these are not applicable for frequencies below 10 GHz.

The corresponding expression in the 1978 version of Report 382 and in Appendix 28 of Radio Regulations (ITU, 1982) is also closely similar but utilizes a normalized transmission loss L_2 (0.01) defined by

$$[L_2\ (0.01)]_{dB} = (P_{T_i})_{dBW} + (\Delta G)_{dB} - [P_R(p)]_{dBW} - F(p,f) \tag{8.28a}$$

The normalized transmission loss is based on a gain G_T of 42 dB of the terrestrial station antenna. The factor ΔG is the difference between the maximum gain of the terrestrial antenna and 42 dB, and tables are given showing ΔG for use when the earth station is a transmitting antenna and when it is a receiving station. A term $-F(p,f)$ is also included in the texts cited as a correction factor to relate conditions for the percentage of time p to the case when

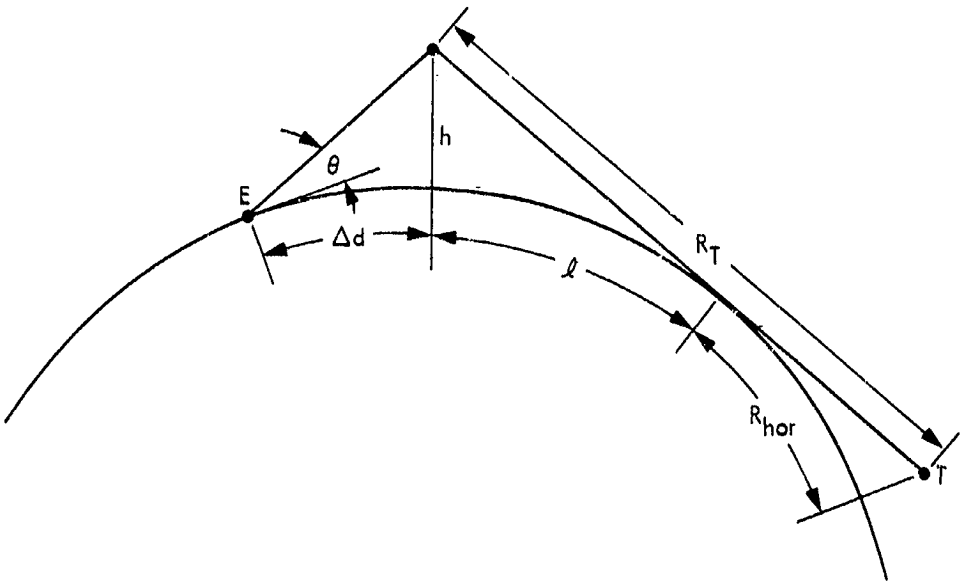

Figure 8.10.- Considering rain scatter involving a transhorizon path from a terrestrial station, T, a grazing ray at the horizon will reach a height of $\ell^2/2kr_0 = (R_T - R_{hor})^2/2kr_0$ at the distance $R_T - R_{hor}$ from where the ray is tangential to the Earth's spherical surface. The elevation angle θ corresponding to the height h as seen from the earth station, E, is $\tan^{-1} h/\Delta d$.

the percentage is 0.01, in the frequency band under consideration, but in Report 382 of 1982, the normalized loss L_2 does not refer specifically to the percentage of 0.01 and no correction factor is included. The equation defining L_2 then becomes

$$[L_2(p)]_{dB} = (P_{T_i})_{dBW} + (\Delta G)_{dB} - [P_{R_i}(p)]_{dBW} \qquad (8.28b)$$

In order to determine a form for L_2 (0.01) in terms of propagation parameters, one can subtract 42 from the 199 of Eq. (8.26) to obtain 157, thus taking account of the assumed gain G_T of the terrestrial antenna of 42 dB. Also one can express -10 log Z as -26 - 14 log R + $(R_T - 40)^2/17{,}000$ but combine the -26 + 157 to obtain a numerical coefficient of 131. The form of L_2 (0.01) as utilized in the 1978 version of Report 382 then becomes, after combining numerical factors and with $\Delta G = 0$,

$$\begin{aligned}[L_2(0.01)]_{dB} &= 131 - 20 \log(R_T)_{km} - 20 \log f_{GHz} \\ &\quad -10 \log C + \gamma_o r_o - 14 \log R + (R_T - 40)^2/17{,}000 \\ &\quad - 10 \log D_{km}\end{aligned} \qquad (8.29)$$

Equation (8.29) can be solved for the rain-scatter distance R_T by an iterative process. The distance R_T, however, is not the same quantity as d_2, the rain-scatter coordination distance, as R_T is measured from the common scattering volume rather than from the earth station. Thus the center of the circle representing the locus of R_T is displaced from the earth station by the distance Δd where

$$\tan \theta = \frac{h}{\Delta d} = \frac{(R_T - 40)^2}{17{,}000\ \Delta d}$$

and

$$\Delta d = \frac{(R_T - 40)^2 \cot \theta}{17{,}000} \qquad (8.30)$$

where θ is the elevation angle of the main beam of the earth station antenna. The basis for the expression for tan θ is shown in Fig. 8.10. The distance Δd is measured from the earth station along the azimuth of the main beam of the earth station. A circle of radius R_T is drawn about the point so reached. The circle is referred to as the rain scatter coordination contour. The rain-scatter coordination distance d_2 is the distance from the earth station to the rain scatter coordination contour on the azimuth under consideration.

We now mention briefly the 1982 versions of Report 569, 724, and 382. In the 1982 form of Report 569, Eq. (8.26) has been modified and for frequencies below 10 GHz takes the form of

$$[L_t(p)]_{dB} = 199 + 20 \log(R_T)_{km} - 20 \log f_{GHz} - 10 \log M - 10 \log C + \gamma_o r_o - 10 \log Z - 10 \log B \quad (8.31)$$

The quantity B is now entirely different from that of B of Eq. (8.26) and is an integral expression that includes the factors D and G_T and also attenuation due to rain outside the common scattering volume (see Appendix 8.3).

Still slightly different expressions are given in Reports 724 and 382 for 1982. The form of Report 724 for frequencies below 10 GHz is

$$[L_t(p)]_{dB} = 168 + 20 \log (R_T)_{km} - 20 \log f_{GHz} - 10 \log C + \gamma_o r_o + \Gamma - 13.2 \log R - 10 \log G_T \quad (8.32)$$

In this equation, a 10 log D form does not appear nor is D accounted for in a complex term like -10 log B of Eq. (8.31). Instead, D in km has been taken to be given by

$$D = 3.5\ R^{-0.08} \quad (8.33)$$

where R is rain rate in mm/h. This variation of D with R introduces an 0.8 log R term which when combined with the -14 log R term (of 10 log Z = 26 + 14 log R) yields -13.2 log R. The coefficient 3.5 of Eq. (8.33) results in a factor of about -5 dB (10 log 3.5 $\simeq$ 5) which when combined with 199 and -26 from 10 log Z gives the numerical coefficient of 168. The quantity Γ represents attenuation outside the common scattering volume.

The corresponding equation in the 1982 version of Report 382 is

$$[L_2]_{dB} = 126 + 20 \log(R_T)_{km} - 20 \log f_{GHz} - 10 \log C + \gamma_o r_o + 10 \log B - 13.2 \log R \qquad (8.34)$$

Here $[L_2]_{dB}$ is a normalized transmission loss, and the numerical coefficient of 126 is 42 dB less than the 168 of Eq. (8.32). Otherwise the same factors are included, as 10 log B in this case is actually the same as Γ of Eq. (8.32).

8.5 INTERFERENCE BETWEEN SPACE STATIONS AND THOSE ON THE EARTH'S SURFACE

Interference between a space station and one on the Earth's surface may take place, for example, when an earth station receives unwanted transmissions from an interfering satellite as well as wanted transmissions from the satellite that serves the earth station. The analysis of Sec. 8.2, presented there as an introduction to the analytical aspects of interference, applies directly to this case, and some additional considerations follow.

Scatter from rain, which was not considered in Sec. 8.2 but may also cause interference can be analyzed by a modification of the approach of Sec. 8.4 with R_T and G_T now taken to refer to the interfering satellite transmitter rather than to a terrestrial transmitter.

Solar power satellites, which would intercept solar energy and transmit energy to the Earth's surface as microwave radiation at a frequency of 2450 MHz according to preliminary plans, present a potential interference problem

for communication satellite systems. According to one analysis (CCIR, 1982d) based upon likely harmonic content, the interfering signal scattered from rain, even at the fourth harmonic, would be comparable with the signal level received in the fixed satellite service.

In the absence of precipitation, the signal on a line-of-sight path from a satellite will be attenuated by the atmospheric gases and perhaps by defocusing but may experience a gain Gp due to multipath and scintillation effects as mentioned in Sec. 8.3.2. The gain due to multipath effects and scintillation may be assumed to be zero for elevation angles above 5° and for percentages of time greater than one percent (CCIR 1982d).

8.6 PROCEDURES FOR INTERFERENCE ANALYSIS

8.6.1 Introduction

Previous sections of this chapter have outlined the theoretical basis for interference analysis, with emphasis on basic concepts. Some empirically derived relations and other details are reproduced in the appendices. In this Sec. 8.6, practical considerations, including procedures for determining coordination distances, are summarized.

The procedures for interference analysis are subject to continuing development and updating, and a number of variations in approach have been illustrated in this chapter. The procedures of Appendix 28 of Radio Regulations (ITU, 1982) carry legal authority, but they may be revised in the future. (Resolution No. 60 of WARC-79 called for a revision in Appendix 28 of Radio Regulations, and the 1982 version of Report 382, utilizing certain data from Reports 724, 563, and 569, has been proposed as a basis for any changes in the Radio Regulations.) The differences in the treatments of the several CCIR reports are in detail and refinement and relate to what losses are taken into account and how to achieve the necessary compromise between a satisfactory degree of precision on one hand and convenience and practicality on the other. A basic problem is that some of the phenomena, such as ducting, must be treated in a largely empirical way and the available data bases are limited.

8.6.2 Off-axis Antenna Gain

For calculating the predicted intensity of a terrestrial interfering signal at an earth station, it is necessary to know the gain of the earth station antenna at the horizon at the azimuth of the terrestrial station (or for determining coordination distance at all azimuthal angles). To determine the gain, one must first find the angle of the horizon from the axis of the main antenna beam at the azimuth of interest. For the case that the horizon is at zero elevation angle, the horizon angle ϕ, measured from the axis of the antenna beam, is found by applying the law of cosines for sides of a spherical triangle, namely

$$\cos\phi = \cos\theta_s \cos(\alpha-\alpha_s) \tag{8.35}$$

where θ_s is the elevation angle of the satellite the earth station is servicing, α_s is the azimuth of the satellite, and α is the azimuthal angle of interest. If the horizon is at an elevation angle θ, the corresponding relation becomes

$$\cos\phi = \cos\theta \cos\theta_s \cos(\alpha - \alpha_s) + \sin\theta \sin\theta_s \tag{8.36}$$

Having determined ϕ, it remains to specify a value for the antenna gain at this angle. If the actual antenna gain is known as a function of ϕ, it should be used. If the gain is not known and the antenna diameter to wavelength ratio D/λ is 100 or greater, the following relation, from CCIR Report 391 (CCIR, 1978d) and 382, and Appendix 28 of Radio Regulations, can be used for angles greater than that of the first side lobe

$$G = 32 - 25 \log\phi \text{ dB} \tag{8.37}$$

If the D/λ ratio is less than 100, the corresponding relation is

$$G = 52 - 10 \log(D/\lambda) - 25 \log\phi \text{ dB} \tag{8.38}$$

The same sources give relations between the maximum gain G_{max} and D/λ, that in Report 382 and Appendix 28 being

$$20 \log D/\lambda = G_{max} - 7.7 \quad dB \tag{8.39}$$

More precisely and completely than stated above, Report 382 and Appendix 28 gives the following set of relations

For $D/\lambda \geq 100$,

$$G(\phi) = G_{max} - 2.5 \times 10^{-3} \left(\frac{D\phi}{\lambda}\right)^2 \qquad 0 < \phi < \phi_m \tag{8.40a}$$

$$G(\phi) = G_1 \qquad \phi_m < \phi < \phi_r \tag{8.40b}$$

$$G(\phi) = 32 - 25 \log \phi \qquad \phi_r < \phi < 48^\circ \tag{8.40c}$$

$$G(\phi) = -10 \qquad 48^\circ < \phi < 180^\circ \tag{8.40d}$$

where

$$\phi_m = \frac{20\lambda}{D} \sqrt{G_{max} - G_1} \quad deg$$

$$\phi_r = 15.85 \left(\frac{D}{\lambda}\right)^{-0.6} \quad deg$$

$$G_1 = 2 + 15 \log D/\lambda = \text{gain of first side lobe} \tag{8.41}$$

For $D/\lambda \leq 100$

$$G(\phi) = G_{max} - 2.5 \times 10^{-3} \left(\frac{D\phi}{\lambda}\right)^2 \qquad 0 < \phi < \phi_m \tag{8.42a}$$

$$G(\phi) = G_1 \qquad \phi_m < \phi < 100\ \lambda/D \tag{8.42b}$$

$$G(\phi) = 52 - 10 \log D/\lambda - 25 \log \phi \qquad \frac{100\lambda}{D} < \phi < 48^\circ \tag{8.42c}$$

$$G(\phi) = 10 - 10 \log D/\lambda \qquad 48^\circ < \phi < 180^\circ \tag{8.42d}$$

For satellite antennas, CCIR Report 558 (1978e) gives the following relations:

$$G(\phi) = G_{max} - 3\left(\frac{\phi}{\phi_o}\right)^2 \qquad \phi_o < \phi < 2.6\phi_o \qquad (8.43a)$$

$$G(\phi) = G_{max} - 20 \qquad 2.6\,\phi_o < \phi < 6.3\phi_o \qquad (8.43b)$$

$$G(\phi) = G_{max} - 25\log\left(\frac{\phi}{\phi_o}\right) \qquad 6.3\phi_o < \phi < \phi_1 \qquad (8.43c)$$

$$G(\phi) = -10 \qquad \phi_1 < \phi \qquad (8.43d)$$

where ϕ_o is one half the 3 dB beamwidth and ϕ_1 is the value ϕ when $G_{max} - 25 \log\left(\frac{\phi}{\phi_o}\right)$ equals -10. In other words, $G(\phi)$ is never assumed to drop below -10.

8.6.3 Procedures for Determining Coordination Distance for Great Circle Propagation

For determining coordination distances d_1 for great circle propagation, it is necessary to first determine the basic transmission loss, L_b, as defined by Eq. (8.11), that can be tolerated for the percentage or percentages of time specified (commonly 0.01 percent and perhaps 20 percent as well). The allowable value of L_b is based primarily on factors other than propagation. For determining the gain of the earth station towards the horizon, which value is needed in Eq. (8.11) in order to find L_b, find the angle ϕ and then the gain G in the ϕ direction by using the procedure of Sec. 8.6.2. The quantity $P_{R_i}(p)$, the maximum permissable interference level for p percent of the time that appears in Eq. (8.11), is defined in Appendix 8.1.

Having decided on a value for L_b, one can solve for distance d of Eq. (8.18) of Report 569 (1982a) or for d from the very similar relation of Report 724 (1982b) or one can solve for d_1 of Eq. (8.20) of Report 382 (1982c) and Appendix 28 of the Radio Regulations. In all three cases, the distances whether d or d_1 originally are to be taken as coordination distance d_1. Equation (8.18) follows more directly from the basic theory than Eq.(8.20) but if

legal requirements are to be met, it is necessary to use the approach given in Radio Regulations. The effect of ducting is accounted for empirically in all cases.

For zones B and C (Sec. 8.3.3), if coordination distances turn out to be greater than the values in Table 8.3, the values in the table should be used instead as the coordination distance.

Table 8.3 Maximum Coordination Distances, Propagation Mode 1.

	Percentages of Time			
Zone	0.001	0.01	0.1	1.0
B	2000 km	1500 km	1200 km	1000 km
C	2000 km	1500 km	1200 km	1000 km

8.6.4 Procedures for Determining Coordination Distance for Rain Scatter

For determining the coordination distance for scatter by rain, one must first find the total transmission loss L_t that can be tolerated for some specified percentage of time, commonly 0.01 percent of the time. This loss is that of the interfering signal that is scattered by rain and is the ratio of the transmitted interfering power to the received interfering power as shown in Eqs. (8.10) and (8.22). In addition, or alternatively, certain approaches including that of Report 382 of the CCIR and Appendix 28 of Radio Regulations for both 1978 and 1982, utilize the normalized transmission loss L_2 which is based upon the assumption that the terrestrial antenna being considered has a gain of 42 dB. The loss L_2 is reduced with respect to L_t by 42 dB for this reason, but its final value may differ from L_t by a different amount. For finding the value of L_t, use the definition of L_t of Eq. (8.10). For finding

L_2, use Eq. (8.28b). In both cases, it is necessary to first determine $P_{R_1}(p)$, and the procedure for doing this, the same procedure as when working with great circle propagation, is given in Appendix 8.1.

When the required loss factor, L_t or L_2, has been found, then one must determine the rainfall rate R in mm/h that applies for the specified percentage of time for the location or climatic region being considered. If appropriate long-term data are available for the location in question, it should be used. Otherwise one must use one of several models which show rain rate exceeded as a function of percentage of time for the various geographical areas of the world.

Several such models are described in Sec. 4.3.3, and values of R, as a function of percentage of time exceeded, are given in Table 4.4 for regions defined for North America in Fig. 4.10 and in slightly more detail for the United States in Fig. 4.9. Also, Table 4.5 gives values of R for regions of Canada defined in Fig. 4.10. An additional geographical model, presented in CCIR Reports 563 (CCIR, 1982e) and 724 (CCIR, 1982b) for 1982 is included in Sec. 9.3.2 which deals with estimation of attenuation due to rain. Data concerning this model are presented in two ways. The regions of the world utilized are shown in Figs. 4.12 - 4.14 and Table 4.6 shows the corresponding rain rates as a function of percentage of time exceeded. In addition, Figs. 9.8 - 9.10 from Report 563 shows contours of fixed values of R that are exceeded for 0.01 percent of the time.

Once the values of L_t and R have been settled on, one can solve for the value of R_T, the distance of the rain scatter region from the terrestrial station, by use of Eqs. (8.26), (8.29), (8.31), (8.32), or (8.34) Equation (8.29) is that utilized also in Appendix 28 of Radio Regulations and must be followed if legal requirements are to be met.

The value of R_T is the radius of a circle centered on the region of rain scatter. The center of this circle is displaced form the earth station by the distance Δd of Eq. (8.30), and d_2, the coordination distance for rain scatter, is the distance from the earth station to the circle at the azimuth under consideration.

If coordination distances for rain scatter turn out to be greater than those shown in Table 8.4, the values of the table should be used instead.

Table 8.4 Maximum Rain Scatter Distances (km).

Percent of time	Latitude (deg) 0-30	30-40	40-50	50-60	60-70
1.0	360	340	290	260	240
0.1	360	340	310	290	260
0.01	370	360	340	310	280
0.001	380	370	360	340	300

8.7 SITING OF EARTH STATIONS

The siting of earth stations in basins or valleys surrounded by hills is highly advantageous for minimizing radio interference. It is recommended in CCIR Report 385 (1978f), however, that the angles of elevation of obstructions should not exceed about 3° in order to ensure maximum satellite availability. Where sufficient natural shielding cannot be found, artificial shielding may be desirable. Rada fences built for suppression of signals at low elevation angles have provided 20 dB of protection (Crane, 1981). Placement of the earth station antenna in a pit is reported in CCIR Report 390 (1978g) to have provided 25 dB of protection in the 4 and 6 GHz fixed satellite bands. Ducting has the potential for producing the highest-level interference fields, but the effect of ducting can be reduced by the measures mentioned. Other siting precautions mentioned in Report 385 include avoiding line-of-sight paths between earth stations and interfering transmitters, avoiding locating the earth station with less than a 5° discrimination angle at the interfering transmitter between the path to the earth station and the main beam of the interfering transmitter antenna, and maintaining a minimum distance of 50 km when shielding of 3° to 4° is available. A distance of only 20 km is said to be sufficient when the shielding has an elevation angle of 10°.

Reflections from aircraft can cause interference, and earth stations should preferably not be located near areas of especially heavy aircraft traffic. In the Federal Republic of Germany, some 19,000 events attributed to aircraft reflections were observed during a period of 10,000 hours on a 1.9 GHz troposcatter link 420 km in length. The average basic transmission loss on this link was about 236 dB but for 0.1, 0.02, and 0.005 percent of the time the losses were 216, 213, and 210 dB respectively. The low levels of loss attributed to aircraft (CCIR, 1982a) show the advisability of considering potential interference due to reflections from aircraft.

Although apparently not mentioned in the literature, reflections from flocks of birds can also cause interference, and the vicinity of major waterfowl refuges or flyways should be avoided if possible. As far as the reflection of electromagnetic waves is concerned, birds act like large blobs of water. They are thus effective scatterers of electromagnetic waves and readily detectable by radar at L band and higher frequencies (near 1.5 GHz and higher) (Eastwood, 1967). Migrating birds commonly fly at altitudes up to about 3.6 km or higher.

Battan, L. J., Radar Observation of the Atmosphere. Chicago: University of Chicago Press, 1973.

CCIR, "The evaluation of propagation factors in interference problems between stations on the surface of the earth at frequencies above about 0.5 GHz," Report 569, Vol. V, Propagation in Non-ionized Media, Recommendations and Reports of the CCIR, 1978. Geneva: Int. Telecomm. Union, 1978a.

CCIR, "Propagation data required for the evaluation of coordination distance in the frequency range 1 to 40 GHz," Report 724, Vol. V. Propagation in Non-ionized Media, Recommendations and Reports of the CCIR, 1978. Geneva: Int. Telecomm. Union, 1978b.

CCIR, "Determination of coordination area," Report 382, Vol. IX, Fixed Service Using Radio-relay Systems. Frequency Sharing and Coordination Between Systems in the Fixed Satellite Service and Radio-relay Systems, Recommendations and Reports of the CCIR, 1978. Geneva: Int. Telecomm. Union, 1978c.

CCIR, "Radiation diagrams of antennae for earth stations in the fixed satellite service for use in interference studies and for the determination of a design objective," Report 391, Vol. IV, Fixed Service Using Communication Satellites, Recommendations and Reports of the CCIR, 1978. Geneva: Int. Telecomm. Union, 1978d.

CCIR, "Satellite antenna patterns in the fixed satellite service," Report 558, Vol. IV, Fixed Service Using Communication Satellites, Recommendations and Reports of the CCIR, 1978. Geneva: Int. Telecomm. Union, 1978e.

CCIR, "Feasibility of frequency sharing between systems in the fixed satellite service and terrestrial radio services. Criteria for the selection of sites for earth-stations in the fixed satellite service," Report 385, Vol. IV, Fixed Service Using Communication Satellites, Recommendations and Reports of the CCIR, 1978. Geneva: Int. Telecomm. Union, 1978f.

CCIR, "Earth station antennae for fixed satellite service." Report 390, Vol. IV, Fixed Service Using Communication Satellites, Recommendations and Reports of the CCIR, 1978. Geneva: Int. Telecomm. Union, 1978g.

CCIR, "The evaluation of propagation factors in interference problems between stations on the surface of the earth at frequencies above about 0.5 GHz,"

Report 569, Vol. V, Propagation in Non-ionized Media, Recommendations and Reports of the CCIR, 1982. Geneva: Int. Telecomm. Union, 1982a.

CCIR, "Propagation data required for the evaluation of coordination distance in the frequency range 1 to 40 GHz," Report 724, Vol. V, Propagation in Non-ionized Media, Recommendations and Reports of the CCIR, 1982. Geneva: Int. Telecomm. Union, 1982b.

CCIR, "Determination of coordination area," Report 382, Vol. IX, Fixed Service Using Radio-relay Systems. Frequency Sharing and Coordination Between Systems in the Fixed Satellite Service and Radio-relay Systems, Recommendations and Reports of the CCIR, 1982. Geneva: Int. Telecomm. Union, 1982c.

CCIR, "Propagation data required for evaluating interference between stations in space and those on the surface of the earth," Report 885 Vol. V, Propagation in Non-ionized Media, Recommendations and Reports of the CCIR, 1982. Geneva: Int. Telecomm. Union, 1982d.

CCIR, "Radiometeorological data," Report 563, Vol. V, Propagation in Non-ionized Media, Recommendations and Reports of the CCIR, 1982. Geneva: Int. Telecomm. Union, 1982e.

Crane, R. K., "A review of transhorizon propagation phenomena," Radio Science, vol. 16, pp. 649-669, Sept.-Oct. 1981.

Dougherty, H. T., A Consolidated Model for UHF/SHF Telecommunication Links Between Earth and Synchronous Satellites, NTIA Report 80-45, U.S. Dept. of Commerce, Aug. 1980.

Dougherty, H. T. and B. A. Hart, "Recent progress in duct propagation predictions," IEEE Trans. on Antennas and Propagation, vol. AP-27, pp. 542-548, July 1979.

Eastwood, E., Radar Ornithology. London: Methuen, 1967.

ITU (International Telecommunications Union), Appendix 28, Method for the Determination of the Coordination Area Around an Earth Station in Frequency Bands Between 1 GHz and 40 GHz, Radio Regulations, Edition of 1982. Geneva: Int. Telecomm. Union, 1982.

APPENDIX 8.1

PERMISSIBLE LEVEL OF INTERFERING EMISSION

Information on the permissible level of interfering emission that is included in Appendix 28 of Radio Regulations (ITU, 1982) is reproduced below. Reference is made in the following material to two tables containing detailed listing of parameters for the various frequency bands. These tables are not included here, but notes 1 through 4 discuss the parameters and provide information about their magnitudes.

2.3 *Derivation and tabulation of interference parameters*

2.3.1 *Permissible level of the interfering emission*

The permissible level of the interfering emission (dBW) in the reference bandwidth, to be exceeded for no more than p% of the time at the output of the receiving antenna of a station subject to interference, from each source of interference, is given by the general formula below:

$$P_r(p) = 10 \log (kT_eB) + J + M(p) - W \quad (3)$$

where:

$$M(p) \cong M(p_0/n) = M_0(p_0) \quad (4)$$

with:

k: Boltzmann's constant (1.38×10^{-23} J/K);

T_e: thermal noise temperature of the receiving system (K), at the output of the receiving antenna (see *Note 1*);

B: reference bandwidth (Hz) (bandwidth of the interfered-with system over which the power of the interfering emission can be averaged);

J: ratio (dB) of the permissible long term (20% of the time) interfering emission power to the thermal noise power of the receiving system, referred to the output terminals of the receiving antenna (see *Note 2*);

p_0: percentage of the time during which the interference from all sources may exceed the permissible value;

n: number of expected entries of interference, assumed to be uncorrelated;

p: percentage of the time during which the interference from one source may exceed the permissible value; since the entries of interference are not likely to occur simultaneously: $p = p_0/n$;

$M_0(p_0)$: ratio (dB) between the permissible powers of the interfering emission, during p_0% and 20% of the time, respectively, for all entries of interference (see *Note 3*);

$M(p)$: ratio (dB) between the permissible powers of the interfering emission during p% of the time for one entry of interference, and during 20% of the time for all entries of interference;

W: equivalence factor (dB) relating interference from interfering emissions to that caused by the introduction of additional thermal noise of equal power in the reference bandwidth. It is positive when the interfering emissions would cause more degradation than thermal noise (see *Note 4*).

Tables I and II list values for the above parameters.

In certain cases, an administration may have reason to believe that, for its specific earth station, a departure from the values associated with the earth station, as listed in Table II, may be justified. Attention is drawn to the fact that for specific systems the bandwidths B or, as for instance in the case of demand assignment systems, the percentages of the time p and p_0 may have to be changed from the values given in Table II. For further information see § 2.3.2.

Note 1: The noise temperature, in kelvins, of the receiving system, referred to the output terminals of the receiving antenna, may be determined from:

$$T_r = T_a + (e - 1)\,290 + eT_r \qquad (5a)$$

where:

T_a: noise temperature (K) contributed by the receiving antenna;

e: numerical loss in the transmission line (e.g. a waveguide) between antenna and receiver front end;

T_r: noise temperature (K) of the receiver front end, including all successive stages, referred to the front end input.

For radio-relay receivers and where the waveguide loss of a receiving earth station is not known, a value of $e = 1.0$ is to be used.

Note 2: The factor J (dB) is defined as the ratio of total permissible long term (20% of the time) power of interfering emissions in the system, to the long term thermal radio frequency noise power in a single receiver. In the computation of this factor, the interfering emission is considered to have a flat power spectral density, its actual spectrum shape being taken into account by the factor W (see below). For example, in a 50-hop terrestrial hypothetical reference circuit, the total allowable additive interference power is 1 000 pW0p (CCIR Recommendation 357-3) and the mean thermal noise power in a single hop may be assumed to be 25 pW0p. Therefore, since in a frequency-division multiplex/frequency modulation (FDM/FM) system the ratio of a flat interfering noise power to the thermal noise power in the same reference band is the same before and after demodulation, J is given by the ratio 1 000/25 expressed in dB, i.e. $J = 16$ dB. In a fixed-satellite service system, the total allowable interference power is also 1 000 pW0p (CCIR Recommendation 356-4), but the thermal noise contribution of the downlink is not likely to exceed 7 000 pW0p, hence $J \geq -8.5$ dB.

In digital systems interference is measured and prescribed in terms of the bit error rate or its permissible increase. While the bit error rate increase is additive in a reference circuit comprising tandem links, the radio frequency power of interfering emissions giving rise to such bit error rate increase is not additive, because bit error rate is not a linear function of the level of the radio frequency power of interfering emissions. Thus, it may be necessary to protect each receiver individually. For digital radio-relay systems operating above 10 GHz, and for all digital satellite systems, the long term interference power may be of the same order of magnitude as the long term thermal noise, hence $J = 0$ dB. For digital radio-relay systems operating below 10 GHz, long term interference power should not decrease the receiver fade margin by more than 1 dB. Thus the long term interference power should be about 6 dB below the thermal noise power and hence $J = -6$ dB.

Note 3: $M_0(p_0)$ (dB) is the "interference margin" between the short term (p_0%) and the long term (20%) allowable powers of an interfering emission.

For analogue radio-relay and fixed-satellite systems in bands between 1 GHz and 15 GHz, this is equal to the ratio (dB) between 50 000 and 1 000 pW0p (17 dB).

In the case of digital systems, system performance at frequencies above 10 GHz can, in most areas of the world, usefully be defined as the percentage of the time p_0 for which the wanted signal is allowed to drop below its operating threshold, defined by a given bit error rate. During non-faded operation of the system, the desired signal will exceed its threshold level by some margin M_s which depends on the rain climate in which the station operates. The greater this margin, the greater the enhancement of the interfering emission which would

degrade the system to threshold performance. As a first order estimate it may be assumed that, for small percentages of the time (of the order of 0.001% to 0.003%), the level of interfering emissions may be allowed to equal the thermal noise which exists at the demodulator input during faded conditions. Thus, M_0 in Tables I and II may, for digital systems operating above 10 GHz, be assumed to be equal to the fade margin M_f of the system. For digital radio-relay systems operating below 10 GHz it is assumed that the short term power of an interfering emission can be allowed to exceed the long term power of the interfering emission by an amount equal to the fade margin of the system minus J, i.e. 41 dB, where $J = -6$ dB.

Note 4: The factor W (dB) is the ratio of radio frequency thermal noise power to the power of an interfering emission in the reference bandwidth when both produce the same interference after demodulation (e.g. in a FDM/FM system it would be expressed for equal voice channel performance; in a digital system it would be expressed for equal bit error probabilities). For FM signals, it is defined as follows:

$$W = 10 \log \left\{ \frac{\text{Thermal noise power at the output of the receiving antenna in the reference bandwidth}}{\text{Power of the interfering emission at the radio frequency in the reference bandwidth, at the output of the receiving antenna}} \times \frac{\text{Interference power in the receiving system after demodulation}}{\text{Thermal noise power in the receiving system after demodulation}} \right\} \quad (5b)$$

The factor W depends on the characteristics of the wanted and the interfering signals. To avoid the need for considering a wide range of characteristics, upper limit values were determined for the factor W. When the wanted signal uses frequency modulation with r.m.s. modulation indices which are greater than unity, W is not higher than 4 dB. In such cases, a conservative figure of 4 dB will be used for the factor W in (3), regardless of the characteristics of the interfering signal. For low-index FDM/FM systems a very small reference bandwidth (4 kHz) implies values of W not greater than 0 dB. In such case., a conservative figure of 0 dB will be used for W in (3), regardless of the characteristics of the interfering signal.

When the wanted signal is digital, W is usually equal to or less than 0 dB, regardless of the characteristics of the interfering signal.

APPENDIX 8.2

EXPRESSIONS FOR ATTENUATION CONSTANTS

1. a(p), b(p), and g(f) of $\gamma_D = a(p)+b(p)g(f)$ [Eq. (8.18), Sec. 8.3.3, from Report 724].

The quantity γ_D is a duct attenuation constant, describing the attenuation of a signal propagating beyond the horizon in a surface duct (dB/km). The quality p stands for percentage of occurrence, and f is frequency if GHz.

	a(p)	b(p)	g(f)
Zone A	$0.052 + 0.020 (\log p + 3)^{1.3}$	$0.080 + 0.013 (\log p + 3)^{1/3}$	$\log f - 0.07 (\log f)^5 + 0.002 (\log f)^{10}$
Zone B	$0.013 + 0.009 (\log P + 3)^{1.5}$	$0.026 + 0.011 (\log P + 3)^{1.5}$	$\log f-0.4 (\log f-0.5)^3 + 0.001 (\log f)^{10}$
Zone C	$0.013 + 0.009 (\log p + 3)^{1.1}$	$0.026 + 0.011 (\log p + 3)^{1.3}$	$\log f-0.4 (\log f-0.5)^3 + 0.001 (\log f)^{10}$

2. β_z of Eq. (8.20), Sec. 8.3.3, from Report 382 (dB/km).

Zone A $\beta_{ZA} = 0.05 + (0.12 + 0.15 \log f)p^{0.12}$

Zone B $\beta_{ZB} = (0.03 + 0.09 \log (f+1))\ p^{0.18}$

Zone C $\beta_{ZC} = (0.03 + 0.08 \log (f+1))\ p^{0.17}$

APPENDIX 8.3

TERMS OF EQ. (8.26) OF REPORT 569, 1978 AND EQ. OF REPORT 569, 1982

The expression for 10 log C, representing the attenuation due to rain within the common scattering volume is given below. This term is the same in the 1978 and 1982 versions of Report 569.

$$10 \log C = \left(\frac{1 - \cos \alpha_T}{2}\right) \quad 10 \log \left[\frac{2.17}{\lambda_R d_a}\left(1 - 10^{-\gamma_R d_a/5}\right)\right] - \lambda_R d_a \left(\frac{1 + \cos \alpha_T}{2}\right) \text{dB}$$

$\gamma_R = kR^{\alpha}$, the rain attenuation coefficient in the rain cell (dB/km); (see Report 721);

d_a = the earth station main beam section lying in the rain cell below the 0° C isotherm (km);

α_T is the azimuth of the terrestrial station relative to the earth station beam azimuth, measured at the scatter volume (α_T = 0°: forward scatter; α_T = 180° : back scatter);

The quantity B of Eq. (8.26) is a terrain blocking factor which may have a value of about 3 dB under some circumstances. For best accuracy in determination of B, it should be determined on the basis of the geometry in question. In the 1982 version of Eq. (8.26), the terrain blocking factor B is omitted, and a term 10 log B refers to an entirely different phenomenon. In the 1982 report, 10 log B accounts for attenuation outside the common scattering volume and has the form of

$$10 \log B = 10 \log \left[10^{-\Gamma_1/10} \int_{D_o}^{D_a} g_T dx + 10^{-\Gamma_2/10} \int_{D_a}^{D} g_T \, 10^{-0.65(h-H_R)} dx\right] \text{dB}$$

g_T is the numerical antenna gain component of the terrestrial station in the direction of an integration element dx along the earth station main beam from D_0 to D:

H_R is the rain ice-crystal transition height (km) (see §4.3 of Report 563-1) and above the height H_R in the reflectivity is assumed to decrease by 6.5 dB per km of additional height.

The quantities Γ_1 and Γ_2 are attenuation coefficients derived on the basis of the Crane path profile model (Sec. 4.3.2, No. 8). This approach is also utilized in Report 882, "Scattering by precipitation,: CCIR, Vol. V, Propagation in Non-ionized Media, 1982. In the expression for 10 log B, D_0 is the distance from the earth station to the intersection of the earth station main beam axis with the horizon ray from the terrestrial station, and D_a is the distance from the earth station along the beam to the 0°C isotherm at height H_R. D is the distance from the earth station to the edge of the rain cell. The 1982 version of Report 569 provides further information about Γ_1 and Γ_2 and points out that when the gain g_T does not vary much along the path from D_0 to D. or D_a to D, it may be taken outside the integral sign.

CHAPTER 9
ESTIMATION OF PROPAGATION IMPAIRMENTS

9.1 INTRODUCTION

Background material on the various propagation effects on satellite communications has been presented in previous chapters, and in this chapter attention is devoted to consideration of the magnitudes of the effects for use in system design. The phenomena are treated in essentially the same order as in Chaps. 1-8. Thus ionospheric effects are considered first. Table 9.1 (same as Table 2.2) provides a summary of ionospheric effects (not including ionospheric scintillation).

9.2 IONOSPHERIC EFFECTS

9.2.1 Faraday Rotation: Determination of Longitudinal Component of Magnetic Field

Many satellite communications systems employ circularly polarized waves and therefore need not be concerned with Faraday rotation. Some satellites transmit linearly polarized waves which are subject to Faraday rotation, however, and attention is given here to its estimation. One reason for using linearly polarized transmission may be to obtain information about ionospheric total electron content (TEC) which contributes to excess range delay and other effects in addition to Faraday rotation. At high frequencies, Faraday rotation along a path is given in SI units by

$$\Phi = \frac{2.36 \times 10^4}{f^2} \int NB \cos\theta_B \, d\ell \qquad \text{rad} \qquad (9.1)$$

where Φ is the Faraday rotation angle in radians, f is frequency in Hz, N is electron density in el/m^3, B is the magnetic flux density of the Earth's field, and θ_B is the angle between the path and the B vector. The SI unit for B is the tesla (T), also commonly referred to as Webers/m^2 (Wb/m^2). Evaluation of the integral involves the values of N, B, and cos θ_B along the path, but for some situations, for both geostationary and orbiting earth

satellites, it is sufficiently accurate to replace B cos θ_B by an average or effective value B_L and take it outside the integral. Then the relation has the form of

$$\phi = \frac{2.36 \times 10^4 \, \overline{B}_L}{f^2} \int N \, d\ell$$

$$= \frac{2.36 \times 10^4 \, \overline{B}_L}{f^2} (TEC) \qquad \text{rad} \qquad (9.2)$$

where

$$B_L = \frac{\int NB \cos \theta_B \, d\ell}{\int N \, d\ell} \qquad \text{T or Wb/m}^2 \qquad (9.3)$$

Table 9.1 Estimated Maximum Ionospheric Effects in the United States for Elevation Angles of About 30 Degrees and One-way Paths [derived from Table VI, Report 263-4 (CCIR, 1978), first appeared in Smith, E. K. and E. Reinhart, JPL Publication 77-71, October 31, 1977].

Effect	Frequency Dependence	100 MHz	300 MHz	1GHz	3 GHz	10 GHz
Faraday Rotation	$1/f^2$	30 rot.	3.3 rot.	108°	12°	1.1°
Propagation delay	$1/f^2$	25 μs	2.8 μs	0.25 μs	0.028 μs	0.0025 μs
Refraction	$1/f^2$	$\leq 1°$	$\leq 7'$	$\leq 0.6'$	$\leq 4.2"$	$\leq 0.36"$
Variation in the direction of arrival	$1/f^2$	20 min of arc	2.2 min of arc	12 sec of arc	1.32 sec of arc	0.12 sec of arc
Absorption (auroral and polar cap)	$1/f^x$ $1 < x \leq 2$	5 dB	1.1 dB	0.2 dB	0.04 dB	0.008 dB
Absorption (mid latitude)	$1/f^2$	<1 dB	0.1 dB	<0.01 dB	0.001 dB	$<10^{-4}$ dB
Dispersion	$1/f^3$ ps/Hz	0.4 ps/Hz	0.015 ps/Hz	0.0004 ps/Hz	1.5×10^{-5} ps/Hz	4×10^{-7} ps/Hz

A variation of this procedure has been employed by Davies who uses

$$\phi = \frac{8.447 \times 10^{-7}}{f^2} \int f_L \, N \, d\ell \qquad \text{rad}$$

$$= \frac{8.447 \times 10^{-7}}{f^2} \, F \, (\text{TEC}) \qquad \text{rad} \qquad (9.4)$$

with F defined by

$$\bar{F} = \frac{\int N f_H \cos \theta_B d\ell}{\int N \, d\ell} \qquad (9.5)$$

As the electron gyrofrequency f_H in Hz equals 2.8×10^{10} B and $(2.8 \times 10^{10}) \times (8.44 \times 10^{-7}) = 2.36 \times 10^4$, the two variations are seen to be compatible. The values of TEC obtained by use of Eqs. (9.2) and (9.4) are values for slant paths. If it is desired to determine TEC values for equivalent vertical paths, one may use

$$\phi = \frac{2.36 \times 10^4}{f^2} \, M \, (\text{TEC}) \qquad \text{rad} \qquad (9.6)$$

with

$$\bar{M} = \frac{\int N \, B \cos \theta_B \sec \chi \, dh}{\int N \, dh} \qquad (9.7)$$

where χ is the zenith angle and dh represents an element of length in the vertical direction (Titheridge, 1972). Davies (1980) has pointed out that the use of an effective vertical content is advantageous when comparing contents over different paths but may be somewhat misleading because there may be no existing vertical path that has the inferred vertical content.

Equations (9.3), (9.5), and (9.7) show what the values of $\bar{B}_L$, $\bar{F}$, and $\bar{M}$ represent but in practice it is generally considered that for $\bar{B}_L$, for example, the value at a height of 400 km, or at a height near 400 km such as 420 km, represents a sufficiently good approximation to what would be obtained by evaluation of the integral expression.

The approach to be used to estimate Faraday rotation depends on the degree of accuracy required. If only a very rough estimate is needed for paths between an earth station and a geostationary satellite in the conterminous United States one may refer to Table 9.1 or Fig. 9.1 if an

estimate of TEC is available. If somewhat greater accuracy is needed, it may be advisable to determine a value for $\bar{B}_L$ for the path and to then use Eq. (9.2) for calculating Faraday rotation as a function of TEC. In determining $\bar{B}_L$, one has a choice of using a simple dipole model of the Earth's field or more sophisticated models. The dipole model is useful for preliminary estimates or when funding, facilities, and location do not justify the use of more accurate models. The need for a more accurate model than the dipole model tends to be greater at low geomagnetic latitudes than at the higher latitudes of the conterminous United States. It should be recognized in any case that Faraday rotation is proportional to ionospheric TEC, which is highly variable, and high accuracy in determining $\bar{B}_L$ may not be justifiable. Also the use of a fixed value of $\bar{B}_L$ introduces errors and if the highest precision is desired one should theoretically evaluate Faraday rotation by using the integral formulation or by use of a summation obtained by separating the ionosphere into layers of known or assumed values of N, B, and cos θ_B.

The view is taken here that it is useful in some cases to employ a value for $\bar{B}_L$ obtained by using a dipole model for the Earth's field, and a procedure for doing so is presented as Appendix 9.1. If one wishes to be assured of greater accuracy than about 25 percent for determining $\bar{B}_L$, one can make use of the Environmental Data and Information Service (EDIS) of NOAA, Boulder, Colorado. They can supply values of the Earth's magnetic field and its components by using one or more of several mathematical models. Alternatively they will also supply program decks for carrying out the needed calculations. A leaflet describing their services is available (Environmental Data and Information Service, 1981). Also use can be made of the spherical harmonic coefficients of the International Geomagnetic Reference Field (Peddie, 1982) and a computer algorithm for synthesizing the geomagnetic field such as that by Malin and Barraclough (1981). A special issue of the Journal of Geomagnetism and Geoelectricity (vol. 34, no. 6, 1982) will be devoted to the International Geomagnetic Reference Field. The following Example 9.1 illustrates the calculation of $\bar{B}_L$, using a dipole model of the Earth's field. The example utilizes the procedure described in Appendix 9.1.

Example 9.1 Determination of $\bar{B}_L$

Considering an earth station at Fairbanks, Alaska (65°N, 148°W) and a geostationary satellite at 148°W (on the same geographic meridian), this example illustrates how to find a value for $\bar{B}_L$ for evaluating Faraday rotation, using the dipole model of the Earth's magnetic field. In the example the geographic coordinates of the intersection of the dipole axis and the Earth's surface in the northern hemisphere are taken as 78.3°N and 69°W, the values used by Davies (1965). Recent values given by Dawson and Newitt (1982) are 78.8°N and 70.9°W.

From Eqs. (A9.14) and (A9.15) with $\theta'_g = 65°$, $\theta'_p = 78.3°$, and $\phi_g - \phi_p = 148° - 69° = 79°$,

$\theta'_m = 64.667°$N (geomagnetic latitude of Fairbanks)

$\phi_m = 75.822°$W (geomagnetic longitude of Fairbanks)

By a graphical construction, it is found that the path to the satellite intersects the 400 km height of the ionosphere at about 55°. The coordinates of this point, found by using Eqs. (A9.14) and (A9.15) again, now with $\theta'_g = 55°$, are

$\theta'_m = 55.519°$N

$\phi_m = 84.014°$W

From Eqs. (A9.5) and (A9.6), using B_0 as 0.31 G (10,000 G = 1 Wb/m^2) and $a/r = 6378/(6378 + 400)$,

$H = 0.146$ G

$Z = 0.425$ G

$F = 0.449$ G

and $\mathbf{F} = \mathbf{a}_r\, 0.425 + \mathbf{a}_\theta\, 0.146$

Converting to rectangular coordinates by using Eqs. (A9.17) and (A9.18),

$$\mathbf{F} = 0.0376\mathbf{a}_x + 0.359\,\mathbf{a}_y + 0.268\,\mathbf{a}_z.$$

Next one needs to determine $\mathbf{d} = \mathbf{S} - \mathbf{G}$, where $\mathbf{S}$ is the geostationary satellite position and $\mathbf{G}$ is the earth-station position. For $\mathbf{S}$, $\theta'_m = 2.302°$ and $\phi_m = 79.24°$ from Eqs. (A9.14) and (A9.15) with $\theta'_g = 0°$. Measuring distances in earth radii with the satellite at 6.6 earth radii and expressing in rectangular coordinates by use of Eqs. (A9.19-A9.21).

$$\mathbf{S} = \mathbf{a}_x\, 1.231 + \mathbf{a}_y\, 6.479 + \mathbf{a}_z\, 0.2651.$$

For G, $\theta'_m = 64.667°$ and $\phi_m = 75.822°$ and with **G** at a distance of 1 earth radius from the center of the Earth

$$\mathbf{G} = \mathbf{a}_x\ 0.107 + \mathbf{a}_y\ 0.415 + \mathbf{a}_z\ 0.904$$

Thus for $\mathbf{d} = \mathbf{S} - \mathbf{G}$ the result is that

$$\mathbf{d} = \mathbf{a}_x\ 1.12 + \mathbf{a}_y\ 6.06 - \mathbf{a}_z\ 0.639.$$

Then using $\mathbf{F}\cdot\mathbf{d} = Fd \cos \theta_B$

$$2.048 = 2.784 \cos \theta_B$$

$$\cos \theta_B = 0.736$$

$$\theta_B = 42.6°$$

and $\bar{B}_L = F \cos \theta_B = (0.449)(0.736) = 0.330\ G = 3.30 \times 10^{-5}\ Wb/m^2$

If the earth station and satellite are not on the same longitude, one can use the angle Z of Eq. (1.16) in place of C' in a graphical construction to find the smaller angle Z' for the intersection of the earth-space path with the 400 km level in the ionosphere. Then in a figure like those of Fig. 1.2, Z' can be shown as lying along the same path as Z but shorter in length. Values for θ' and ϕ' for the 400 km intersection can be obtained from those for Z' and α by using relations for right spherical triangles (ITT, 1968 of Chap. 1) namely

$$\sin \phi' = \sin Z' \sin \alpha$$

$$\sin \theta' = \tan \phi' \cot \alpha$$

where α is the azimuth angle calculated by use of Eq. (1.17) and shown in Fig. 1.2.

9.2.2 Propagation Effects Directly Dependent on TEC

The total electron content (TEC) along a path is the number of electrons in a column one square meter in cross-section (el/m^2) that coincides in position with the path. The TEC of the ionosphere has a pronounced diurnal variation as illustrated in Fig. 2.6 and also varies with solar activity, especially with geomagnetic storms which may result from solar activity. Faraday rotation, excess time delay and associated range delay, phase advance, and time-delay and phase-advance dispersion are directly proportional to TEC. Most ionospheric effects in fact tend to be more severe for high values of TEC than for low values. Note that whereas much emphasis in this handbook is on effects on the loss factor L and the system noise temperature T_{sys}, both introduced in Chap. 1, in this subsection consideration is given to additional parameters, including excess time and range delay, which are important to navigation and ranging systems.

9.2.2.1 Faraday Rotation

The Faraday rotation angle is proportional to TEC as indicated by Eq. (9.2) which is repeated below

$$\phi = \frac{2.36 \times 10^4}{f^2} \bar{B}_L (TEC) \quad \text{rad} \qquad (9.2)$$

The theory of Faraday rotation was developed in Sec. 2.2, and Eq. (9.2) was further justified in Sec. 9.2.1 which was devoted primarily to consideration of $\bar{B}_L$, the longitudinal component of the Earth's magnetic field.

For systems using linear polarization, uncompensated Faraday rotation can cause a polarization mismatch loss $20 \log \delta$ where $\delta = \cos \theta_i$ and θ_i is the polarization mismatch angle. This angle may equal the Faraday rotation angle Φ but may also be less than ϕ (if a certain value of Φ was anticipated and compensated for but the actual value of ϕ encountered was different). In addition to the diurnal variations of Faraday rotation and the variations with the solar cycle, rapid variations, having periods of fractions of a minute, are also sometimes observed. At Ascension Island at the equatorial anomaly crest, rapid variations of about 90° at 136 MHz were observed at the same time that intense scintillation was recorded on 1.54 GHz MARISAT transmissions (Lee et al, 1982). Although Faraday rotation can sometimes be troublesome or at least must be taken into account to ensure satisfactory system performance, it can be a valuable tool for determining ionospheric TEC which causes excess time delay that is important for radionavigation and positioning satellite systems. Representative values of Faraday rotation are shown in Fig. 9.1 as a function of frequency and TEC.

9.2.2.2 Excess Time and Range Delay

The excess time delay Δt due to the TEC along a path is given by

$$\Delta t = \frac{40.3\ (TEC)}{cf^2} = \frac{1.34 \times 10^{-7} (TEC)}{f^2} \quad \text{s} \qquad (9.8)$$

and the excess range delay ΔR due to the TEC is specified by

$$\Delta R = \frac{40.3}{f^2} (TEC) \quad \text{m} \qquad (9.9)$$

In Eqs. (9.8) and (9.9), f is frequency in Hz and TEC is total electron content in el/m^2. It is evident that determination of Δt and ΔR requires information concerning TEC.

Figure 9.2 shows time and range delay as a function of frequency for a one-way path for TEC values of 10^{-17} and 10^{-18} el/m^2. Sometimes a known or estimated value of TEC is available for a vertical path and it is desired to estimate delay for a path as a function of elevation angle. Figure 9.3 shows the excess range delay or error as a function of elevation angle for a TEC of 10^{18} el/m^2 on a vertical path for frequencies of 100 MHz, 400 MHz, and 1200 MHz (Millman, 1980).

9.2.2.3 Phase Advance

The phase advance $\Delta\phi$ of an electromagnetic wave with respect to the value of phase for propagation through a vacuum is also directly proportional to TEC as expressed by

$$\Delta\phi = \frac{8.44 \times 10^{-7}}{f} (TEC) \qquad \text{rad} \qquad (9.10)$$

The change in phase associated with a change in TEC is often of interest. For example, one may wish to relate the change in phase due to a traveling ionospheric disturbance (TID) to the change in TEC. Using $\delta\phi$ for the change in phase associated with an increment $\Delta(TEC)$ in TEC,

$$\delta\phi = \frac{8.44 \times 10^{-7}}{f} \Delta(TEC) \qquad \text{rad} \qquad (9.11)$$

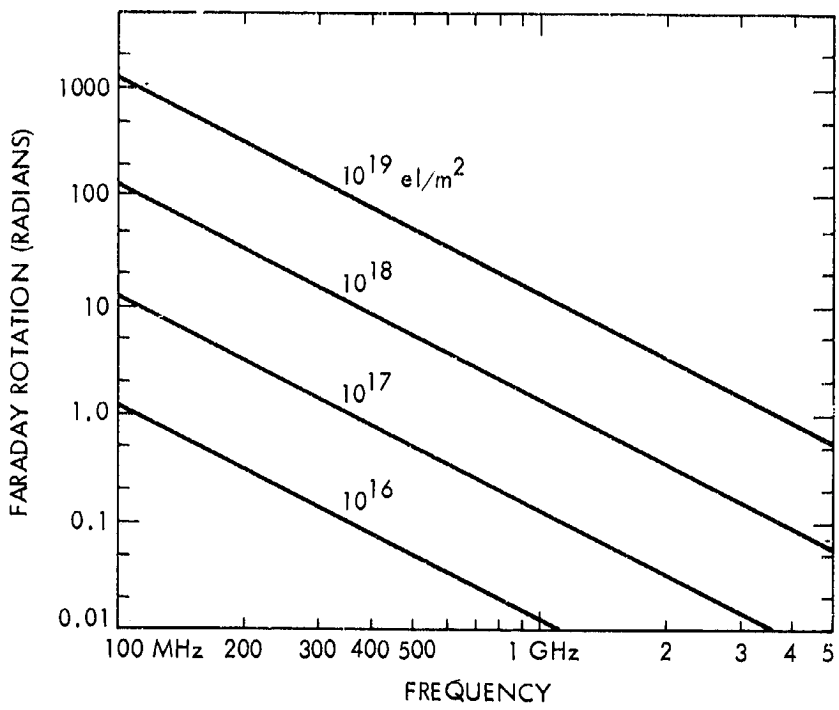

Figure 9.1. Faraday rotation as a function of ionospheric TEC and frequency (after Klobuchar, 1978).

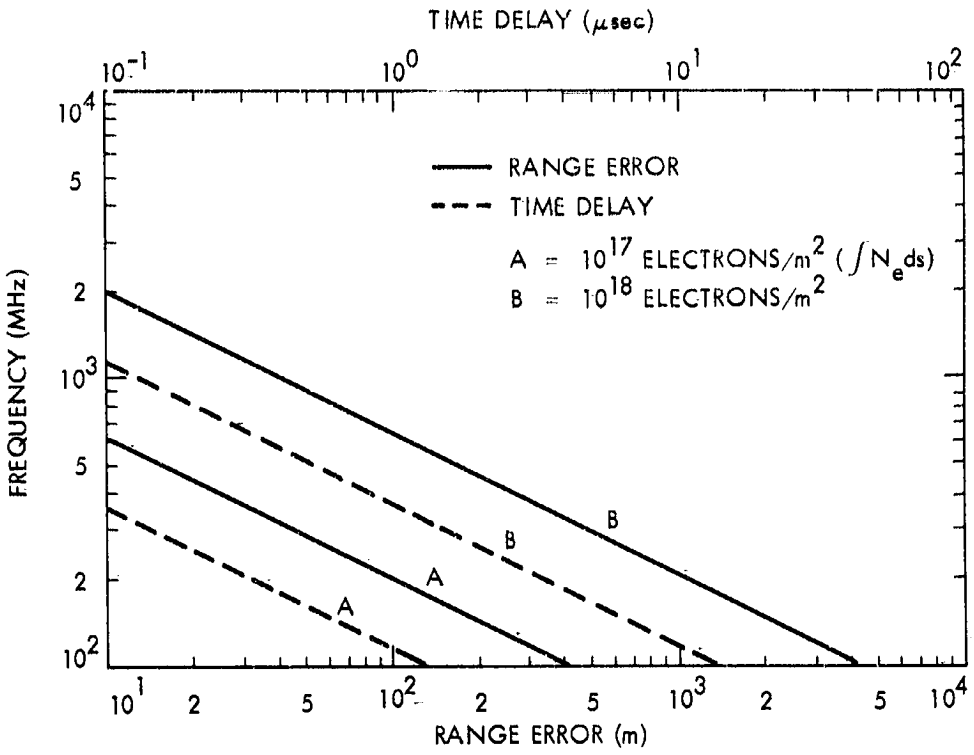

Figure 9.2. Ionosphere range error and time delay for a one-way path (Millman, 1980).

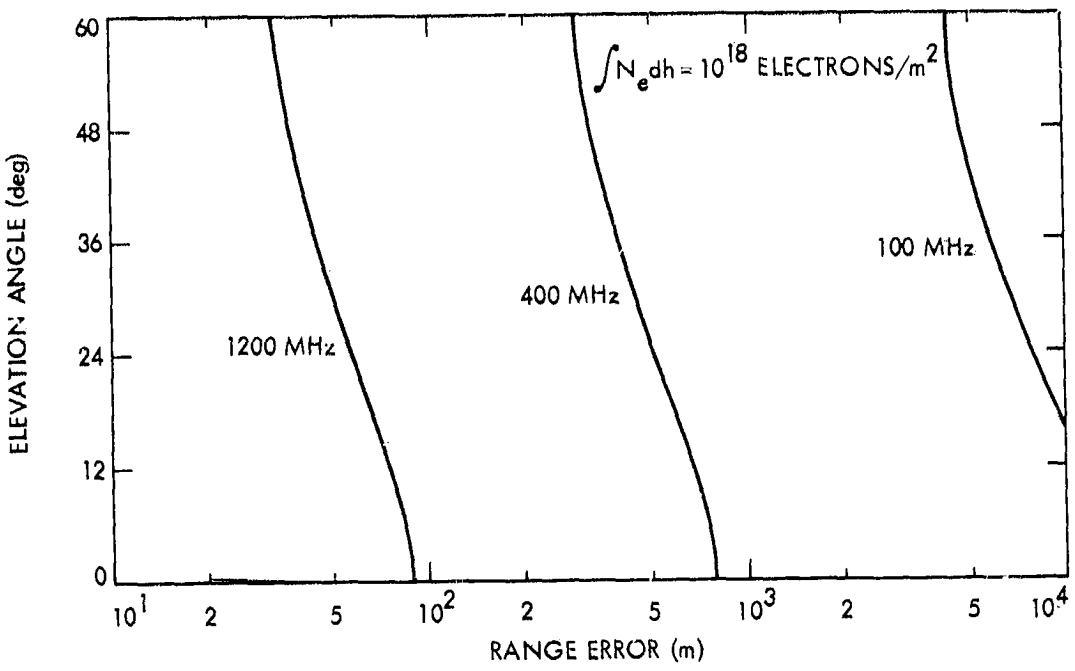

Figure 9.3. Ionospheric range error as a function of elevation angle (Millman, 1980).

9.2.2.4 Doppler Frequency

Frequency f and phase ϕ are related by $f = (1/2\pi)(d\phi/dt)$, and the Doppler shift in frequency f_D associated with a change in phase due to a TEC that is varying with time is given by

$$f_D = \frac{1.34 \times 10^{-7}}{f} \frac{d(TEC)}{dt} \quad \text{Hz} \qquad (9.12)$$

The average Doppler frequency during a time interval or count time T_c in which the TEC changes by Δ(TEC) is given by

$$f_D = \frac{1.34 \times 10^{-7}}{f} \frac{\Delta(TEC)}{T_c} \quad \text{Hz} \qquad (9.13)$$

9.2.2.5 Dispersion

The rate of change of time delay with frequency, or the time-delay dispersion, is

$$\frac{dt}{df} = -\frac{2.68 \times 10^{-7}}{f^3} (TEC) \quad \text{s/Hz} \qquad (9.14)$$

Applied to a pulse of length τ for which the associated bandwidth $\Delta f = 1/\tau$, the difference in time delay Δt between the two extreme frequencies of the pulse is given by

$$\Delta t = -\frac{2.68 \times 10^{-7}}{f^3} \Delta f \, (TEC) \quad \text{s} \qquad (9.15)$$

The effect of dispersion on a pulse propagating through the ionosphere is to decrease the amplitude, increase the length, and introduce frequency modulation (Millman, 1980). Whether the effects are significant or not depends on the values of f, Δf, and TEC.

9.2.2.6 Refractive Bending

It develops that the refractive bending or change in direction of a ray traversing the ionosphere is proportional to the TEC also. The expression given by Millman and Reinsmith (1974) for the elevation angle error $\Delta\theta$ for a

satellite for which the range R is considerably larger than $r_0 \sin \theta_0$, where r_0 is earth radius and θ_0 is elevation angle, is

$$\Delta\theta = \frac{\cos \theta_0}{2h_1} \Delta R \quad \text{rad} \tag{9.16}$$

The quantity h_1 is the height where the median electron content occurs and is generally between 300 and 450 km. As ΔR is the range error along the path and is proportional to TEC, $\Delta\theta$ is also proportional to TEC.

As irregularities in electron density such as TID's move across the line of sight and cause variations in TEC, the same variations are reflected in ΔR and $\Delta\theta$ and variations in direction of arrival thus occur.

9.2.2.7 Prediction and Measurement of TEC

TEC along a path is highly variable and difficult to predict accurately, but advance estimates or predictions of TEC may be needed for system planning and in system operations. Techniques are available for measuring TEC and these will be mentioned shortly, but their expense may preclude their use.

For some purposes it may be sufficient to estimate the maximum Faraday rotation or excess range delay that could be encountered. To obtain this estimate one may assume a maximum TEC of 10^{18} el/m^2 for a zenith one-way path (CCIR, 1978a). At night the value of TEC may drop to about 1/8th of the maximum value. Figure 9.3 illustrates how effects proportional to TEC will tend to vary as a function of elevation angle θ in the range from 0° to 60°. When the value of TEC is given without qualification it normally refers to the zenith value, but the content along a slant path is often what is wanted. This value is commonly assumed to be the zenith value multiplied by the secant of the zenith angle χ at an ionospheric height h somewhat above that of the F layer maximum, thus taking into account the preponderence of ionization on the topside of the layer. A relation giving the zenith angle χ in terms of the elevation angle θ of the path at the surface is

$$\chi = \sin^{-1}\left[\frac{r_0}{r_0 + h} \cos \theta\right] \tag{9.17}$$

where r_0 is the Earth's radius and h is ionospheric height, commonly 300 to 400 km (CCIR, 1978b). For example if $\phi = 30°$ and h = 350 km

$$\chi = \sin^{-1}\left[\frac{350}{6370 + 350}\,0.866\right] = 55.175^{0}$$

Then sec $\chi = 1.75$ and the TEC for the slant path equals about 1.75 times the value for a zenith path.

The problem of predicting time delay due to TEC was considered carefully by Klobuchar and the working group of which he was the leader (Klobuchar and Working Group, 1979) at the Solar-Terrestrial Predictions Workshop Program in Boulder in 1979. It was concluded that monthly median values of TEC could be predicted to within an rms deviation of 20 to 25 percent in the daytime and 30 to 35 percent at night but that geomagnetic activity causes about a 25 percent deviation from the median values. For highest accuracy in TEC, real-time or near-real time data are needed. A service is available for registered SELDADS users that provides hourly TEC values from satellite data. SELDADS is an operational, real-time, solar-terrestrial environment monitoring system. Further information about SELDADS and the TEC data that it can provide can be obtained by writing to the Chief Forecaster, Space Environment Services Center, R432, National Oceanic and Atmospheric Administration, 325 Broadway, Boulder, Colorado 80303.

One means for obtaining real-time data on ionospheric TEC is to measure the Faraday rotation of signals from beacons on satellites. In addition to the ionospheric TEC, however, the total TEC along a path to a satellite or space vehicle may include a contribution from the plasmasphere that is about 15 percent of the ionospheric TEC by day and 50 percent by night (Klobuchar and Working Group, 1979). Measurements of time delay at two frequencies can provide the value of the total TEC along a path. As discussed more fully in Sec. 2.3.1, the total TEC is given in that case by Eq. (2.38) which is repeated below.

$$\text{TEC} = \frac{\delta t\, c}{40.3}\,\frac{f_1^{\,2} f_2^{\,2}}{f_1^{\,2} - f_2^{\,2}} \qquad (2.38)$$

The quantities f_1 and f_2 are the two frequencies, c is the velocity of light, and Δt is the difference in the time delays (Δt_2 - Δt_1) at the two frequencies.

Example 9.3 Effects Dependent on TEC

To illustrate the effects dependent on total electron content (TEC), frequencies of 870 MHz and 2.3 GHz, a TEC value of 10^{18} el/m^2, and a longitudinal component of the Earth's magnetic field B_L of 0.38 G will be utilized.

1. Faraday Rotation

870 MHz, 10^{18} el/m^2, 0.38 G = 3.8×10^{-5} Wb/m^2

$$\phi = \frac{2.36 \times 10^4 \, B_L \, (TEC)}{f^2} = \frac{2.36 \times 10^4 (3.8 \times 10^{-5})(10^{18})}{(8.7 \times 10^8)^2}$$

$$= 1.17 \text{ rad} = 67.6^\circ$$

2.3 GHz, 10^{18} el/m^2, 3.7×10^{-5} Wb/m^2

$$\phi = \left(\frac{8.7 \times 10^8}{2.3 \times 10^9}\right)^2 67.6^\circ = 9.67^\circ$$

2. Time and Range delay (one-way transmission)

870 MHz, 10^{18} el/m^2

$$\Delta R = \frac{40.3 \, (TEC)}{f^2} = \frac{40.3 \, 10^{18}}{(8.7 \times 10^8)^2} = 53.24 \text{ m}$$

$$\Delta t = \frac{53.24}{2.9979 \times 10^8} = 1.775 \times 10^{-7} \text{s} = 0.1775 \, \mu\text{s}$$

2.3 GHz, 10^{18} el/m^2

$$\Delta R = \left(\frac{8.7 \times 10^8}{2.3 \times 10^9}\right)^2 (53.24) = 7.618 \text{ m}$$

$$\Delta t = \frac{7.618}{2.9979 \times 10^{8}} = 0.0254\ \mu s$$

3. Phase Advance (one-way transmission)

870 MHz, 10^{18} el/m^2

$$\Delta\phi = \frac{8.44 \times 10^{-7}}{f}(TEC) = \frac{8.44 \times 10^{-7}\ (10^{18})}{8.7 \times 10^{8}}$$

$$= 970.1 \text{ rad or } \frac{970.1}{2\pi} = 154.4 \text{ cycles}$$

This very large advance in phase is probably of less interest than that due to a change in TEC, $\Delta(TEC)$. Suppose that a traveling ionospheric disturbance modulates the TEC by a factor of 0.01 so that $\Delta(TEC) = 10^{16}$. Then

$$\delta\phi = \frac{8.44 \times 10^{-7}\ \Delta(TEC)}{f}$$

= 9.701 rad
= 1.544 cycles
= 555.84 deg

This is still a large change in phase.

2.3 GHz, 10^{18} el/m^2

$$\Delta\phi = \frac{8.7 \times 10^{8}}{2.3 \times 10^{9}}\ (9.701)$$

= 367 rad
= 58.4 cycles

For modulation of TEC by a factor of 0.01

$\delta\phi$ = 3.67 rad = 0.584 cycle = 210 deg

4. Doppler Frequency

870 MHz, TEC = 10^{16} el/m^2 in 100 s

Suppose that the change in TEC assumed for calculating $\delta\phi$ (namely $0.01 \times 10^{18} = 10^{16}$ el/m^2) took place in a period of 100 s. Then

$$f_D = \frac{1.34 \times 10^{-7}}{f}\ \frac{\Delta(TEC)}{T_c} = \frac{1.34 \times 10^{-7}(10^{16})}{8.7 \times 10^{8}(100)}$$

$$= 0.015 \text{ Hz}$$

2.3 GHz, TEC = 10^{16} el/m^2 in 100 s

$$f_D = \frac{8.7 \times 10^8}{2.3 \times 10^9}(0.015) = 0.0057 \text{ Hz}$$

5. Dispersion

870 MHz, TEC = 10^{18} el/m^2, Δf = 50 MHz

To consider dispersion we take as an example a bandwidth of 50 MHz which might be utilized to reproduce a pulse of width $\tau = 1/\Delta f = 2 \times 10^{-2}$ μs.

$$|\Delta t| = \frac{2.68 \times 10^{-7}}{f^3} \Delta f \text{ TEC}$$

$$= \frac{2.68 \times 10^7 (5 \times 10^7) 10^{18}}{(8.7 \times 10^8)^3}$$

$$= 2.2 \times 10^{-8} \text{ s} = 2.2 \times 10^{-2} \text{ μs}$$

The time dispersion is seen to be slightly greater than the pulse width. It thus appears that dispersion limits the bit rate (data rate for digital transmission) to something less than 50 Mbps.

2.3 GHz, TEC = 10^{18} el/m^2, Δf = 50 MHz

$$|\Delta t| = \left(\frac{8.7 \times 10^8}{2.3 \times 10^9}\right)^3 (2.2 \times 10^{-2})$$

$$= 1.19 \times 10^{-3} \text{ μs}$$

At a frequency of 2.3 GHz, a data rate of 50 Mbps appears to be possible.

6. Elevation Angle Error

870 MHz, 10^{18} el/m^2

$$\Delta\theta = \frac{\cos \theta_o}{2h_i} \Delta R$$

A range delay ΔR of 53.24 m was determined for this frequency and TEC. Using 400 km for h_i and taking θ_0 to be 40°

$$\Delta\theta = \frac{0.766}{2(4 \times 10^5)} (53.24) = \frac{40.78}{8 \times 10^5}$$

$$= 5.1 \times 10^{-5}$$

$$= 0.051 \text{ mrad}$$

2.3 GHz, 10^{18} el/m^2

$$\Delta\theta = \frac{0.766}{2(4 \times 10^5)} (7.618) = \frac{5.835}{8 \times 10^5}$$

$$= 0.0073 \text{ mrad}$$

9.2.3 Ionospheric Scintillation

Scintillation is most severe in the equatorial region within ± 20° of the magnetic equator and at high latitudes, where two regions of peak scintillation activity have been reported. One corresponds to the auroral oval, and one is over the polar cap above 80° of geomagnetic latitude. In the equatorial zone, scintillation is higher in the region of the equatorial anomaly from about 15° to 20° north and south of the magnetic equator than near the equator itself. In between the equatorial and high-latitude regions are the middle latitudes where activity is less intense. In all sectors pronounced nighttime maxima occur. The general pattern is as shown in Fig. 9.4. A recent review of the global morphology of ionospheric scintillation has been provided by Aarons (1982). Some data concerning scintillation levels are shown in Table 9.2 for the low frequencies of 137 and 254 MHz for which scintillation tends to be intense. At Ascension Island in the equatorial anomaly 27 dB peak-to-peak fading was recorded at 1.54 GHz compared to 7-9 dB at Huancayo and Natal near the magnetic equator during the sunspot peak in 1979 and 1980 (Aarons, et al., 1981).

At equatorial latitudes, significant scintillation has been recorded in the 4 and 6 GHz bands. In one case involving transmission on a 6 GHz uplink and a 4 GHz downlink, fading reached 8 dB peak-to-peak (Aarons, 1982). Examples of scintillation fading on 6 GHz links are also shown in Fig. 2.16.

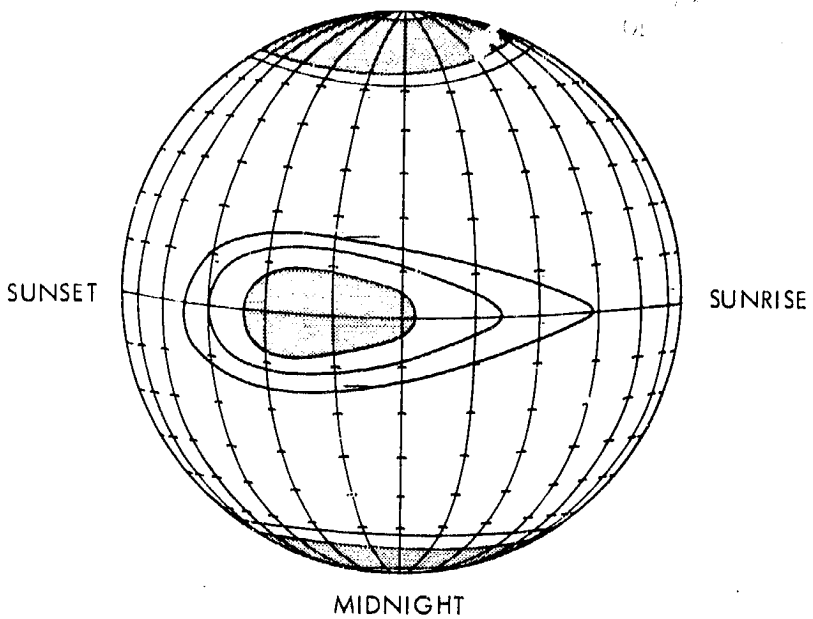

Figure 9.4. Pattern of occurrence of ionospheric scintillation (CCIR, 1978).

Although scintillation at middle latitudes is generally not as intense as at equatorial and high latitudes, some cases of severe scintillation have been recorded. During a magnetic storm on March 22, 1979, peak-to-peak scintillation of 18, 10, 15, and 3.5 dB were recorded at 136 MHz and 1.7, 4, and 12 GHz, respectively, on different paths in and around Japan (Minakoshi, et al., 1981).

Considerable data have been accumulated on ionospheric scintillation and the values quoted here give a rough idea of what margins may be needed to protect against ionospheric scintillation. Table 9.3 gives values of fade depths due to scintillation at midlatitudes (CCIR, 1982). Much of the data has not been presented or analyzed and summarized and made readily available on a statistical basis, however, and it is difficult to reach firm conclusions about margins. The data have commonly been presented as peak-to-peak values,

Table 9.2 Percentage of Occurrence of Scintillation (CCIR, 1978).

(a) ≥ 10 dB peak to peak, equatorial latitudes

Site	Frequency	Day	Night
		(0400-1600 LT)	(1600-0400 LT)
Huancayo (Peru)	137 MHz	3	14
	254 MHz	2	7
		(0600-1800 LT)	(1800-0600 LT)
Accra (Ghana)	137 MHz	0.4	14

(b) ≥ 12 dB peak to peak at 137 MHz, sub-auroral and auroral latitudes

Site	K_p	Day (0500-1700 Lt)	Night (1700-0500 LT)
Sagamore Hill (Massachusetts)	0 to 3+	0	1.4
	> 3+	0.1	2
Goose Bay (Labrador)	0 to 3+	0.1	1.8
	> 3+	1.6	6.8
Narssarssuaq (Greenland)	0 to 3+	2.9	18
	> 3+	19	45

(c) ≥ 10 dB peak to peak at 254 MHz, auroral latitudes

Site	K_p	Day (0600-1800 LT)	Night (1800-0600 LT)
Goose Bay (Labrador)	0 to 3+	0.1	0.1
	> 3+	0.3	1.2
Narssarssuaq (Greenland)	0 to 3+	0.1	0.9
	> 3+	2.6	8.4

LT: Local time.

Table 9.3 Distribution of Mid-Latitude Fade Depths Due to Ionospheric Scintillation (dB) (CCIR, 1982a).

Percentage of time Percent	Frequency (MHz) 100	200	500	1000
1.0	5.9	1.5	0.2	0.1
0.5	9.3	2.3	0.4	0.1
0.2	16.6	4.2	0.7	0.2
0.1	25.0	6.2	1.0	0.3

and in the case of the 8 dB figure mentioned for 6 GHz-4 GHz links not much more than half of the 8 dB range appeared to involve a signal decrease and nearly half a signal increase above the unperturbed level. Thus, the needed margin is less than the peak-to-peak value and may possibly approach a value as low as one half the peak-to-peak value. The increase in signal level may in some cases cause a problem of overload.

A WBMOD empirical computer model of global scintillation behavior has been prepared by Fremouw and co-workers over a period of years. This model has been described in the review paper by Aarons (1982) and in more detail by Fremouw (1982). Persons wishing to pursue the application of this model to the estimation of ionospheric scintillation may contact Dr. Edward J. Fremouw, Physical Dynamics, Inc., P.O. Box 3027,Bellevue, Washington, 98009.

9.3 TROPOSPHERIC CLEAR-AIR EFFECTS

9.3.1 Introduction

Clear-air effects on propagation are influenced strongly by the elevation angle of the path. For elevation angles above about 10° and for frequencies below about 10 GHz, the effects on communication satellite operations tend to be slight. For elevation angles of only a few degrees, the effects may be severe. The low-elevation-angle effects have long been familiar to persons concerned with terrestrial line-of-sight paths, for which margins up to about 45 dB may be utilized to combat atmospheric multipath fading. For downlinks from satellites, it is difficult to supply large margins and it has been generally assumed that it would not be necessary to do so because large elevation angles would normally be utilized for satellite communications. It turns out, however, that in a number of situations it is desirable to be able to utilize satellite communications at low elevation angles. The problems of low-angle propagation are well illustrated in a paper on measurements of 1.5 GHz MARISAT signals (Fan, Tseng, and Calvit, 1982). It was reported that MARISAT services were not available for paths having elevation angles below 10° because of severe signal degradation. Reflections from the sea surface probably contributed to the problem, but atmospheric effects surely played a major role.

The time delay due to the atmosphere may be important for navigation, ranging, and time-transfer purposes (Spilker, 1977). The excess range delay caused by the ionosphere on earth-space transmissions can be determined and taken into account by transmitting two different frequencies but that technique cannot be applied to the troposphere as the tropospheric index of refraction does not vary with frequency within the frequency range of interest.

9.3.2 Refraction and Multipath Fading

The variation of the index of refraction of the troposphere with height causes ray paths to experience bending rather than to be straight lines. The bending results in elevation-angle errors. The exact amount of bending and the resulting elevation-angle error on a path depends on the index of reflection profile as well as elevation angle but representative values can be determined for assumed index of refraction profiles. The results of such

calculations for a U.S. standard atmosphere are shown in Table 9.4. The differences in bending and elevation-angle error values apply to the path heights of 80 km and less that are shown. For the much greater heights of geostationary satellites, elevation-angle error is equal to bending, rather than smaller as for lower heights. Table 9.5 shows values of bending (equal to elevation angle error for earth-space paths) for polar continental air and tropical maritime air (CCIR, 1982b).

Table 9.4 Ray Parameters for a Standard Atmosphere[a,b] (Crane, 1976).

Initial Elevation Angle (deg)	Height (km)	Range (km)	Bending (mdeg)	Elevation-Angle Error (mdeg)	Range Error (m)
0.0	0.1	41.2	97.0	48.5	12.63
	1.0	131.1	297.8	152.8	38.79
	5.0	289.3	551.2	310.1	74.17
	25.0	623.2	719.5	498.4	101.0
	80.0	1081.1	725.4	594.2	103.8
5.0	0.1	1.1	2.6	1.3	0.34
	1.0	11.4	25.1	12.9	3.28
	5.0	55.2	91.7	52.4	12.51
	25.0	241.1	175.7	126.3	24.41
	80.0	609.0	181.0	159.0	24.96
50.0	0.1	0.1	0.2	0.1	0.04
	1.0	1.3	1.9	1.0	0.38
	5.0	6.5	7.0	4.0	1.47
	25.0	32.6	14.3	10.3	3.05
	80.0	104.0	14.8	13.4	3.13

[a]U.S. Standard Atmosphere Supplements, 1966, Environmental Sci. Serv. Administration, Dept. of Commerce, Washington, D.C. (1966).

[b]N. Sissenwine, D. D.Grantham, and H. A. Salmela, AFCRL-68-0556, Air Force Cambridge Res. Lab., Bedford, Massachusetts (October 1968).

Table 9.5 Ray Bending Values (CCIR, 1982b).

Elevation angle	Average total ray-bending,	
	Polar continental air	Tropical maritime
1°	0.45°	0.65°
2°	0.32°	0.47°
4°	0.21°	0.27°
10°	0.10°	0.14°
	Day-to-day variation in $\Delta\theta$	
1°	0.1° r.m.s.	
10°	0.007° r.m.s.	

Atmospheric multipath fading is a serious problem for very-low-elevation-angle paths, whether terrestrial paths or earth-space paths. The amount of fading is best determined by experimental data for the particular path, and the margin to be utilized for fading depends on the grade of service needed. An effort is made here to distinguish between refractive multipath fading or multipath propagation on the one hand and scintillation on the other, but the distinction is not always made clearly in the literature nor is it always possible to distinguish the two phenomena in practice. Atmospheric multipath fading is generally restricted to angles less than 10° and is most serious only for angles up to a few degrees. It is considered to result from large-scale changes in refractivity and involves relatively long fading periods, generally from around 10 s to a few minutes. Scintillation results from the smaller-scale structure of turbulence and clouds and has short periods in the order of a second and less. Though most intense for low elevation angles, it does not decrease as rapidly with increasing elevation angle as does multipath fading. Tropospheric multipath fading tends to be insensitive to frequency over the microwave frequency range. It is often closely associated with the occurrence of temperature inversions and disappears when the temperature inversion is destroyed by the passage of cyclonic storms (Flock, 1960).

Although sometimes referred to as scintillation, the fading observed at 4 and 6 GHz in the Canadian Arctic at an elevation angle of 1° (Strickland, et al., 1977) is undoubtedly atmospheric multipath fading. The margins judged to be required for such operation for three values of reliability or availability are shown in Table 9.6. The refractivity in the Arctic tends to be less than in other sections of the world, perhaps excluding desert areas, and similar or higher margins would probably be required elsewhere for the same elevation angle. On a path in Hawaii at the slightly larger elevation angle of 2.5°, Thompson et al. (1975) observed fading of 20 dB.

Table 9.6 6 GHz Link Margins for Tropospheric Fading at Eureka, Canada, Elevation Angle 1 Degree (Strickland, et al 1977).

Time Duration	Reliability		
	90%	99%	99.9%
Worst two-hours	8.0 dB	18.0 dB	28.0 dB (Rayleigh)
Worst summer day	6.8 dB	15.5 dB	24.5 dB
Worst summer week (5 days)	5.4 dB	13.0 dB	22.0 dB
Worst month, July (15 days)	3.8 dB	10.8 dB	20.3 dB

9.33.3 Tropospheric Scintillation

The term tropospheric scintillation is used here to refer to generally low-amplitude, rapid variations (periods typically around 1 s and less) in signal intensity. Such scintillation tends to be associated with small-scale structure such as that of turbulence and clouds. The amplitude variance due to scintillation has been modeled as a function of frequency and elevation angle (Ippolito, Kaul, and Wallace, 1981). The results of this analysis show that scintillation amplitude increases with frequency and elevation angle (Fig. 9.5).

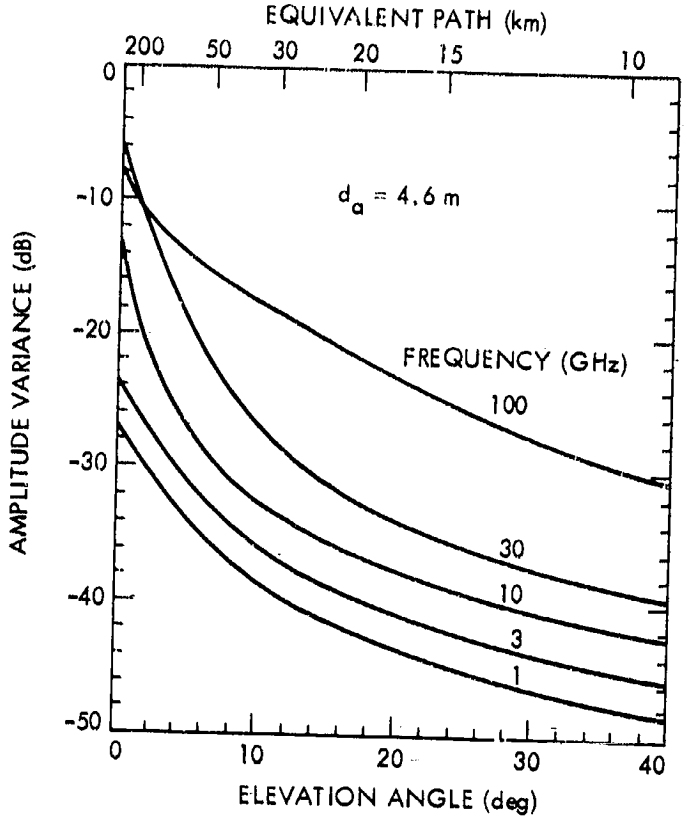

Figure 9.5. Amplitude variance for a 4.6m diameter aperture for 1 to 100 GHz (Ippolito, Kaul, and Wallace, 1981).

Example 9.3 Tropospheric Refraction

The term tropospheric refraction includes elevation-angle error, ducting, and multipath fading. The materials of this Sec. 9.3 and Chap. 3 include illustrative values of elevation-angle error and multipath fading, but it is difficult to establish quantitative recommendations concerning the magnitudes

of these effects. All are a function of index of refraction. Calculation of refractivity N is illustrated in this example.

The refractivity of the troposphere is described by the following equation (Eq. 3.2).

$$N = \frac{77.6\ p}{T} + \frac{3.73 \times 10^5 e}{T^2}$$

where $N = (n-1) \times 10^6$ with n the index of refraction, p the total pressure in mb, e the partial pressure of water vapor in mb, and T the temperature in kelvins. A value of N that could apply to Denver, Colorado will now be calculated for the pressure of a standard atmosphere, a surface temperature of 20°C, and water vapor specified in two ways--first, as a water vapor density of 7.5 g/m^3 and secondly as a relative humidity of 60 percent.

From the U.S. Standard Atmosphere, the pressure p at an altitude of 1600 m or 1 mile is 835 mb (compared to 1013 mb at sea level). The temperature of 20°C gives a temperature in kelvins of 273.15 + 20 = 293 K.

1. ρ, water vapor density, = 7.5 g/m^3

Using Eq. (3.5), $e = \frac{\rho T}{216.5} = \frac{(7.5)(293)}{216.5} = 10.15$ mb

$$N = \frac{77.6\ (835)}{293} + \frac{3.73 \times 10^5\ (10.15)}{(293)^2}$$

$$= 222.1 + 44.1$$

$$= 265.2$$

2. R.H. (relativity humidity) = 60 percent

From Table 3.1 for T = 20°C, e_s (the saturation water vapor pressure) = 23.4 mb.

$$e = e_s(\text{R.H.}) = (23.4)(0.60) = 14.04 \text{ mb}$$

$$N = \frac{77.6\ (835)}{293} + \frac{3.73 \times 10^5\ (14.04)}{(293)^2}$$

$$= 222.1 + 61.0$$

$$= 282.1$$

The above values of N are rather low because of the reduced pressure at the altitude of Denver. For the same water vapor contents of 7.5 g/m^3 and 60 percent relative humidity but the sea level pressure of 1013 mb, the corresponding values of N are 313.5 and 330.5 respectively.

To illustrate what is probably the maximum value of N that might be encountered consider the temperature of 34°C and a partial pressure of water vapor of 53.2 mb (values recorded at Sharjah, Saudi Arabia). For this case

$$N = \frac{77.6\ (1013)}{307} + \frac{3.73 \times 10^5\ (53.2)}{(307)^2}$$

$$= 256.1 + 210.5$$

$$= 466.6$$

It is the variation of N with height that has the greatest effect on wave propagation, a decrease of 157 N/km being sufficient to cause trapping or ducting of a wave launched at an elevation angle of 0 degrees. Still higher rates of decrease can trap waves having elevation angles slightly greater than 0 degrees. An expression provided by Bean and Dutton (1966)

$$\frac{\Delta n}{\Delta r} = -1 \left[\frac{1}{r} + \frac{\theta_p^2}{2h_A} \right]$$

allows determining that for a decrease of 300 N/km ($\Delta n/\Delta r = -0.000300$) in a layer of thickness h_A of 0.1 km at the Earth's surface ($r_o = 6370$),

$$\theta_p = 5.3 \text{ mrad} = 0.3 \text{ deg}$$

The angle θ_p is the penetration angle. Rays having smaller values will be subject to ducting.

9.3.4 Defocusing

Bending of rays is proportional to dN/dh, the variation of refractivity N with height (Sec. 3.2), and when dN/dh itself varies across a wavefront rays crossing the wavefront experience different amounts of bending. As the result the rays become more widely separated than previously and signal intensity is reduced. Figure 8.5 shows the attenuation due to defocusing as a function of elevation angle and ΔN, the decrease in refractivity in the first km above the surface. Figure 9.6 shows the defocusing loss in a different way. Here the loss corresponding to the average of many index of refraction profiles and the standard deviation of the loss are shown as a function of elevation angle.

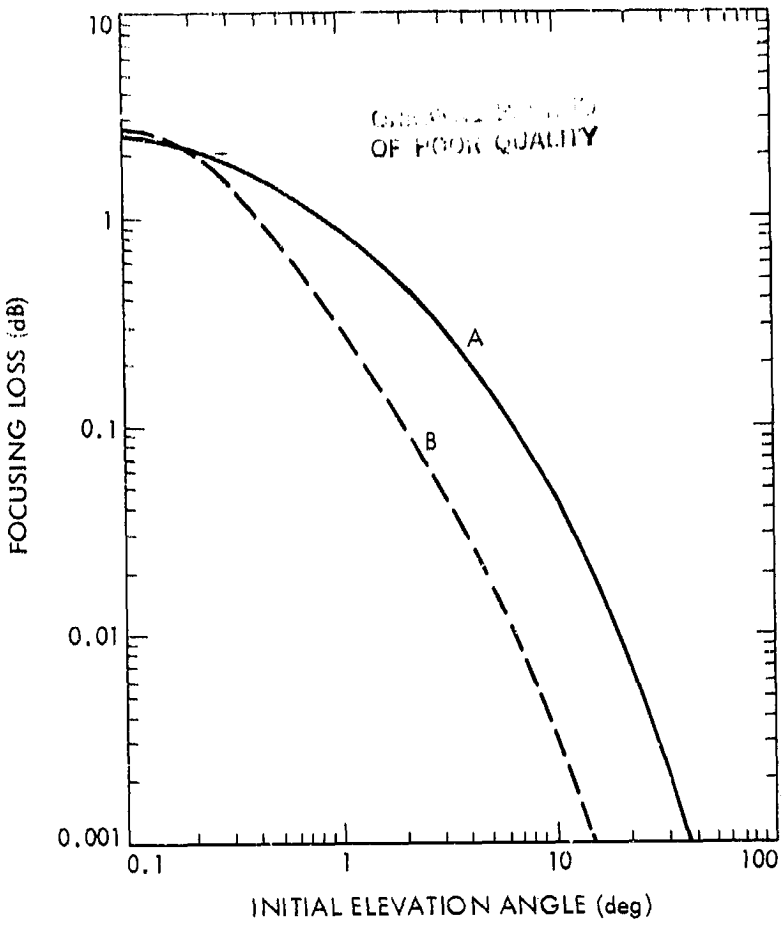

Figure 9.6. Average focusing loss (A) and standard deviation about the average (B) (CCIR, 1982b).

The results were obtained [illegible] New York and can be considered to be representative of an inland continental location. The loss is only significant for low elevation angles.

9.3.5 Gaseous attenuation

The attenuation constants for oxygen and water vapor are shown in Fig. 3.11 for sea-level pressure, a temperature of 20°C, and a water vapor density of 7.5 g/m^3. At 10 GHz, the attenuation for oxygen is about 0.007 dB/km and it decreases only slowly to about 0.005 dB/km at 1 GHz. For water vapor the value is about 0.0085 dB/km at 10 GHz, but the attenuation drops rapidly to 0.001 dB/km near 4 GHz. The values quoted are given by the dotted curves provided by J.W. Waters of the Jet Propulsion Laboratory and for water vapor are higher than the values previously used by the CCIR.

The total vertical one-way attenuation due to the gaseous constituents of the atmosphere from specified heights to the top of the atmosphere for a water vapor density of 7.5 g/m^3 is shown in Fig. 3.10. For 10 GHz and 0 km, corresponding to sea level, the value is nearly 0.06 dB; for 10 GHz and a height of 4 km the value is slightly over 0.02 dB.

In treatments of coordination distance, it is usually considered that attenuation due to water vapor can be neglected below 10 GHz but that attenuation due to oxygen should be included. This conclusion should be modified slightly in light of the values provided by Waters, as the attenuation due to oxygen and water vapor for a water vapor density of 7.5 g/m^3 are comparable near 10 GHz. However for coordination distance analysis, the recommended values of water vapor density range from 1 to 5 g/m^3 and use of these lower densities is conservative when considering interference. It appears reasonable then to continue to neglect water vapor for frequencies below 10 GHz.

9.3.6 Time and Range Delay

The excess time and range delays for propagation of signals through the Earth's atmosphere consist of components caused by the ionosphere and by the troposphere. The delay due to the ionosphere was considered in Sec. 9.2.2.

Time delay Δt and range delay ΔR are related by $\Delta R = c\Delta t$, where c is the velocity of light, 2.9979 x 10^8 m/s. The discussion in this section is in terms of ΔR.

The excess tropospheric range delay can be separated into the delay due to dry air ΔR_d and the delay due to water vapor ΔR_w or, somewhat more conveniently, it can be separated into ΔR_1 and ΔR_2 corresponding to the two terms of the expression for the refractivity N of the troposphere (Sec. 3.7; Flock, Slobin, and Smith, 1982). The equation for N is

$$N = \frac{77.6\ p}{T} + \frac{3.73 \times 10^5 e}{T^2} \tag{9.18}$$

The range delay ΔR_1 for a vertical path due to the first term N_1 of Eq. (9.18) is given by

$$\Delta R_1 = 10^{-6} \int N_1 dh = 10^{-6} \int \frac{77.6\ p}{T}\, dh = 2.757 \times 10^{-3}\ p_o \qquad \text{m} \tag{9.19}$$

for a latitude of about 45° (only slightly different elsewhere) where p_o is total surface pressure in mb. For p_o = 1013 mb, the approximate value for sea level, ΔR_1 = 2.31 m. The total pressure $p = p_d + e$ where p_d is the pressure of dry air and e is water vapor. As p_d is much larger than e, ΔR_1 is largely but not entirely due to dry air. Hopfield (1971) has determined that ΔR_1 can be determined to an accuracy of 0.2 percent or about 0.5 cm by measuring p_o.

It is shown in Sec. 3.7 that ΔR_2 for a vertical path is given by

$$\Delta R_2 = 10^{-6} \int N_2 dh = 1.731 \times 10^{-3} \int \frac{\rho}{T}\, dh \tag{9.20}$$

where ρ is the density of water vapor in g/m^3. Water vapor density ρ in g/m^3 and water vapor pressure e in mb are related by $\rho = e\ 216.5/T$ where T is in kelvins (derivation in Appendix 3.1). Determining a value for ΔR_2 requires information on ρ and T as a function of height. As ρ is highly variable and difficult to predict from surface parameters, water vapor is responsible for a larger error in range than is dry air even though the magnitude of ΔR_2 is typically only about 10 cm for ρ = 7.5 g/m^3 at the surface. By the use of radiometer techniques, however, ΔR_2 can be determined to an accuracy of 1 or 2 cm.

Table 9.4 includes values of total excess tropospheric range delay for paths to 80 km at several different elevation angles.

Example 9.4 Tropospheric range delay

To illustrate the magnitude of excess range delay due to the troposphere, consider first a zenith path at Denver, Colorado where the surface pressure (for a standard atmosphere) is 835 mb. From Eq. (9.19) the typical delay corresponding to the first term of the expression for N is

$$\Delta R_1 = 2.2757 \times 10^{-3} p_o$$

$$= 1.9 \text{ m}$$

A more precise value at a particular time could be obtained by using a measured value of p_o rather than the value for a standard atmosphere. For a relative humidity of 60 percent and other conditions likewise as in Example 9.3, the delay corresponding to the second term of the expression for N could be obtained approximately by first calculating the value of N_2 by use of

$$N_2 = \frac{3.73 \times 10^5 \ (14.04)}{(293)^2}$$

$$= 61.00$$

Then assuming an exponential decrease of N_2 with a scale height of 2 km

$$\Delta R_2 = 10^{-6} \int 61.00 \ e^{-h/2000} \ dh$$

$$= 10^{-6} \ (61.00) \ (2000)$$

$$= 12.2 \text{ cm.}$$

The total delay ΔR for a zenith-path would then be

$$\Delta R = \Delta R_1 + \Delta R_2 = 2.02 \text{ m}$$

For a path at an elevation angle of 30°, the corresponding delay would be 4.04 m. The calculation of ΔR_2 is illustrative only, and the precise determination of ΔR_2 requires the use of radiometer techniques (Sec. 3.7).

9.4 ATTENUATION AND DEPOLARIZATION CAUSED BY PRECIPITATION

9.4.1 Introduction

Attenuation due to rain increases with frequency throughout the microwave range and has sometimes been considered to be important only for frequencies above 10 GHz. However, while it is true that attenuation decreases rapidly with decreasing frequency below 10 GHz, values of attenuation are nevertheless potentially troublesome for frequencies of 8 GHz or lower. In addition the attenuation due to rain is accompanied by an increase in antenna noise temperature which further degrades the carrier-power-to-noise ratio (Sec. 9.7).

Depolarization due to rain is caused by the differences in attenuation and phase shift of electric-field-intensity components that are parallel to the major and minor axes of rain drops, which are roughly spheroidal in form. For the differences in these quantities to be high, the absolute values must generally be high. Thus depolarization tends to be most severe when attenuation is high, and it might be expected that as attenuation is low for frequencies below 8 GHz depolarization would also be low. Attenuation at 4 GHz, for example, is only about 0.05 dB/km for a rain rate of 35 mm/h. Depolarization does tend to decrease with decreasing frequency, but it does so less rapidly than attenuation because differential phase shift as well as differential attenuation contributes to depolarization, and differential phase shift is relatively high for frequencies below 10 GHz. (Phase shift is proportional to the real part of the effective index of refraction of a medium, and this value is relatively high below 10 GHz for rain as shown in Fig. 4.3a). It thus develops that depolarization due to rain may be important for frequencies of 4 GHz or lower.

Scatter of electromagnetic waves by rain is significant for frequencies of 1.5 GHz or lower, as the intense echoes from rain on L-band radar displays indicate. Such scatter is a potential source of interference.

Basic concepts and definitions concerning the propagation effects of rain were presented in Chap. 4. Consideration is directed here to procedures for estimating the magnitude of the effects.

9.4.2 Estimation of Attenuation Due to Rain

9.4.2.1 Step-by-step Procedure

In the design of telecommunication links, data on propagation effects are needed in statistical form in order to provide as much assurance as possible that a certain signal level will be available for a specified percentage of time. A sufficient data base is not available for all propagation effects to allow link design on this basis, but a considerable effort has been devoted to the development of satisfactory data bases and models to account for the effects of rain in this way.

If satisfactory statistical data on rain rate or attenuation due to rain are available for the particular location in question they should be used. Lin (1977) and Lee (1979) have described procedures for obtaining the needed rain rate statistics from data supplied by the National Climatic Center in the United States. Lacking the information needed to proceed on the basis of local weather data or not wishing to formulate statistical data from Weather Service records, use can be made of models that have been developed for rain rate and attenuation due to rain. The steps to be taken in estimating attenuation are listed below.

1. Estimate Rain Rate

The first step in obtaining a value for attenuation due to rain is to estimate the rain rate R_p that is exceeded for a certain small percentage (or certain percentages) of time, commonly 0.01 percent corresponding to 53 minutes per year. For this purpose, use should be made of statistical data for the particular location, if satisfactory data are available, or of several models described in Sec. 4.3.3. Prominent among these is the 1980 Global Model by Crane (1980a, b). Figure 4.8 shows the rain-rate regions of the world according to this model, and Fig. 9.7 shows rain-rate regions of the United States in more detail. The rain-rate values for these regions are given in Table 9.7. Figure 4.10 shows rain-rate regions for Canada, and Table 4.5 gives corresponding rain-rate values for Canada.

The 1982 CCIR model uses similar but somewhat different rain-rate regions (CCIR, 1982c). These are shown in Figs. 4.12-4.14, and the corresponding rain-rate values are given in Table 4.6. Contours based on the model of constant rain rate exceeded for 0.01 percent of the time are provided in CCIR Report 563 and are reproduced here as Figs. 9.8-9.10. This type of presentation provides considerable information at a glance.

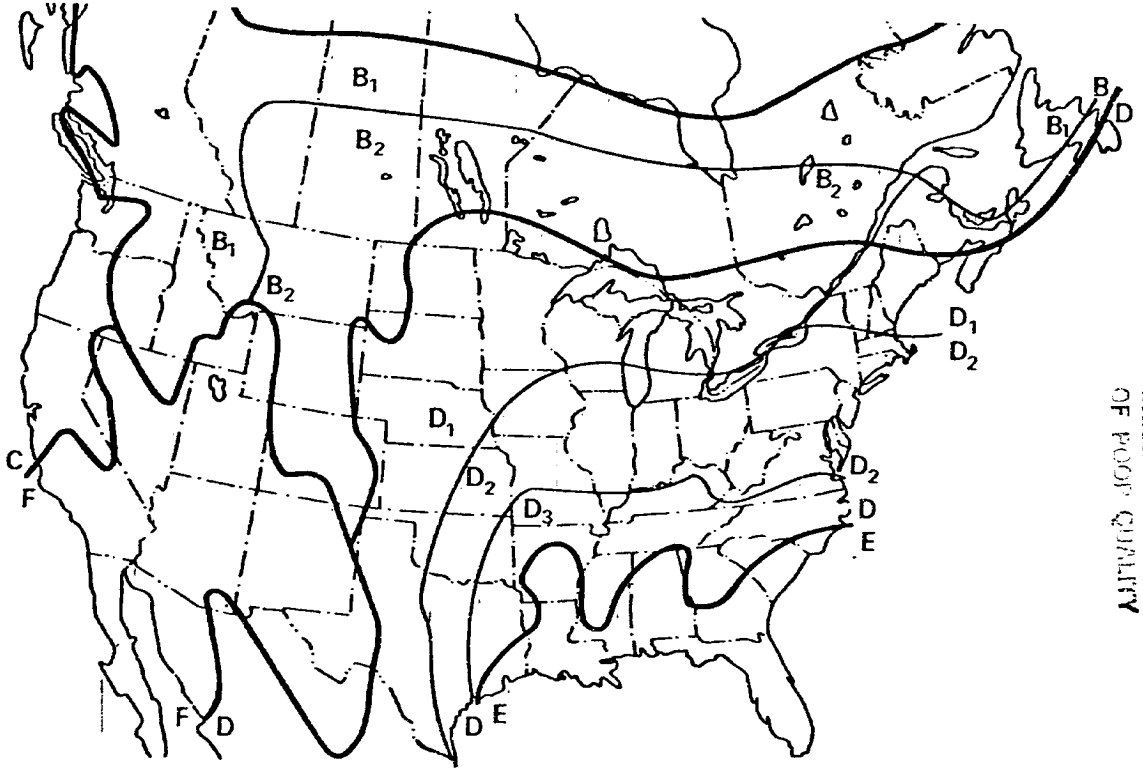

Figure 9.7. Rain-rate regions for conterminous United States and southern Canada (Crane, 1980b).

Table 9.7 Point Rain Rate Distribution Values (mm/hr) Versus Percent of Year Rain Rate is Exceeded (Crane, 1980b).

Percent of Year	RAIN CLIMATE REGION												Minutes per Year	Hours per Year
	A	B_1	B	B_2	C	D_1	$D=D_2$	D_3	E	F	G	H		
0.001	28.5	45	57.5	70	78	90	108	126	165	66	185	253	5.26	0.09
0.002	21	34	44	54	62	72	89	106	144	51	157	220.5	10.5	0.18
0.005	13.5	22	28.5	35	41	50	64.5	80.5	118	34	120.5	178	26.3	0.44
0.01	10.0	15.5	19.5	23.5	28	35.5	49	63	98	23	94	147	52.6	0.88
0.02	7.0	11.0	13.5	16	18	24	35	48	78	15	72	119	105	1.75
0.05	4.0	6.4	8.0	9.5	11	14.5	22	32	52	8.3	47	86.5	263	4.38
0.1	2.5	4.2	5.2	6.1	7.2	9.8	14.5	22	35	5.2	32	64	526	8.77
0.2	1.5	2.8	3.4	4.0	4.8	6.4	9.5	14.5	21	3.1	21.8	43.5	1052	17.5
0.5	0.7	1.5	1.9	2.3	2.7	3.6	5.2	7.8	10.6	1.4	12.2	22.5	2630	43.8
1.0	0.4	1.0	1.3	1.5	1.8	2.2	3.0	4.7	6.0	0.7	8.0	12.0	5260	87.7
2.0	0.1	0.5	0.7	0.8	1.1	1.2	1.5	1.9	2.9	0.2	5.0	5.2	10520	175
5.0	0.0	0.2	0.3	0.3	0.5	0.0	0.0	0.0	0.5	0.0	1.8	1.2	26298	438

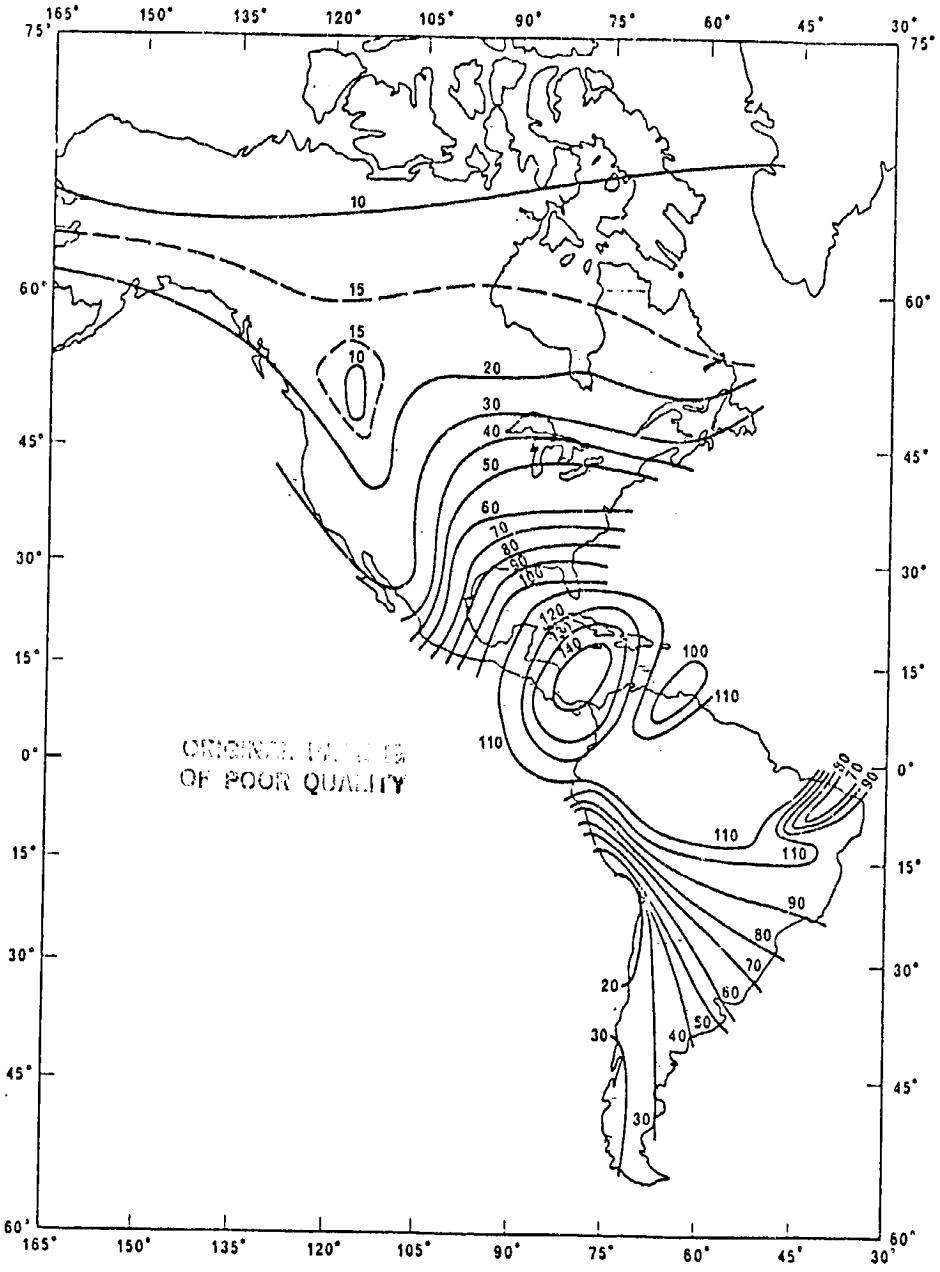

Figure 9.8. Rainfall contours for 0.01 percent of the time for the Americas.

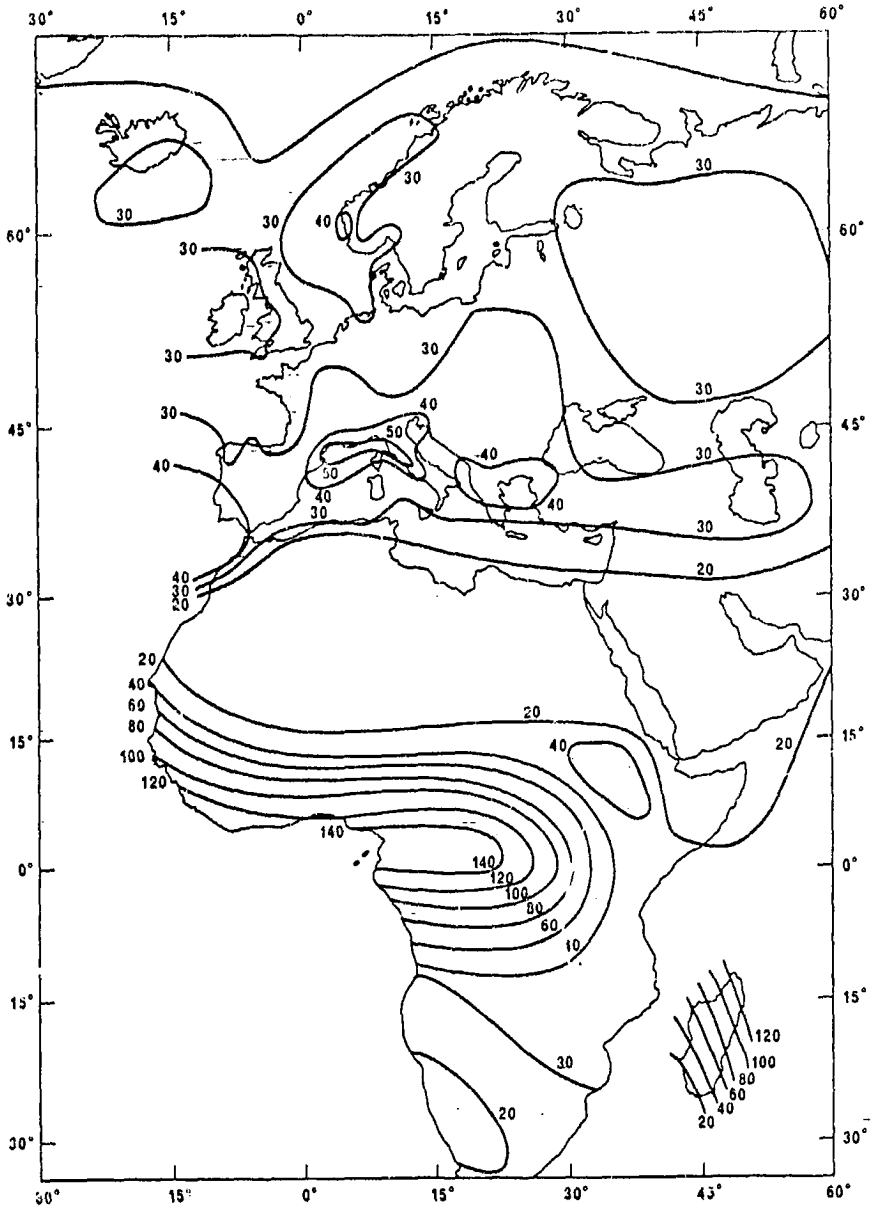

Figure 9.9. Rainfall contours for 0.01 percent of the time for Europe and Africa.

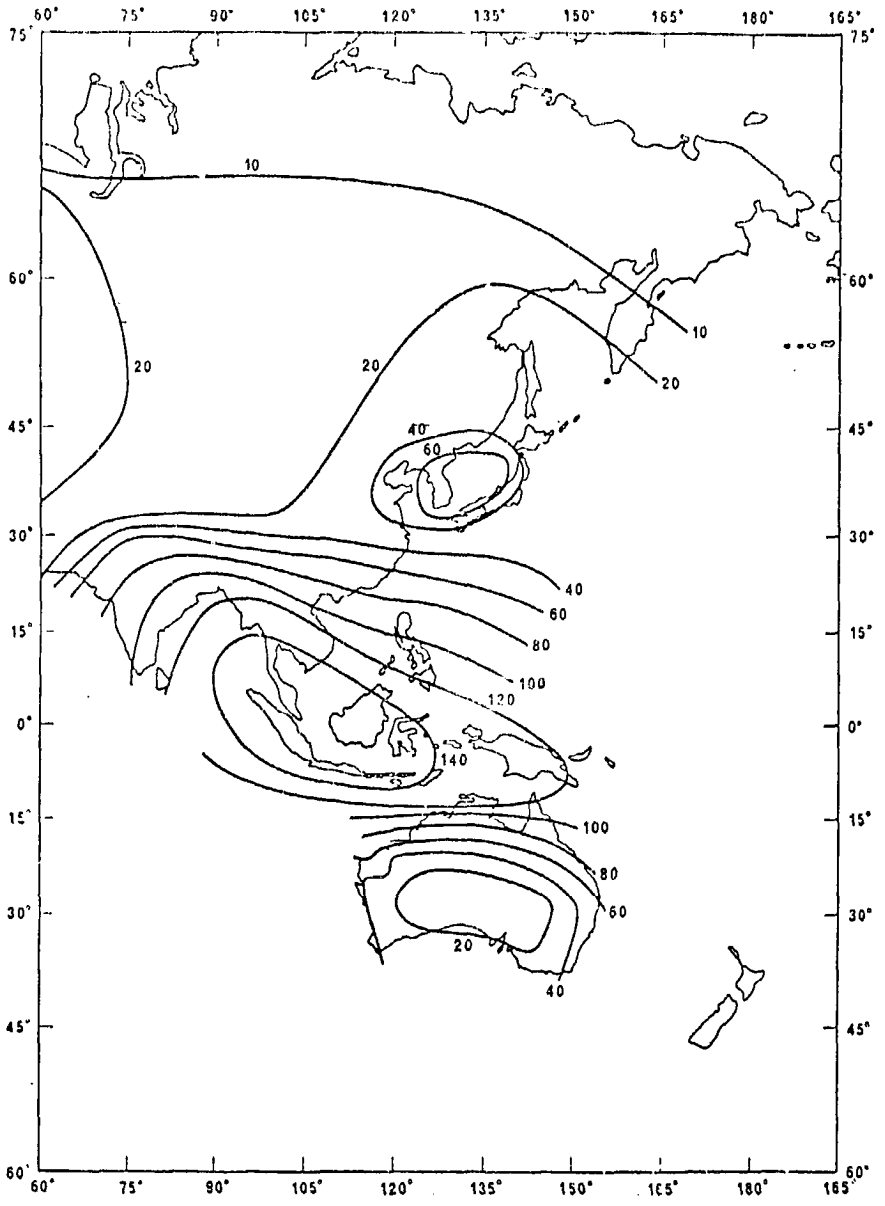

Figure 9.10. Rainfall contours for 0.01 percent of the time for Asia and Oceania.

The large-scale world-wide or continent-wide maps of rain-rate regions are extremely valuable but suffer from lack of detail. This statement is especially applicable to the western United States where large variations in rain rate occur within short distances. Rain rates on opposite sides of mountain ranges, for example, are often drastically different. As pointed out in CCIR Report 563, additional data are needed to improve the accuracy and resolution of the information on rain rates. An observation period of many years and rain gauges with adequate sensitivity and time resolution are required for this purpose. A considerable amount of data on the effects of rain have been accumulated for the eastern United States and are reflected in Fig. 9.7. For the United States, we recommend using the rain-rate regions of Fig. 9.7 and the values of Table 9.7. For Canada, we favor the regions of Fig. 4.10 and the values of Table 4.5. For the rest of the world, we favor the regions and values of the 1982 CCIR model. (Figs. 4.12-4.14 and Table 4.6 or Figs. 9.8-9.10 for a percentage of occurrence of 0.01.)

2. Determine Attenuation Constant (dB/km) Corresponding to Rain Rate

For the rain rate R_p determined in step 1, find the corresponding attenuation constant α_p by use of an expression of the form of $\alpha_p = aR^b$. Values of the coefficients of a and b have been provided by Olsen, Rogers, and Hodge (1978) and their values for frequencies of 15 GHz and lower are reproduced as Tables 4.2 and 9.8. The table includes values LP_H and LP_L calculated in accordance with analyses for high and low rain rates. It is recommended that the LP_L values be used for rain rates of 30 mm/h and less and that the LP_H values be used for rates above 30 mm/h.

If it is desired to distinguish between horizontal and vertical linear polarization, values of a and b for the two linear polarization are given for a limited number of frequencies in Table 9.9 (CCIR, 1982d). For circular polarization, the value of a (a_c) is given by

$$a_c = [a_H + a_V + (a_H - a_V) \cos^2\theta \cos^2\tau\ ]/2 \qquad (9.21)$$

and the value of b is given by

$$b_c = [a_H b_H + (a_H b_H - a_V b_V) \cos^2\theta \cos^2\tau\ ]/2a_c \qquad (9.22)$$

Table 9.8 Values of a and b of Eq. (4.11) from Olsen, Rogers, and Hodge (1978) for T = 0°C and for Laws and Parsons Low and High Rain Rates.

Freq. (GHz)	a		b	
	LP_L	LP_H	LP_L	LP_H
1.0	6.41×10^{-5}	5.26×10^{-5}	0.891	0.947
1.5	1.45×10^{-4}	1.14×10^{-4}	0.908	0.976
2.0	2.61×10^{-4}	1.96×10^{-4}	0.930	1.012
2.5	4.16×10^{-4}	2.96×10^{-4}	0.955	1.054
3.0	6.15×10^{-4}	4.12×10^{-4}	0.984	1.100
3.5	8.61×10^{-4}	6.42×10^{-4}	1.015	1.150
4.0	1.16×10^{-3}	6.84×10^{-4}	1.049	1.202
5.0	1.94×10^{-3}	1.12×10^{-3}	1.113	1.274
6.0	3.05×10^{-3}	1.99×10^{-3}	1.158	1.285
7.0	4.55×10^{-3}	3.36×10^{-3}	1.180	1.270
8.0	6.49×10^{-3}	5.35×10^{-3}	1.187	1.245
9.0	8.88×10^{-3}	8.03×10^{-3}	1.185	1.216
10.0	1.17×10^{-2}	1.14×10^{-2}	1.178	1.189
11.0	1.50×10^{-2}	1.52×10^{-2}	1.171	1.167
12.0	1.86×10^{-2}	1.96×10^{-2}	1.162	1.150
15.0	3.21×10^{-2}	3.47×10^{-2}	1.142	1.119

where H and V refer to horizontal and vertical polarization, θ is the elevation angle of the path, and τ is the polarization tilt angle (see Sec. 9.4.3.2).

Other means are available to obtain a value of α_p as a function of frequency and rain rate. Figures 4.3b and 4.5, for example, can be used for this purpose with α_p given by $(2\pi/\lambda)m_i$ if Fig. 4.3b is used. As in some cases these figures can provide only an approximate value because of the way they are plotted, they are perhaps best used as a rough check on the values obtained by using $\alpha_p = aR^b$.

Table 9.9 The Coefficients a and b for Calculating Attenuation for Horizontal and Vertical Polarization (CCIR, 1982d).

Frequency (GHz)	a_H	a_V	b_H	b_V
1	0.0000387	0.0000352	0.912	0.880
2	0.000154	0.000138	0.963	0.923
4	0.000650	0.000591	1.12	1.07
6	0.00175	0.00155	1.31	1.27
8	0.00454	0.00395	1.33	1.31
10	0.0101	0.00887	1.28	1.26
12	0.0188	0.0168	1.22	1.20
15	0.0367	0.0347	1.15	1.13

3. Determine path length L and horizontal projection D

In addition to the attenuation constant, α_p in dB/km, information on the path length L through rain is needed to determine total attenuation along the path. Rain is essentially confined to the region below the height of the 0°C isotherm, and this height has been considered to vary with latitude and percentage of time as shown in Fig. 4.7. By use of this figure, one can determine the height H of the 0°C isotherm for the latitude and percentage or probability of occurrence. The height H can be expressed as the difference H_0

- H_g, where H_0 is the elevation of the 0° isotherm and H_g is the ground elevation. The more recently prepared Fig. 9.11 shows the same curves for height H as Fig. 4.7 but refers to them as Method 2 curves, where Method 2 applies to continental climates and/or percentages of occurrence greater than 0.1 percent. Also, Fig. 9.11 includes a curve for 0.01 percent for Method 1, which has been formulated for maritime climates. It is now believed, however, that both the original Method 1 and Method 2 curves give values of H that are too large for the lower latitudes (tropical regions), and Fig. 9.11 includes a dotted modification of the Method 1 curve that has been proposed by a 1982 CCIR working party (IWP 5/2) for the lower latitudes. The relative advantages of Methods 1 and 2 for locations in the United States where the modification for lower latitudes is not applicable are under continuing review. The modified Method 1 curve appears to be preferable for use in tropical regions.

For elevation angles above 10°, determine the length L of the path through rain by use of

$$L = \frac{H}{\sin\theta} = \frac{H_0 - H_g}{\sin\theta} \tag{9.23}$$

where θ is elevation angle. For elevation angles less than 10°, various expressions have been devised, that included in CCIR Report 564 (CCIR, 1982) being

$$L = \frac{2H}{(\sin^2\theta + 2H/kr_0)^{1/2} + \sin\theta} \tag{9.24}$$

where kr_0 is the effective radius of the Earth (Sec. 3.2) and can be taken to be 8500 km for k = 4/3 in the absence of contrary information. If using the Crane Global Model, however, determine L and its horizontal projection D by the procedure of Appendix 4.1 for elevation angles less than 10°.

For elevation angles greater than 10°, find D by using

$$D = L\cos\theta \tag{9.25}$$

4. Path reduction factor; effective path length

The average rain rate along a path through rain tends to differ from the rain rate at a particular point. For high values of rain rate R_p, the average rate tends to be less than R_p, as intense rain is generally restricted to localized areas. A common approach to the estimation of attenuation is to

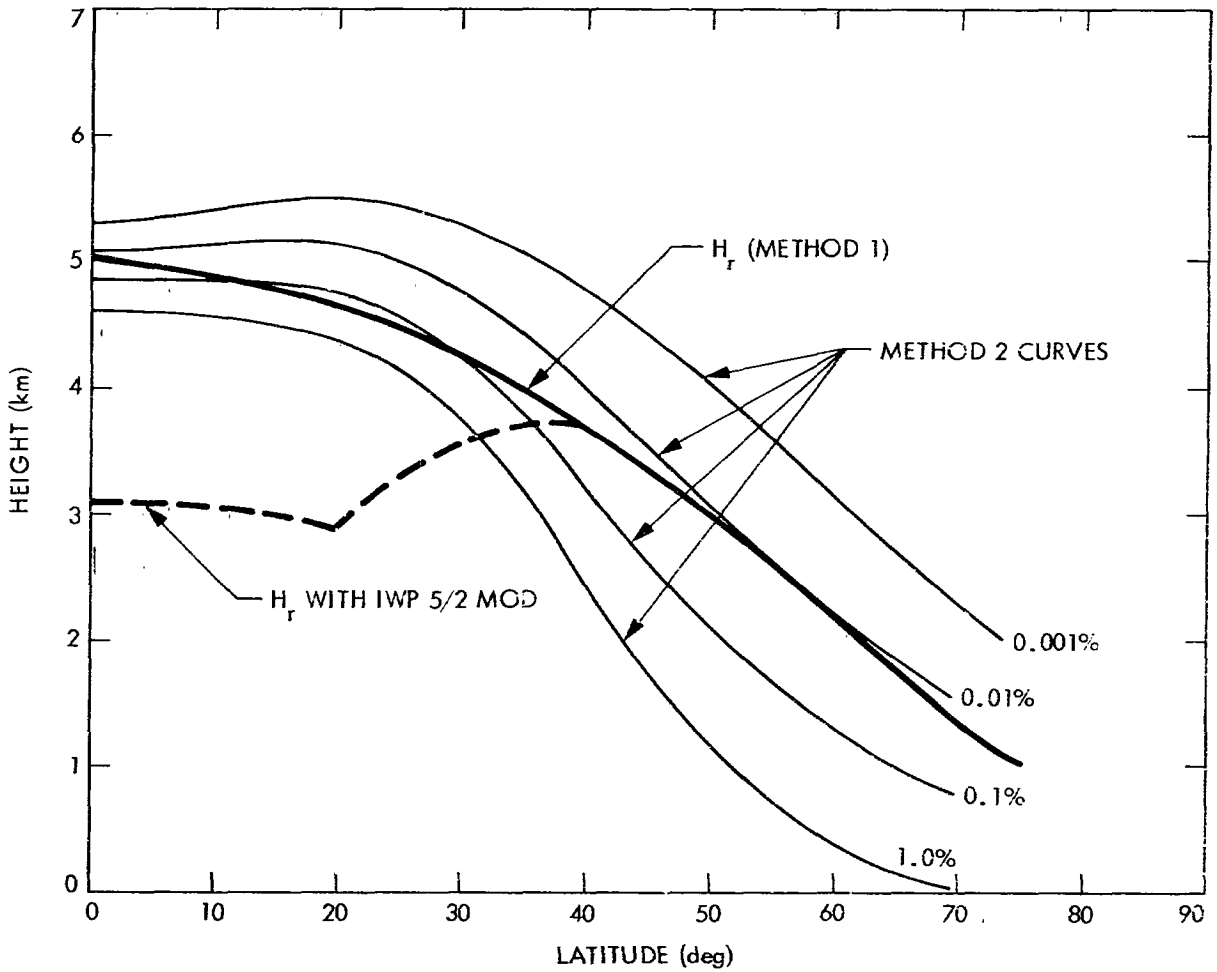

Fig. 9.11. Heights of 0°C isotherm for CCIR prediction methods.

determine a path reduction factor which can be viewed as modifying the value of R_p to obtain an effective value of R or as modifying L to obtain an effective path length. Crane (1980), however, determines a value of D as mentioned for step 3 but instead of calculating an effective rain rate or path length determines attenuation by an expression using three exponential functions that have been devised to account for the expected variation of rain rate with distance from a recording location, as a function of rain rate.

Following CCIR Report 564 for 1982, we determine a reduction factor r_p, which for continental climates and Method 2 has the form of

$$r_p = \frac{90}{90 + C_p D} \tag{9.26}$$

where D is in km and C_p is given by Table 9.10.

Table 9.10 Coefficient C_p for Determining Reduction Factor r_p for Continental Climates (CCIR, 1982e).

Percent of year	.0001	0.01	0.1	1.0
C_p	9	4	0.5	0

Note that for the commonly used percentage of p = 0.01,

$$r_p = \frac{90}{90 + 4D}$$

This relation for p = 0.01 is considered to hold for both maritime and continental climates (and thus for both Methods 1 and 2). For other percentages than 0.01 for maritime climates (Method 1), however, the recommended procedure is to first determine the total attenuation $A_{0.01}$ for p = 0.01 and to then use the relation given by Eq. (9.28) for percentages of 0.1 and less (rather than referring to Table 9.10 for these percentages).

5. Calculate attenuation

Having determined the values of α_p, L, and r_p, attenuation A in dB can be calculated by using the simple relation

$$A = \alpha_p L r_p \quad \text{dB} \tag{9.27}$$

This relation applies for all percentages of occurrence for continental climates (using Method 2) and for p = 0.01 or p > 0.1 for maritime climates (using Method 1). For values of p other than 0.01 (but 0.1 or less) for maritime climates first calculate $A_{0.01}$ for p = 0.01 and then use

$$A_p = A_{0.01} \left(\frac{p}{0.01} \right)^{-a} \tag{9.28}$$

with a = 0.33 for $0.001 \leq p \leq 0.01$ and a = 0.41 for $0.01 \leq a \leq 0.1$.

It should be kept in mind that attenuation due to rain is accompanied by an increase in system noise temperature. Thus the degradation in signal-to-noise ratio due to rain is more severe than that caused by attenuation alone, especially for low-noise systems. Section 9.7 and Chap. 7 are devoted to the subject of noise.

Example 9.5 Attenuation Due to Rain

For an example of attenuation due to rain, we use the rain rate exceeded for 0.01 percent of the time at a frequency of 8.5 GHz and a latitude of 40° in region D_1 of North America or in central Spain. The procedure followed is generally that of the 1982 CCIR model but differs from it in some details.

1. For North America, Table 9.7 shows a value of 35.5 mm/h, and Fig. 9.9 indicates that about 35 mm/h is suitable for central Spain. Also reference to Fig. 4.13 and Table 4.6 confirm that 35 mm/h is a reasonable figure for central Spain. We therefore settle on 35 mm/h as being suitable for both the D_1 region of North America and central Spain.
2. To determine the attenuation constant α_p, use

   $$\alpha_p = a(f)\, R^{b(f)}$$

   where R is rain rate and a and b are given by Olsen, Rogers, and Hodge (1978) for 0°C. Table 9.8 gives values of these constants for frequencies of 8.0 and 9.0 GHz, and reference to the original paper indicates that linear interpolation should be suitable. For a rain rate of 35 mm/h, use the LP_H values.

The values of a, b, and α_p for 8.0 GHz and 9.0 GHz and the interpolated values for 8.5 GHz are as follows:

f(GHz)	a	b	α_p (dB/km)
8.0	5.35×10^{-3}	1.245	0.447
9.0	8.03×10^{-3}	1.216	0.606
8.5	6.69×10^{-3}	1.231	0.532

3. For determining the path length L and the horizontal projection D, use Fig. 9.11. For a latitude of 40°, the original and modified Method 1 curves agree. It is only for lower latitudes that they differ. From Fig. 9.11, the height from the Method 1 curve is about 3.7 km. To determine L and D, information on elevation angle is needed. For purposes of illustration, the elevation angle is arbitrarily taken to be 42°. Then

$$L = \frac{H}{\sin \theta} = \frac{3.7}{0.669} = 5.53 \text{ km}$$

and

$$D = L \cos \theta = (5.53)(0.743)$$

$$= 4.11 \text{ km}$$

4. The path reduction factor r_p is given by

$$r_p = \frac{90}{90 + 4D} = \frac{90}{90 + 16.44} = \frac{90}{106.44} = 0.846$$

5. The total attenuation A is calculated by using $A = \alpha_p L r_p$, resulting in

$$A = (0.532)(5.53)(0.846)$$

$$= 2.49 \text{ dB}$$

See Example 9.7 for consideration of the decrease in C/X due to the noise associated with an attenuation of 2.49 dB. If the Method 2 curve for 0.01 percent were used the value of H would be about 4 km, D would be 4.44 km, r_p would be 0.835, and A would be 2.66 dB.

9.4.3 Depolarization

9.4.3.1 Introduction

The degree of depolarization may be described in several ways. The terms cross polarization discrimination (XPD) and depolarization or cross polarization have an inverse relation. The quantity XPD was defined by Eq. (4.32) as 20 log E_{11}/E_{12} where E_{11} is the copolarized or wanted signal and E_{12} is the cross polarized or unwanted signal which may have been produced by a process of depolarization. The terms depolarization and cross polarization may be used, however, to represent 20 log E_{12}/E_{11}. It can be noted that a high value of XPD, for example 40 dB, represents a favorable condition corresponding to a small value of depolarization or cross polarization, namely -40 dB. Also the low value of XPD or 10 dB for example represents an unfavorable conditions corresponding to the quite high level of depolarization of -10 dB.

9.4.3.2 Relation between XPD and A for rain for frequencies above 8 GHz

For frequencies above 8 GHz and for attenuation values above about 1 dB, XPD and copolarized attenuation A have been related by

$$\begin{aligned} XPD = {} & 30 \log f_{GHz} - 40 \log (\cos \theta) \\ & - 10 \log \tfrac{1}{2} \left[1 - \cos (4\tau) e^{-\kappa_m^2}\right] \\ & + \kappa^2 - 20 \log A \end{aligned} \qquad (9.29)$$

This expression is given in CCIR reports 563 and 722 for 1982 and differs slightly from an earlier version which did not include κ^2 and for variation with τ used the form of -20 log [sin 2|ϕ - τ|], sometimes written with ϕ taken as zero as -20 log sin 2τ. In Eq. (9.29), θ is the elevation angle of the path, τ is the polarization tilt angle (of the electric field vector of the wave) with respect to the horizontal, and A is attenuation in dB. The quantity κ equals 0.0053 σ^2 where σ is the effective standard deviation of the raindrop canting angle distribution and can be set equal to zero as a conservative design measure, and $\kappa_m^2 = 0.0024\ \sigma_m^2$ where σ_m is the standard deviation of the canting angle ϕ, assuming it to have zero mean and a Gaussian

distribution. The angles σ and σ_m are in degrees. For application of Eq. (9.29), one can use 5° for σ_m (CCIR, 1982f).

The term - 40 log (cos θ), where θ is elevation angle shows that XPD increases as elevation angle increases. The term is positive for $\theta > 0°$ as cos θ is then less than unity and log (cos θ) is negative. The relation between XPD and θ, however, should only be used for $10° \leq \theta \leq 60°$, or for a smaller range of θ. The term involving τ shows that XPD is the lowest for tilt angles τ of 45° and highest for horizontal and vertical polarizations for which the electric field intensity vectors are essentially parallel to the major and minor axes, respectively, of raindrops. Circular polarization is equivalent to linear polarization with a tilt angle of 45° as far as depolarization is concerned, and circularly polarized waves have lower XPD (higher depolarization) than linearly polarized waves unless the latter have a tilt angle near 45°. In summary

1. XPD is higher (depolarization lower) for paths at large elevation angles than for paths at low elevation angles.
2. XPD is higher (depolarization lower) for vertical and horizontal polarization than for circular polarization or linear polarization at an angle of 45°.
3. For frequencies above about 8 GHz, taking only rain into account, XPD has the form of U - V log A, with A copolarized attenuation and U and V as indicated in Eq. (9.29). Use Eq. (9.29) with the appropriate values of A, θ, and τ and with $\kappa^2 = 0$ and $\kappa_m^2 = 0.06$ for estimating XPD. The value of attenuation A can be estimated by the procedure of Sec. 9.3.2.

It should be recognized that the use of Eq. (9.29) provides only a rough estimate of XPD. If statistical data relating XPD and rain rate or XPD and attenuation are available for the particular frequency and location they should be used instead.

Example 9.6 Depolarization at 10 GHz

Applying Eq. (9.29) to the case of a linearly polarized wave with f = 10 GHz, θ = 40°, τ = 80°, and A = 4 dB, corresponding to a very heavy rain, the calculated value of XPD is 31.15, meaning that the desired copolarized signal is 31.15 dB above the unwanted cross polarized signal. For a circularly

polarized wave corresponding to $\tau = 45°$ but with other parameters the same, the calculated value of XPD is 22.72. If the polarization is linear at the same frequency, tilt angle, and attenuation as originally but the elevation angle is 10°, the calculated value of XPD is 26.79 but if the attenuation increases to 10 dB, as might possibly be the case for a path at a lower elevation angle and the same rain rate, the calculated XPD is 18.83. The values of the parameters mentioned are summarized in the following table and the calculation giving the first entry then follows.

Illustrative Calculations of XPD

f (GHz)	(deg)	(deg)	A (dB)	XPD (dB)
10	40°	80°	4	31.15
10	40°	45°	4	22.72
10	10°	80°	4	26.79
10	10°	80°	10	18.83

For the first row of the table

$$XPD = 30 \log f_{GHz} - 40 \log (\cos \theta) - 10 \log \tfrac{1}{2} [1 - \cos 4\tau e^{-\kappa^2 m}] - 20 \log A$$

$$= 30 - 40 (-0.1157) - 10 \log \tfrac{1}{2} [1 - \cos 3200(0.9418)] - 20 \log A$$

$$= 30 + 4.628 + 8.561 - 12.041$$

$$= 31.15$$

9.4.3.3 Depolarization due to ice particles

Clouds above the 0°C isotherm consist at least in part of ice particles. These have a variety of shapes but are asymmetric and when they have a preferred orientation may cause depolarization not accompanied by appreciable attenuation (Bostian and Allnut, 1979; Cox, 1981). The depolarization in this case is produced primarily by differential phase shift. Rapid changes in depolarization due to ice particles have been correlated with lightning strokes, (Howell, 1977; McEwan et al., 1977). The relative amounts of rain and ice depolarization vary considerably with

location and weather. Also when attenuation is high, depolarization is due primarily to rain but when depolarization is accompanied by only low values of attenuation a larger amount of the depolarization is due to ice. Chu (1980) has suggested the simple procedure of adding 2 dB to the depolarization due to rain alone (subtracting 2 dB from the XPD) in order to account for the effects of ice particles. Elsewhere it has been stated that an allowance of 2 dB may be sufficient for North America but that a value as much as 4 or 5 dB may be needed for the maritime climate of northwestern Europe (CCIR, 1982e).

9.4.3.4 Depolarization as a function of differential phase shift and differential attenuation

For frequencies below about 8 GHz, Eq. (9.29) which relates XPD to attenuation is not suitable for estimating XPD because at these frequencies differential phase shift plays an important role in causing depolarization. One may then need to place greater reliance on any suitable experimental data concerning XPD that may be available. However expressions have been developed for XPD that take into account both differential phase shift and differential attenuation. For circular polarization, Taur (1975) and Miya (1981) use

$$XPD = 20 \log \left[\frac{1 + e^{A+jB}}{1 - e^{A+jB}} \right] \qquad (9.30)$$

and for linear polarization they use

$$XPD = 20 \log \left[\frac{1 + \tan^2 \tau \, e^{A+jB}}{(1 - e^{A+jB}) \tan \tau} \right] \qquad (9.31)$$

where A represents differential attenuation and B represents differential phase shift. Also Chu (1980) has concluded that depolarization is proportional to the differential propagation constant $\sqrt{(\Delta\alpha)^2 + (\Delta\beta)^2}$ where $\Delta\alpha$ is differential attenuation and $\Delta\beta$ is differential phase. This differential propagation constant, furthermore, is proportional to frequency from about 4 to 30 GHz. Thus while $\Delta\alpha$ decreases more rapidly that frequency below 10 GHz, $\sqrt{(\Delta\alpha)^2 + (\Delta\beta)^2}$ decreases at essentially the same rate that frequency decreases.

Based on these considerations, Chu (1980) has developed a procedure for estimating depolarization at any frequency, elevation angle, polarization, and

location where rain statistics are available by extrapolation of data from other sources, including 19/28 GHz COMSTAR beacon measurements. For converting depolarization D from one path to another when rain distributions are available for both paths, Chu gives

$$(D_1)_{dB} - (D_2)_{dB} = P_1 - P_2 + 20 \log \left[\frac{\left(\sqrt{(\Delta\alpha)^2 + (\Delta\beta)^2}\right)_1 \cos^2\theta_1 L_1}{\left(\sqrt{(\Delta\alpha)^2 + (\Delta\beta)^2}\right)_2 \cos^2\theta_2 L_2} \right] \quad (9.32)$$

where the P's represent polarization factors which are zero for circular polarization and for linear polarization are given by

$$P = 10 \log \frac{1}{2} [1 - \cos 4\tau e^{-8\sigma^2 m}] \pm \frac{\Delta A}{2} \quad (9.33)$$

The expression involves the same dependence on elevation angle θ and essentially the same dependence on polarization tilt angle τ as in Eq. (9.29). The quantities $\sqrt{(\Delta\alpha)^2 + (\Delta\beta)^2}$ for the two paths represent differential propagation constants per km and the L's are path lengths. The term A/2 equals 5 $\log(\alpha_V/\alpha_H)^2$ where α_V is the attenuation constant of a vertically polarized wave and α_H is the attenuation constant of a horizontally polarized wave. The sign of $\pm$ ΔA/2 should be chosen to favor (give a higher value of P for) quasivertical polarization than quasihorizontal polarization. Chu includes curves giving $\sqrt{(\Delta\alpha)^2 + (\Delta\beta)^2}$ (for zero elevation angle) as a function of rain rate and frequency (Fig. 9.12), and α_V and α_H can be determined by using Table 9.9 with $\alpha_V = a_V R^{b_V}$ and $\alpha_H = a_H R^{b_H}$.

Figure 9.13 shows the application of the procedure outlined to comparison of depolarization at 4 GHz for linearly polarized transmissions on a path with an elevation angle of 38.6° in New Jersey with depolarization on a path with an elevation angle of 9° in Japan where circular polarization was employed.

Further information on the low values of XPD which may be encountered at the low elevation angles utilized on some 4 GHz earth-space paths from Japan is shown in Fig. 9.14 (Kobayashi,1976). Low values of XPD have also been reported to Taur (1974) at 4 GHz on paths terminating at Washington, D.C. and having higher elevation angles.

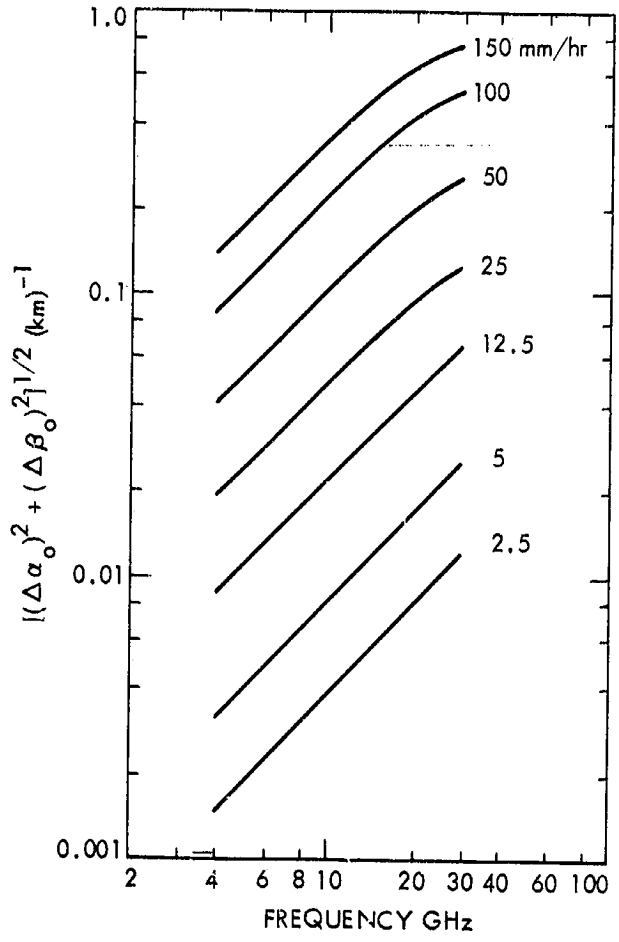

Figure 9.12. Calculated differential propagation constant at zero elevation angle as a function of frequency for various rain rates (Chu, 1980).

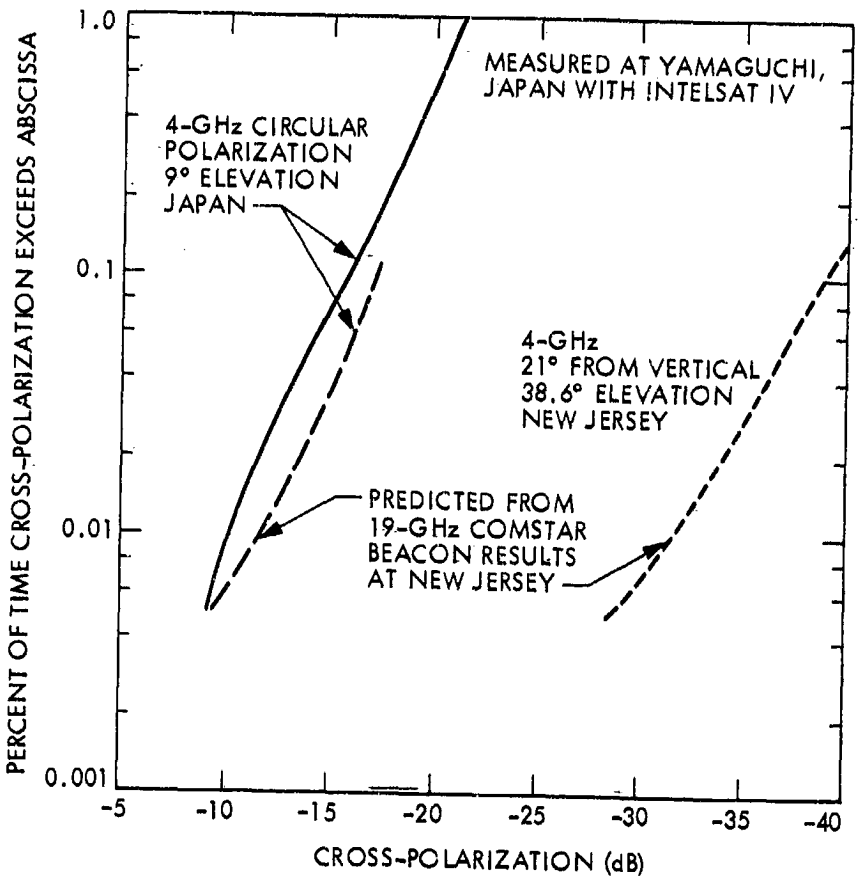

Figure 9.13. Comparison between measured 4 GHz circularly polarized INTELSAT IV depolarization statistics at 9° elevation angle and predictions from COMSTAR measurements (Chu, 1980).

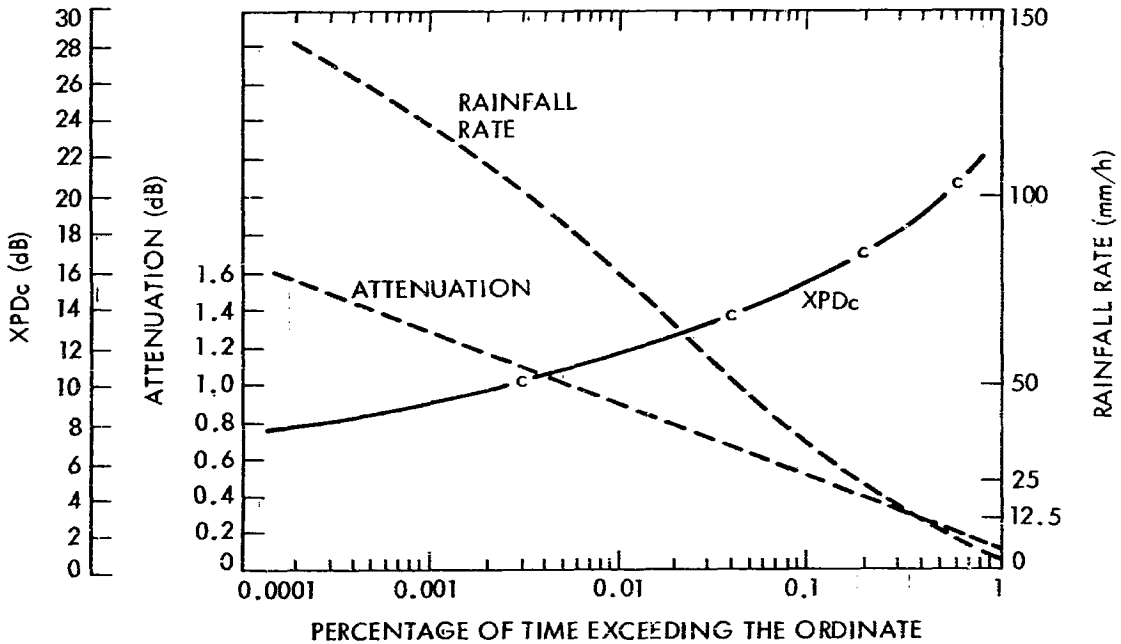

Figure 9.14. Pre-estimation of XPD on a satellite communication circuit, 4 GHz, 8° elevation angle, circular polarization, Yamaguchi station (Kobayashi, 1976).

Example 9.7 Comparison of Depolarization for Different Paths

The application of Eq. (9.32) to the comparison of depolarization on two different paths will now be illustrated. Let Station 1 have an elevation angle of 10° and circular polarization. Let Station 2 have an elevation angle of 40° and quasivertical polarization with a tilt angle τ of 75°. Assume that both stations operate at 4 GHz, that Station 2 is reported to have a depolarization of -30 dB, and that it is desired to determine the depolarization of Station 1. The comparison will be made for the same rate of 35 mm/h at both stations. Station 1 can be expected to have a higher depolarization (less favorable condition for frequency sharing) than Station 2 so that $D_1 - D_2$ should be positive.

As Station 1 has circular polarization P_1 is zero. The principal term of P_2, namely

$$10 \log \frac{1}{2} [1 - \cos 4 e^{-8\sigma_m^2}] = 10 \log \frac{1}{2} [1 - \cos 3000 (0.9418)] = - 5.77$$

where the exponential term has the same value as in Example 9.6. [In Eq. (9.33), σ_m is in radians whereas it is in degrees in Eq. (9.29)]. By using values of a_H, a_V, b_H, and b_V from Table 9.9 it is determined that $A/2$ is 1.19. Therefore

$$P_1 - P_2 = 0 - (-5.77 - 1.19) = 6.96.$$

Considering next the second term of Eq. (9.32), the propagation constants are the same if the same rain rate is assumed and the difference in depolarization due to this term is

$$20 \log \left[\frac{\cos^2 \tau_1 L_1}{\cos^2 \tau_2 L_2} \right] = 20 \log \left[\frac{\cos^2 10^\circ \left(\frac{1}{\sin 10^\circ} \right)}{\cos^2 40^\circ \left(\frac{1}{\sin 40^\circ} \right)} \right]$$

$$= 15.73$$

Thus

$$(D_1)_{dB} - (D_2)_{dB} = 6.96 + 15.73 = 22.69$$

and

$$(D_1)_{dB} - (-30) = 22.69$$

$$(D_1)_{dB} = 22.69 - 30 = -7.31$$

To take account of different frequencies or rain rates use can be made of Fig. 9.12. For example if Station 2 operated at 8 GHz with the same depolarization of -30 dB, but station 1 remained at 4 GHz, the ratio of propagation constants of Eq. (9.32) would be roughly 1/2 and in place of 15.73 for the second term of Eq. (9.32) one would have about 9.7. Then $(D_1)_{dB}$ would be about -13.3.

Note that whereas Station 2 was known to operate with a depolarization of -30 dB (or XPD of +30 dB), Station 1, at the same frequency and rain rate but a different path, was predicted to have an unsatisfactory depolarization value of -7.3 dB (XPD of +7.3 dB) in the first case considered.

9.5 EFFECTS OF CLOUDS, DUST, AND VEGETATION

Attenuation due to clouds is normally no greater than 0.5 dB for a vertical (zenith) path for frequencies of 10 GHz and less. For the same conditions otherwise, the attenuation would be 1 dB for an elevation angle of 30° and 2.88 dB for an elevation angle of 10° if the attenuation were 0.5 dB for a vertical path. As every dB of attenuation may be important, clouds may be of significance for frequencies as low as 10 GHz and somewhat lower (as well as for higher frequencies for which the attenuation is greater). Also as was indicated for the case of rain, dissipative attenuation is accompanied by an increase in noise and both effects contribute to a degradation in signal-to-noise ratio. Section 9.7 and Chap. 7 specify and discuss further the relation between attenuation and noise. Table 7.1 gives noise temperature and attenuation values for 12 different cloud models.

Although effects due to clouds do not become as intense as those due to rain, they occur for larger percentages of the time. For operations for which propagation impairments occurring for relatively high percentages of the time (such as 1 to 10 percent of greater) are pertinent (rather than or in addition to small percentages such as 0.01), the effects of clouds assume the greatest relative importance. In a study of effects of clouds by Slobin (1982), the United States has been divided into 15 regions shown in Fig. 9.15. For these regions data on cumulative distributions of zenith atmospheric noise temperatures due to clouds have been provided. Figure 9.16 shows such distributions for 5 of the 15 regions mentioned.

Very little data on attenuation due to sand and dust are available. For earth stations in desert areas where serious sand or dust storms are known to

occur, an allowance of 1 dB for attenuation due to sand and dust on a one-way path appears to be advisable if high-quality service is required.

Attenuation due to vegetation could be a factor for land mobile systems. The questions of whether to provide a margin for attenuation caused by vegetation and how much of a margin to provide if the answer to the first question is affirmative appear to be primarily questions of policy rather than questions that can be answered on the basis of quantitative, technical considerations. The view could be taken that vegetation causes a degree of shadowing and that providing for shadowing is impractical. Or one could arbitrarily specify a margin of a dB or two if it is planned to operate extensively in forested terrain. Background material on the effects of vegetation is presented in Sec. 5.3. Additional experimental data are required if this topic is to be treated in a satisfactory quantitative manner.

9.6 PROPAGATION EFFECTS ON MOBILE SYSTEMS

Two of the systems used as examples in Chap. 10 are mobile systems, and the link equations for these systems include margins for propagation effects.

9.7 RADIO NOISE

9.7.1 Basic Relations

The system noise temperature, T_{sys}, and the noise temperature, T_s, of the receiving system of Fig. 9.17 are given by

$$T_{sys} = T_A + (\ell_a - 1)T_o + \ell_a T_R \tag{9.34}$$

and

$$T_S = T_A g_a + (1 - g_a)T_o + T_R \tag{9.35}$$

In these equations, T_A is the antenna noise temperature, T_o is the attenuator temperature (taken here to be 290 K), and T_R is the receiver noise temperature. The factor g_a is the attenuator gain and has a maximum value of one; the factor ℓ_a equals $1/g_a$ and has a minimum value of one. If there is no attenuation $T_{sys} = T_s = T_A + T_R$.

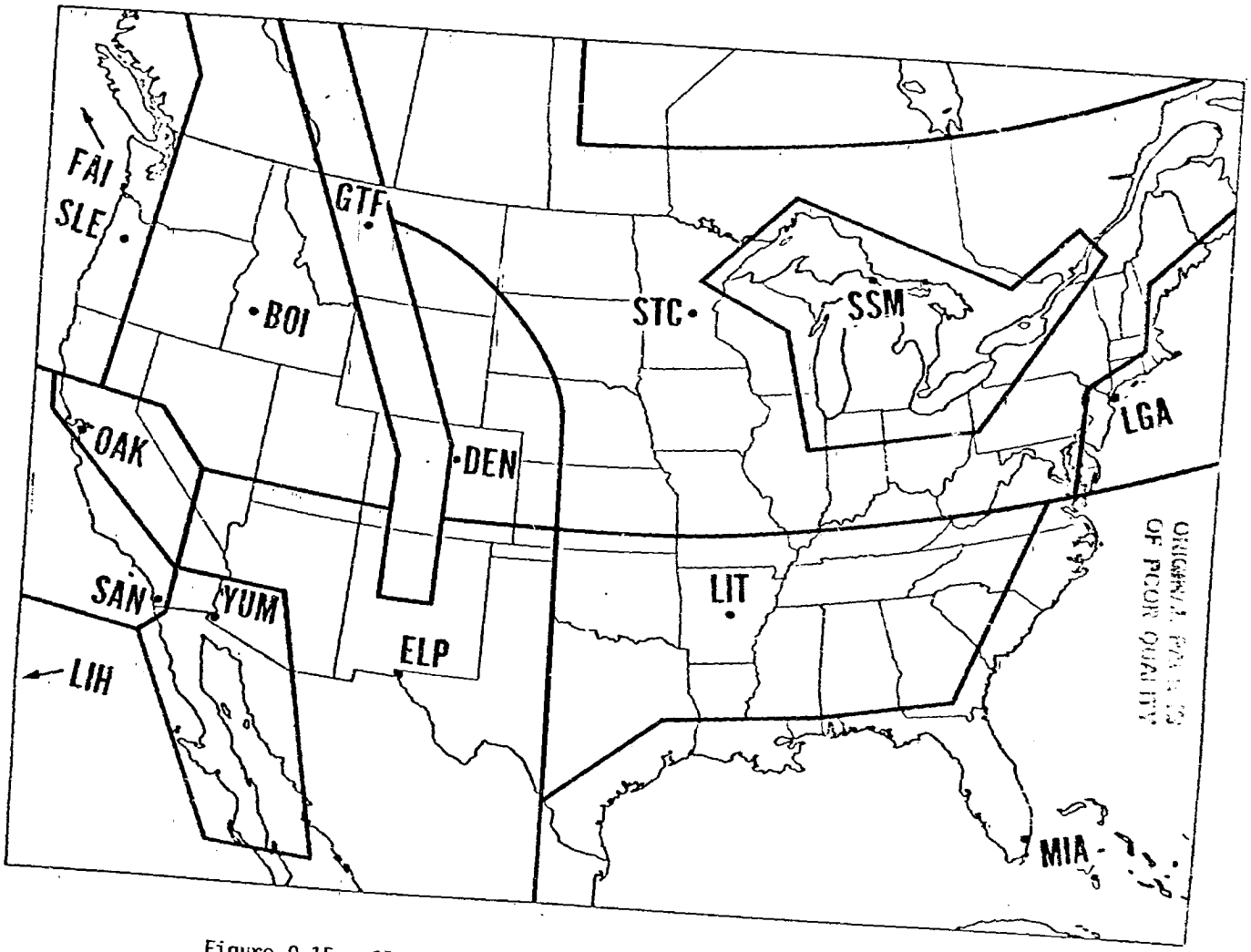

Figure 9.15. Cloud regions of the United States (Slobin, 1982).

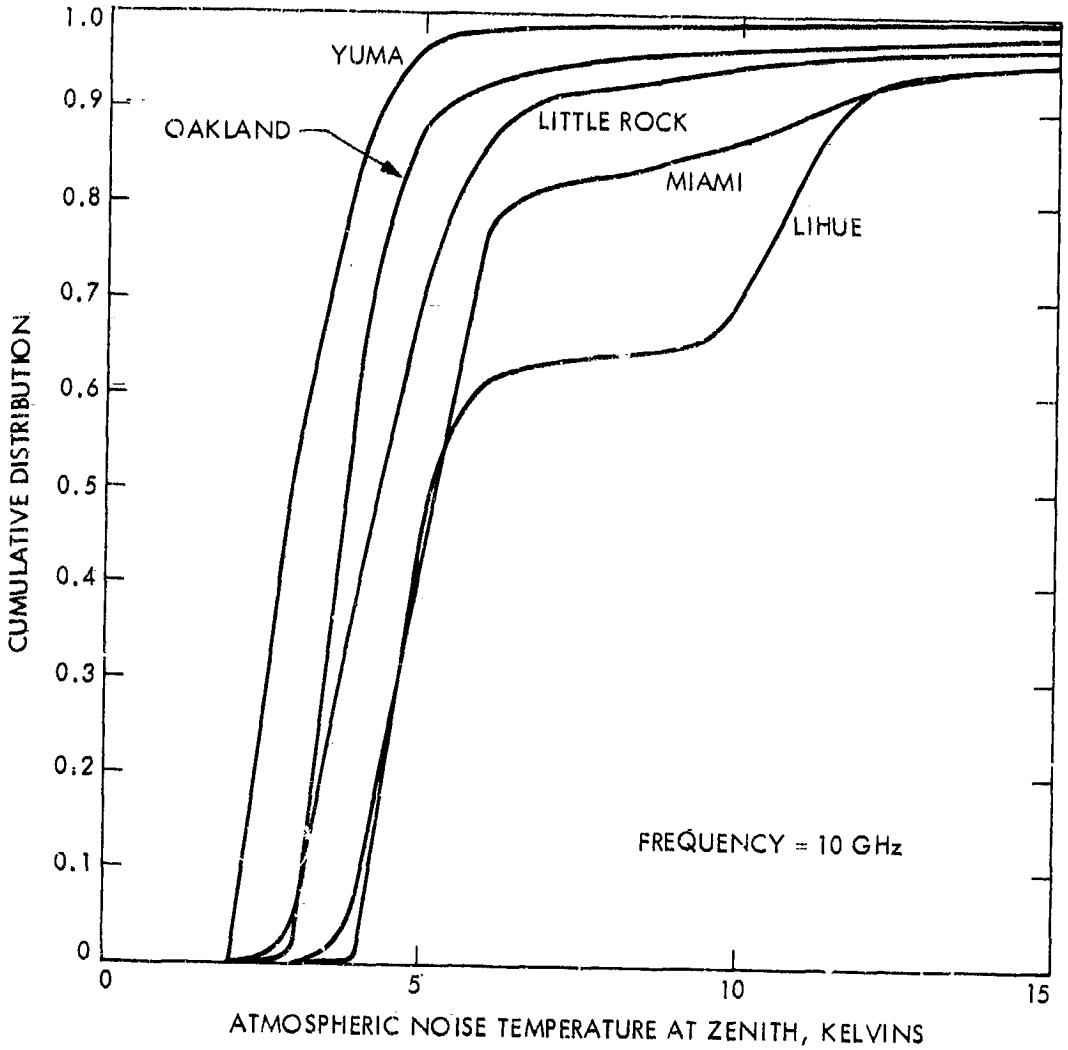

Figure 9.16. Total-year cumulative distributions of zenith atmospheric noise temperature for five regions at 10 GHz (Slobin, 1982).

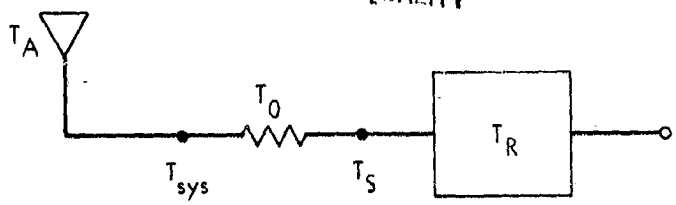

Figure 9.17. Noise temperatures of a receiving system.

The brightness temperature T_b, recorded when observing a noise source T_s through an absorbing region having an intrinsic temperature T_i and causing an attenuation represented by $e^{-\tau}$ is given by

$$T_b = T_s e^{-\tau} + T_i(1 - e^{-\tau}) \tag{9.36}$$

Note that g_a and $e^{-\tau}$ are alternative ways of representing attenuation and that if $T_R = 0$, Eqs. (9.35) and (9.36) are identical in form. In the above three equations, noise temperature is used as a measure of noise power. To obtain a value for noise power itself, multiply the temperature by Boltzmann's constant k (1.381×10^{-23} J/K) and by the bandwidth B. The differences in Eqs. (9.35) and (9.36) when $T_R = 0$ lies only in the fact that the attenuation of Eq. (9.35) is considered to be due to a transmission line or device whereas the attenuation of Eq. (9.36) is that experienced by a wave in propagating through an absorbing region of the atmosphere. In both cases the noise generated in the absorbing medium is thermal noise.

In the case of a satellite receiving system, T_A may be approximately equal to T_b. That is, the antenna noise may be primarily that due to an absorbing region along the path possibly plus noise of distant origin that is attenuated by the absorbing region. Actually other noise sources, such as terrestrial noise picked up by the antenna sidelobes and backlobe make at

least a small contribution to T_A as well. In some situations the value of the term $T_s e^{-\tau}$ of Eq. (9.58) may be much smaller than that of the second term and

$$T_b = T_i (1 - e^{-\tau}) \tag{9.37}$$

Also in some cases absorption may be negligible and then $T_b = T_A = T_s$.

Consider that a signal is propagating through an absorbing region, for example a region where rain is falling. The signal is attenuated by a factor $e^{-\tau}$ or by A_{dB} where $A = 4.34\,\tau$. Also the antenna receives noise given by Eq. (9.37) as $T_i (1 - e^{-\tau})$. Values of T_i have been determined empirically and may range from 260 to 290 K. The degradation in signal-to-noise ratio (C/X), compared to the case when no rain is present is given by

$$\Delta(C/X)_{dB} = A_{dB} + 10 \log \frac{T_2}{T_1}$$

or

$$\Delta(C/X)_{dB} = A_{dB} + 10 \log \frac{T_1 + T_b}{T_1} \tag{9.38}$$

where T_1 is the system noise temperature in the absence of the absorbing region and $T_2 = T_1 + T_b$ is the system noise temperature in the presence of the absorbing region

The concept presented here applies regardless of what the absorptive attenuation is due to (rain, clouds, or atmospheric gases). Note that the magnitude of $10 \log [(T_1 + T_b)/T_1]$ depends on the relative magnitudes of T_1 and T_b. If $T_1 >> T_b$, $10 \log [(T_1 + T_b)/T_1]$ is small. For a low-noise system, however, for which T_1 is small, $10 \log [(T_1 + T_b)/T_1]$ tends to be relatively large and may be larger than A_{dB}. Thus for low-noise systems and for attenuations up to about 10 dB, the degradation in the C/X ratio due to noise may be larger than that due to attenuation. This result is illustrated by Fig. 9.18 for $T_i = 280$ K.

9.7.2 Noise Sources

9.7.2.1 Extraterrestrial Noise

In the lower decade of the frequency range of this handbook from 100 MHz to 1000 MHz (1 GHz), extraterrestrial or cosmic noise is the dominant type of noise. Atmospheric thermal noise clearly dominates above 10 GHz, and the

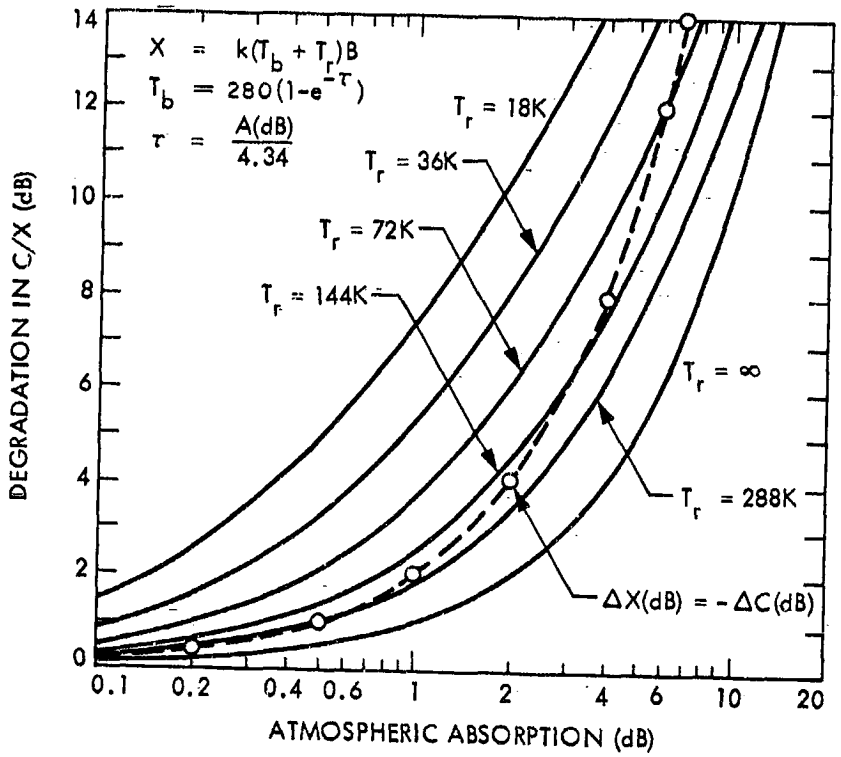

Figure 9.18. Degradation in signal-to-noise ratio (C/X) versus atmospheric absorption, for various values of T_1 (taking T_1 as equal to T_r).

frequency range from 1 to 10 GHz has the least noise of natural origin of the radio-frequency spectrum.

The most intense extraterrestrial radio noise sources other than the Sun are non-thermal and have positive spectral indices, which means that their noise powers increase with wavelength and decrease with frequency. Figure 7.11 shows radio emission from that part of the celestial sphere of interest to telecommunications utilizing geostationary satellites (declination angles from +8.7° to -8.7°) and includes data for larger declination angles as well. The plot is in celestial coordinates with declination angle δ measured from the celestial equator which is an extension into space of the Earth's equator. Declination angles of $\pm$ 8.7° correspond to the highest possible latitudes ($\pm$ 81.3°) which can be used for communication with geostationary satellites. For an earth station in the northern hemisphere at a latitude of θ', the extraterrestrial noise received is that from a strip of sky behind the satellite having a declination angle δ given by

$$\delta = -\tan^{-1}\left[\frac{\sin\theta'}{6.6 - \cos\theta'}\right] \qquad (9.39)$$

and equals -6.3° for $\theta' = 40°$. The fraction $\sin\theta'/(6.6 - \cos\theta')$ is a ratio of distances measured in earth radii, geostationary satellites being at 6.6 earth radii from the center of the Earth. By examination of Fig. 7.11 (or a clearer original version) and from the accompanying discussion of Chap. 7, it can be determined that the maximum noise temperature at 250 MHz for an earth station at a latitude of 40° that is communicating with a geostationary satellite is 850 K. For other frequencies an equivalent blackbody temperature T can be determined by assuming that T varies as f^{-2+n} where n is the spectral index and can be taken as 0.75 for frequencies less than 250 MHz (Smith, 1982a). In addition, for microwave frequencies, the microwave background temperature of 2.7 K should be included in T_b, the total brightness temperature. Thus for a microwave frequency f_i

$$T_b(f_i) = T_b(f_0)\left(\frac{f_i}{f_0}\right)^{-2.75} + 2.7 \text{ K} \qquad (9.40)$$

where f_0 = 250 MHz.

9.7.2.2. Atmospheric Thermal Noise

Thermal noise generated by the atmospheric gases, clouds, and rain is related to attenuation in these same media by Eqs. (9.36) and (9.37) of Sec. 9.7.1. Knowledge of attenuations and the intrinsic temperatures of the media allow estimation of noise temperatures.

Detailed analyses of the attenuation and noise due to gases (Smith, 1981, 1982b) and clouds (Slobin, 1981, 1982) have been prepared. Values of attenuation due to gases are shown in Fig. 3.11 and discussed in Sec. 9.3. Table 5.3 provides some data on attenuation and atmospheric thermal noise due to clouds, and Table 7.1 presents more detailed information on the same topics. For many purposes the attenuation and noise due to the gases can be neglected for frequencies of 10 GHz and lower, but for low-angle paths and for coordination-area analyses the effects of oxygen may need to be taken into account. As discussed in Sec. 9.5, the effects of clouds may need to be taken into account for frequencies of 10 GHz and somewhat lower.

9.7.2.3 Terrestrial Noise

A principal consideration about terrestrial noise is that the receiving antenna of an uplink to a satellite points at the Earth which has commonly been taken to be at a temperature of 290 K. Evidence is accumulating, however, that the brightness temperature of the Earth may be considerably less than 290 K. The receiving antenna of a downlink from a satellite points at the sky but nevertheless picks up at least a small amount of terrestrial noise, ranging from one or a few degrees for a very-high-quality antenna to tens of degrees or more.

Example 9.8 Decrease in Signal-to-noise Ratio Caused by Absorbing Region

a. Consider a receiving system with a system noise temperature $T_{sys} = T_1 =$ 100 K in the absence of attenuation along the transmission path. Assume next that an attenuation of 1 dB occurs along the path in an absorbing region where the intrinsic temperature is 280 K. Because of the absorbing region T_{sys} increases to a new value T_2. This example demonstrates how to

calculate T_2 and the total decrease, $\Delta(C/X)_{dB}$, in signal-to-noise ratio. The relation between τ of $T_b = T_1(1 - e^{-\tau})$ and attenuation A in dB is

$$\tau = \frac{A_{dB}}{4.34}$$

For this case $\tau = 1/4.34 = 0.23$ and $e^{-\tau} = 0.794$. Thus using $T_b = T_1(1 - e^{-\tau})$

$$T_b = 280\ (1 - 0.794) = 57.6\ K$$

and from Eq. (9.38)

$$\Delta(C/X)_{dB} = 1 + 10 \log \frac{100 + 57.6}{100}$$

$$= 1 + 1.98 = 2.98\ dB$$

b. Next determine $(C/X)_{dB}$ for the extremely low value of T_1 of 25 K, with conditions otherwise as in part a. Now

$$(C/X)_{dB} = 1 + 10 \log \frac{25 + 57.6}{25}$$

$$= 1 + 5.19 = 6.19\ dB$$

For the very-low-noise system of part b, the total degradation in the C/X ratio is over six times that due to attenuation alone, and even for the T_{sys} of 100 K of part a. the total degradation is three times that for attenuation alone.

c. For the attenuation due to rain of 2.49 dB of Example 9.5, assuming T_1 = 100K,

$$\tau = \frac{2.49}{4.34} = 0.574 \text{ and } e^{-\tau} = 0.563$$

Then

$$T_b = 280(1 - 0.563) = 122.24$$

and

$$(C/X)_{dB} = 2.49 + 10 \log \frac{100 + 122.24}{100}$$

$$= 2.49 + 3.47$$

$$= 5.96\ dB$$

REFERENCES

Aarons, J., H. E. Whitney, E. Mackenzie, and S. Basu, "Microwave equatorial scintillation intensity during solar maximum," Radio Science, vol. 10, pp. 939-945, Sept.-Oct. 1981.

Aarons, J. "Global morphology of ionospheric scintillations," Proc. IEEE, vol. 70, pp. 360-378, April 1982.

Bean, B. R. and E. J. Dutton, Radio Meteorology. Washington, D.C.: Supt. of Documents, U.S. Government Printing Office, 1966.

Bostian, C. W. and J. E. Allnut, "Ice-crystal depolarization on satellite-earth microwave radio paths," Proc. IEEE, vol. 126, p. 951, 1979.

CCIR, "Ionospheric effects upon earth-space propagation," Report 263, Vol. VI, Propagation in Ionized Media, Recommendations and Reports of the CCIR, 1978. Geneva: Int. Telecomm. Union, 1978.

CCIR, "Propagation data for maritime and land mobile satellite systems-above 100 MHz," Report 884, Vol. V, Propagation in Non-ionized Media, Recommendations and Reports of the CCIR, 1982. Geneva: Int. Telecomm. Union, 1982a.

CCIR, "Effects of large-scale tropospheric refraction on radiowave propagation," Report 718, Vol. V, Propagation in Non-ionized Media, Recommendations and Reports of the CCIR, 1982. Geneva: Int. Telecomm. Union, 1982b.

CCIR, "Radiometeorological data," Report 563, Vol. V., Propagation in Non-ionized Media, Recommendations and Reports of the CCIR, 1982. Geneva: Int. Telecomm. Union, 1982c.

CCIR, "Attenuation by precipitation and other atmospheric particles," Report 721, Vol. V, Propagation in Non-ionized Media, Recommendations and Reports of the CCIR, 1982. Geneva: Int. Telecomm. Union, 1982d.

CCIR, "Propagation data required for space telecommunication systems," Report 564, Vol. V, Propagation in Non-ionized Media, Recommendations and Reports of the CCIR, 1982. Geneva: Int. Telecomm. Union, 1982e.

CCIR, "Cross-polarization due to the atmosphere," Report 722, Vol. V, Propagation in Non-ionized Media, Recommendations and Reports of the CCIR, 1982. Geneva: Int. Telecomm. Union, 1982f.

Chu, T. S., "Microwave depolarization of an earth-space path," Bell System Tech. Jour., vol. 59, pp. 987-1007, July-Aug. 1980.

Cox, D. C., "Depolarization of radio waves by atmospheric hydrometers in earth-space paths: a review," Radio Science, vol. 16, pp. 781-812, Sept.-Oct. 1981.

Crane, R. K., "Refraction effects in the neutral atmosphere," in Methods of Experimental Physics, Vol. 12, Astrophysics, Part B: Radio Telescopes (M. L. Meeks, ed.), pp. 186-200. New York: Academic Press, 1976.

Crane, R. K., "Prediction of attenuation by rain," IEEE Trans. on Communications, vol. COM-28, pp. 1717-1733, Sept. 1980a.

Crane, R. K., "Earth-space and terrestrial microwave propagation-estimation of rain attenuation with the global model," ERT Technical Report P-A414-TR, prepared for NASA Headquarters, October 1980b.

Davies, K., Ionospheric Radio Propagation. Washington, D.C.: Sup. of Documents, U.S. Government Printing Office, 1965.

Davies, K., "Recent progress in satellite radio beacon studies with particular emphasis on the ATS-6 radio beacon experiment," Space Science Reviews, vol. 25, pp. 357-430, April 1980.

Dawson, E. and L. R. Newitt, "The magnetic poles of the Earth," J. Geomag. Geoelectr., vol. 34, no. 4, pp. 225-240, 1982.

Environmental Data Service, Values of Earth's Magnetic Field From Mathematical Models (Availability of Recent Geomagnetic Field Models and Associated Data Services), 81-TGB-18, 1981. National Oceanic and Atmospheric Admin., EDIS/NGSDC (D62), 325 Broadway, Boulder CO 80303. Telephone: (303) 497-6478, FTS: 320-6478.

Fang, D. J., F. T. Tseng, and T. O. Calvit, "A low elevation angle propagation measurement of 1.5-GHz satellite signals in the Gulf of Mexico," IEEE Trans. on Antennas and Propagation, vol. AP-30, pp. 10-15, Jan. 1982.

Flock, W. L., "Propagation at 36,000 MC in the Los Angeles basin," IRE Trans. on Antennas and Propagation, vol. AP-8, pp. 235-241, May 1960.

Flock, W. L., S. D. Slobin, and E. K. Smith, "Propagation effects on radio range and noise in earth-space telecommunications," Radio Science, vol. 17, pp. 1411-1424, Nov.-Dec. 1982.

Fremow, E. J., "A computer model of high-latitude scintillation," 82-0150, Technical Papers, Aerospace Sciences Meeting, 20th, Orlando, FL, Jan. 11-14, 1982, 9 pp. New York: American Institute of Aeronautics and Astronautics, 1982.

Hopfield, H. S., "Tropospheric effect on electromagnetically measured range: prediction form surface weather data," Radio Science, vol. 6, pp. 357-367, March 1971.

Howell, R. G., "Cross-polar phase variations at 20 and 30 GHz on a satellite-earth path," Electronic Letters, vol. 13, pp. 405-406, 1977.

Ippolito, L. J., R. D. Kaul, and R. G. Wallace, Propagation Effects Handbook for Satellite Systems Design, A Summary of Propagation Impairments on 10 to 100 GHz Satellite Links With Techniques for System Design, NASA Reference Pub. 1082, Washington, D.C.: NASA Headquarters, 1981.

Klobuchar, J. A. (leader) and Working Group, "B. Transionospheric propagation predictions," in R. F. Donnelly (ed.), Vol. 2: Working Group Reports and Reviews of Solar-Terrestrial Predictions Proceedings, p. 217, Boulder, CO: Environmental Research Labs, NOAA, 1978.

Klobuchar, J. A., "Ionospheric effects on satellite navigation and air traffic control systems," in Recent Advances in Radio and Optical Propagation for Modern Communications, Navigation, and Detection Systems, AGARD Proceedings-LS-93, ISBN 92-835-1280-4. NTIS: Springfield, VA 22161, April 1978.

Kobayashi, T., "Pre-estimation of cross-polarization discrimination due to rain," J. Radio Res. Labs. (Japan), vol. 23, pp. [illegible]-64, March 1976.

Lee, M. C., A DasGupta, J. A. Klobuchar, S. Basu, and S. Basu, "Depolarization of VHF geostationary satellite signals near the equatorial anomaly crests," Radio Science, vol. 17, pp. 399-409, Mar.-Apr. 1982.

Lee, W. C. Y., "An approximate method for obtaining rain statistics for use in signal attenuation estimating," IEEE Trans. on Antennas and Propagation, vol. AP-27, pp. 407-413, May 1979.

Lin, S. H., "Nationwide long-term rain rate statistics and empirical calculation of 11-GHz microwave rain attenuation," Bell System Tech. Jour., vol. 56, pp. 1581-1604, Nov. 1977.

McEwan, N. J., P. A. Watson, A. W. Dissanayake, D. P. Haworth, and V. T. Vakili, "Crosspolarization from high altitude hydrometeors on a 20 GHz satellite radio path," Electronics Letters, vol. 13, pp. 13-14, 1977.

Millman, G. H. and G. M. Reinsmith, An Analysis of the Incoherent Scatter-Faraday Rotation Technique for Ionospheric Propagation Error Correction (R 74EMH2). Syracuse, NY 13221: General Electric Co., Feb. 1974. [Available from HMES Technical Publications, Box 1122 (CSPA-24), Syracuse, N.Y. 13201.]

Millman, G. H., Ionospheric Electron Content Effects on Earth-space Radio Propagation - A Review (R80EMH11). Syracuse, NY 13221: General Electric Co., Dec.1980.

Minakoshi, H. et al., "Severe ionospheric scintillation associated with magnetic storm on March 22, 1979," J. Radio Res. Labs. (Japan), vol. 28,pp. 1-9, March-July 1981.

Miya, K., Satellite Communications Technology. KDD Bldg. 3-2, Nishi-Shinjuku 2-chome, Shinjuku-ku, Tokyo/60, Japan, 1981.

Olsen, R. L., D. V. Rogers, and D. B. Hodge, "The aR^b relation in the calculation of rain attenuation," IEEE Trans. on Antennas and Propagation, vol. AP-26, pp. 318-329, March 1978.

Slobin, S. D., Microwave Noise Temperature and Attenuation of Clouds at Frequencies Below 50 GHz, JPL Publication 81-46, Pasadena, CA: Jet Propulsion Lab., 1981.

Slobin, S. D., "Microwave noise temperature and attenuation of clouds: statistics of these effects at various sites in the United States, Alaska, and Hawaii," Radio Science, vol. 17, pp. 1443-1454, Nov.-Dec. 1982.

Smith, E. K. and J. W. Waters, Microwave Atenuation and Brightness Temperature Due to the Gaseous Atmosphere, A Comparison of JPL and CCIR Values, JPL Publication 81-81, Pasadena, CA: Jet Propulsion Lab., 1981.

Smith, E. K., "The natural radio noise source environment," Proceedings of 1982 IEEE International Symposium on Electromagnetic Compatibility, Santa Clara, CA (Sept. 6-8, 1982). New York: The Institute of Electrical and Electronics Engineers, 1982a.

Smith, E. K., "Centimeter and millimeter wave attenuation and brightness-temperature due to atmospheric oxygen and water vapor," Radio Science, vol. 17, pp. 1455-1464, Nov.-Dec. 1982b.

Spilker, J. J., Digital Communication by Satellite. Englewood Cliffs, NJ: Prentice-Hall, 1977.

Strickland, J. I, R. I. Olsen, and H. L. Werstiyk, "Measurements on low angle fading in the Canadian Arctic," Ann. Tellecomm., vol. 32, pp. 530-535, 1977.

Taur, R. R., "Rain depolarization measurements on a satellite-earth propagation path at 4 GHz," IEEE Trans. on Antennas and Propagation, vol. AP=23, pp. 854-858, Nov. 1975.

Thompson, M. C., L. E. Wood, H. B. Janes, and D. Smith, "Phase and amplitude scintillations in the 10 to 40 GHz band," IEEE Trans. on Antennas and Propagation, vol. AP-23, pp. 792-797, Nov. 1975.

Titheridge, J. E., "Determination of ionospheric electron content from the Faraday rotation of geostationary satellite signals," Planet. Space Sci., vol. 20, pp. 353-369, 1972.

C-5

APPENDIX 9.1

DETERMINATION OF $\bar{B}_L$ USING DIPOLE MODEL

In this appendix, a procedure is described for determining a value of $\bar{B}_L$, for estimating Faraday rotation as a function of ionospheric TEC. The procedure can be applied to any ionospheric height; it is recommended that the value at a height of 400 km be used in the absence of information pointing to a different choice. For a particular earth-station location and path, the geographic latitude and longitude of the intersection of the path with the 400 km height level can be determined by graphical or other means.

The dipole model may be described by assuming a scalar magnetic potential V given by $V = -M \cos\theta / r^2$, where M is dipole magnetic moment, θ is the angle measured from the dipole axis, and r is the distance from the center of the Earth. Then $F = -\nabla V$, where F is the total magnetic flux density vector and has a vertical component Z given by $Z = \partial V/\partial r = 2 M \cos\theta / r^3$ and a horizontal component H given by $H = \frac{1}{r}\frac{\partial V}{\partial \theta} = M \sin\theta / r^3$. The dipole axis should ideally pass through the observed north and south magnetic dip poles but their positions, which vary with time, are not directly opposite from each other or consistent with a purely dipole field. The north magnetic dip pole is near Ellef Ringnes Island in the Canadian Arctic. The axis of the dipole model that best approximates the observed field overall intersects the Earth's surface at different locations, namely the north and south geomagnetic poles. The north geomagnetic pole is in Greenland, very close to the northwest coast. Its position was taken to be 78.3^{o}N and 69^{o}W in 1965 (Davies, 1965). In a 1982 paper on the magnetic poles of the Earth, Dawson and Newitt (1982) give values of 78.8^{o}N and 70.9^{o}W.

Rather than specifying a value for M, the magnetic moment, the expressions for Z and H can be given in terms of B_0, the magnetic flux density at the Earth's surface at the geomagnetic equator. They then become

$$Z = 2 B_0 \left(\frac{a^3}{r}\right) \cos\theta \qquad \text{(A9.1)}$$

and

$$H = B_0 \left(\frac{a}{r}\right)^3 \sin\theta \qquad \text{(A9.2)}$$

with

$$F = (H^2 + Z^2)^{1/2} \tag{A9.3}$$

where a is the Earth's radius (mean value about 6371 km). Substituting the expressions for H and Z into Eq. (A9.3), it becomes

$$\begin{aligned} F &= B_0 \left(\frac{a}{r}\right)^3 [\sin^2 \theta + 4 \cos^2 \theta]^{1/2} \\ &= B_0 \left(\frac{a}{r}\right)^3 [\sin^2 \theta + 3 \cos^2 \theta + 1 - \sin^2 \theta]^{1/2} \\ &= B_0 \left(\frac{a}{r}\right)^3 [1 + 3 \cos^2 \theta]^{1/2} \end{aligned} \tag{A9.4}$$

Equations (A9.1), (A9.2), and (A9.4) refer to the angle θ measure from the polar axis, but for some purposes it is more convenient to use the magnetic latitude θ', which is measured from the magnetic equator. In terms of latitude, θ', the expressions become

$$Z = 2 B_0 \left(\frac{a}{r}\right)^3 \sin \theta' \tag{A9.5}$$

$$H = B_0 \left(\frac{a}{r}\right)^3 \cos \theta' \tag{A9.6}$$

and

$$F = B_0 \left(\frac{a}{r}\right)^3 [1 + 3 \sin^2 \theta']^{1/2} \tag{A9.7}$$

If in Eq. (A9.7) F is held constant, it develops that the radial coordinate r corresponding to a particular value of F is given by

$$r = k' a [1 + 3 \sin^2 \theta']^{1/6} \tag{A9.8}$$

where

$$k' = (B_0/F)^{1/3}$$

The quantity F represents the magnitude of the total magnetic flux density. To obtain a plot showing the direction of the magnetic flux density vector (or showing the magnetic flux lines), note that the direction of the vector at a particular point is as indicated by

$$\frac{dr}{r d\theta} = \frac{Z}{H} \tag{A9.9}$$

where an increment of length along a field line, $d\ell$, has a component dr in the radial direction and a component $rd\theta$ in the horizontal direction. Rearranging Eq. (A9.9) leads to

$$\frac{dr}{r} = \frac{Z}{H}\, d\theta = 2 \cot\theta \; d\theta \tag{A9.10}$$

Integrating this expression from the point on the geomagnetic equator where r = ka to r = r and from $\theta = \pi/2$ to

$$\int_{ka}^{r} \frac{dr}{r} = \int_{\pi/2}^{\theta} 2 \cot\theta \; d\theta$$

and

$$\ell n \frac{r}{ka} = 2 \ell n \sin\theta = \ell n \sin^2\theta$$

from which

$$r = ka \sin^2\theta \tag{A9.11}$$

or, in terms of latitude θ',

$$r = ka \cos^2\theta' \tag{A9.12}$$

Note that a particular field line that crosses the equator at r = ka will intersect the Earth's surface at $\cos\theta' = (1/k)^{1/2}$.

An additional parameter describing the Earth's magnetic field is the dip angle I which can be determined from

$$\tan I = \frac{Z}{H} = 2 \cot\theta = 2 \tan\theta' \tag{A9.13}$$

To estimate the value of $\overline{B}_L$ for a particular path, one can first determine the geographic coordinates of the point where the path intersects the 400 km height level. Then one can convert the locations of the ground station, the 400 km intercept, and the satellite to the spherical coordinates of the Earth's geomagnetic field. The applicable relations are

$$\sin\theta'_m = \sin\theta'_g \sin\theta'_p + \cos\theta'_g \cos\theta'_p \cos(\phi_g - \phi_p) \tag{A9.14}$$

and

$$\sin\phi_m = \frac{\cos\theta'_g \sin(\phi_g - \phi_p)}{\cos\theta'_m} \tag{A9.15}$$

where the primes represent latitudinal quantities, θ'_m is the magnetic latitude of the location of interest, θ'_g is its geographic latitude, θ'_p is the geographic latitude of the north geomagnetic pole (the intersection of the dipole axis and the Earth's surface), ϕ_m is the magnetic longitude of the location of interest, ϕ_g is its geographic longitude, and ϕ_p is the geographic longitude of the north geomagnetic pole.

Having expressed all quantities in magnetic coordinates [previously the subscript m was not used but Eqs. (A9.1)-(A9.13) are all in magnetic coordinates], one can then obtain vector representations of d, the path from the earth station to the satellite and F, the total geomagnetic field at the 400 km intercept. One can then determine the angle between the magnetic field and the path at 400 km by using

$$Fd \cos \theta_B = \mathbf{F} \cdot \mathbf{d} \tag{A9.16}$$

where θ_B is the angle desired and $\mathbf{F} \cdot \mathbf{d}$ is the scalar dot product of vectors. The magnetic field F and the locations of the satellite (S) and the earth station (G) can be most conveniently described in spherical coordinates initially, but to find $\mathbf{d} = \mathbf{S} - \mathbf{G}$ and to take the dot product they are converted to rectangular coordinates by use of

$$\mathbf{a}_r = \sin\theta \cos\phi \, \mathbf{a}_x + \sin\theta \sin\phi \, \mathbf{a}_y + \cos\theta \, \mathbf{a}_z \tag{A9.17}$$

$$\mathbf{a}_\theta = \cos\theta \cos\phi \, \mathbf{a}_x + \cos\theta \sin\phi \, \mathbf{a}_y - \sin\theta \, \mathbf{a}_z \tag{A9.18}$$

for F and

$$x = r \sin\theta \cos\phi \tag{A9.19}$$

$$y = r \sin\theta \sin\phi \tag{A9.20}$$

$$z = r \cos\theta \tag{A9.21}$$

for the locations of the earth station and satellite. Note that in these expressions θ is colatitude, the polar angle of spherical coordinates, rather than latitude θ' ($\theta' = \pi/2 - \theta$). Once the magnitude of F and the angle θ_B are known one has $\overline{B}_L$ from

$$\overline{B}_L = F \cos\theta_B \tag{A9.22}$$

As shown by Eq. (9.2), Faraday rotation is proportional to $\overline{B}_L$ and TEC and inversely proportional to frequency squared. Section 9.2.2 considers the value of the TEC.

CHAPTER 10
SPACE-COMMUNICATIONS SYSTEM DESIGN

10.1 INTRODUCTION

10.1.1 Performance Requirements

The role of propagation phenomena in earth-space telecommunications system design is illustrated in this final chapter, and it is necessary to include consideration of related aspects of design as well. The propagation loss L and the system noise temperature T_{sys}, introduced in Chap. 1, appear in the telecommunication link power budget equation, and reference to system design in this chapter refers primarily to formulation of link budgets. In earlier chapters, including Chap. 9, Estimation of Propagation Impairments, this handbook treats additional topics, including time and range delay, phase advance and Doppler frequency, and refractive bending. Also Chap. 8 is devoted to propagation effects on interference and determination of coordination area.

The system designer may have the function of meeting system requirements posed by the user, but in the process of attempting to do so it may develop that the requirements present problems and may need to be modified. To minimize this possibility, it is advantageous for the system designer, or someone with experience with system design and performance, to be involved in specifying the requirements. The design of a complicated system like a telecommunication system, however, is in any case largely an iterative process, starting with a preliminary design, rather than a true synthesis. The amount of readily available information dealing specifically with system design is limited. One useful treatment of the subject has been provided by Ippolito, Kaul, and Wallace (1981) in the final chapter of NASA Reference Publication 1082 for the design of systems operating at frequencies from 10 to 100 GHz.

Some minimum signal-to-noise ratio is needed for satisfactory operation of a telecommunications system, and information must be available or a decision must be reached in some way as to what this value is. We will use C/X generally as in Eq. (1.6) for this ratio but certain related quantities may be

used instead in particular cases]. Because of the characteristics of the propagation medium, C/X tends to be a random variable and, as it is usually impractical to design a system so the C/X never drops below any particular desirable level, a specification should normally be made, if possible, of the permissable percentage of time for which C/X may be below the desired level. This specification also defines the signal availability, namely the percentage of time that a specified C/X ratio should be available. Alternatively, or additionally, a specification may be made concerning outage, such as the mean outage duration, the distribution function applying to the time until the next outage, etc. In some cases the statistical nature of the phenomena affecting C/X may not be known, and it may not be possible to design a system to have a predetermined availability or specific outage characteristics. In such cases, one may nevertheless need to estimate the margins to be provided for the phenomena under consideration. For example, a margin of so many dB must be allotted in some cases to take account of the reduction in signal level associated with ionospheric scintillation or multipath fading due to reflections from terrain even though a satisfactory statistical description of these phenomena may not be available.

10.1.2 Digital Systems

For digital systems performance quality is generally measured in terms of the bit error rate (BER), and the BER is a function of the energy-per-bit to noise-power-density ratio, E_b/N_o. (When referring specifically to digital systems, we will use N_o instead of the X_o of Chap. 1 and elsewhere). The energy per bit E_b is related to C, the carrier power, by

$$E_b R = C \tag{10.1}$$

where R is the information rate in bits per second. Therefore,

$$\frac{E_b}{N_o} = \frac{C}{N_o R} \tag{10.2}$$

Equation (10.2) shows that $C/N_o = RE_b/N_o$ and that if bandwidth B equals bit rate R, $E_b/N_o = C/N_oB = C/N$ (same quantity as C/X). More generally $C/N = E_b R/N_oB$. The ratio R/B depends on the type of modulation and coding used. For uncoded binary phase-shift modulation (BFSK) employing phase values of 0°

and 180°, B may be equal to R. For uncoded quadriphase modulation (QFSK) employing phase values of 0°, 90°, 180°, and 270°, the bandwidth B may be only half the bit rate R, as for each phase there are two corresponding bits (Feher, 1983; Freeman, 1981). Coding of digital transmissions is used as a means of minimizing errors or to reduce the needed E_b/N_0 ratio and therefore the power C needed for a fixed BER. Coding involves adding redundant symbols to an information symbol sequence and requires additional bandwidth beyond that of the original uncoded signal. The ratio of the number of information bearing symbols to the total number is known as the rate of the code and has values such as 3/4, 2/3, etc., with 1/3 usually being the minimum value of the rate that is used. A number of error correcting codes and procedures for decoding at the receiving terminal have been devised. Convolutional coding and Viterbi decoding (Heller and Jacobs, 1971) are widely used. The performance of a Viterbi decoder depends upon the rate R, the number K of consecutive information bits encoded (e.g., 4, 6, or 8), the levels of quantization Q (1 to 8), and path length (e.g., 8-, 16-, or 32-bit). Figure 10.1 shows illustrative plots of BER versus E_b/N_0 for Viterbi decoding and for no coding.

10.1.3 Analog Systems

The allowable noise in analog systems used for voice communications may be specified in pWOp, standing for noise power in picowatts (pW) at a point of zero relative level (0) with psophometric weighting (p) utilized. We consider here how the system designer, given the permissable value of pWOp, can determine the corresponding minimum signal-to-noise ratio C/X.

In Recommendation 353, the CCIR (1978) advises that the noise power at a point of zero relative level in any telephone channel used in FDM-FM (frequency division multiplex-frequency modulation) telephony in the fixed satellite service should not exceed the following values:

10,000 pWOp psophometrically-weighted one-minute mean power for more than 20 percent of any month

50,000 pWOp psophometrically-weighted one-minute mean power for more than 0.3 percent of any month

1,000,000 pWO unweighted power (with an integration time of 5 ms) for more than 0.01 percent of any year.

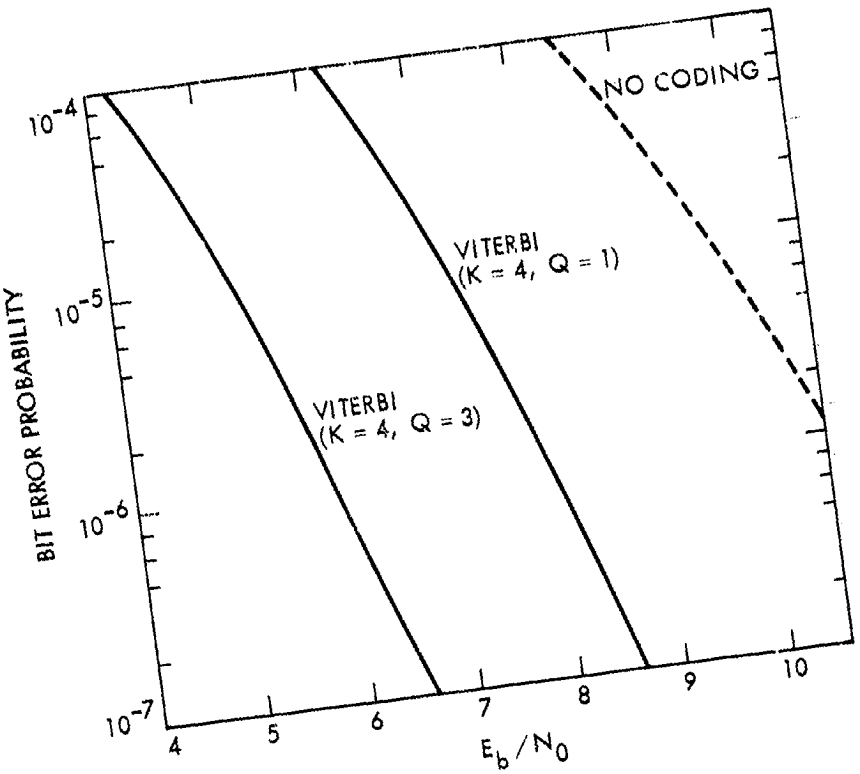

Figure 10.1. Bit error rate versus E_b/N_0 (Van Trees, 1979).

For RF levels above the FM threshold (commonly 10 dB above the noise level), the noise expressed in pW0p can be related to carrier power C by (GTE, 1972)

$$10 \log pW0p = - C_{dBm} - 48.6 + F_{dB} - 20 \log \Delta f/f_{ch} \qquad (10.3)$$

where F is the receiver noise figure, Δf is the peak frequency deviation of the channel for a signal of test tone level, and f_{ch} is the center frequency occupied by the channel in the baseband.

Solving for C_{dBm} and then subtracting $10 \log kT = 10 \log kT_o + F_{dB} = -174$ dBm + F_{dB} for $T_o = 290$ K, yields

$$(C/X_o)_{dB} = (C/kT)_{dB} = 125.4 - 20 \log \Delta f/f_{ch} - 10 \log pW0p \qquad (10.4)$$

For determining C/X, use $X = X_o B$ where B is bandwidth. Values of $20 \log \Delta f/f_{ch}$ are given in GTE (1972) as -1.82 dB for an 120-channel system with emphasis, -9.2 dB for a 300-channel system with emphasis, etc.

10.1.4 Allocation of Noise and Signal-to-Noise Ratio

A communications satellite system consisting of an uplink and a downlink is subject to thermal noise generated in the uplink and downlink, to intermodulation noise generated in the satellite transponder in an FDMA system, and to interfering signals which may be received on the uplink or downlink or both. Considering all the individual noise sources to be additive at the downlink receiver input terminal, the ratio of carrier power C to total noise density $(X_o)_T$ is given by

$$\frac{C}{(X_o)_T} = \frac{C}{(X_o)_U + (X_o)_D + (X_o)_{IM} + (X_o)_I} \qquad (10.5)$$

where $(X_o)_D$ is generated in the downlink, $(X_o)_{IM}$ represents intermodulation noise, and $(X_o)_I$ represents interference noise. The quantity $(X_o)_U$ is derived from but not equal to the noise $(X'_o)_U$ at the satellite (uplink) receiver input terminal. In particular $(X_o)_U = (X'_o)_U \, g/L_t$ where g is the gain of the satellite transponder and L_t is the total downlink loss factor (defined so as to be

greater than unity). Starting from. Eq. (10.5), it can be shown by a process of algebraic manipulation that

$$\frac{1}{(C/X_o)_T} = \frac{1}{(C/X_o)_U} + \frac{1}{(C/X_o)_D} + \frac{1}{(C/X_o)_{IM}} + \frac{1}{(C/X_o)_I} \qquad (10.6)$$

The ratio $(C/X_o)_T$ appears at the downlink receiver input terminal; the ratio $(C/X_o)_D$ would be observed at this location if the input signal for the downlink was noiseless and interference noise was negligible. The ratio $(C/X_o)_U$ applies at the satellite-receiver input (uplink) terminal and also at the downlink (earth station) receiver input terminal if the X_o in the latter case is recognized as $(X_o)_U$ mentioned above. [The values of C at the two locations are related in the same way as $(X_o)_U$ and $(X'_o)_U$.]

If one knows the values of all of the terms of Eq. (10.6) but one, that unknown quantity can be determined from Eq. (10.6).

The noise contributions to a satellite system can be divided or allotted in various ways. The total allowable noise of 10,000 pW0p is separated in the INTELSAT system noise budget into the three major categories shown below.

Space segment	8,000	pW0p
Earth stations	1,000	
Terrestrial interference	1,000	
Total noise	10,000	pW0p

By the space segment, reference is made to noise in the uplink and downlink, intermodulation noise generated in the satellite transponder, and interference other than terrestrial interference.

10.2 DIVERSITY RECEPTION

Diversity reception of several types, most prominently site diversity, space diversity, and frequency diversity, may be advantageous for particular applications. For satellite communications site diversity can be used to reduce the effect of attenuation due to rain. Site diversity takes advantage

of the fact that high rain-rates tend to occur only over areas of limited extent. For example, the probability that rain rates greater than 50 mm/h will occur jointly at two locations 20 km apart is reported to be about 1/15th the probability that a rain rate greater than 50-mm/h will occur at one location (Miya, 1981). Most interest in site diversity has been directed to frequencies above 10 GHz for which attenuation due to rain is most severe (Ippolito, Kaul, and Wallace, 1981).

For terrestrial line-of-sight paths, space and frequency diversity are used to combat fading due to atmospheric multipath fading and reflections from surfaces (GTE, 1972). The form of space diversity most commonly used involves vertical separation of two receiving antennas on the same tower.

The performance of a diversity system can be characterized by diversity gain and diversity advantage, which are shown in Fig. 10.2. Diversity gain is the difference in dB, for the same percentage of time, between the attenuation exceeded on a single path and that exceeded jointly on the two paths to two sites. Diversity advantage is defined as the ratio of the percentage of time that a given attenuation is exceeded on a single path to that exceeded jointly on two paths.

Site diversity to minimize the effects of attenuation due to rain may be useful for critical applications at frequencies below 10 GHz (but above about 6 GHz) but must be weighed against the alternative of providing a margin to cover the expected attenuation. For the higher attenuations and consequently the higher values of diversity gain and diversity advantage that tend to be encountered at higher frequencies, the advantage is more apt to be on the side of site diversity.

Likewise, space diversity may be helpful on low-angle satellite paths where atmospheric multipath fading or reflections from sea or land surfaces are a problem. An example of this type is provided by the Canadian arctic where, in the 6/4 GHz band, a space diversity system involving two arctic receiving sites is expected to reduce the required propagation margin from 20 to 8 dB (Mimis and Smalley, 1982)

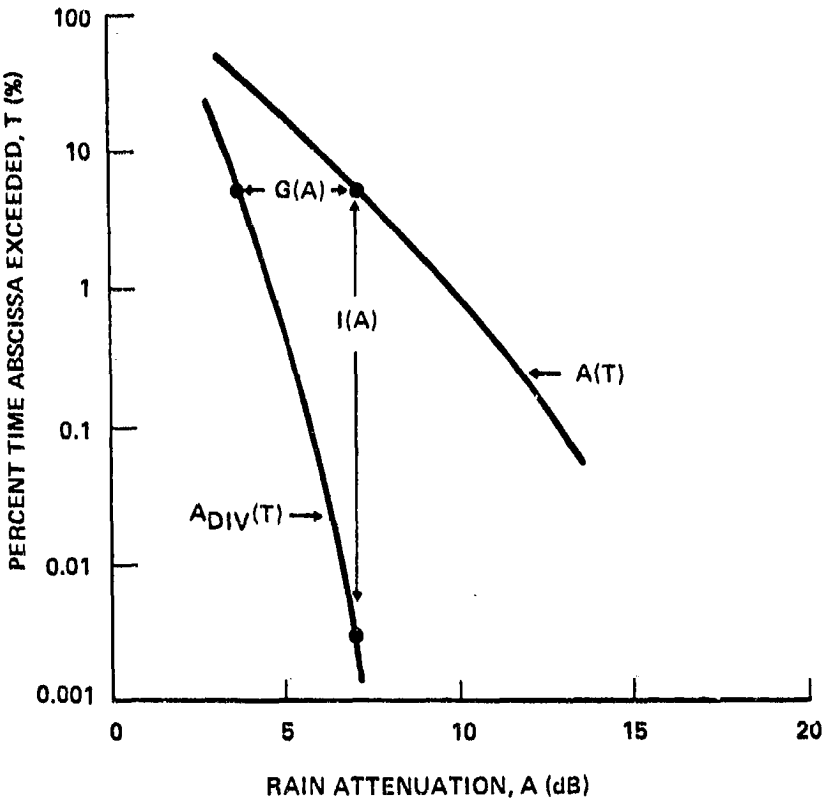

Figure 10.2. Definition of diversity gain G(A) and diversity advantage I(A). The curve A(T) represents performance when only one path is employed, while $A_{DIV}(T)$ represents performance when two paths are employed in a diversity system (Ippolito, Kaul, and Wallace, 1981).

10.3 TELECOMMUNICATION LINK BUDGETS

Provision of a satisfactory signal-to-noise ratio for a specified percentage of time is the aspect of system design that is treated here, and the link power budget equation is used for this purpose. The equation may be written for $C/kT_{sys} = C/X_0$ where C is carrier power (W), k is Boltzmann's constant (1.38×10^{-23} J/K), and T_{sys} is the system noise temperature (K). The ratio C/X_0 is referred to as the carrier power to noise density ratio, as $k\,T_{sys}$ is the noise power in a 1 Hz bandwidth. To obtain C/X, the carrier power to noise ratio in a bandwidth B, one can simply divide C/X_0 by B as X, the noise power in a bandwidth B, equals $k\,T_{sys}\,B$. The quantity C/X_0 was introduced in Chap. 1 where it was written in the form of

$$\frac{C}{kT_{sys}} = C/X_0 = \frac{EIRP\ G_R}{k\ L_{FS}\ L\ T_{sys}} \tag{10.7}$$

where EIRP stands for equivalent isotropic radiated power, G_R is the gain of the receiving antenna, L_{FS} is the free space basic transmission loss, and L is a loss factor defined to be greater than unity for a true loss. The propagation medium plays a major role in determining L and T_{sys}, and Eq. (10.7) shows that C/X_0 varies inversely with L and T_{sys}. In carrying out telecommunication systems design, one works in detail with the expression for C/X_0 (or C/X) usually expressing it in decibel form and carefully considering the factors contributing to L and T_{sys}. Attention must be given to both the uplink and downlink as they both affect the C/X_0 ratio observed at the downlink receiver input terminal.

For applying Eq. (10.7), it is customary to convert to decibel values. Following this practice

$$(C/X_0)_{dB} = (P_T)_{dBW} + (G_T)_{dB} + (G_R)_{dB} - k_{dBW} \tag{10.8}$$

$$- (L_{FS})_{dB} - L_{dB} - (T_{sys})_{dB}$$

where for k we have used Boltzmann's constant times 1 K times 1 Hz (-228.6 dBW) so that T_{sys} and B, the bandwidth, are then treated as being nondimensional. Equation (10.8) is often written with $(P_T)_{dBW}$ and $(G_T)_{dB}$ combined into $(EIRP)_{dBW}$ and with $(G_R)_{dB}$ and $(T_{sys})_{dB}$ combined into $(G_R/T_{sys})_{dB}$, which is

considered as a figure of merit of the receiving system. When the terms are combined as indicated, the resulting form is

$$(C/X_o)_{dB} = (EIRP)_{dBW} - (L_{FS})_{dB} - L_{dB} - k_{dBW} + (G_R/T_{sys})_{dB} \qquad (10.9)$$

When referring specifically to digital systems, we use N_o in place of X_o but the meaning is the same.

The treatment of telecommunication power link budgets here is primarily by example. The first example, 10.1, illustrates some of the basic types of calculations pertinent to link budgets, and the second example deals with a hypothetical system operating at 8.5/8.0 GHz. Following examples deal with particular systems using values quoted in the literature.

Example 10.1 System Concepts

Some of the basic calculations pertinent to system design and operation are illustrated in this example.

1. System noise temperature, T_{sys}

The system noise temperature, T_{sys}, is a measure of noise power as X_o, the noise power density or noise power per Hz (same as N_o) equals k T_{sys} where k is Boltzmann's constant (1.38×10^{-23} J/K). Also X, the total noise power, equals k T_{sys}B where B is bandwidth. System noise temperature is defined at the antenna terminal as suggested in Fig. 10.3, which shows an antenna having a noise temperature of T_A, a lossy transmission line at the standard reference temperature T_o (taken here as 290 K), and a receiver having a noise temperature of T_R.

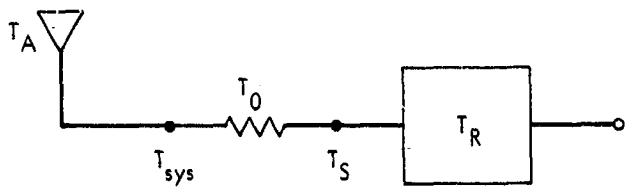

Figure 10.3. Receiving system, with location of T_{sys} specified.

For the receiving system of Fig. 10.3, T_{sys} is given by

$$T_{sys} = T_A + (\ell_a - 1)T_o + \ell_a T_R$$

To illustrate the calculation of T_{sys}, let T_R equal 100 K and T_A equal 50 K and consider that the transmission line has a loss of 1 dB. In the expression for T_{sys}, $\ell_a = 1/g_a$ where g_a is less than unity and is the power "gain" of the transmission line, considering it as a lossy attenuator. The relation between g_a and attenuation A in dB is

$$-A_{dB} = 10 \log g_a$$

and for A = 1

$$-1 = 10 \log g_a$$

$$g_a = 0.794$$

$$\ell_a = 1/g_a = 1.26$$

Substituting values into the expression for T_{sys}

$$T_{sys} = 50 + (1.26-1)\ 290 + 1.26\ (100)$$

$$= 50 + 75.4 + 126$$

$$= 251.4 \text{ K}$$

Note that if there were no attenuation between the antenna and receiver g_a and ℓ_a would equal unity and T_{sys} would equal $T_A + T_R = 150$ K.

The noise power density X_o corresponding to $T_{sys} = 251.4$ K is given by

$$X_o = k\ T_{sys} = (1.38 \times 10^{-23})\ (251.4)$$

$$= 3.47 \times 10^{-21} \text{ W}$$

and

$$(X_o)_{dBW} = 10 \log (3.47 \times 10^{-21}) = -204.6$$

Also

$$(X_o)_{dBm} = -174.6$$

Thus X_o is 204.6 dB below one watt (W), and 174.6 dB below one milliwatt (mW).

2. Antenna gain, G

The gain of an antenna having an effective aperture area A_{eff} is given by

$$G = \frac{4\pi A_{eff}}{\lambda^2}$$

where λ is wavelength. The effective area equals the geometric area times an efficiency factor κ which generally falls between about 0.5 and 0.7. To illustrate the calculation of G consider a frequency of 3 GHz, a paraboloidal antenna having a diameter of 3 m, and an efficiency factor of 0.54. The wavelength $\lambda = 3 \times 10^8/3 \times 10^9 = 0.1$ m and

$$A_{eff} = \left(\frac{\pi d^2}{4}\right) = \frac{\pi 9}{4}(0.54) = 3.817 \text{ m}^2$$

Thus

$$G = \frac{4\pi(3.817)}{0.01} = 4797$$

and

$$G_{dB} = 10 \log G = 36.8$$

3. Distance and elevation angle of geostationary satellite

Consider a receiving earth station at 65°N and a geostationary satellite on the same meridian. The distance d between the station and satellite is given by (Eq. 1.13).

$$d^2 = r_0^2 + (h + r_0)^2 - 2r_0(h + r_0) \cos \theta'$$

where r_0 is the earth radius, h is the height of the satellite above the Earth, and θ' is latitude. Thus

$$d^2 = (6378)^2 + (35,785 + 6378)^2$$

$$- 2(6378)\ (35,785 + 6378) \cos 65^\circ$$

$$d = 39,888.6 \text{ km}$$

To determine the elevation angle, the following expression (Eq. 1.15) can be solved for ψ which equals the elevation angle θ plus 90°

$$(h + r_0)^2 = d^2 + r_0^2 - 2r_0 d \cos \psi$$

$$(42,163)^2 = (39,888.6)^2 + (6378)^2$$

$$- 2(6378)\ )39,888.6)\ \cos \psi$$

$$\cos \psi = - 0.2868$$

$$\psi = 106.67^\circ$$

$$\theta = 16.67^\circ$$

If the earth station were displaced by 10° from the longitude of the satellite then in place of cos θ' = cos 65° = 0.4226 one would use cos 65° cos 10° = 0.4162. The result would be that d = 39,931.9 km and θ = 16.24°. If the difference in longitude were 20°, the distance would be 40,060 km and the elevation angle would be 15.00°.

Example 10.2 Link Power Budget Equation for Hypothetical 8.5/8.0 GHz System

For an example of a link power budget, consider a hypothetical analog system using 8.5 GHz for the uplink and 8.0 GHz for the downlink. The system has a performance objective of 99.99 percent availability in an environment in which a rain rate of 35 mm/h is exceeded for 0.01 percent of the time. The elevation angle of the path is taken as 42° which allows using the results of Example 9.5 for attenuation due to rain. A small earth-station antenna which would be suitable for a portable system is considered.

The distance d to the satellite corresponding to the elevation angle of 42°, can be found from Eq. (1.15),

$$(h + r_0)^2 = d^2 + r_0^2 - 2r_0 d \cos \psi$$

with $\psi = 42^{\circ} + 90^{\circ} = 132^{\circ}$ and turns out to be about 37,600 km. Ordinarily one would start with a particular location to find the value of d and then find ψ, but here we have determined a value of d consistent with an elevation angle of 42°. Knowing d, $(L_{FS})_{dB}$, the free space loss can be determined from

$$(L_{FS})_{dB} = 20 \log \left(\frac{4\pi d}{\lambda}\right)$$

and is found to be 202.55 dB for 8.5 GHz and 202.02 dB for 8.0 GHz.

To formulate a link equation, some initial assumptions must be made about the characteristics of the equipment to be utilized, the required C/X ratio, the needed bandwidth, etc. The initial assumptions may later need to be modified. We assume a minimum overall or composite C/X ratio of 10 dB, a bandwidth B of 5 MHz, a 3-m portable earth-station antenna having an efficiency factor of 0.54, T_{sys} = 300 K for the earth station, and G_R/T_{sys} = -10 dB for the satellite.

Allowance is made for a carrier-to-interference ratio of 18 dB, as well as for thermal noise on the uplink and downlink. The C/X ratios for the

uplink and downlink could be chosen to be equal, but it is easier to supply relatively high power for the uplink so a somewhat higher C/X ratio is chosen for it. The combination of $(C/X)_U$ = 15 dB for the uplink, $(C/X)_D$ = 13 dB for the downlink, and 18 dB for C/I gives an overall or composite ratio of 10.11 dB, thus satisfying the requirement of 10 dB. As ordinary numbers, the four ratios are 31.62, 19.95, 63.10, and 10.25, corresponding to 15, 13, 18, and 10.11 dB respectively and consistent with Eq. (10.6) without a contribution for intermodulation noise, namely

$$\frac{1}{(C/X)_T} = \frac{1}{(C/X)_U} + \frac{1}{(C/X)_D} + \frac{1}{(C/X)_I}$$

Substituting numbers

$$\frac{1}{10.247} = \frac{1}{31.623} + \frac{1}{19.953} + \frac{1}{63.096}$$

Uplink (8.5 GHz)

Attenuation due to rain is taken to be 2.49 dB (from Example 9.5), gaseous attenuation is assumed to be 0.1 dB, and the pointing error loss is taken as 0.3 dB. The gain of the transmitting antenna is calculated from $G_T = 4\pi A_{eff}/\lambda^2$ (Example 10.1, Sec. 2) to be 38,558 or 45.86 dB. At this stage the needed transmitter power P_T can be determined by rearranging Eq. (10.9) to give

$$(EIRP)_{dBW} = (C/X_o)_{dB} + (L_{FS})_{dB} + L_{dB} + k_{dBW} - (G_R/T_{sys})_{dB}$$

where

$$(C/X_o)_{dB} = (C/X)_{dB} + B_{dB}$$

The quantity B is bandwidth which is 5 MHz and B_{dB} = 67 dB (relative to 1 Hz). Thus

$$(C/X_o)_{dB} = 15 + 67 = 82 \text{ dB}$$

Substituting numbers into the equation for EIRP,

$$(EIRP)_{dBW} = 82 + 202.55 + 2.89 - 228.6 + 10$$

$$= 68.84 \text{ dBW}$$

where

$$(EIRP)_{dBW} = (P_T)_{dBW} + (G_T)_{dB}$$

so that

$$68.84 = (P_T)_{dBW} + 45.86$$

Finally P_T = 22.98 dBW ≃ 200 W. The various system parameters are summarized in Table 10.2A.

Table 10.2A
Uplink (8.5 GHz)

Transmitter Power, P_T	23 dBW (200 W)	
Antenna Gain, G_T	45.86 dB	
EIRP		68.84 dBW
Free Space Loss (L_{FS})		202.55 dB
Losses (L)		
Attenuation due to rain	2.49 dB	
Gaseous attenuation	0.1 dB	
Pointing error	0.3 dB	
Total		2.89 dB
Satellite G_R/T_{sys}		-10 dB
C/X		15 dB
C/X_o		82 dB

Downlink (8.0 GHz)

The gain of the receiving antenna for the downlink (same antenna as for the uplink) is calculated to be 34,159 or 45.34 dB. The system noise temperature T_{sys} is taken to be 300 K or 24.77 dB above 1 K in the absence of attenuation due to rain, and the G_R/T_{sys} ratio is thus 45.34 - 24.77 = 20.57 dB. The assumed rain rate of 35 mm/h introduces an attenuation of 2.092 dB and an additional contribution to the noise temperature given by

$$T_b = 280\ (1 - e^{-\tau}) = 280\ (1 - e^{-2.09/4.34}) = 107.1\ K$$

The total degradation in C/X due to rain is then given by

$$(C/X)_{dB} = 2.092 + 10 \log \frac{107.1 + 300}{300}$$

$$= 2.092 + 1.325$$

$$= 3.42\ dB$$

Gaseous attenuation of 0.1 dB and a pointing error loss of 0.3 dB are assumed. Solving for EIRP and P_T in the same way as for the uplink

$$(EIRP)_{dBW} = (C/X_o)_{dB} + B_{dB} + (L_{FS})_{dB}$$

$$+ L_{dB} + k_{dBW} - (G_R/T_{sys})_{dB}$$

$$= 13 + 67 + 202.02 + 3.82 - 228.6 - 20.57$$

$$= 36.67\ dBW$$

At this point it is necessary to have information on or to make an assumption about the gain of the transmitting antenna. Taking this gain G_T as 24 dB, the transmitter power P_T is given by

$$(P_T)_{dBW} = 36.67 - 24 = 12.67\ dBW$$

$$\approx 20\ W$$

System parameters are summarized in Table 10.2B.

Table 10.2B
Downlink (8.0 GHz)

Transmitter Power, P_T	13 dBW (20 W)			
Antenna Gain, G_T	24 DB			
EIRP			37	dBW
Free Space Loss (L_{FS})			202.02	dB
Losses (L)				
Attenuation due to rain	2.09	dB		
Gaseous attenuation	0.1	dB		
Pointing error	0.3	dB		
Total loss			2.49	dB
Antenna Gain, G_R	45.34	dB		
T_{sys}	24.77	dB (300 K)		
G_R/T_{sys}			20.57	dB
Increase in noise due to rain			1.32	dB
C/X			13	dB
C/X_o			80	dB

Example 10.3 LMSS System

As an example in the UHF band, we consider the planned analog Land Mobile Satellite System (LMSS) (Naderi, 1982). This system will utilize the 806-890 allotment for the satellite-mobile and mobile-satellite links and the S band for satellite-base station and base station-satellite links. For the UHF links, a design has been prepared for a large (55-m) multibeam (87-beam) offset-reflector antenna on the satellite with the separate beams formed by the use of 134 microstrip-patch feed elements excited in clusters of 7. The 87 beams would provide coverage of the entire conterminous 48 states (CONUS) of the United States. Use of the UHF band provides a satellite system which is compatible with the cellular mobile radiotelephone system presently in use on a limited basis in two metropolitan areas and due for expansion to other urban areas. At UHF, 95 voice channels would be available per beam, each requiring a 10.2 kHz bandwidth with a 15 kHz channel separation and a total bandwidth per beam of 10 MHz. The initial system to be used for testing the concept, however, may have a much smaller number of beams and channels. The satellite-to-mobile link operating for design purposes at 871 MHz is the most

critical of the four links, and the items entering into the power link budget for this link are shown in Table 10.3A. Some of the points in the following discussion refer to line items of this table.

Downlink

The required total or overall C/X ratio is taken to be 10 dB, and the required minimum C/I carrier-to-interference ratio is 17 dB. Analysis of intermodulation noise indicates that a 25 dB carrier-intermodulation noise ratio is expected. To initiate the link design process, a 20 dB $(C/X)_U$ ratio (carrier-to-thermal noise ratio for the uplink) is assumed. Using the relation of Eq. (10.6) but applying it to $C/X = C/(X_0 B)$, it is determined that $(C/X)_D$ (for the downlink) must be 11.8 dB in order for the carrier-to-overall ratio to be 10 dB (Line item 1). For designing the links (up and down at UHF and up and down at S band), the link budget in all cases begins with the carrier-to-noise requirement at the receiver terminal and progresses backwards to find the needed transmitter power.

A number of the losses shown in Tables 10.3A are equipmental in nature or due to the fact that the system is a mobile system. For example a 4 dB loss is shown to account for a mobile receiver not being at the center of a beam but at a point of minimum signal (Line item 14). Also losses of 2 dB and 1 dB represent pointing losses for the mobile and satellite antennas respectively (Line items 15 and 16). The mobile antenna has a maximum gain of only 5 dB and a correspondingly large beamwidth but the antenna may not always be pointed towards the satellite as the mobile moves uphill and downhill. The satellite antenna has a pointing stability of 0.04 deg but at a point at the edge of the coverage area of a beam a pointing error of 0.04 deg could cause a loss of 1 dB.

For system noise temperature T_{sys} the use of such a large antenna beamwidth for the mobile receiver indicates a minimum antenna temperature T_A of 290 K. In addition the LMSS must provide satisfactory performance in suburban areas where man-made noise would be encountered. A value of T_A of 1.6(290) or 464 K as suggested in the ITT handbook (ITT, 1968) is used for this reason (Line item 4). Taking into account also a receiver noise figure of 2 dB and 2.25 dB for input circuit losses gives a T_{sys} of 991 K or about 30 dB (relative to 1 K).

For propagation losses, the following considerations apply. At UHF frequencies attenuation and depolarization due to precipitation are negligible. Circular polarization is used, and Faraday rotation is not a factor. Ionospheric scintillation is most severe at equatorial and auroral latitudes, and the design is for the conterminous 48 states. CCIR Report 884 (CCIR, 1982) gives the data of Table 9.2 for mid-latitude fading due to ionospheric scintillation. The smallest percentage of time shown in the table is 0.1, for which the fade depth is 1 dB for 500 MHz and 0.3 dB for 1000 MHz. Thus the 800-900 MHz frequency range is sufficiently high that scintillation effects should not be severe, and as the grade of service for the LMSS calls for a two percent probability of system overload an allowance for ionospheric scintillation has not been included among the losses. Observations of peak-to-peak scintillations of 18, 10, 15, and 3.5 dB at 136 MHz and 1.7, 4, and 14 GHz respectively in and around Japan (Minakoshi et al., 1981), however, indicate that ionospheric scintillation may need to be taken into account in some system designs at temperate latitudes, especially if a high grade of service is required.

Mobile operations are subject to fading due to multipath reception involving interference between rays following direct paths and rays reflected from the Earth's surface. On the basis of measurements made by use of the ATS-6 satellite (Anderson et al., 1981; Hess, 1980; CCIR, 1982b) a 5 dB margin for multipath effects has been utilized in the LMSS design (Line item 13). No allowance has been made for shadowing, as it has been concluded that it is unreasonable to provide service where a line-of-sight path does not exist between the mobile and the satellite.

Uplink

For the uplink opearting at 826 MHz, many of the same considerations apply. A 20 dB $(C/X)_U$ ratio at the satellite was assumed at the outset. This ratio is achieved by using a mobile antenna gain of 5 dB and a transmitter power per channel of 2.45 W or 3.9 dBW. The system noise temperature T_{sys} (or effective receiver temperature, Line item 4) is 580 K rather than 991 K. A principal reason for the difference is that the mobile receiver is assumed to operate in a 464 K suburban noise environment whereas the satellite receiver is assumed to receive radiation from the Earth at 290 K. The same multipath

Table 10.3A

LMSS Satellite-To-Mobile Link Budget

Line Item	Parameter	Value	Comment
1	Downlink Carrier-to-Thermal Noise Ratio (C/X_0B)	11.8 dB	At the input-to-mobile receiver
2	IF Bandwidth (B = 10.2 KHz)	40.1 dB	Assuming Envelope Normalized (EN) FM (Channel Spacing = 15 kHz)
3	Carrier-to-Noise Density Ratio (C/X_0)	51.9 dB	(1) + (2)
4	Effective Receiver Temperature (991 K)	30 dB	Includes: 464 K suburban noise, 2.5 dB input circuit loss and a receiver noise figure of 2 dB
5	Boltzmann Constant	-228.6 dBW	
6	Miscellaneous Receiver Loss	2 dB	
7	Required Received Power	-144.7 dBW	(3) + (4) + (5) + (6)
8	Maximum Mobile Antenna Gain	5 dB	(G/T = -25 dB)
9	Free Space Losses (f = 871 MHz, λ = 34.44 cm)	182.8 dB	Free space loss varies from 182.5 dB for southern CONUS to 183.2 dB for north-eastern CONUS
10	Transmitting Antenna Gain	50 dB	
11	Transmitting Circuit Losses	1 dB	
12	Control Signal Power Requirement	1 dB	
13	Multipath Fading	5 dB	
14	Edge of Coverage Allowance	4 dB	
15	Mobile Antenna Pointing Loss	2 dB	
16	Satellite Antenna Pointing Loss	1 dB	
17	Scanning Loss	0.5 dB	
18	Required Transmitter Power-Per-Channel	-2.2 dBW (0.6 W)	(7) - (8 + 10) + (9+11+12+13 +14+15+16+17) (SCPC EIRP = 46.8 dBW)
19	Average Transmitter Power-Per-Channel Using VOX	-6.2 dBW (0.24 W)	For 40 percent voice activity factor

Table 10.3B

LMSS Satellite-To-Mobile Link Budget

Line Item	Parameter	Value	Comment
1	Downlink Carrier-to-Thermal Noise Ratio (C/X_oB)	20 dB	At the input-to-satellite UHF receiver
2	IF Bandwidth (B = 10.2 KHz)	40.1 dB	
3	Carrier-to-Noise Density Ratio (C/X_o)	60.1 dB	(1) + (2)
4	Effective Receiver Temperature (580 K)	27.7 dB	Includes: 290 K Earth's temperature, 1 dB cable and diplexer loss, 2 dB receiver noise figure
5	Boltzmann Constant	-228.6 dBW	
6	Miscellaneous Receiver Loss	1 dB	
7	Required Received Power	-139.8 dB	(3) + (4) + (5) + (6)
8	Receiving Antenna Gain	49.7 dB	G/T = 22 dB
9	Free Space Loss (f = 826 MHz, λ = 36.32 cm)	182.4 dB	Various from 182 dB for southern CONUS to 182.7 for northeastern CONUS
10	Transmitting Antenna Gain	5 dB	
11	Transmitting Circuit Losses	2.5 dB	
12	Control Signal Power Requirement	1 dB	
13	Multipath Fading	5 dB	
14	Edge of Coverage Allowance	4 dB	
15	Mobile Antenna Pointing Loss	2 dB	
16	Satellite Antenna Pointing Loss	1 dB	
17	Scanning Loss	0.5 dB	
18	Required Transmitter Power-Per-Channel	3.9 dBW (2.45 W)	(7) - (8 + 10) + (9+11+12+13 +14+15+16+17) (SCPC EIRP = 6.4 dBW)

fading allowance of 5 dB is used, and the same values are allotted for pointing and edge of coverage losses. Parameters for the uplink are given in Table 10.3B.

Example 10.4 MARISAT

The MARISAT system provides an example involving L-band operation for the uplink from ship to satellite and C-band operation for the downlink from satellite to ground station. The system parameters utilized in the example and shown in Tables 10.4A and 10.4B are taken from a paper dealing with application of the MARISAT system to the transmission of seismic data at 56 kbps from a ship or seismic vessel, with losses taken into account (Calvit and Heitman, 1981). Table 10.4A follows.

Table 10.4A
Ship to Satellite Uplink (1.6405 GHz)

Transmitter Power, P_T	15.7 dBW	
Diplexer/Feed Loss	0.6 dB	
Antenna Gain, G_T	23.5 dB	
EIRP (Transmitter Power Minus Diplexer/Feed Loss Plus Antenna Gain)		38.6 dBW
Free Space Loss (L_{FS})		188.6 dB
Losses (L)		
Wet Radome	0.5 dB	
Polarization Coupling	0.2 dB	
Atmospheric Absorption	0.4 dB	
Total		1.1 dB
Satellite G_R/T_{sys}		-15.9 dB
C/N_o		61.6 dB

The values in the table are consistent with Eq. (10.9), namely

$$(EIRP)_{dBW} - (L_{FS})_{dB} - L_{dB} - k_{dBW} + (G_R/T_{sys})_{dB} = (C/N_o)_{dB}$$

as can be checked by numerical substitution, giving the result that

$$38.6 - 188.6 - 1.1 - (-228.6) - 15.9 = 61.6 = (C/N_0)_{dB}$$

Next consider Table 10.4B for the downlink.

Table 10.4B
Satellite to Shore Station Downlink (4.197 GHz)

Satellite EIRP		2 dBW
Free Space Loss (L_{FS})		196.9 dB
Losses (L)		
Atmospheric Absorption	0.3 dB	
Rain attenuation	1.2 dB	
Polarization Coupling	0.4 dB	
Total		1.2 dB
Increase in T_{sys} Due to Rain		1.2 dB
Shore Station G_R/T_{sys}		33 dB
C/N_0		64.3 dB

Inserting values from the table into Eq. (10.9) (combining the losses and the increase in T_{sys} to obtain 2.4 dB),

$$2 - 196.9 - 2.4 - (-228.6) + 33 = 64.3 = (C/N_0)_{dB}$$

Overall C/N_0 Ratio

The overall or composite C/N_0 value, neglecting interference, is found from

$$\frac{1}{(C/N_0)_T} = \frac{1}{(C/N_0)_U} + \frac{1}{(C/N_0)_D}$$

in which $(C/N_0)_U = 10^{6.16} = 1.445 \times 10^6$ and $(C/N_0)_D = 10^{6.43} = 2.96 \times 10^6$. The resulting value of $(C/N_0)_T$ is 9.333×10^5 or 59.7 dB.

The E_b/N_0 ratio can then be found from

$$E_b/N_0 = \frac{C}{N_0 R}$$

where R is the data rate, namely 56 kbps in this case. Carrying out the calculation in decibels, 10 log 5.6×10^4 = 47.5 dB and

$$(E_b/N_0)_{dB} = 59.7 - 47.5 = 12.2 \text{ dB}$$

which is a satisfactory value, as it was determined that a bit error rate (BER) of better than 1×10^{-5} could be achieved with an E_b/N_0 ratio above [illegible] 6 dB.

A film of water on an antenna or radome has the potential for creating a loss, and for the uplink a loss of 0.5 dB was assigned for the condition of a wet radome on the uplink. A loss of 0.4 dB was assigned for atmospheric absorption on the uplink, at about 1.6 GHz. At this frequency, true absorption of this magnitude is improbable, but a reduction in signal amplitude of this magnitude due to ionospheric scintillation could very likely occur. For the downlink at about 4.2 GHz, a generous allowance of 0.3 dB is provided for atmospheric absorption, 0.5 dB is assigned for attenuation due to rain, and 1.2 dB is assigned for the increase in noise due to rain. The basis for the rain effects is not stated but they correspond to intense rain such as might be exceeded in region D_3 of the United States for 0.01 of the time (63 mm/h) or slightly higher. A greater margin would be needed at 1.6 GHz for ionospheric scintillation at equatorial latitudes, and a considerably larger margin would probably be needed for the degradation in signal-to-noise ratio on paths at elevation angles below 10°. It appears that the system actually had a larger margin than that specifically assigned. A practical consideration in shipboard operations is that ships are subject to large values of pitch and roll in high seas, and these motions can result in degradation in performance unless the antenna platform is extremely well stabilized.

Example 10.5 Westar V

Westar V serves as an example of a C-band system, with the uplink operating at 6 GHz and the downlink operating at 4 GHz (Piraino and Schoen, 1982). Tables 10.5A and 10.5B give some of the parameters for the uplink and downlink. The system is a digital system having a bit error rate of 1×10^{-6} as a performance objective without encoding and 1×10^{-11} when rate-7/8 convolu-

tional forward-error-correction (FEC) encoding is employed. The overall E_b/N_0 ratio required to meet these objectives is stated to be 14.5 dB. The various contributions to this ratio are stated to be 22.9 dB for the uplink, 18.6 dB for the downlink, 24.3 dB for the adjacent satellite interference, 20.1 dB for cross-polarized transponders, and 23.0 dB for interference from terrestrial microwave systems. When these quantities are taken into account in an equation like Eq. (10.6) (which is written in terms of ordinary numbers rather than decibel values), an overall E_b/N_0 value of 14.3 dB (close to 14.5 dB) is obtained. The calculation is summarized in Table 10.5A. For the various contributions to the overall E_b/N_0 value, the numerical values were calculated from the dB values and then the reciprocals of the numerical values were taken. The reciprocals were added to obtain the corresponding overall reciprocal value, and then the overall numerical and dB values were determined. The bit rate for the system is 60 Mbps (quoted as 77.8 dB-Hz).

Table 10.5A

E_b/N_0

Type	dB	Numerical	Reciprocals of Numerical Values
Uplink	22.9	194.984	0.00512861
Downlink	18.6	72.4436	0.0138038
Adjacent Sat.	24.3	269.153	0.00371535
Cross Polarization	20.1	102.329	0.00977237
Terrestrial	23.0	199.526	0.00501187
Total	14.3	26.7171	0.0374320

Uplink (6 GHz)

Parameters for the 6 GHz uplink are shown in Table 10.5B.

Table 10.5B
6 GHz Uplink Budget

Earth Station EIRP	79.0 dBW
Free Space Loss	200.1 dB
Atmospheric Absorption	0.1 dB
Rain Attenuation	0.4 dB
Wind Effect on Antenna	0.3 dB
Transponder G_R/T_{sys}	-6.0 dB

The values of the table are consistent with Eq. (10.9) repeated below.

$$(C/N_o)_{d/B} = (EIRP)_{dBW} - (L_{FS})_{dB} - L_{dB} - k_{dBW} + (G_R/T_{sys})_{dB}$$

Substituting numbers into the right-hand side of Eq. (10.9)

$$(C/N_o)_{dB} = 79.0 - 200.1 - 0.8 - (-228.6) - 6.0 = 100.7$$

Converting to $(E_b/N_o)_{dB}$ by subtracting

R_{dB} with R = 60 Mbps (Eq. 10.2),

$$(E_b/N_o)_{dB} = (C/N_oR)_{dB} = 100.7 - 10 \log 6 \times 10^7$$

$$= 100.7 - 77.8 = 22.9 \text{ dB}$$

Downlink 4 GHz

Parameters for the 4 GHz downlink are shown in Table 10.5C.

Table 10.5C

4 GHz Downlink Budget

Transmitter EIRP	33.3 dBW
Free Space Loss, L_{FS}	196.6 dB
Atmospheric Absorption	0.1 dB
Rain Attenuation	0.1 dB
Wind Effect on Antenna	0.2 dB
Increase in T_{sys} due to Rain	0.3 dB
Earth Station G_R/T_{sys}	31.8 dB

Substituting numbers into the right-hand side of Eq. (10.9) as following Table 10.5B,

$$(C/N_o)_{dB} = 33.3 - 196.6 - 0.7 - (-228.6) + 31.8$$

$$= 96.4$$

Converting to $(E_b/N_o)_{dB}$

$$(E_b/N_o)_{dB} = 96.4 - 77.8$$

$$= 18.6 \text{ dB}$$

In the numerical equation, 0.7 represents the sum of atmospheric absorption, rain attenuation, wind effect on antenna, and increase in noise due to rain.

For both the uplink and downlink, an allowance of 0.1 dB is made for atmospheric absorption. Absorption due to oxygen and water vapor should be somewhat less than 0.1 dB, and the allowance is generous but still small. An allowance of 0.4 dB is made for rain attenuation on the uplink at 6 GHz, and 0.1 dB for rain attenuation plus 0.3 dB for noise due to rain is assigned for the downlink. The basis for the attenuation values listed for rain is not given, but the values are reasonable. Effects due to rain at these frequencies are small but should still be included in the link equations. The values of attenuation are less than those for the rain rate of 35 mm/h considered in

Example 9.5 and appear to be based on a percentage of occurrence (percentage exceeded) of 0.1 rather than 0.01.

10.4 A GRAPHICAL MARGIN-DESIGN PROCEDURE

Insight into choosing suitable uplink and downlink margins in the presence of rain can be obtained by use of a graphical procedure described by Calo, Schiff, and Staras (1978). Consider first Fig. 10.4 in which the curve illustrates the combination of uplink and downlink C/X ratios which can provide the needed total or composite C/X ratio (10 dB in this case) in the absence of rain. Equal C/X ratios of 13 dB for the uplink and downlink, for example, can provide the composite value of 10 dB.

Now consider how the curve would need to be modified for the presence of rain on the uplink only of a TDMA (time-division-multiple access) system. Numerical values will be used for purposes of illustration. If 3 dB of attenuation is expected to be encountered, with a probability of p percent of being exceeded where p is consistent with performance objectives, the original curve of Fig. 10.4 can be moved to the right by 3 dB in order to provide a 3 dB margin for the uplink. In addition the output power of the satellite repeater, which serves as the transmitter power for the downlink, will have been reduced but, because of the nonlinear characteristic of traveling-wave tubes, by not necessarily the same amount as the reduction in input power. Assuming the reduction is 2 dB, the original curve can be moved upwards to compensate by 2 dB, corresponding to increasing the downlink power and therefore the downlink C/X ratio by 2 dB. In Fig. 10.5, the curve of Fig. 10.4 is redrawn and labeled A and the curve obtained by an upward movement of 2 dB and movement to the right of 3 dB is labeled as B. Next consider rain causing attenuation of 2 dB in the downlink with the same probability as for the attenuation of 3 dB on the uplink. Whereas the receiving antenna of the uplink receives noise corresponding to about 290 K from the Earth, whether there is rain or not, the receiving antenna of the downlink receives additional noise when there is rain along the path. Take the increase in noise to be 2 dB so that the total degradation in C/X ratio for the downlink is 4 dB. To compensate for this degradation, the original curve A can be moved upwards by 4 dB to form curve C which therefore includes a margin of 4 dB. The point where curves B and C intersect now corresponds to C/X values providing suffi-

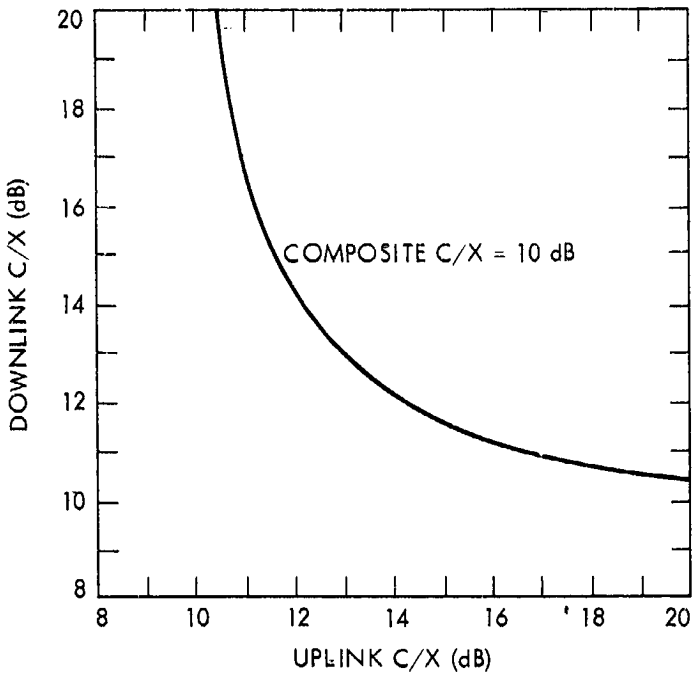

Figure 10.4. Values of downlink and uplink C/X ratios that give a composite ratio of 10 dB in the absence of attenuation.

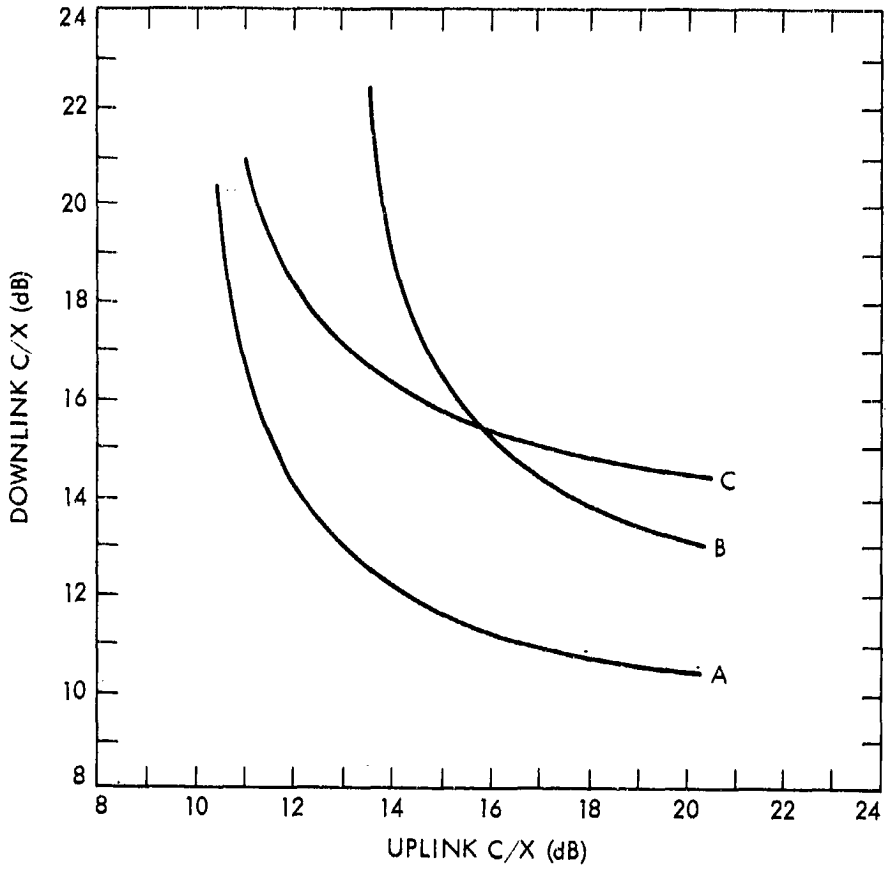

Figure 10.5. Illustration of graphical procedure for determining downlink and uplink C/X ratios such that the composite ratio will be satisfactory when propagation impairments due to rain are encountered.

cient margins to accommodate simultaneous rain causing attenuations as indicated for both the uplink and downlink. Assuming the probabilities of such rain rates on the uplink and downlink are independent, however, the accommodation is now for all but 2p percent of the time rather than for all but p percent. Although the point of intersection of curves B and C may give suitable C/X values for the uplink and downlink (in the absence of rain but providing suitable margins for rain), it may be desirable to choose a point slightly to the right along curve C so that C/X for the uplink is slightly higher than C/X for the downlink.

Further discussion, including consideration of the application of the technique to FDMA (frequency-division-multiple access) is provided in the original reference (Calo, Schiff, and Staras, 1978).

10.5 COVERAGE AREA

It may be necessary in system design to provide for service over a given, possibly extensive, geographical area rather than only one particular earth station. The relation between the service or coverage area, A_{cov}, and other system parameters, including C/X_0, for one antenna beam is shown in Eq. (1.11), from which k and other numerical factors were eliminated. The relation is repeated below but with k and κ_{ANT}, the antenna efficiency, reinserted.

$$A_{cov}(C/X_0) \simeq \frac{P_T A_R \kappa_{ANT}}{kT_{sys} L} \tag{10.10}$$

The relation is still shown as only an approximation for a reason to be explained in the course of deriving the expression. To derive Eq. (10.10) one can start with Eq. (10.7). In this expression make the substitutions $L_{FS} = (4\pi d/\lambda)^2$, $G_R = 4\pi A_R/\lambda^2$, and $G_T = \kappa_{ANT}\, 4\pi/\Omega_A$, where A_R represents the effective area of the receiving antenna and Ω_A is the solid angle of the transmitting antenna beam. Note that $4\pi/\Omega_A$, with Ω_A in rad^2 or steradians, represents antenna directivity by definition and that directivity times antenna efficiency equals gain. After making these substitutions, the resulting expression for C/X_0 is

$$(C/X_0 = \frac{P_T \kappa_{ANT} A_R}{\Omega_A d^2 L k\, T_{sys}} \tag{10.11}$$

By definition the solid angle Ω_A subtended at a point by an area A that is perpendicular to the line of sight from the point at a distance d is given by

$$\Omega_A = \frac{A}{d^2} \tag{10.12}$$

If now A is identified as A_{cov} and Ω_A of Eq. (10.11) is set equal to A_{cov}/d^2, Eq. (10.10) is obtained. The equation is only an approximation, and possibly only a very rough one, because A_{cov} most closely approaches perpendicularity in the vicinity of the subsatellite point and departs increasingly from perpendicularity with increasing distance from the subsatellite point. A precise analysis is beyond the scope of this handbook. Equation (10.10) is of interest, however, in that it shows the product $A_{cov}(C/X_0)$ to be independent of transmitter gain G_T. Increasing gain, for example, increases C/X_0 but decreases A_{cov} such that $A_{cov}(C/X_0)$ remains constant. Also it is obvious that a higher value of transmitter power is required, other factors remaining constant, to provide a certain C/X_0 value over a large area than for a small area.

Contours of constant EIRP for Westar IV and V are shown in Figs. 10.6 and 10.7. These satellites provide coverage over the entire United States, with an EIRP for downlink transmission at 4 GHZ of 34 dBW for the adjacent 48 states and with smaller values of EIRP for Alaska, Hawaii, and Puerto Rico. For uplink transmission at 6 GHz, Fig. 10.7 shows the G_R/T_{sys} value for the adjacent 48 states to be -6 dB.

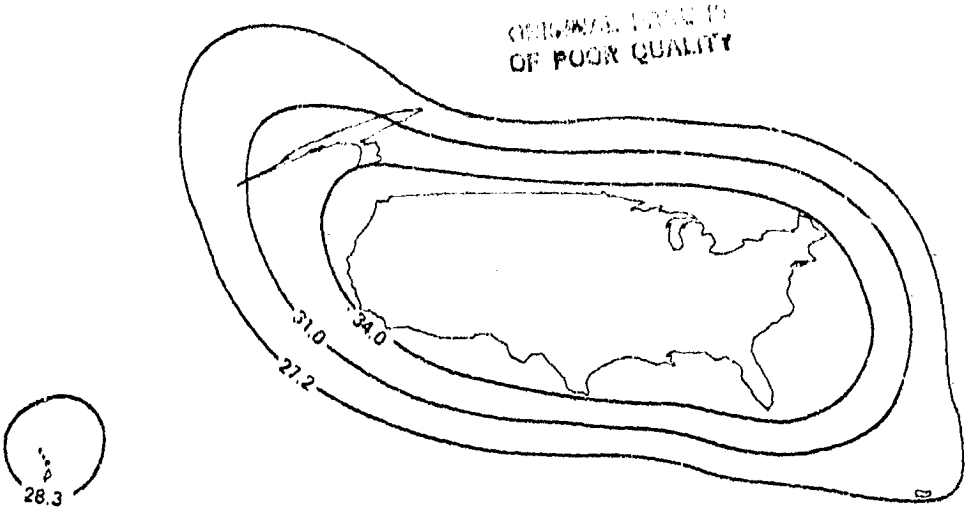

Figure 10.6. EIRP contours for Westar IV and V at 4 GHz.

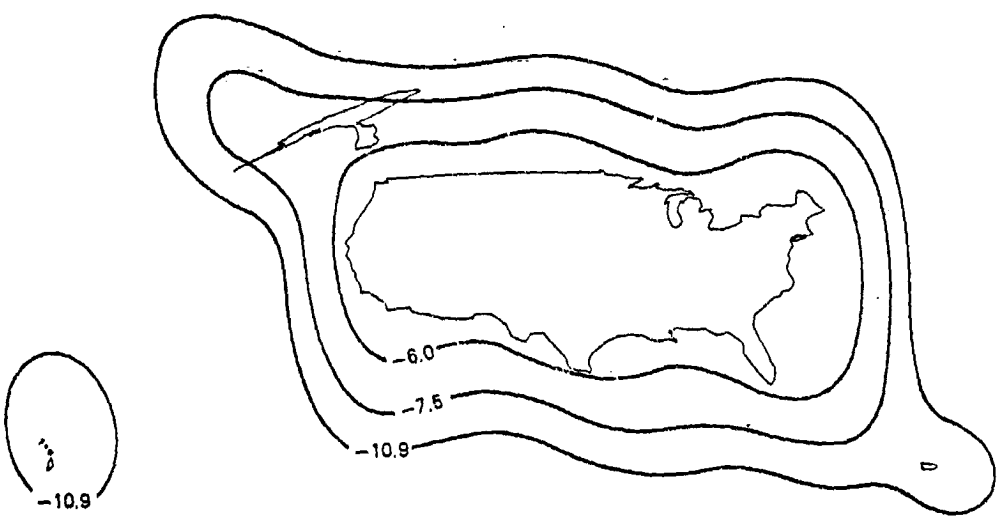

Figure 10.7. Contours of G_R/T_{sys} for Westar IV and V at 6 GHz.

10.6 DISCUSSION

In the examples and other material of this chapter and Chap. 9, some basic, practical considerations about the role of propagation effects have been illustrated. Emphasis has been on link power budgets and propagation phenomena affecting these, but depolarization was considered in Sec. 9.4.3, including Examples 9.6 and 9.7. Note also that in Example 10.5 an allowance was made for the depolarization or cross polarization by the approach of specifying a value for the signal-to-cross polarization ratio (20.1 dB in this case). The effect of this procedure is to treat the cross polarized signal as a type of noise. Also interference from adjacent satellites and terrestrial microwave systems was treated in the same way. Diversity systems have been considered only briefly, as appears appropriate for frequencies below 10 GHz, and the reader wishing a more nearly complete treatment is referred to such references as NASA Reference Publication 1082 (Ippolito, Kaul, and Wallace, 1981) and CRI Technical Report 1891 (Wallace, 1981). Excess range delay due to the ionosphere and troposphere was illustrated in Examples 9.2 and 9.3 respectively. Section 10.3 treats a graphical technique for determining suitable C/X values for the uplinks and downlinks of satellite telecommunication systems.

Intermodulation noise, which occurs in multiple carrier systems, was included in Examples 10.3 and 10.5. Intermodulation noise varies, depending on the combination of carriers being simultaneously amplified and on the position of the carrier of interest on a frequency scale. Thus it is difficult to express it in a general form (Miya, 1981). The intermodulation noise generated in the traveling-wave tube or klystron amplifier is greatest when full rated or saturation power is being utilized and can be reduced by reducing input power (and therefore output power). The reduction in power level is referred to as backoff. Intermodulation noise is only a problem for FDMA (frequency-division-multiple access) systems as TDMA (time-division-multiple access) digital systems are single carrier systems.

It is desirable to treat the propagation impairments, and consequently the evaluation of satellite link availability, in a statistical manner. This type of approach has been quite well developed for the case of attenuation due to rain, but less well developed for the other impairments. In the other

cases it is necessary to rely to a considerable extent on operational experience and representative values that have been reported. Some more nearly complete analyses, however, have been made. Bantin and Lyons (1978) in their statistical analysis of propagation effects in northern and southern Canada included rain attenuation, ionospheric scintillation, tropospheric scintillation (including tropospheric multipath fading), gaseous attenuation, and pointing error due to wind.

While mild depolarization of originally orthogonally polarized channels may be treated as noise and accounted for in link design in this way, as in Example 10.5, depolarization in some cases may be so severe as to cause system outage. Adaptive techniques for compensating for depolarization have been developed for frequencies in the 4- and 6- GHz bands where depolarization is caused principally by rain induced differential phase. These techniques involve the use of rotating phase shifters to restore orthogonality (DiFonzo et al., 1965; Krautel et al., 1977; Yamada et al., 1981). Theoretical analysis applicable to this problem was carried out by Chu (1971, 1973). It was reported by Yamada et al. (1981) that XPD under rainy conditions was improved from 18 dB to 45 dB.

The graphical approach of Sec. 10.4 is a useful supplementary design tool. Further discussion of system design procedures can be found in NASA Reference Publication 1982 (Ippolito, Kaul, and Wallace, 1981) and in ORI Technical Report 1890 (McGregor, 1981).

REFERENCES

Anderson, R. E. et al., "Satellite-aided mobile communications: experiments, applications, and prospects," IEEE Trans. Vehicular Technology, vol. VT-30, pp. 54-61; May 1981.

Bantin, C. C. and R. G. Lyons, "The evaluation of satellite link availability," IEEE Trans. Commun., vol. COM-26, pp. 847-853, June 1978.

Calo, S. B., L. Schiff, and H. Staras, "Effects of rain on multiple access transmission of data via satellite," Record, IEEE 1978 International Communications Conference, Toronto, pp. 30.1.1-6.

Calvit, T. O. and L. B. Heitman, "High-speed satellite data transmission of maritime seismic data," 80-0480, Technical Papers, Communication Satellite Systems Conference, 8th, Orlando, FL, April 20-24, 1980, pp. 714-722. New York: American Institute of Aeronautics and Astronautics, 1980.

CCIR, "Allowable noise power in the hypothetical reference circuit for frequency-division multiplex telephony in the fixed satellite service," Recommendation 353, Vol. IV, Fixed Service Using Communication Satellites, Recommendations and Reports of the CCIR, 1978. Geneva: Int. Telecomm. Union, 1978.

CCIR, Propagation Data for Maritime and Land Mobile Satellite Systems Above 100 MHz, Report 884 , vol. V, Propagation in Non-ionized Media, Recommendations and Reports of the CCIR, 1982. Geneva: Int. Telecomm. Union, 1982.

Chu, T. S., "Restoring the orthogonality of two polarizations in radio communication systems, I," Bell System Tech. Jour., vol. 50, pp. 3063-3069, Nov. 1971.

Chu, T. S., "Restoring the orthogonality of two polarizations in radio communication systems, II," Bell System Tech. Jour., vol. 52, pp. 319-327, March 1973.

DiFonzo, D. F., W. S. Trachtman, and A. E. Williams," Adaptive polarization control for satellite frequency reuse systems," COMSAT Tech. Review, vol. 6, pp. 253-283, Fall 1976.

Feher, K., Digital Communications, Satellite/Earth Station Engineering. Englewood Cliffs, NJ: Prentice-Hall, 1983.

Freeman, R.L., Telecommunications Transmission Handbook, 2nd Ed. New York: Wiley, 1981.

GTE Lenkurt, Engineering Considerations for Microwave Communication Systems. San Carlos, CA: GTE Lenkurt, Inc., 1972.

Heller, J. A. and I. W. Jacobs, "Viterbi decoding for satellite and space communications," IEEE Trans. Commun. Technol., vol. COM-19, pp. 835-848, Oct. 1971. Also in Van Trees, H. L. (ed.), Satellite Communications, pp. 273-286. New York: IEEE Press, 1979.

Hess, G. C., "Land-mobile satellite excess path loss measurements," IEEE Trans. Vehicular Technology, vol. VT-29, pp. 290-297, May 1980.

Ippolito, L. J., R. D. Kaul, and R. G. Wallace, Propagation Effects Handbook for Satellite Systems Design, A Summary of Propagation Impairments on 10 to 100 GHz Satellite Links with Techniques for System Design, NASA Reference Pub. 1082. Washington, D. C.: NASA Headquarters, 1981.

ITT, Reference Data for Radio Engineers, Fifth Ed. Indianapolis: Howard W. Sams & Co., 1968.

Kreutel, R. W., D. F. DiFonzo, W. J. English, and R. W. Gruner, "Antenna technology for frequency reuse satellite communications," Proc. IEEE, vol. 65, pp. 370-378, March 1977.

McGregor, D. N., Communication Satellite System Availability Models, ORI Technical Report 1890, prepared under contract NASW-3436 for NASA Headquarters, 1981.

Mimis, V. and A. Smalley, "Low elevation angle site diversity satellite communications for the Canadian arctic," Record, IEEE 1982 International Communications Conference, Philadelphia, PA, June 13-17, 1982, pp. 4A.4.1-5.

Minakoshi, H. et al., "Severe ionospheric scintillation associated with magnetic storm on March 22, 1979," J. Radio Res. Labs. (Japan), vol. 28, pp. 1-9. March/July 1981.

Miya, K., Satellite Communications Technology. KDD Bldg. 3-2, Nishi-Shinjuku 2-chome, Shinjuku-ku, Tokyo 160, Japan, 1981.

Naderi, F. (ed.), Land Mobile Satellite Service (LMSS), Part II: Technical Report, JPL Publication 82-19. Pasadena, CA: Jet Propulsion Lab., 1982.

Piraino, S. M. and A. P. Schoen, "CITISATCOM: Citicorp's digital satellite network," 82-0513, Technical Papers, Communications Satellite Systems Conference, 9th, San Diego, CA, March 7-11, 1982, pp. 309-404. New York: American Institute of Aeronautics and Astronautics, 1982.

Van Trees, H. L. (ed.), Satellite Communications. New York: IEEE Press, 1979.

Wallace, R. G., Site Diversity Effects on Communications Satellite System Availability, ORI Technical Report 1891, prepared under contract NASW-3436 for NASA Headquarters, 1981.

Yamada, M. et al. "Compensation techniques of rain depolarization in satellite communications," Abstracts of URSI XXth General Assembly, Aug. 10-19, 1981, Washington, D. C., p. 294.

☆U.S. GOVERNMENT PRINTING OFFICE: 1982-733-010/44